SEPTEMBER 2020 PhD. İn Civil Engineering AHMET HİLMİ DERİNGÖL

REPUBLIC OF TURKEY

GAZİANTEP UNIVERSITY

GRADUATE SCHOOL OF NATURAL & APPLIED SCIENCES

A COMPARATIVE STUDY ON INELASTIC SEISMIC DEMANDS OF FRICTION DAMPED AND BASE ISOLATED STRUCTURES

PhD. THESIS
IN
CIVIL ENGINEERING

BY

AHMET HİLMİ DERİNGÖL

SEPTEMBER 2020

A Comparative Study on Inelastic Seismic Demands of Friction Damped and Base Isolated Structures

PhD. Thesis

in

Civil Engineering

University of Gaziantep

Supervisor

Prof. Dr. Esra METE GÜNEYİSİ

by

Ahmet Hilmi DERİNGÖL

September 2020

REPUBLIC OF TURKEY
UNIVERSITY OF GAZİANTEP
GRADUATE SCHOOL OF NATURAL & APPLIED SCIENCES
CIVIL ENGINEERING DEPARTMENT

Name of the Thesis : A Comparative study on inelastic seismic demands of friction damped and base isolated structures

Name of the Student : Ahmet Hilmi DERİNGÖL

Exam Date : 23.09.2020

Approval of the Graduate School of Natural and Applied Sciences

Prof. Dr. A. Necmeddin YAZICI
Director

I certify that this thesis satisfies all the requirements as a thesis for the degree of Doctor of Philosophy.

Prof. Dr. Aytaç GÜVEN
Head of Department

This is to certify that we have read this thesis and that in our consensus/majority opinion it is fully adequate, in scope and quality, as a thesis for the degree of Doctor of Philosophy.

Prof. Dr. Esra METE GÜNEYİSİ
Supervisor

Examining Committee Members:	Signature
Prof. Dr. Mustafa GÜNAL	…………………..
Prof. Dr. Ali Fırat ÇABALAR	…………………..
Prof. Dr. Esra METE GÜNEYİSİ	…………………..
Assoc. Prof. Dr. Kasım MERMERDAŞ	…………………..
Asst. Prof. Dr. Süleyman İPEK	…………………..

I hereby declare that all information in this document has been obtained and presented in accordance with academic rules and ethical conduct. I also declare that, as required by these rules and conduct, I have fully cited and referenced all material and results that are not original to this work.

Ahmet Hilmi DERİNGÖL

ABSTRACT

A COMPARATIVE STUDY ON THE INELASTIC SEISMIC DEMANDS OF FRICTION DAMPED AND BASE ISOLATED STRUCTURES

DERİNGÖL, Ahmet Hilmi
Ph.D. in Civil Engineering
Supervisor: Prof. Dr. Esra METE GÜNEYİSİ
September 2020
163 pages

This study addresses the nonlinear seismic response of the buildings retrofitted with a series of passive protective systems. Friction damper (FD) as an energy dissipation device and lead rubber bearing (LRB), friction pendulum bearing (FPB), and high damping rubber bearing (HDRB) as base isolators were considered. Two sets of steel buildings were used. The first one included three 5 storey frames and two 10 storey frames while the second one contained 3, 6, and 9-storey steel moment resisting frames. To study the application and effectiveness of different seismic protective systems in the buildings, four cases were adopted. The first case investigated the utilization of FD and LRB considering their design properties. The second and third cases examined the influence of design parameters of FPB (i.e., the isolation period T, effective damping ratio ß, and yield strength to weight ratio Fy/W) and HDRB (i.e., T, ß, and post-yield stiffness ratio λ), respectively. Finally, the fourth case compared the overall performance of the protective systems through the single and combined use of energy dissipation devices (i.e., FD) and base isolation devices (i.e., LRB, FPB, HDRB). The most favourable isolation parameters of the isolators and slip load of FD were utilized in the design of the structural protective systems. They are modelled using a finite element program, and evaluated by the nonlinear time history analyses through ground motion records. The results were discussed in terms of various engineering demand parameters. It was shown that single protective system could not always satisfy fully operational performance level while the combined systems effectively achieved for the case studied structures.

Keywords: Friction damper, Base isolation, Friction pendulum bearing, High damping rubber bearing, Lead rubber bearing, Seismic protection.

ÖZET

SÜRTÜNME SÖNÜMLEYİCİLİ VE TABAN İZOLATÖRLÜ YAPILARIN ELASTİK ÖTESİ SİSMİK TALEPLERİ ÜZERİNE KARŞILAŞTIRMALI BİR ÇALIŞMA

DERİNGÖL, Ahmet Hilmi
Doktora Tezi, İnşaat Mühendisliği
Danışman: Prof. Dr. Esra METE GÜNEYİSİ
Eylül 2020
163 Sayfa

Bu çalışma bir dizi pasif koruyucu sistemlerle güçlendirilmiş binaların elastik ötesi tepkilerini ele almaktadır. Enerji sönümleyici olarak sürtünme sönümleyici (SS), taban izalatörü olarak kurşun çekirdekli kauçuk mesnet (KÇKM), sürtünme sarkaçlı mesnet (SSM) ve yüksek sönümlü kauçuk mesnet (YSKM) çalışılmıştır. 2 tip çelik bina kullanılmıştır. İlki üç adet 5 katlı, iki adet 10 katlı, ikincisi ise 3, 6 ve 9 katlı moment aktaran çelik çerçeveleri kapsamaktadır. Binalardaki farklı sismik koruyucu sistemlerin uygulamalarını ve etkinliğini araştırmak için 4 durum belirlenmiştir. İlk durumda, tasarım özellikleri dikkate alınarak SS ve KÇKM'nin kullanımı incelenmiştir. İkinci ve üçüncü durumda, sırasıyla, SSM ve YSKM'nin tasarım parametrelerinin etkileri (izolasyon peryodu T, efektif sönüm oranı ß, akma dayanım oranı Fy/W ve akma sonrası sertlik oranı λ) incelenmiştir. Son olarak dördüncü durumda, tüm koruyucu sistemlerin performansı enerji sönümleyici olarak SS, taban izalatörleri olarak KÇKM, SSM ve YSKM'nin tek ve birlikte kullanımlarıyla karşılaştırılmıştır. Yapısal koruyucu sistemlerin tasarımında izolatörlerin en elverişli izolasyon parametreleri ve sönümleyicinin kayma kuvveti kullanılmıştır. Sonlu eleman programıyla modellenip deprem kayıtları kullanılarak zaman tanım alanında doğrusal olmayan analizlerle değerlenidirlmiştir. Sonuçlar mühendislik istem parametreleri cinsinden tartışılmıştır. Tekli koruyucu sistemin tam düzey performans seviyesini her zaman sağlayamadığı, ancak kombine sistemlerin etkin bir şekilde incelenen yapılar için sağladığı görülmüştür.

Anahtar Kelimeler: Sürtünme Sönümleyici, Taban İzalatörü, Sürtünme Sarkaçlı Mesnet, Yüksek Sönümlü Kauçuk Mesnet, Kurşun Çekirdekli Kauçuk Mesnet, Sismik Koruma.

''Dedicated to my family''

ACKNOWLEDGEMENTS

I would like to express my sincere gratitude to my supervisor Associate Prof. Dr. Esra METE GÜNEYİSİ for her invaluable guidance, advices, and supervision.

My special thanks are reserved for my parents, all my family and my wife Tuğba DERİNGÖL They have given me an endless enthusiasm and encouragement.

I owe special thanks to the exam committee members, Prof. Dr. Mustafa GÜNAL, Prof. Dr. Ali Fırat ÇABALAR, Assoc. Prof. Dr. Kasım MERMERDAŞ, and Asst. Prof. Dr. Süleyman İPEK for their encouragement, advices, and valuable guidances.

My sincere appreciation also extends to my wife who were directly or indirectly involved in the process of producing this research report, for their generous assistance.

Without their support and contribution, this thesis would not have been completed.

Finally, I would like to thank to those who took part in completion of this thesis.

TABLE OF CONTENTS

Page

LIST OF TABLES

Page

LIST OF FIGURES

LIST OF SYMBOLS

3D	Three dimensional model
B	Damping reduction factor
B_D	Damping coefficient
BIS	Base isolation system
c	Coefficient of dashpot
C_{VD}	Seismic coefficient
D	Displacement
d_r	Diameter of rubber
d_l	Diameter of lead core
D_y	Yield displacement
EPRRC	Elasto-plastic response reduction curves
FB	Fixed-base frame
FD	Friction damper
FO	Fully Operational
Fy	Yielding strength
Fy/W	Yield strength ratio
g	Gravitational acceleration
HDRB	High damping rubber bearing
IMF	Intermediate moment frame
IM	Intensity measure
KÇKM	Kurşun çekirdekli kauçuk mesnet
k_1	Iinitial stiffness
k_2	Post-yield stiffness
k_{eff}	Effective stiffness
LRB	Lead rubber bearing
LS	Lifes safety
m	Mass
MD	Metallic dampers
M_w	Moment magnitude
OMF	Ordinary moment frame
OP	Operational

PEER	Pacific Earthquake Engineering Research Centre
PGA	Peak ground acceleration
PGD	Peak ground displacement
PGV	Peak ground velocity
PPS	Passive protective systems
Q	Characteristic strength
R	Radius of curvature of the dish.
R_m	Response modification factors
RC	Reinforced concrete
R_{jb}	Surface projection distance
R_{rup}	Rupture distance
SPS	Seismic protective systems
SMF	Special moment frame
SMRF	Steel moment resisting frame
SP1	Fully operational
SP2	Operatinal
SP3	Lifes safety
SP4	Near collapse
SS	Sürtünme sönümleyici
SSM	Sürtünme sarkaçlı mesnet
ß	Effective damping ratio
T	Isolation period
T_D	Target period
TMD	The tuned mass dampers
UDR	uniform damping ratio
VD	Viscous dampers
VE	Viscoelastic dampers
V_{s30}	Mean shear velocity over the top 30 m
W	Total of the load
W_D	Area of the hysteresis loop
YSKM	Yüksek sönümlü kauçuk mesnet
λ	Post-yield stiffness ratio
μ	Friction coefficient

CHAPTER 1

INTRODUCTION

1.1 General

Civil engineering structures are designed to withstand the external forces induced by tsunamis windstorm, hurricane, and earthquakes. It is an indisputable fact that the earthquake can be accepted as the most devastating disaster because it causes many injuries, fatalities, and severe damage to the public buildings and bridges [1]. For instance, on August 17, 1999, more than 17,000 people died, 44,000 people injured, 30,000 buildings collapsed or were heavily damaged, 20 billion US dollars lost because of Düzce earthquake with a magnitude of 7.4 struck the Northwestern of Turkey [2] where the probability of a 7.4 magnitude earthquake is nearly 70 % over the next 30 years [3]. Therefore, the aged buildings having poor strength capacity should be retrofitted to minimize the casualties. However, beyond the traditional retrofitting concept that is depend on increasing the stiffness and strength of the structure, there is special requirement for the critical structures such as medical centers, power supply stations, and transportation buildings. They have to preserve functionality and also remain fully operational even during and just after earthquakes that can be only provided through utilization of the seismic protective systems (SPS) [4]. The first attempt on SPS dates back to 1970s in earthquake prone regions such as New Zealand, China, Japan and USA [5]. SPS can be categorized into four major groups: passive, active, semi-active, and hybrid systems. The base isolation system (BIS) and dampers are considered as passive devices that are very popular among the engineers and researchers because they neither need to supplemental energy, nor require maintenance during the operation, even mitigate the dynamic forces exerted to buildings whose seismic performance improved as well [6].

There are many types of dampers (e.g., viscous, viscoelastic, metallic, and friction) utilized to dissipate the hysteretic energy exerted by the dynamic loadings [7].

Among those dampers, friction damper (FD) can be acknowledged as the one of the most favourable dampers due to its enormous energy absorption capability, satisfactory lateral robust strength, relatively low cost (namely, manufacturing, implementation, and operation), long service life, independent to velocity and temperature, not include fluidity and corrosive surface, exist a wide range of design models such as X-type, diagonal and chevron braces [8]. Likewise, the configuration and implementation process of FD do not alter the architectural perspective of the buildings [9]. The mechanism of FD depends on the movement of frictional interface between two solid bodies which act opposite direction thereby dissipates the developed seismic energy [10]. The friction-based devices firstly inspired from automobile braking system was developed to design seismically isolated structures, however first attempt on FD was originally recognized by Pall and Marsh [11]. In addition to the dampers, BIS also has been successfully adapted both for poorly constructed structures and newly designed buildings in earthquake-prone regions. After 1994 Northridge and 1995 Kobe earthquakes BIS made use of many buildings in US and Japan, and also extended to developing countries as well [12]. For instance, 2020 Elazig earthquake Mw-6.8 hit the Northwestern of Turkey and caused to die more than 40 people, injure 1,600 people, damage 1,700 buildings, but the newly built base-isolated Elazıg City Hospital has continued to serve during and after earthquake without any damage to nonstructural element as well [13]. Eventually, the ongoing implementation on SPS encouraged the preparation of the seismic codes and standards like ASCE [14], Eurocode [15], TSCB [16] stimulating new provision for the design of buildings with BIS. The notion of the BIS can be summarized as follows: the structure decoupled from the ground level, BIS are placed between upper part of the footing and underneath of the columns to protect from destructive effect of the lateral forces [17]. BIS have enormous vertical stiffness to bear the service loads, but sufficient horizontal rigidity is respectively required for the translation of the isolated buildings during excitation. The low horizontal stiffness easily enhances lateral movement capacity for the isolated building whose fundamental period is lengthened and moved away from the predominant mode of the seismic excitation [18]. Two different BIS are introduced as elastomeric and sliding bearings. The former dissipate the seismic energy by inelastic deformations of the vulcanized materials, on the other hand the latter use up the imparting seismic force through friction-based mechanism generated curvedly surface of friction pendulum bearing (FPB). High damping rubber bearing (HDRB) and lead rubber bearing (LRB) can be admitted as representative of the elastomeric bearings. In the years following, several analytical models of BIS have been proposed and also some of those implemented in the civil structures.

1.2 Research Significance

The main aim of this thesis is to evaluate the seismic performance of the buildings with a series of passive protective systems consisted of an energy dissipation device of friction damper (FD) and base isolation systems of lead rubber bearing (LRB), friction pendulum bearing (FPB), and high damping rubber bearing (HDRB). In the design of the structural protective systems, the key design parameters and slip load were regarded for the base isolators and FD, respectively. Two types of steel buildings were considered as fixed-base (FB) frame. The first one consisted of three 5 storey steel frames (i.e., ordinary moment frame OMF, intermediate moment frame IMF, special moment frame SMF) and two 10 storey steel frames (i.e., IMF and SMF). The other buildings were 3, 6, and 9-storey steel moment resisting frames.

Four different cases were considered. In the first case, 5-storey buildings (i.e., OMF, IMF, SMF) and 10-storey buildings (i.e., IMF, SMF) were equipped with FD, LRB, and combination of those (i.e., FD+LRB) to examine the effectiveness of the dampers, base isolators, and combination of those together. The second case investigated the effectiveness of FPB. For this, 3, 6, and 9-storey frames equipped with FPB having various isolation characteristics such as T, ß, Fy/W. In the third case, HDRB characterized with the isolation parameters of T, ß, λ to upgrade 3, 6, and 9-storey frames with more favourable base isolators. The fourth case was aimed to develop seismically more efficient novel friction damped and isolated frames. For this, in order to see overall performance, the seismic response of 5-storey OMF was upgraded with FD as an energy dissipation device, LRB, FPB, HDRB as base isolators, and combination of those. FD is placed to mid bay over the height of FB frame considering the distribution of the slip load to each storey. In addition, each base isolator (i.e., LRB, FPB, and HDRB) characterized with distinctive mechanical behaviour and installed underneath of the column. The combination of the dampers with the base isolators together (i.e., FD+LRB, FD+FPB, and FD+HDRB) were used to enhance the seismic performance of FB. The overall case study frames were modelled using a finite element program, and evaluated by the nonlinear time history analyses through ground motion records. The obtained analysis results were elaborately discussed.

1.3 Outline of the Thesis

Chapter 1- Introduction: Objectives of the thesis were introduced.

Chapter 2- Literature review and Background: In this chapter a brief review of previous studies about seismic upgrading methods including friction damper and base isolation systems with lead rubber bearing, friction pendulum bearing, and high damping rubber bearing were given.

Chapter 3- Methodology: In this chapter, the analytical models of the case study frames with and without protective systems were introduced. Design methods, bearing characteristics, earthquake records were elaborately given.

Chapter 4- Results and Discussions: In this chapter, the results of the nonlinear time-history analyses were presented. The effect of single and combined use of friction dampers and base isolators for seismic upgrading of different frames were evaluated and the effectiveness of the seismic protective systems was discussed.

Chapter 5- Conclusions: The conclusions obtained from the results of the analyses were given.

CHAPTER 2

LITERATURE REVIEW AND BACKGROUND

2.1 Introduction

The traditional seismic retrofit technique is only interested in enhancing strength and ductility demand of the structural members. However, the passive protective systems (PPS) also develop extra stiffness for the buildings by inducing additional damping to the isolated structures [19]. PPS not only improved the seismic performance of the buildings convenient with the current seismic codes but also provided the serviceability during and after the earthquakes. Therefore, PPS have been favourably reached large audiences and implemented in many civil engineering structures, especially for critical buildings such as hospitals, terminals, nuclear plants etc. [20]. In this chapter, the notion and implementation of some PPS, namely, viscoelastic dampers, viscous dampers, metallic dampers and tuned dampers were superficially presented. In addition, the friction dampers and base isolation systems were elaborately explained.

2.2 Viscous Dampers

The principle of Viscous Damper (VD) depends on the movement of the viscous fluid material one chamber to the other when the external force acted to the device. The energy dissipation occurs by means of the pressure variation along the orifice. Figure 2.1 describes the cross-sectional view of VD whose main parts are a cylindrical orifice plate, a piston rod made of stainless steel, a control valve, and compressible fluidity viscous material, namely silicone oil [21]. The implementation of VD starts with suspension systems for automotive industry as a shock absorber, and then developed with the military missions and aircraft systems. VD have been utilized for the retrofitting of the structures or newly designed buildings since 1980s [22]. For instance, Güneyisi and Altay [23] constructed fragility curves to compare the nonlinear response of RC building with VD and different damping ratios (i.e., 10,

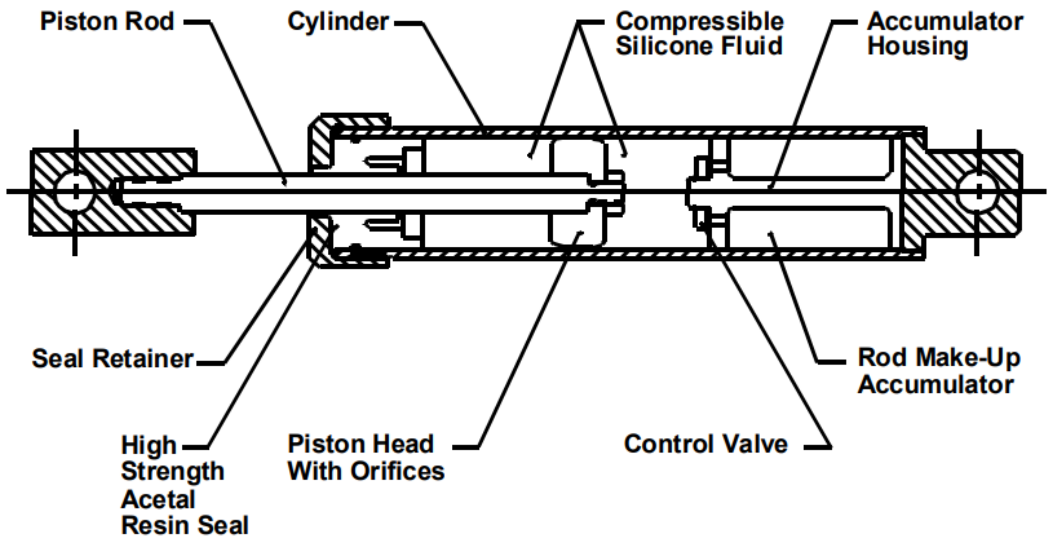

Figure 2.1 The cross-sectional view of Viscous Damper [21]

15, 20 %) were considered as the main subject. It was observed that the utilization of VD was significantly reduced the deformations as well as improved the fragility curves of the benchmark building especially for the greater damping ratio. Zhou et al. [24] studied the design of VD for an office building that was subjected to Wenchuan earthquake with a magnitude of 7.9, and heavily damaged. The amount of the dampers, design parameters of VD, and the configuration over the height of the building were considered. The utilization of VD decreased the shear force at ground floor from 21,270 to 14,220 kN under major earthquake scenario. Tabar [25] proposed a linearization method for nonlinear analysis of the case study frame with VD consisted of a series of damping exponents (i.e., 0.1, 0.2, and 0.5) using perturbation method. For this, 3-storey frame with VD was analyzed under Tabas earthquake as shown in Figure 2.2. The results showed that the proposed method was more reliable than the equivalent damping ratio of VD. Dicleli and Mehta [26] upgraded the seismic performance of chevron type steel braced 1, 2, 4, and 8-storey frame with VD. Not only the intensity and frequency of the earthquake records but also the damping ratio and exponent of the damper were regarded to evaluate the effectiveness of VD. It was observed that the interstorey drift ratio decreased in case of the damping ratio and velocity exponent increased. In addition, Landi et al. [27] examined the influence of the distribution methods of VD height of the buildings. 3, 6, and 9-storey reinforced concrete (RC) regular and irregular frames were evaluated using the nonlinear time-history analyses. They introduced various distribution methods. One of them was the efficient storeys method depend on the distribution of VD placed to the storey if only the shear strain energies higher than the average shear strain energy. The analysis results confirmed that efficient storeys method presented much more advantage than the other methods in terms of the damper force and residual interstorey drifts. Kim et al. [28] used the special truss members for designing the beam of 3 and 10-storey frame with and without VD. The effectiveness of the VD assessed by means of the fragility curves constructed using 44-earthquake records. The results showed that the probability of the limit state for 10-storey frame with VD was greater than 3-storey frame with VD. Sullivan and Lago [29] introduced a new design method based on the direct displacement seismic design for 9-storey RC with VD placed in the middle bay over the height of the building. The proposed method provided freedom to the designer choosing required isolation period, stiffness, and base shear for the isolated building with VD. Jamshidiha et al. [30] predicted the collapse capacity behaviour of 3, 6, and 9-storey frame with VD considering two sets of intensity measures (IM) presented three scalars IM and also contained the spectral shape and duration of the ground motion records. It was observed that the spectral shape IM was much more decisive for SMRF with VD.

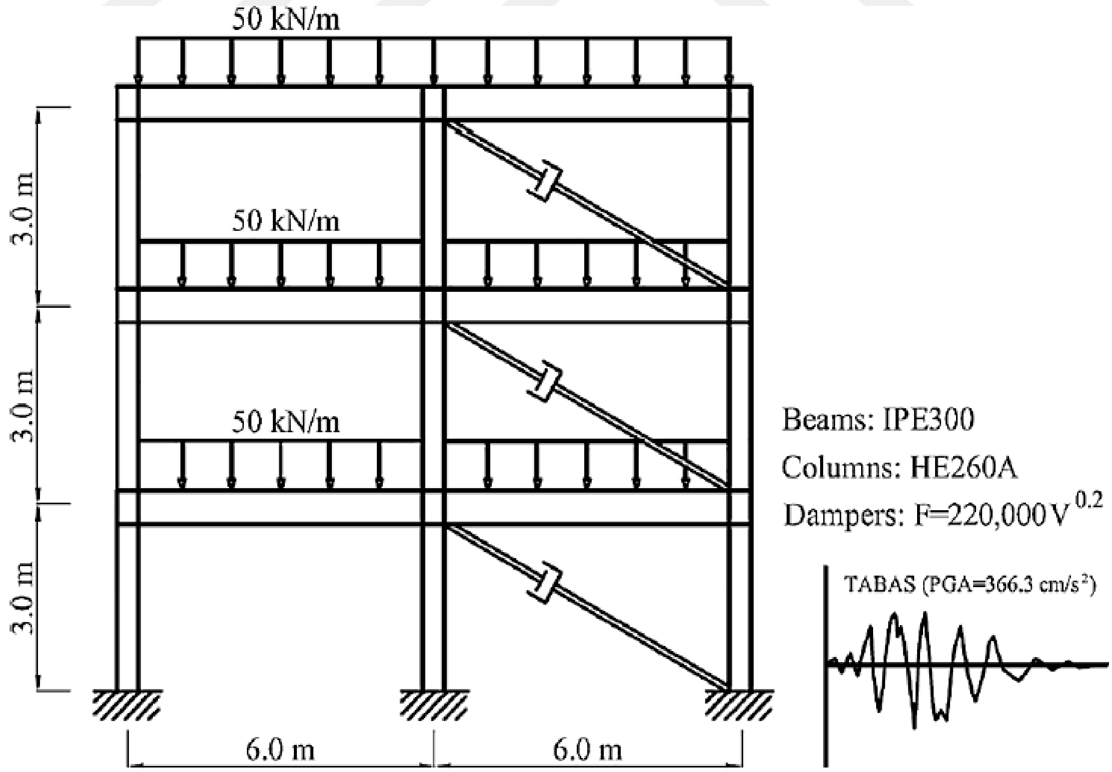

Figure 2.2 The elevation of the frame with VD [25]

2.3 Viscoelastic Dampers

Viscoelastic damper (VE) typically consists of alternating steel plate layers and located between viscoelastic pads as shown in Figure 2.3 [31].

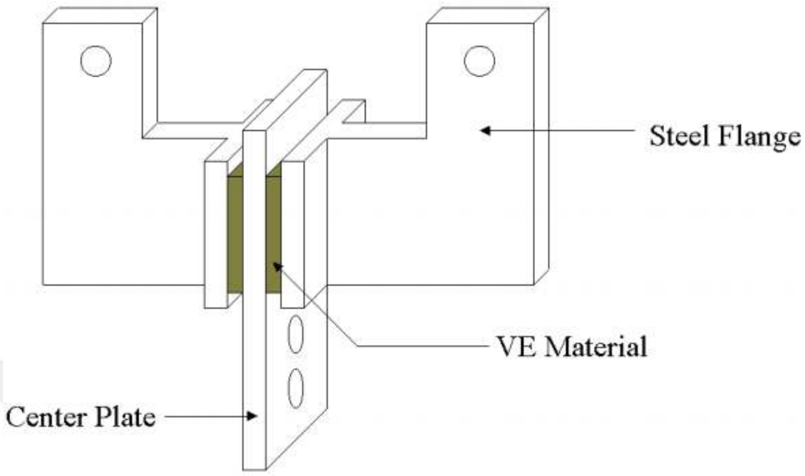

Figure 2.3 The schematic view of VE [31]

The energy dissipation occurs as the relative displacement of the steel layers induce shear strain in the elastic materials (e.g., acrylic copolymers) thereby the higher seismic energy converted into less much heat energy. The most popular examples of VE are World Trade Center in New York City and Two Union Square Building in Seattle that is developed to control the wind excitation high-rise buildings. Many researchers have been investigated the effect of the damping factor, the nonlinearity, configuration and implementation of VE over the few decades. For instance, Guo et al. [32] studied the seismic reliability of 10-storey RC frame with and without VE. The maximum interstorey drift, storey weight, strorey stiffness, and damping ratio were taken into account as IM thereby the damage level of the damper was evaluated. It was observed that the installation of VE reduced the probability of failure. Kim and Bang [33] developed an effective strategy to distribute the VE for minimizing the torsional effect of the 5-storey frame under earthquakes. The nonlinear response of the model frame with VE was also evaluated by changing the modal damping ratio, eccentricity, and edge stiffness (e.g., rigid and flexible). The increase of the damper stiffness and the lower eccentricity improved the response of the model frame. Min et al. [34] performed an experimental study to validate the effectiveness of VE considering the damping ratio and size of the device by the modal strain energy method. For this, VE placed only first and second level of 5-

storey case study frame and subjected to sinusoidal waves. The test results showed that the response of the model was changed with the vibration frequency and temperature. Zhang et al. [35] considered the plastic behaviour of the model frame to determine the design variables of VE by the elasto-plastic response reduction curves (EPRRC). As a case study frame, 6-storey RC was adopted and equipped with VE and also characterized with EPRRC. When subjected to a series of ground motion records, it was observed that the interstorey drifts was effectively mitigated for the benchmark building with VE designed in the light of EPRRC, hence the proposed model can be admitted as more reliable and effective. Shu et al. [36] introduced a new VE that was capable of providing additional damping for SMRF against wind or earthquake motions. The seismic performance of the proposed VE was tested by experimental and analytical studies. It was shown that the endplate and bolted-demountable segment of the damper dissipated the induced energy. The latter can be immediately replaced by the new one in the end of the service life. The undesired strength degradation can be occurred when the stiffness suddenly changed over the height of the building. To overcome this deficiency in high-rise RC frame, Alam et al. [37] utilized the VE characterizing the damping ratios (2.5, 7, 11, and 14 %). The results showed that VE improved the overall responses, but beyond the level of 11 % the effectiveness of the damper was lost. Xie et al. [38] developed a straightforward method to design VE as a retrofit strategy depending on the uniform damping ratio (UDR) for 6-storey RC. It was shown that UDR based on the method of UDR was effectively diminished the storey shear force as shown in Figure 2.4.

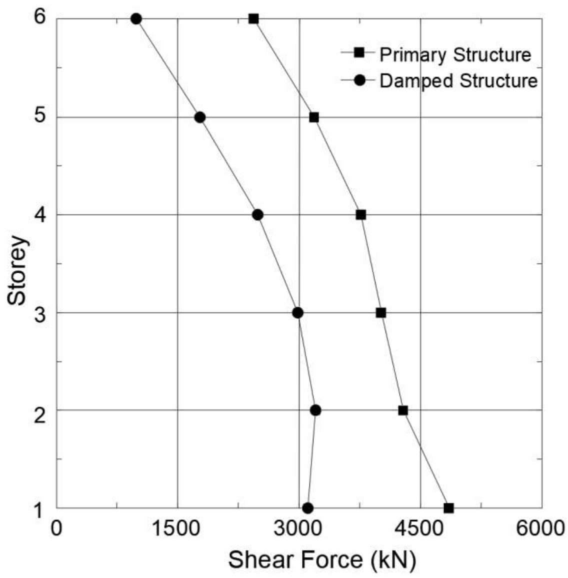

Figure 2.4 The variation of shear forces with and without VE [38]

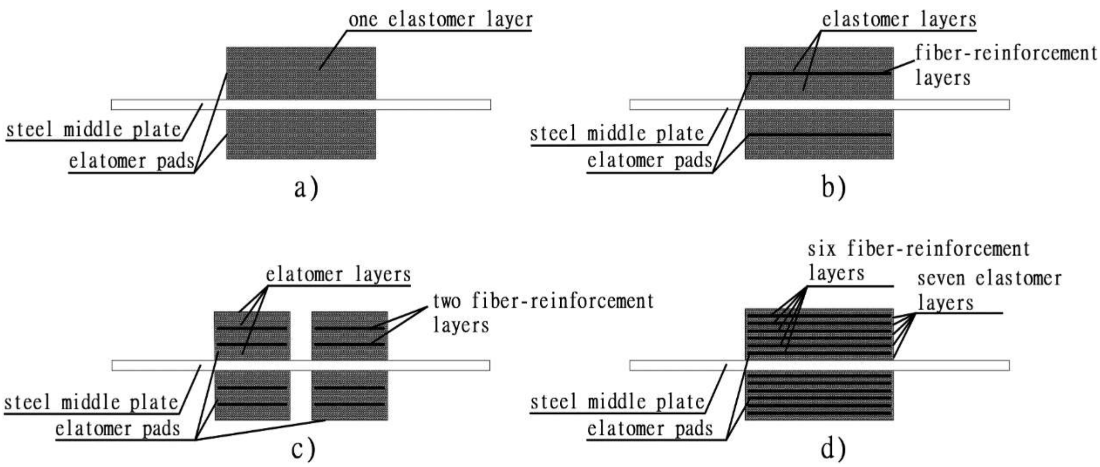

Figure 2.5 The elastomeric pads of VE [39]

Ghotb and Toopchi-Nezhad [39] fabricated four various VE whose characteristic of the elastomeric pads were differentiated as shown in Figure 2.5. They tested the specimens of VE by subjecting harmonic lateral displacement controller. The lowest and highest effective stiffness and loss factor were experienced for the type-A and D, respectively.

2.4 Tuned Mass Dampers

The tuned mass damper (TMD) has been used as a vibration control device for the civil engineering structures such as high-rise buildings and long span bridges subjected to moderate and major seismic excitations (i.e., winds and earthquakes) [40]. The mathematical model of the damped structure with TMD was presented in Figure 2.6 [41].

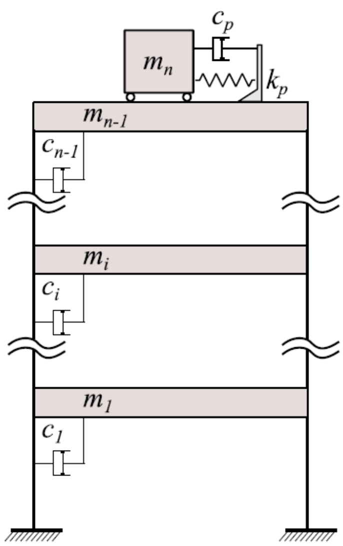

Figure 2.6 The mathematical model of damped structure with TMD [41]

TMD was linked with the main structure by means of the spring and dashpot. The m, c, and k represented the mass, coefficient, and stiffness matrices, respectively. Many researchers studied the utilization of TMD for controlling the seismic response of the structures. For instances, Pinkaew et al. [42] investigated the effectiveness of TMD on 20-storey RC frame under harmonic and ground motion. It was found that TMD significantly prevented the occurrence of the yielding up to a certain level of the peak ground acceleration (PGA) as shown in Figure 2.7. As PGA increased, TMD was capable of the reducing the damage level, otherwise the main structure was severely suffered.

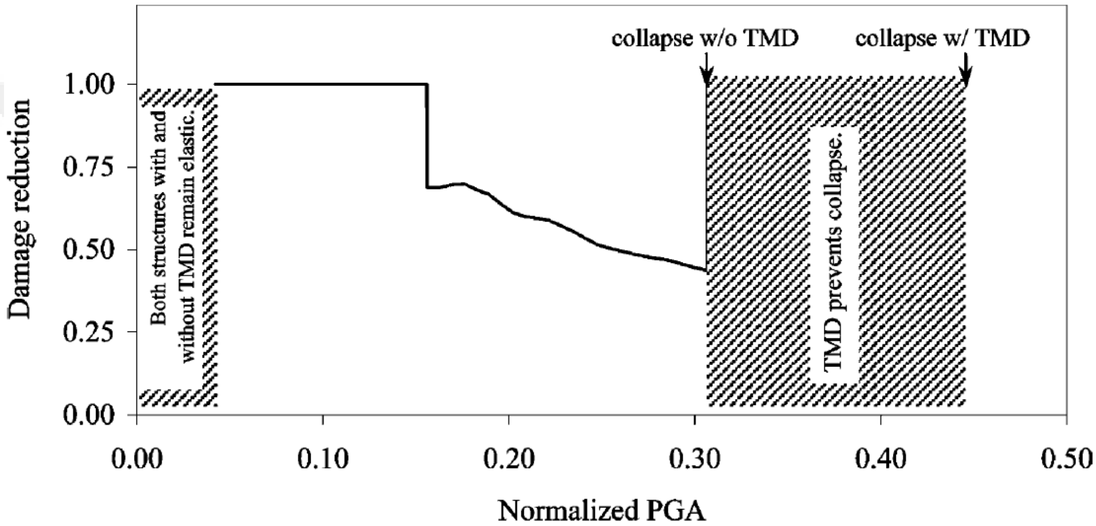

Figure 2.7 Damage reduction of the damped structure with TMD [42]

Taniguchi et al. [43] investigated the mitigation of the displacement demand of the base-isolated building with TMD characterized with various mass ratios (0.02, 0.05, and 0.10) and damping ratios (5, 10, 15, and 20 %) through near and far-field earthquakes. It was obtained that the TMD was favourable when its mass increased, the damping ratio was 10 %, and subjected to near-field earthquakes, Greco and Marano [44] examined the TMD in terms of the displacement reduction and energy dissipation which were used to optimize the response of the damper by Genetic Algorithm. The displacement reduction and energy dissipation correlated as a result of the optimization of TMD variables. Petrini et al. [45] proposed an optimum TMD for 74-storey steel frame building subjected to the wind excitation. The effectiveness of the TMD against wind forces was proved when enhanced the inertial properties or spanned more than one storey.

2.5 Metallic Dampers

Metallic damper (MD) dissipates the seismic energy by means of the hysteretic behaviour of the metals when encountered the inelastic range. MD are generally selected by the engineering community since they have inexpensive manufacturing and simple installation, maintenance procedure [46]. Therefore, many studies have been performed about MD. The implementation of MD in the structure can be observed in Figure 2.8.

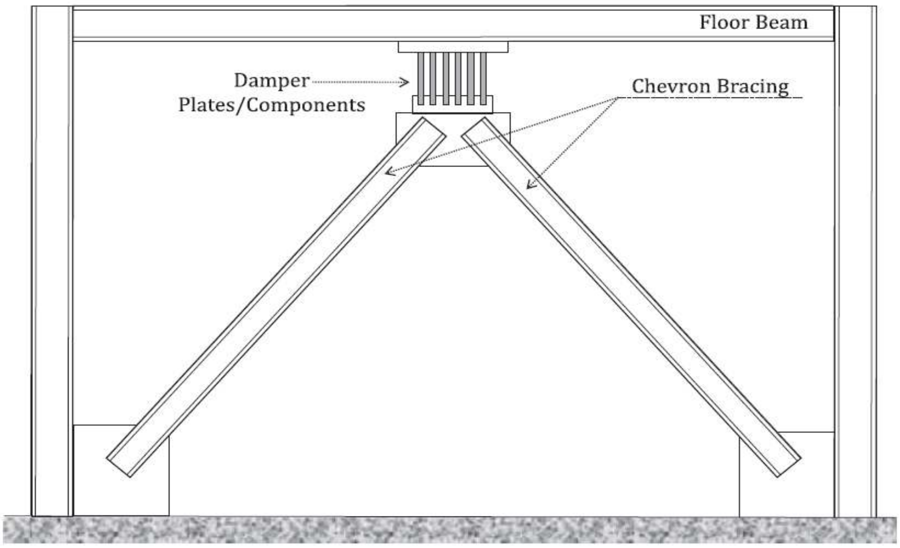

Figure 2.8 The implementation of MD in the structure [47]

The connectivity of the device was provided by the Chevron type bracing systems. Aliakbari et al. [47] proposed the energy-balance approach to predict the energy dissipation of 4, 6, 8, and 10-storey buildings with MD subjected to seven different artificial and twenty real ground motion records. The analysis results showed that the proposed method was valid for the structures with MD when their isolation periods were lower than 2 s. Sahoo et al. [48] experimentally tested the ductility, hysteretic behaviour, load carrying and energy dissipation capacity of MD. It was obtained that the equipment of thin plate in the web of MD improved the mechanical properties (i.e., stiffness, strength) of the damper. It was also valid when increased the size of the device. The addition of the flexural plate on the notched corners not only assisted the energy dissipation but also provide extra drift without any fractures. Li et al. [49] developed a new type of MD that was added a shear panel and K shaped plate. The former and latter were proposed to behave as shear and bending components under cyclic tests, respectively. Both properties enhanced the dissipated energy, and improved the hysteretic behaviour. They also provided excessive strength owing to strain-hardening depend on the yielding point of the steel.

2.6 Friction Dampers

Unlike from the other dampers, friction damper (FD) can be remarkably utilized to reduce the nonlinear response of the structures subjected to any external forces. FD has the advantage of remarkable energy dissipation capacity by means of their hysteretic behaviour. They are independent of temperature and velocity. In addition, they are economical and their design is simple since the maximum force in the FDs that remains constant is predefined in the design stage [50-52]. There are a wide range of design models such as diagonal and chevron, X-type, and Toggle type brace with FD as shown in Figure 2.9 [53].

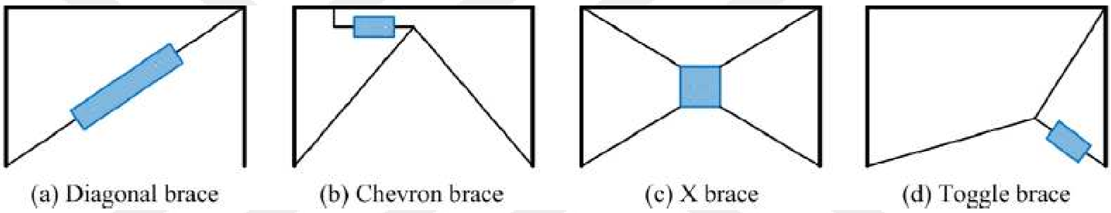

Figure 2.9 The typical configuration of FD [53]

When subjected to the major earthquakes, FD starts to slip at a predetermined yield force in which the structural members do not yield as the slippage in the device enables a mechanism for the dissipation of energy by means of frictional surface. After Pall and Marsh [54] firstly introduced FD, many analytical and experimental researches have already studied in this framework. The typical hysteretic curves and layout of FD described in Figure 2.10 [55].

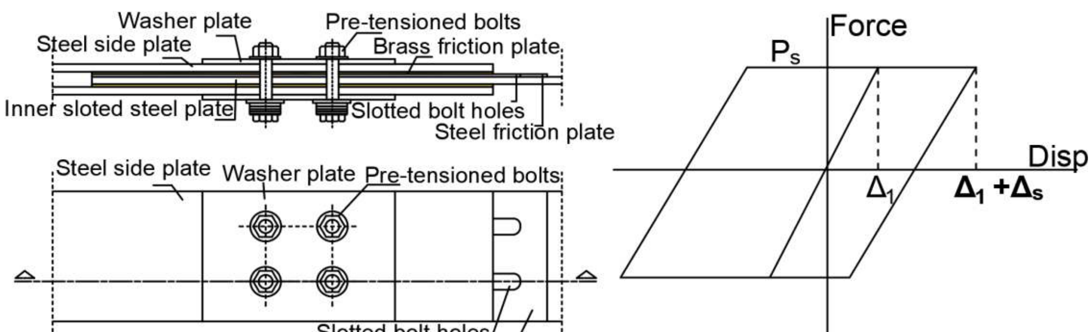

Figure 2.10 Typical configuration and hysteretic behaviour of FD [55]

Lee et al. [58] provided a new type FD in which the clamping piece improved by utilization of the low-steel material for the bolted connection in order to assure better frictional performance within higher friction coefficient and stability as shown in Figure 2.11.

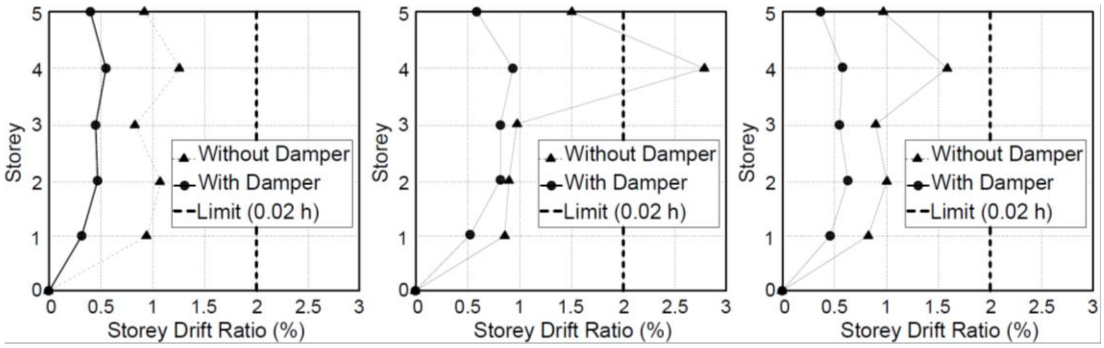

a) Imperial Valley (1940) b) Loma Prieta (1989) c) Northridge (1994)

Figure 2.11 The variation of interstorey drift ratio with and without FD [58]

Lu [59] investigated the efficiency of semi active system including variable FD whose clamping force also determined to reduce the floor displacement and acceleration as well. Armali et al. [60] studied the nonlinear response of four different FD installed to 40-storey RC building in earthquake-prone regions. When placed to optimum location with sufficient number, FD improved the seismic response compared to traditional building as shown in Figure 2.12.

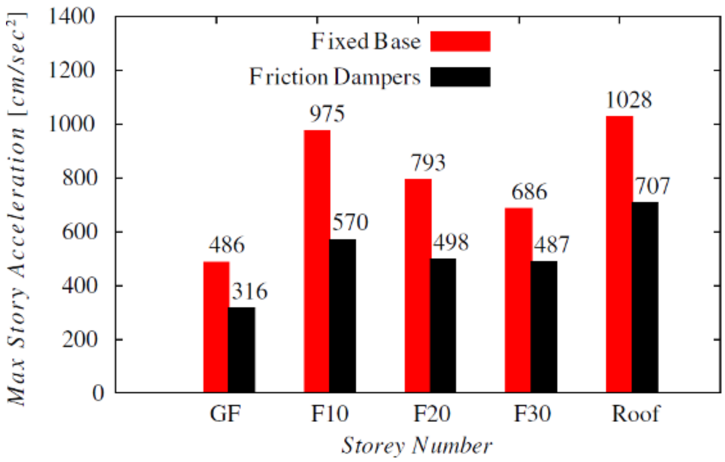

Figure 2.12 The variation of storey acceleration with and without FD [60]

Amjadian and Agrawal [61] developed electromagnetic FD and implemented to 6-storey seismically base-isolated building. The frictional force governed between non-magnetic pads and ferromagnetic plate inhibited the excessive displacement demand originated from BIS and also significantly regulated the interstorey drift. Santos et al.

[62] performed an analytical study in which the nonlinear response of FD performed by the quasi static and impact tests considering the influence of the stress-strain rates on the behaviour of the device. Quintana et al. [63] offered a semi active control system that was capable of adjusting the placement of FD, identifying the threshold of the slip load, enhancing the adaptability of the passive control device under various ground motions. Qu et al. [64] investigated the seismic performance of FD utilized in coupling beam at mid-span of the structure through the cyclic loading test. FD absorbed most of the shear deformations and forces in the coupling beam. Ontiveros-Pérez et al. [65] proposed a new algorithm method for increasing the reliability of FD by optimizing simultaneously both the yield force and the passive device placement. The proposed control device FD effectively diminished the storey displacement as shown in Figure 2.13.

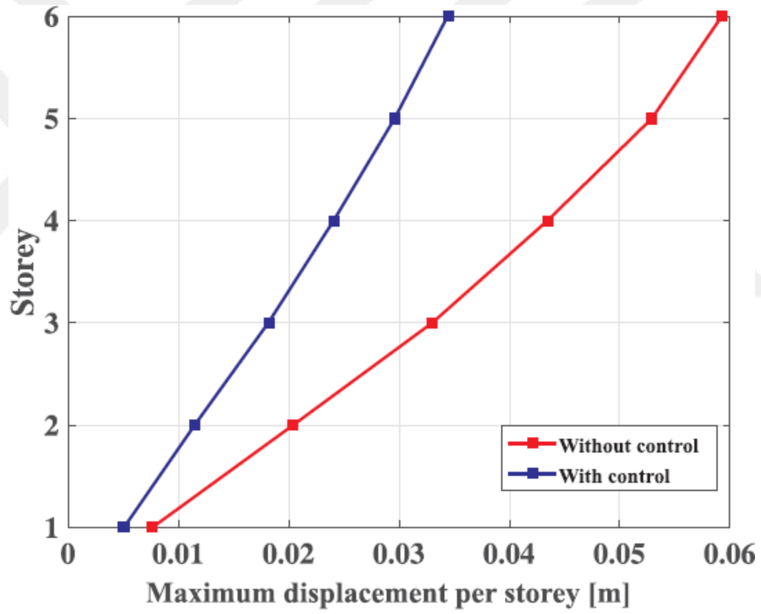

Figure 2.13 The variation of storey displacement with and without FD [65]

Dos Santos and Coelho [66] presented a friction-based semi-active dissipative device, attached to ground level of the structure, utilized to adjust the auxiliary mass system. The offered tunable FD faciliated 50 % mass mitigation and developed significant progress in the seismic protection. Piluso et al. [67] asserted a novel idea depends on the use of FD both end of the beams and connection of the chevron braces. When S_a = 1.2 g, it was observed that the maximum displacement of the beam-column connection equipped with FD never exceed 30 cm. Nabid et al. [68] developed an optimization method using uniform distribution of deformation (UDD) to decrease the computational work of the nonlinear analyses for 3, 5, and 10-storey buildings with FD under earthquakes. The supremacy of UDD was acquired when the iteration numbers, the sensitivity and speed of the optimization compared with genetic algorithm.

2.7 Base Isolation Systems

BIS can be admitted as mature passive seismic isolation technique that is developed against seismic and dynamic actions to resume the service lifespan of the civil engineering structures. For the last a few decades, BIS have been implemented not only new structures but also existing buildings in order to meet the current limit state of the seismic design codes [69]. It is well known that the utilization of BIS increases the fundamental period of the base-isolated structures since the isolator provides additional damping, which hereby enables to smoothly lateral movement, but this relative displacement partially centered on the region of bearing device [70]. BIS decoupled from the ground and placed a flexible layer between the superstructure and its foundation thereby eliminating the seismic energy that is transmitted from ground to the structure as shown in Figure 2.14 [71].

Figure 2.14 The implementation of BIS [71]

BIS have enormous vertical stiffness to bear the service loads, but sufficient horizontal rigidity is respectively required for the translation of the isolated buildings during excitation [72]. The low horizontal stiffness easily enhances lateral movement capacity for the isolated building whose fundamental period is lengthened and moved away from the predominant mode of the seismic excitation [73]. Two different BIS are introduced as elastomeric and sliding bearings. The former dissipate the seismic energy by inelastic deformations of the vulcanized materials, while the latter use up the imparting seismic force through friction-based mechanism generated curvedly surface of friction pendulum bearing (FPB). High damping rubber bearing (HDRB)

and lead rubber bearing (LRB) can be admitted as representative of the elastomeric bearings [74-75]. The typical layout and force-deformation relationship for considered isolators of LRB, FPB, and HDRB were presented in Figure 2.15(a-c) [76]. In the years following, several analytical models of BIS have been proposed and also some of those implemented in the civil structures. For instance, Zhang and Huo [76] constructed fragility curves to interrogate the effectiveness of three different BIS (e.g., FPB, LRB, and elastomeric bearing) and compared their isolator behaviours. The post yield stiffness ratio identified as the key design parameter.

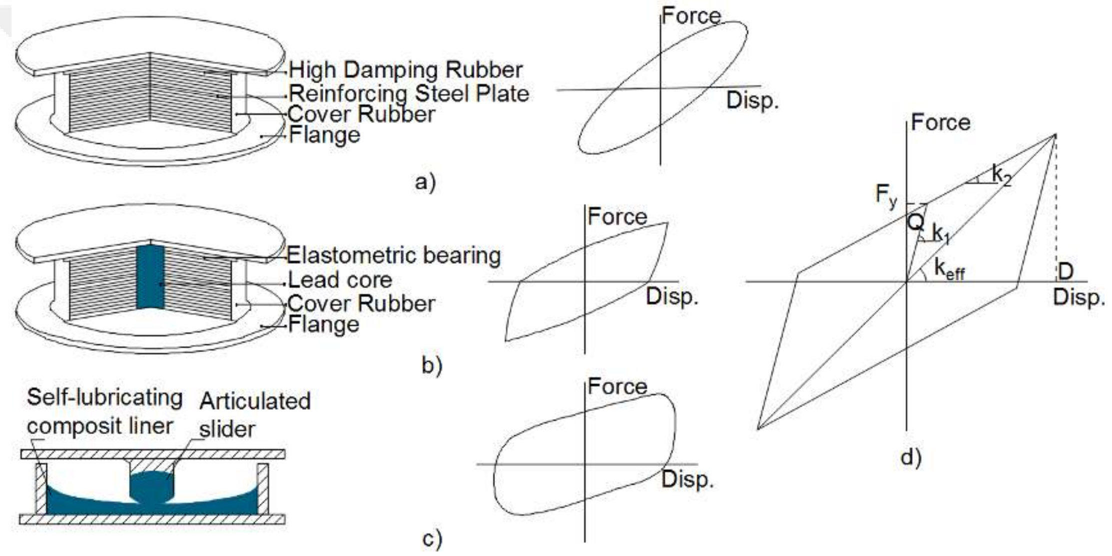

Figure 2.15 The configuration and hysteretic behaviour of LRB, FPB, and HDRB [76]

Jangid [77] evaluated the friction coefficient (μ) of FPB considering a set of variants (e.g., isolation period damping ratio, storey level, mass ratio). The greater μ effectively reduced the isolator displacement while the acceleration was enhanced as shown in Figure 2.16. In another study of Jangid [78], the optimal μ of FPB was determined in the range of 0.05 to 0.15 for multi-storey building subjected to six different near fault ground motions. Deringöl and Güneyisi [79] highlighted the characteristics of FPB (namely, isolation period T, effective damping ratio ß, yield strength ratio Fy/W) using nonlinear time-history analyses. The use of the greater T and ß with lower Fy/W produced the lowest interstorey-drifts as shown in Figure 2.17. Xu et al. [80] studied two different seismic upgrading plans designed both for aboveground and underground buildings equipped with FPB under beneath of the structure and on top of the column. The latter substantially reduced the shear force,

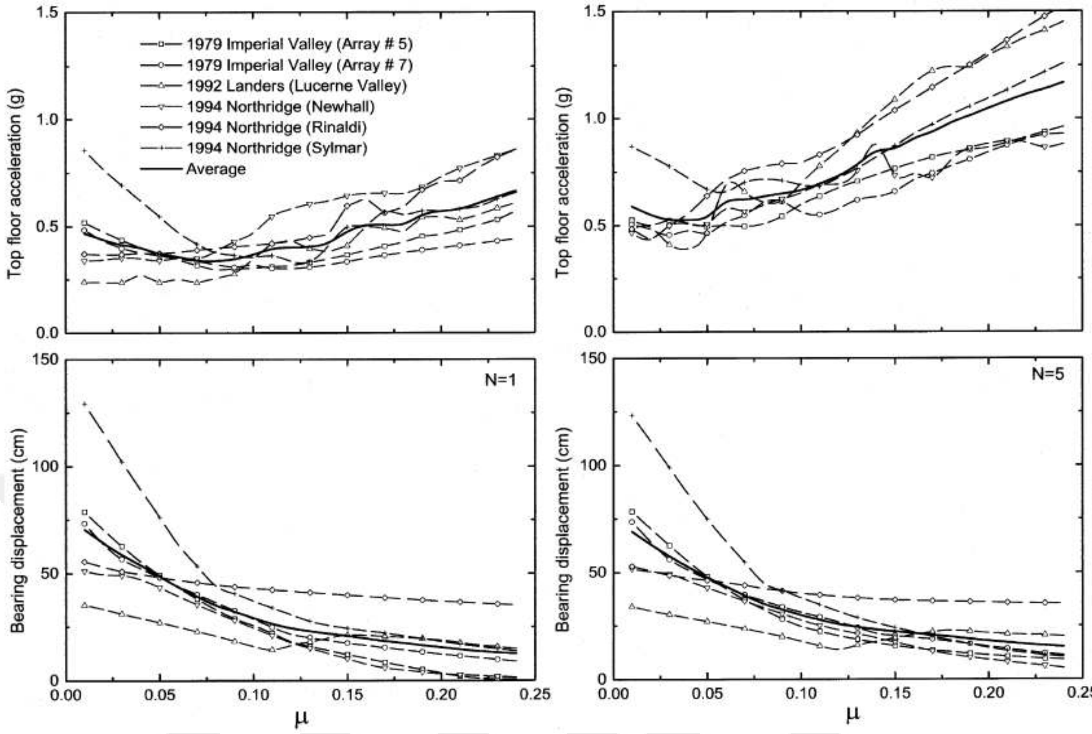

Figure 2.16 The variation of the bearing displacement and top floor acceleration of the base-isolated frames with FPB against friction coefficient under earthquakes [77]

bending moment and displacement. In the study of Ren et al. [81], shake table test was set up and also developed analytical model for specimen of the large space truss structure scaled down (as 1/25) and isolated with FPB. When compared the nonlinear response of the specimen and model, the maximum shear forces and average displacements error were below 16 and 24 %, respectively.

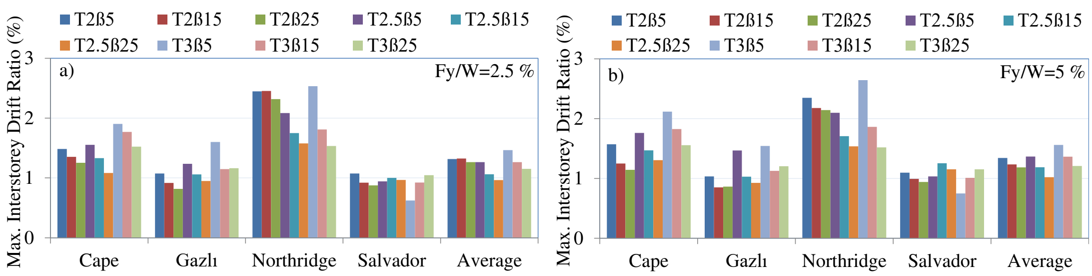

Figure 2.17 The variation of the maximum interstorey drift ratio of the 6-storey base-isolated frames with FPB under earthquakes [79]

Bao and Becker [82] studied 3D numerical modelling of FPB. The proposed model was confirmed by quasi-static and dynamic analysis considering uplift and impact effect of FPB. Calhoun and Harvey [83] investigated the 3D printing simplified the analytical modelling, implementation, and numerical expression of FPB exploring more comprehend the sliding mechanism, incorporating the isolator dimension, considering the supplemental damping. Thus, it enabled to design and test state of the art of the bearings as shown in Figure 2.18.

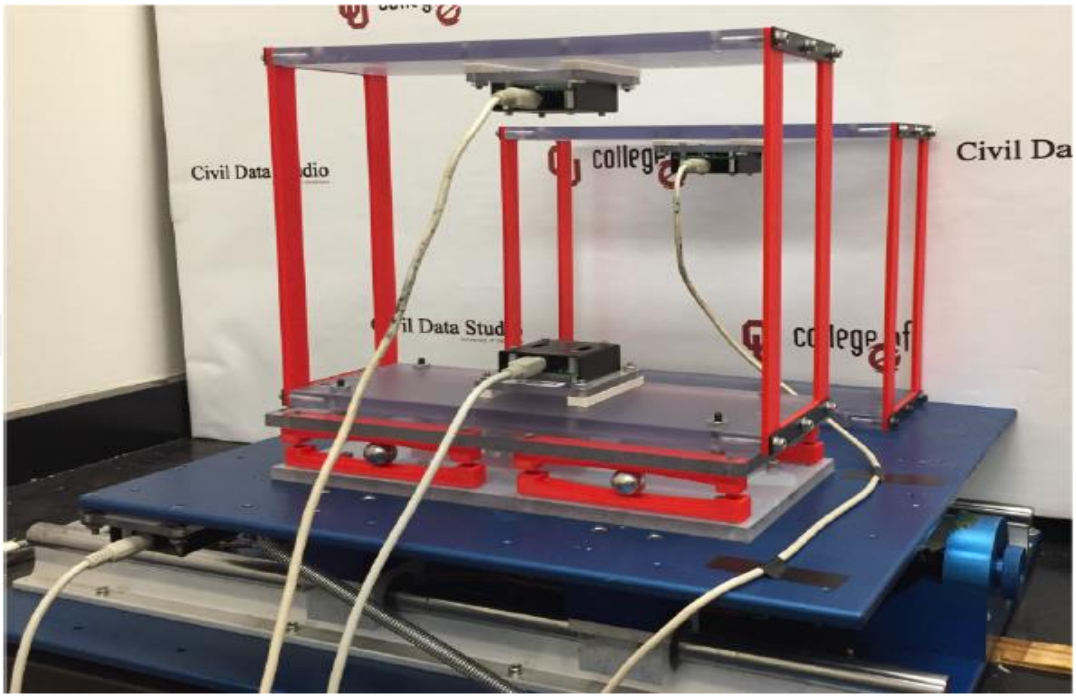

Figure 2.18 The test of the base-isolated frame with FPB [83]

Castaldo and Alfano [84] carried out an extensive sensitivity analyses using equivalent effective period, the mass ratio, the behaviour factor, hardening stiffness ratio, post-yield slope for constructing fragility curves of single and double FPB. The latter can be favourable if less behaviour factor used for the design of the structures. Shau et al. [85] studied on the augmenting the performance of FPB included following three provisions; isolators with predefined strain, isolators with physical barrier, isolators equipped with self-stopping mechanism. The isolator displacements should be enhanced to meet the limits of ASCE 7–16 [86]. The key role of FPB was identified as the energy dissipation and re-centering ability in the study of Domenico et al. [87]. The lower friction coefficient and additional damping device (i.e., gap damper) used in the design of FPB to overcome the negative effect of the re-centering and excessive displacement demand of the isolators, respectively. Bao et al. [88] studied on the collapse analyses of 3-storey moment and braced fames using

FPB with various restrainers (i.e., rigid and flat rims). The latter acquired better prediction for the bearing failure as shown in Figure 2.19.

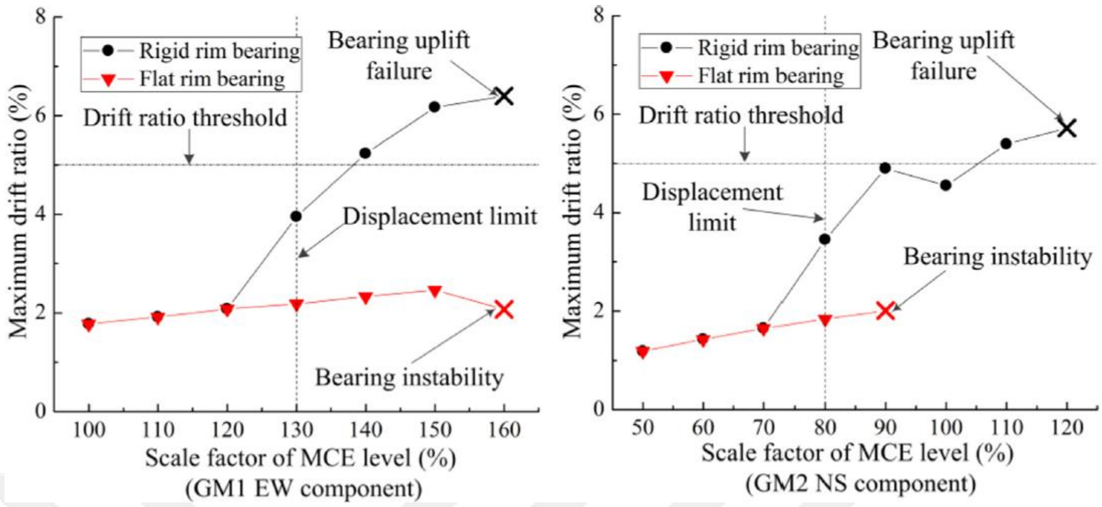

Figure 2.19 The maximum drift ratio of the base-isolated frame with FPB for the rigid and flat rims under earthquakes [88]

Habieb et al. [89] investigated the effective BIS retrofitting techniques, for this valuable masonry tower isolated with FPB, LRB, and HDRB under moderate and high seismic earthquakes. LRB and FPB exhibited better seismic performance than HDRB in terms of drift reduction and roof displacement. Castaldo et al. [90] examined the effect of the isolator characteristics (e.g., radius of curvature, isolation period) on the life-cycle costs of 4-storey RC with FPB. The lower life-cycle cost obtained in case of the higher values was valid. Calabrese et al. [91] utilized the recycled rubber material to design as safe as traditional BIS (i.e., LRB and FPB) for cheap residential building in the developing countries.The interstorey drift reduction of the proposed BIS, LRB, and FPB were determined as 83, 90, and 84 %, respectively. Alhan and Sahin [92] performed a series of nonlinear analyses to query the isolator characteristics of LRB on the nonlinear response of 3, 6, and 10-storey buildings. The results showed that the supplemental damping ranged between 4-8 % effectively reduced the storey accelerations. Moslemi and Kianoush [93] investigated the seismic response of the liquid filled elevated tanks considering the interactivity between fluid and structure. The tank geometry, location of the bearing, and shaft strength considered as key parameters. The higher shaft stiffness and slender tank produced more favourable LRB. Alhan and Oncu-Davas [94] studied the seismic performance thresholds of 5-storey building with LRB for various isolation characteristics under near-field earthquakes contained at different fault distances and velocity pulse. Mansouri et al. [95] plotted fragility curves for the isolation periods (i.e., 2.5, 4, 5.5 s) and damping ratios (i.e., 26, 52, 71 %) of 3 and 9-storey with LRB using nonlinear analyses. Enhancing of the isolator period decreased the failure probability as shown in Figure 2.20. The maximum acceleration ranged from 0.05 to 0.1 g (namely slight damage) was observed for fire damaged building with LRB.

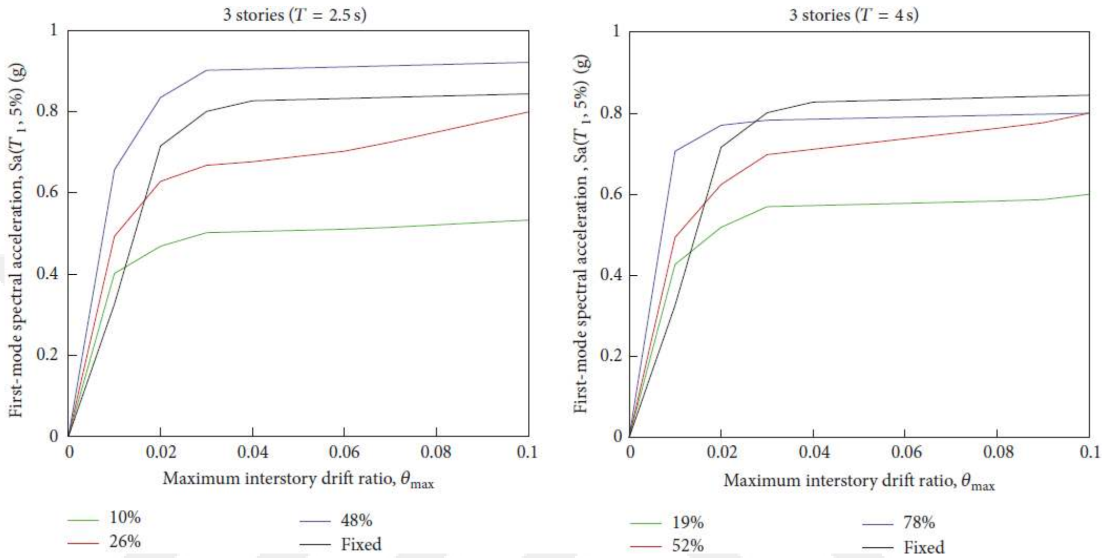

Figure 2.20 The incremental dynamic analysis curves for 3-storey frame with LRB against isolation period [95]

Kim et al. [98] tested two various specimens of LRB under seismic loading cases in which different shape factors governed to eliminate the buckling effect for nuclear power plant. The shear failures were experienced when the shear strain reached to nearly 500 % as shown in Figure 2.21.

Figure 2.21 The views of the typical shear failures of LRB [98]

Ahmadipour and Alam [99] performed a sensitivity analysis on the mechanical properties of LRB including geometry of the lead and rubber. The radious of the lead plug significantly influenced the strength of the bearing and energy dissipation capability as well. Kumar and Whittaker [100] proposed an advanced link element of LRB contributing the deficiency of existing finite element programs such as buckling, cavitation, and heating. In the study of Markou et al. [101], traditional RC buildings were retrofitted using HDRB and friction based sliders. The stochastic response was evaluated using Monte Carlo (MC) simulation to examine the effectiveness of the isolation parameter variation on the seismic response of BIS. Dao et al. [102] presented a study depend on the statistical evaluation for determining the most significant parameter effecting the results of the nonlinear analysis (i.e., maximum displacement) of the isolated frame with HDRB. The post-yield stiffness ratio and characteristic of the ground motion were observed as the strongest parameter for predicting the reliability grades. Wei et al. [103] analyzed the effect of the compression loading on rate-dependent HDRB through monotonic and shear tests, for this three stress and strain levels regarded. It was observed that the slower strain rates clearly caused the more shear stress with different stress levels. Cancellara and Angelis [104] carried out response spectrum and nonlinear dynamic analysis for irregular multi-storey RC, in which HDRB was adopted as BIS. The results of the latter were much more conservative than the former in terms of bending moments at supports. Mazza and Vulcano [105] investigated the emphasis of both components of near-fault earthquakes on the nonlinear response of HDRB with reference to different isolator stiffness ratio ranged between 200 and 2000.

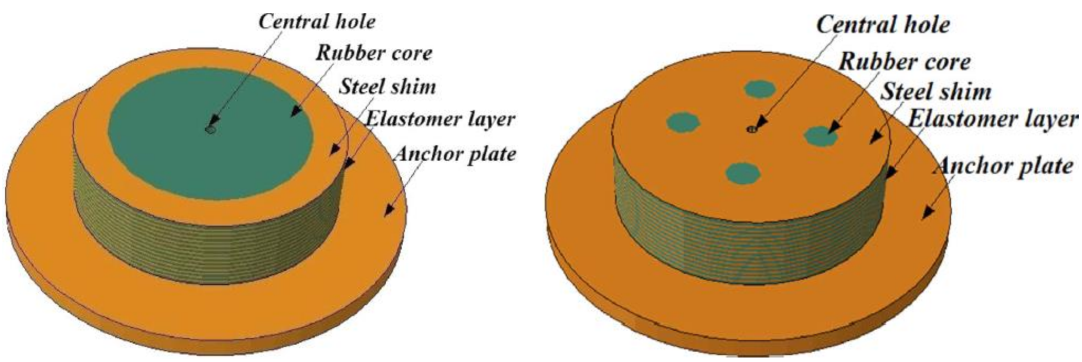

a) b)

Figure 2.22 The view of HDRB with single and multiple rubber cores [107]

The greater values of those increased the ductility demand of the structure. Clemente et al. [106] examined the mechanical behaviour of HDRB varying the shear strain from 5 to 200 % through less intensity ground motions. Actually, the less shear strain enhanced the isolator stiffness. Rahnavard and Thomas [107] studied the nonlinear response of the rubber isolators considering the effect of the type of loadings, magnitude and direction of the exposed loads. It was shown that the stiffness of the bearing enhanced when the rubber isolator subjected to tensile axial load and multiple circular-scattered rubber cores surpassed the only one central rubber core as shown in Figure 2.22. Zuniga-Cuevas and Teran-Gilmore [108] investigated the dynamic response of 2, 4, and 8-storey base-isolated systems subjected to a set including 22 severe earthquakes whose database obtained from firm soils. It was assumed that the isolators are capable of exhibiting different damping levels, period ratio, and mass ratio. When the effective damping ratio increased, the velocity and accelerations significantly decreased especially for moderate period as shown in Figure 2.23.

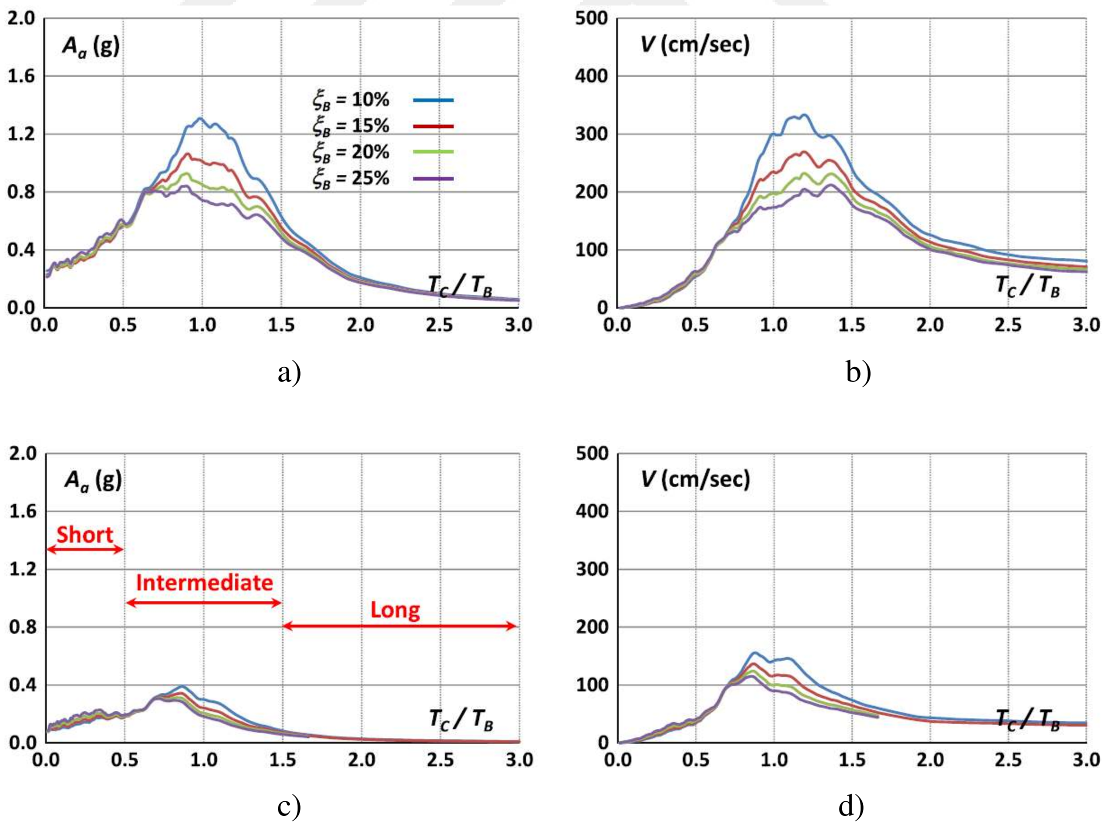

Figure 2.23 The mean acceleration and velocity variation of the roof storey for base-isolated frame with LRB: a and b) TB/TS = 10.00, TB = 1.50 s, TS = 0.15 s, c and d) TB/TS = 20.00, TB = 3.00 s, TS = 0.15 [108]

CHAPTER 3

METHODOLOGY

3.1. Introduction

In this study, the nonlinear seismic response of the buildings retrofitted with a series of passive protective systems was investigated. For this, friction damper (FD) as an energy dissipation device and lead rubber bearing (LRB), friction pendulum bearing (FPB), and high damping rubber bearing (HDRB) as base isolation devices were taken into account. Four different cases were introduced to evaluate the effectiveness the seismic protective systems of FD, LRB, FPB, HDRB and combination of those on the buildings. In the first case, 5 and 10-storey steel frames were introduced with FD, LRB and the combination of FD with LRB. In the second case, the other benchmark buildings of 3, 6, and 9-storey steel frames were equipped with FPB having different design characteristics. In the third case, 3, 6, and 9-storey steel frames were equipped with HDRB considering various isolation parameters. Finally, in the fourth case, for comparison purposes, all seismic protective systems were utilized for retrofitting 5-storey steel frame. The case study frames were modelled using a finite element program, and then they were evaluated through the nonlinear time-history analyses under seven ground motion records. The details of the investigation are given below.

3.2 Case-1 (FD, LRB, and FD with LRB)

The effectiveness of FD, LRB, and combination of those on the buildings were evaluated. For this, three 5-storey steel moment resisting frames (MRFs) as ordinary moment frame (OMF), intermediate moment frame (IMF) and special moment frame (SMF), and two 10-storey MRFs as IMF and SMF were utilized. Firstly, as energy dissipation device, FDs were applied at the middle bay of the frame through the height of the framed structures. Then, as seismic isolation system, LRB were applied. Finally, both structural protective systems, FDs and LRB isolation systems were applied to the case study MRFs together. The nonlinear time history analyses were performed on two-dimensional models of bare and upgraded MRFs using seven ground motion records.

3.2.1 Designing and Modelling of the Case Study Frames

The steel moment resisting frames (SMRF) can be admitted as one of the most favourable gravity load carrying system. The high ductility behaviour of SMRF roots in the capable of restricting the lateral deformations by means of the flexibility of the structural members [109]. In this investigation, as the first case study frames, 5-storey special moment frame (SMF), intermediate moment frame (IMF), and ordinary moment frame (OMF) and 10-storey SMF and IMF were utilized, and originially designed by Asgarian et al. [110] according to Iranian Seismic Code 2800 [111] which is similar to AISC [112] and FEMA 350 [113]. Elevation views of 5 and 10-storey fixed base frames are given in Figure 3.1. All the storeys have the same width of 5 m. The beams and columns are IPE and square TUBE sections, respectively, varied over the frame height as shown in Figure 3.1. The values of response modification factors (R_m) considered in the design of the OMF, IMF and SMF were 5, 7, and 10, respectively. Moreover, inelastic rotation capacities of OMF, IMF and SMF were specified 0.01, 0.02 and 0.03, respectively. The fundamental periods of vibration of 5-storey SMF, IMF and OMF were obtained as 0.82 s, 0.77 s and 0.72 s, respectively and for 10-storey SMF and IMF as 1.55 s and 1.44 s, respectively.

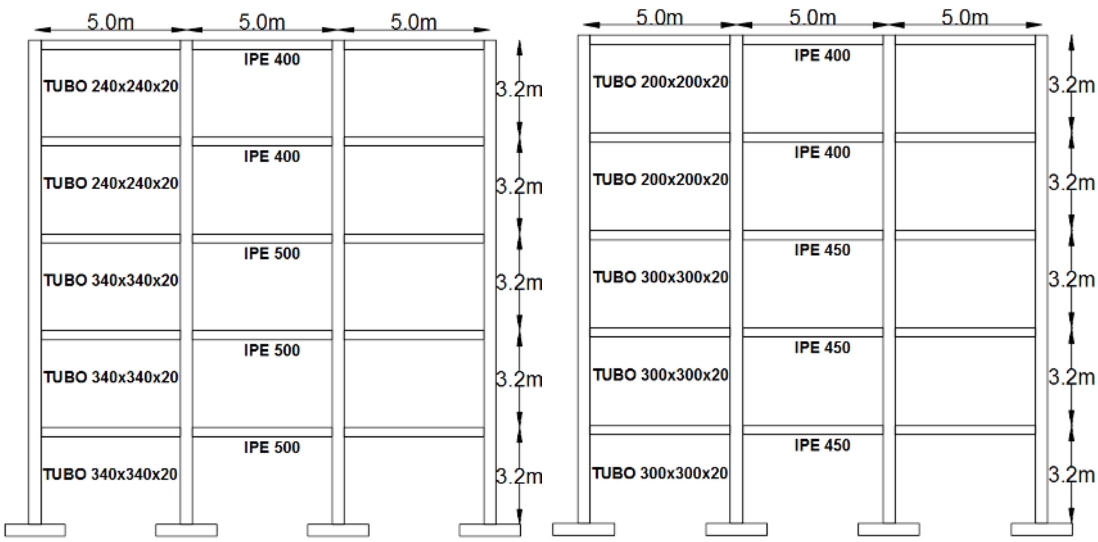

a) b)

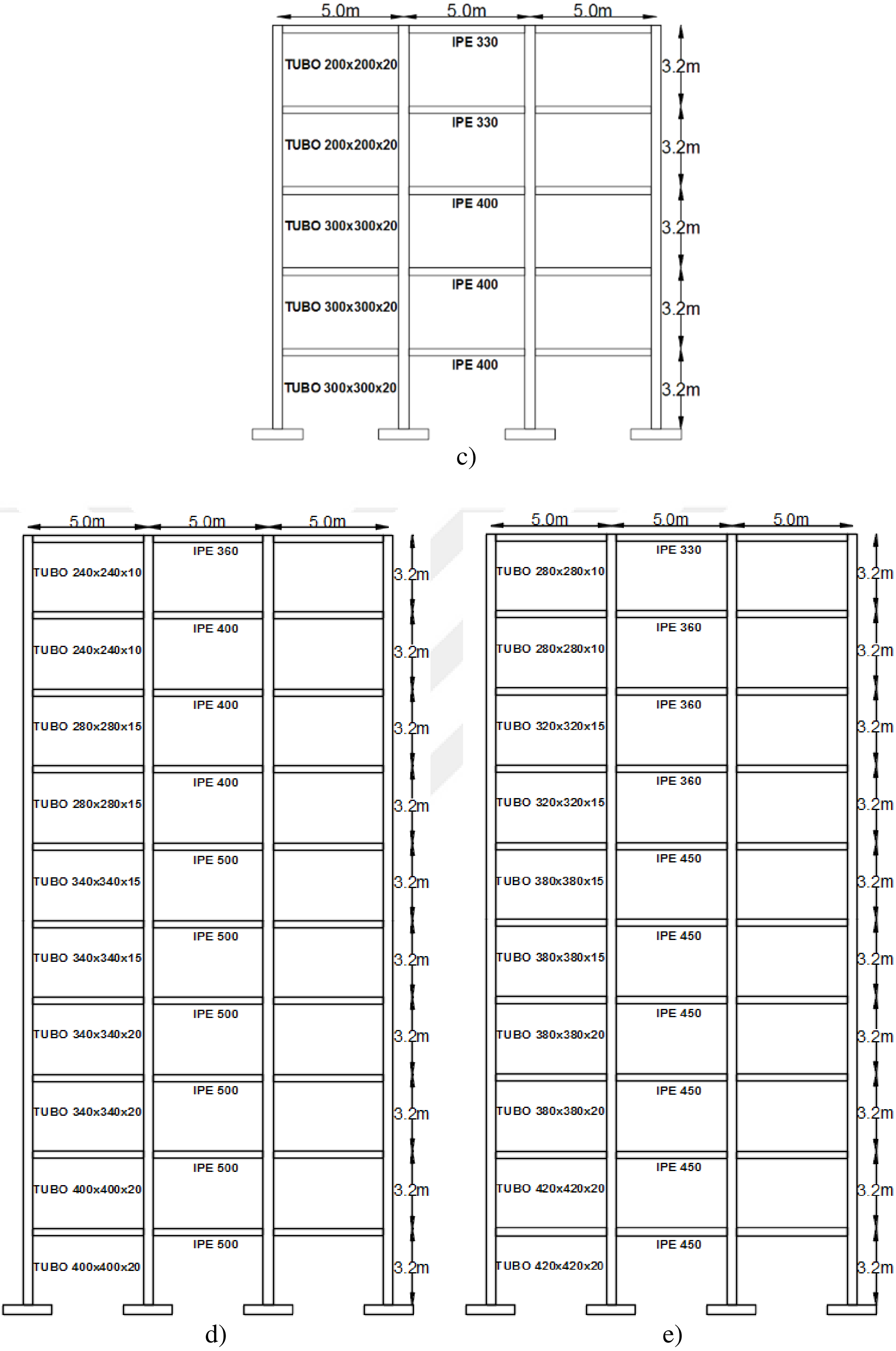

Figure 3.1 Elevation views of 5-storey a) OMF, b) IMF, c) SMF and 10-storey d) IMF and e) SMF [110]

The original buildings are deemed to be located in very high seismic zone whose earthquake acceleration is 0.35 g. Moreover, the soil type is assumed as B corresponded to average shear wave velocity to a depth of 30 m, V_{s30} = 360-750 m/s. Additional information on the case study frame could be found in Asgarian et al. [110].

3.2.2 Friction Damped Frames

Recent studies showed that the sliding motion of the solid bodies in the frictional damping system (e.g., FD) accounted for the energy dissipation through the friction mechanism based on the characteristic of the surface, frequency of the motion, incorporation of the device. It is not required that FD to be active during minor excitations. However, it should just slip only for major earthquakes thereby restraining the structural members yielding. When the exerted frictional force on the solid surface reaches to the projected slip load of FD, the energy dissipation on the device starts by virtue of the activation of the slippage. One the one hand it behaves only a rigid element if it is lower than this threshold, on the other hand it acts as conventional moment resisting frame if it is higher [114]. This state of affairs is required to determine the optimum slip load value of FD which results in the maximum energy dissipation and decreasing the response under excitations. A series of the loads are predetermined and taking into account to attain the optimum slip load for the case study frame. For this, nonlinear time history analyses are carried out up to obtain reasonable nonlinear response similar to study of Mirtaheri et al. [115].

Table 3.1 The values of slip loads (kN) of FDs at each storey

			Frames		
Storey	5 IMF	5 OMF	5 SMF	10 IMF	10 SMF
1	300	300	300	300	300
2	279	279	279	291	291
3	240	240	275	275	275
4	180	180	180	255	255
5	123	111	180	234	234
6	-	-	-	210	211
7	-	-	-	186	186
8	-	-	-	157	158
9	-	-	-	107	124
10	-	-	-	74	300

After all, the load of 300 kN is assigned as the slip load for ground level of case study frame with FD. Furthermore, it is necessary that the slip load should be proportionally distributed to each of the storeys considering the actual demand of the corresponded storey as stated in Ref. [63] and [116]. Therefore, the slip load was distributed as a function of the shear force in the building. That is to say, the proportion of the storey shear force height of the buildings is used to distribute the slip load for each FD whose slip loads are given in Table 3.1. It is known that the nonlinear response of FD generated rectangular hysteretic cycles similar to elasto-plastic behaviour [117]. FD modelled herein using single diagonal brace (see Figure 2.9(a)) represented by Plastic Wen element in SAP2000 [118] simulated the elasto-plastic shear force displacement hysteresis with the post yield stiffness ratio of 0.0001 and yielding exponent of 10.

3.2.3 Lead Rubber Bearing

LRB consists of rubber layers, lead plug and steel plates. Rubber layers provide flexibility horizontally. Steel plates almost carry the whole load and enable to necessary stiffness vertically. The steel plates force the lead plug deforms in shear and dissipate the seismic energy and restrain the isolator displacement. In this study, the design procedure suggested by Naeim and Kelly [1] was followed: firstly, target periods, T_D of 5-storey SMF, IMF and OMF were assumed to be 2.7 s, and that of the 10-storey SMF and IMF were assumed to be 3.0 s. The effective values of the design parameters were calculated by the following equations [1].

Design displacement, D_D:

$$D_D = \frac{gC_{VD}T_D}{B_D(4\pi^2)} \tag{3.1}$$

where C_{VD} is the seismic coefficient and B_D is the damping coefficient, T_D is target period and g is the gravitational acceleration.

Effective stiffness, k_{eff} :

$$k_{eff} = \frac{4\pi^2 W}{(T_D{}^2)g} \tag{3.2}$$

where W is total of the dead and live load.

Characteristic strength, $\mathrm{Q_D}$:

$$\mathrm{Q_D} = \frac{W_\mathrm{D}}{4\mathrm{D_D}} \tag{3.3}$$

where W_D is area of the hysteresis loop (the energy dissipated per cycle).

Post-yield stiffness, $\mathrm{k_2}$:

$$\mathrm{k_2} = \mathrm{k_{eff}} - \frac{\mathrm{Q_D}}{\mathrm{D_D}} \tag{3.4}$$

where $\mathrm{Q_D}$ is determined again according to the yield force and area of lead-plug:

$$\mathrm{Q_D} = \mathrm{A_{pb}} x\, \mathrm{F_{ypb}} \tag{3.5}$$

Then, by assuming elastic stiffness, $\mathrm{k_1} = 10\mathrm{k_2}$, $\mathrm{D_y} = \frac{\mathrm{Q_D}}{\mathrm{k_1 - k_2}}$ is estimated.

Yielding strength, $\mathrm{F_y}$:

$$\mathrm{F_y} = \mathrm{Q_D} + \mathrm{k_2} x \mathrm{D_y} \tag{3.6}$$

where $\mathrm{D_y}$ is the yield displacement.

By using these equations, the design parameters for LRB were computed in accordance with Naim and Kelly [1] and given in Table 3.2. The schematic view and hysteretic cycles are plotted in Figure 2.15(b). For all frames, two different bearings (inner and outer) were designed according to the vertical loads on column. Designed LRBs were placed below the each column of all examined frames. The applications of FD, LRB, and FD with LRB on 5-storey and 10-storey frames are illustrated in Figure 3.2 and 3.3, respectively.

Table 2.2 The outer bearing characteristics of LRB

	Frames				
	5 IMF	5 OMF	5 SMF	10 IMF	10 SMF
T_D (s)	2.7	2.7	2.7	3.0	3.0
W (kN)	254	311	234	675	701
D_D (m)	0.159	0.159	0.159	0.177	0.177
k_{eff} (kN/m)	140	171.5	129	301.5	313.1
Q_D (kN)	4.9	4.9	4.9	7.1	7.1
k_1 (kN/m)	1092.6	1406.9	982.3	2615.8	2731.9
k_2 (kN/m)	109.3	141	98.2	261.6	273.2
F_y (kN)	5.5	5.7	5.4	8.6	8.72
d_r (mm)	500	500	500	600	600
d_l (mm)	25	25	25	30	30

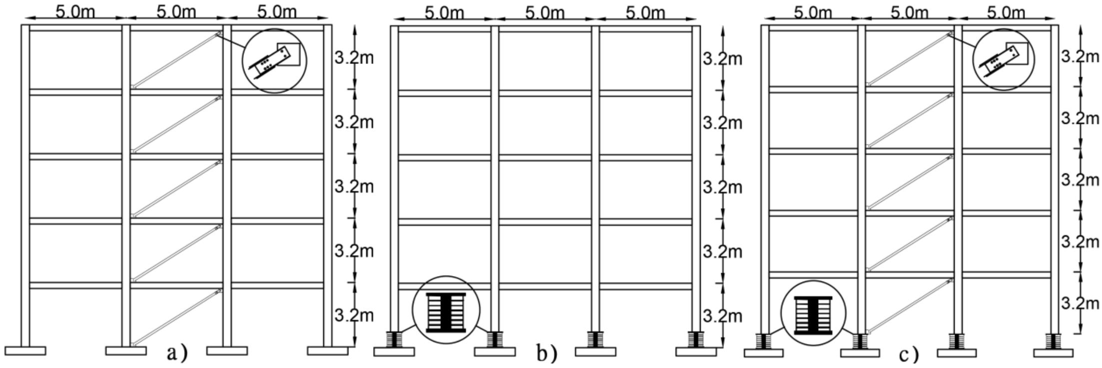

Figure 3.2 Elevation views of 5-storey frames with a) FD, b) LRB, c) FD+LRB under investigation

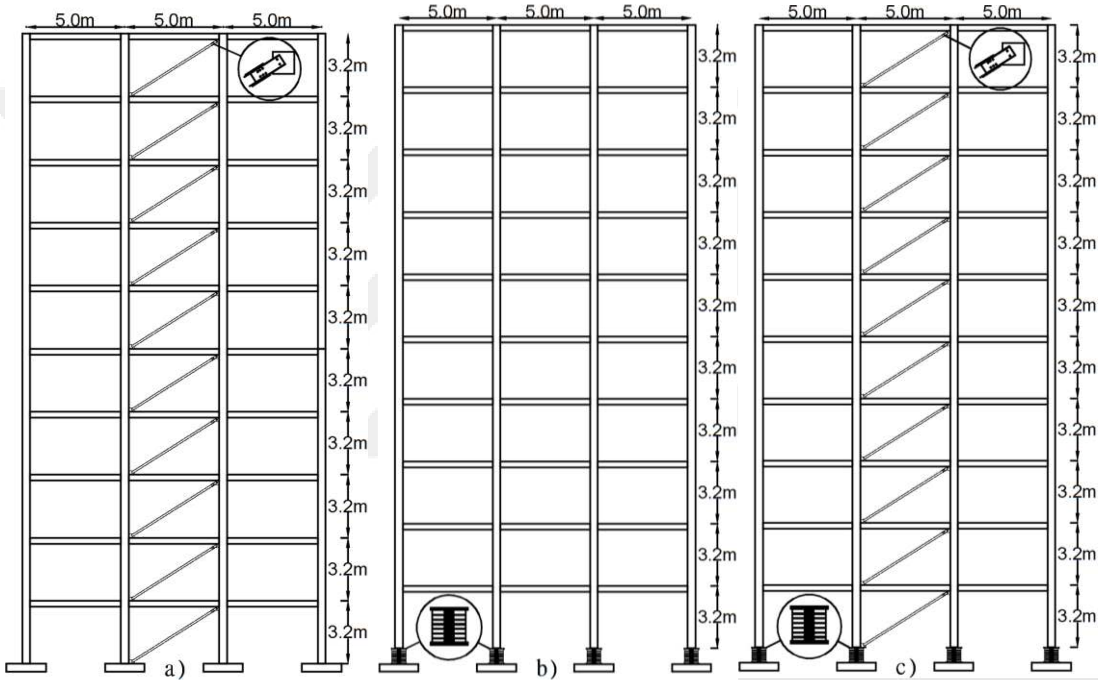

Figure 3.3 Elevation views of 10-storey frames with a) FD, b) LRB, c) FD+LRB under investigation

3.3 Case-2 (FPB)

The inelastic seismic response of steel moment resisting frames equipped with FPB systems was examined. To this aim, 3, 6, and 9-storey frames with FPB having various design properties of isolation period (T), effective damping ratio (ß), and yield strength to weight ratio (Fy/W) in accordance with the code specification of ASCE [14] were taken into account. In the FPB design, T, ß, and Fy/W values varied from 2 to 3 s, 0.01 to 0.25, and 0.025 to 0.10, respectively. The isolated frames were evaluated by means of the nonlinear time history analysis using four ground motion records. The analysis of the results were given and discussed comparatively.

3.3.1 Designing and Modelling of the Case Study Frames

As the second case study frames, three different steel moment resisting frames, namely, 3, 6, and 9-storey fixed base frames were considered that are initially planned by Karavasilis et al. [119]. The profiles of IPE and HEB are used to building of the beams and columns, respectively. The storey height and bay width are equal to 3 and 5 m, respectively. The general layout of the examined frames, including section of the beams and columns are given in Figure 3.4.

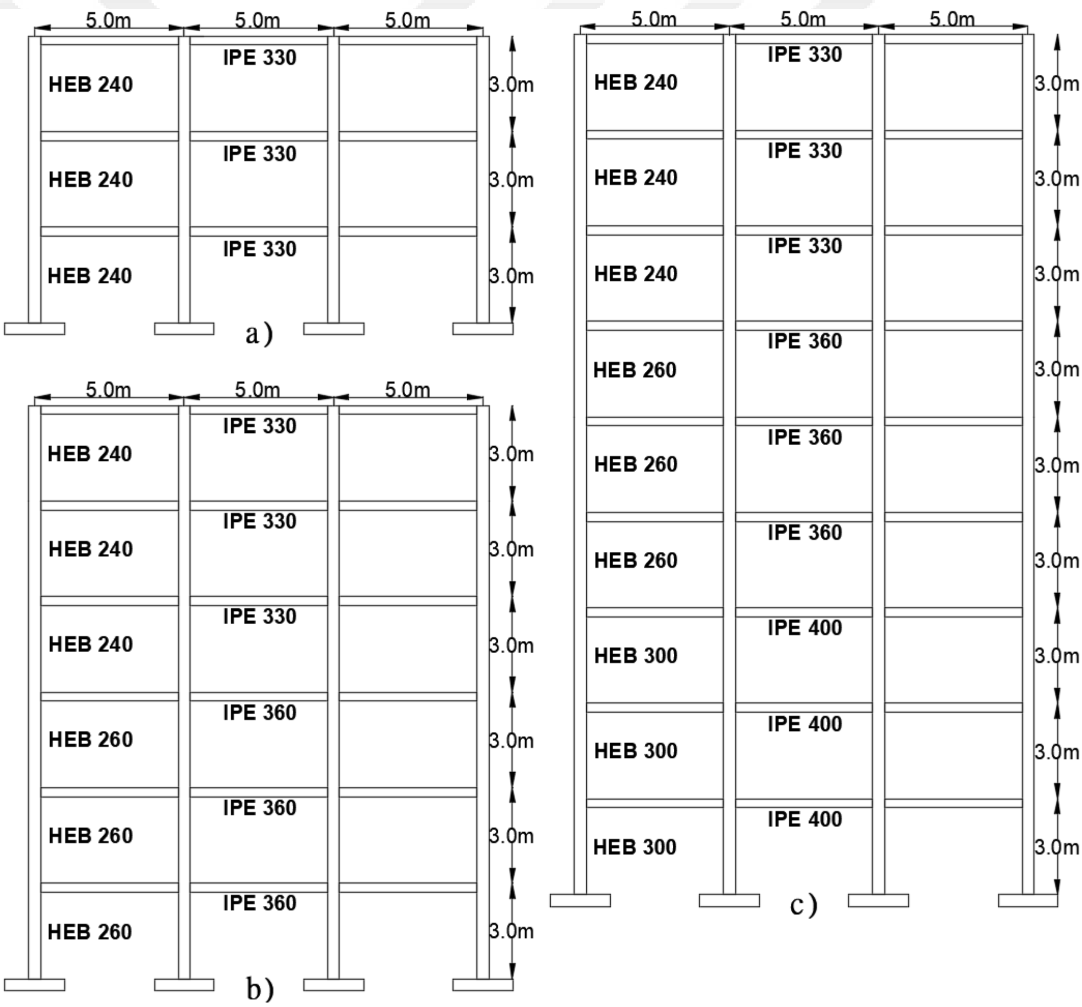

Figure 3.4 Elevation views of a) 3-storey, b) 6-storey, and c) 9-storey SMRF [119]

The fundamental natural periods of free vibration for 3, 6, and 9-storey buildings were determined as 0.73, 1.31, and 1.75 s, respectively. The dead and live loads are only considered in the scenario of the gravity load. The amount of dead and live loads acting on the beams are assigned as 24.5 and 10 kN/m, respectively. The modulus of elasticity and yield strength of steel are taken equal to 200 GPa and 235 MPa, respectively. The post yield stiffness ratio is equal to 0.03. The inherent damping ratio of the original frames is assumed to be 5 %. Moreover, comprehensive information pertained to the original frames can be find out in the study of Karavasilis et al. [119]. The non-linearities considered in the numerical models of the beams and columns were restricted by the plastic hinges. The plastic hinges were assigned at the end of the structural members. FPB system was used to isolate the case study frame structures. The mechanism of FPB depends on the movement of the bearing along the curved surface and the supported mass moved upward, thus the movement would provide the restoring force to the system.

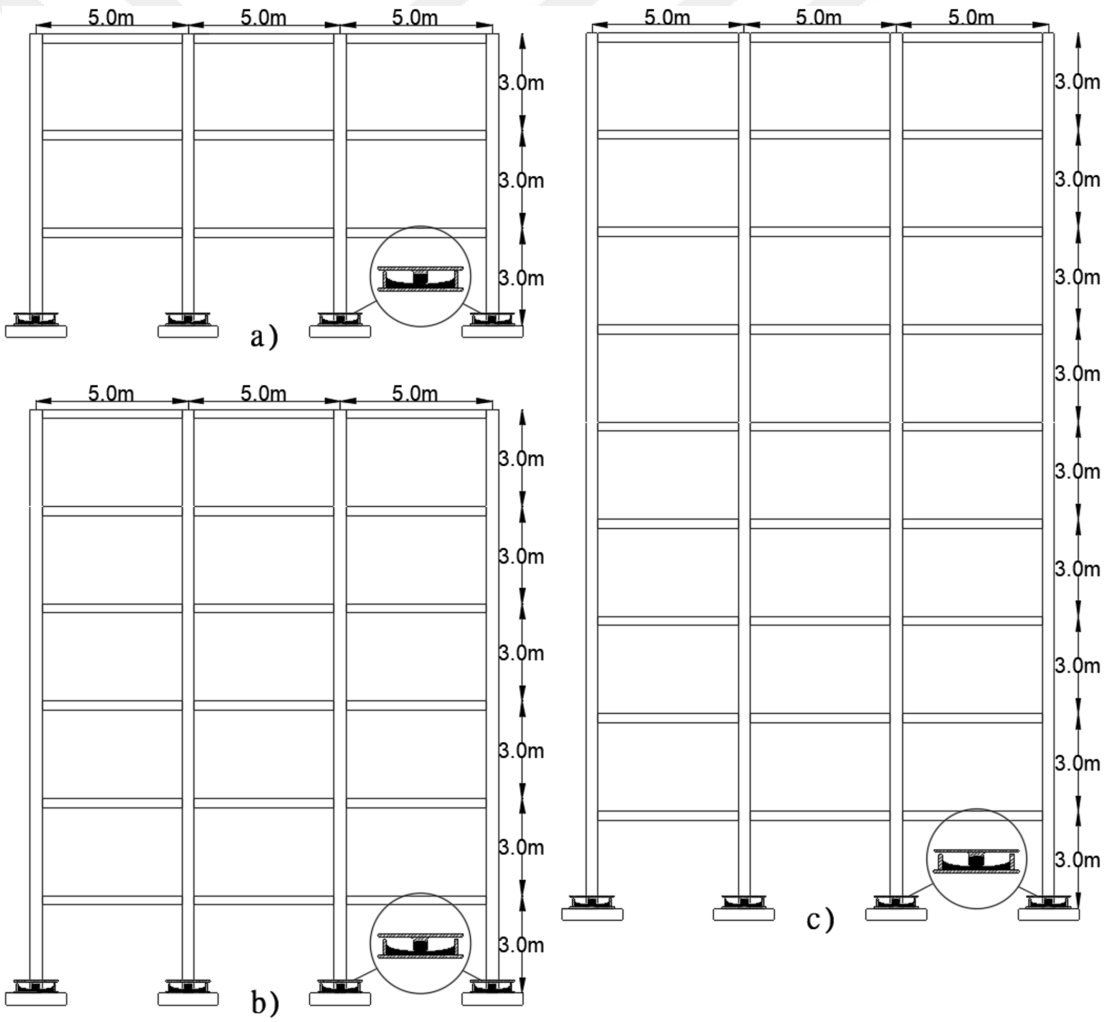

Figure 3.5 Elevation views of a) 3-storey, b) 6-storey, and c) 9-storey SMRF with FPB under investigation

During a seismic excitation, the bearing goes along with curved surface hereby it moves in small arcs like a pendulum. The bearings are expected to decrease the transmission of the seismic forces to the structure by the movement of pendulum and also frictional pad [77]. The effective stiffness and resisting force can be tuned by the design parameters such as assumed isolation period, effective damping ratio, friction coefficient, and radius of the concave surface. Analytical models of the isolated frames as shown in Figure 3.5 were provided using finite element program SAP 2000 [118]. To depict the hysteretic behaviour of the isolators of the FPB, a nonlinear finite element NLlink called as friction pendulum isolator has been used. The mechanical model of the FPS is rooted in the classic Coulomb theory. The cross-sectional view and hysteretic behaviour are plotted in Figure 2.15(c). For the base isolated models, two different bearings (inner and outer) were designed. The isolators located on top of the vertical loads on the column of all evaluated models that include friction isolator as a nonlinear link element employed by Park et al. [120]. Thus, 27 different base-isolated structural models have been designed by employing FPB with different isolation period (T), effective damping ratio (ß), and yield strength ratio (Fy/W). Even though various studies in the literature focus on the parameters such as sliding velocity, axial pressure, temperature, and stick-slip phases which individually affects the friction coefficient of FPBs; to decrease the computational work and make use of nonlinear analysis of the structures having FPBs feasible, in the modeling of FPB, a common moderate value of the sliding friction coefficient was considered as 0.05 during the stick phase according to the study of Jangid [77].The design parameters of the FPB were computed by an iterative solution, in which the following equations were employed in compliance with Naeim and Kelly [1]. The load exerted on the isolator of the FPB is W, the horizontal displacement is D, and the friction coefficient is μ, then the resisting force F is given by

$$F = \frac{W}{R} D + \mu W(\mathrm{sgn} D) \tag{3.7}$$

where R is the radius of curvature of the dish. The first term is the restoring force due to rise of the mass, providing a horizontal stiffness, k_2;

$$k_2 = \frac{W}{R} \tag{3.8}$$

which produces an isolated structure period T given by;

$$T = 2\pi\sqrt{\frac{R}{g}} \tag{3.9}$$

The equivalent stiffness k_{eff} is given by;

$$k_{eff} = \frac{W}{R} + \frac{\mu W}{D} \tag{3.10}$$

and effective damping ratio, ß;

$$ß = \frac{2\mu}{\pi x\left(\frac{D}{R}\right)+\mu} \tag{3.11}$$

where gravitational acceleration is g.

Table 3.3 Properties of FPB for outer columns in 3-storey base-isolated frame

T (s)	$ß_{eff}$ (%)	Fy/W (%)	Fy kN)	k_1 kN/m)	k_2 (kN/m)	D (m)	k_{eff} (kN/m)	Isolation System
	5					0.278	245.4	T2ß5FyW2.5
2	15	2.5	5.2	1040	208	0.202	259.5	T2ß15FyW2.5
	25					0.166	270.5	T2ß25FyW2.5
	5					0.348	164.1	T2.5ß5FyW2.5
2.5	15	2.5	5.2	1040	134.2	0.252	175.4	T2.5ß15FyW2.5
	25					0.208	184.3	T2.5ß25FyW2.5
	5					0.417	118.2	T3ß5FyW2.5
3	15	2.5	5.2	1040	93.2	0.303	127.6	T3ß15FyW2.5
	25					0.249	134.9	T3ß25FyW2.5
	5					0.278	245.4	T2ß5FyW5
2	15	5	10.4	2080	208	0.202	259.5	T2ß15FyW5
	25					0.166	270.5	T2ß25FyW5
	5					0.348	164.1	T2.5ß5FyW5
2.5	15	5	10.4	2080	134.2	0.252	175.4	T2.5ß15FyW5
	25					0.208	184.3	T2.5ß25FyW5
	5					0.417	118.2	T3ß5FyW5
3	15	5	10.4	2080	93.2	0.303	127.6	T3ß15FyW5
	25					0.249	134.9	T3ß25FyW5
	5					0.278	245.4	T2ß5FyW10
2	15	10	20.8	4160	208	0.202	259.5	T2ß15FyW10
	25					0.166	270.5	T2ß25FyW10
	5					0.348	164.1	T2.5ß5FyW10
2.5	15	10	20.8	4160	134.2	0.252	175.4	T2.5ß15FyW10
	25					0.208	184.3	T2.5ß25FyW10
	5					0.417	118.2	T3ß5FyW10
3	15	10	20.8	4160	93.2	0.303	127.6	T3ß15FyW10
	25					0.249	134.9	T3ß25FyW10

Although Naeim and Kelly [1] proposed a constant value for the ratio of post yield stiffness to initial stiffness (k_1), Ryan and Chopra [121] recommended the fixing the yield displacement instead of fixing k_1/k_2 and it is 5 mm for FPB. In this study, various models of steel frame structures have been examined in order to cover a wide range of isolation system characteristics, differing in number of storeys (n_s = 3, 6, and 9), yield strength ratio of the structure (Fy/W= 0.025, 0.05, and 0.10), and effective damping ratio (ß=5, 10, and 25 %). Other properties of the isolation systems were calculated using Eqs. 3.7–3.11 and illustrated in Table 3.3 for 3-storey frame. It was noted that each isolation systems were labeled based on their isolation periods, effective damping (ß ratios), and yield levels (Fy/W ratios) as to use in figures and throughout the rest of the text. For example, T2.5ß25FyW5 denotes an isolation system with T = 2.5 s, ß = 25 %, and Fy/W = 0.05.

3.4 Case-3 (HDRB)

The nonlinear response of a series of buildings embedded with HDRB was examined in order to produce more compact intelligent isolation system by combining the mechanical characteristics of isolators. To this aim, 3, 6, and 9-storey steel frames equipped with HDRB having different design properties of the isolation period T, effective damping ratio ß, and post-yield stiffness ratio λ compatible with the standard of ASCE [14] were considered. For the designing of HDRB, the values of T, ß, and λ changed from 2 to 3 s, 0.05 to 0.15, and 3 to 6, respectively. The examined frames were estimated through dynamic analyses using five ground motion records. The comments obtained from the analyses were presented and addressed comparatively.

3.4.1 Designing and Modelling of the Case Study Frames

As the third case study frames, 3, 6, and 9-storey fixed base frames are considered that are initially planned by Karavasilis et al. [119] were redesigned by added HDRB. The general layout of the examined frames with HDRB is given in Figure 3.6. HDRB has similar notion of BIS and inhibit the seismic energy transferred from the ground to the structure in the event of earthquakes. HDRB consists of alternate laminated thin rubber layers and reinforced steel plates that are bonded by vulcanization [122]. The isolators designed to provide horizontal post-yield elasticity and also ensure the vertical rigidity by supporting the weight of the structure.

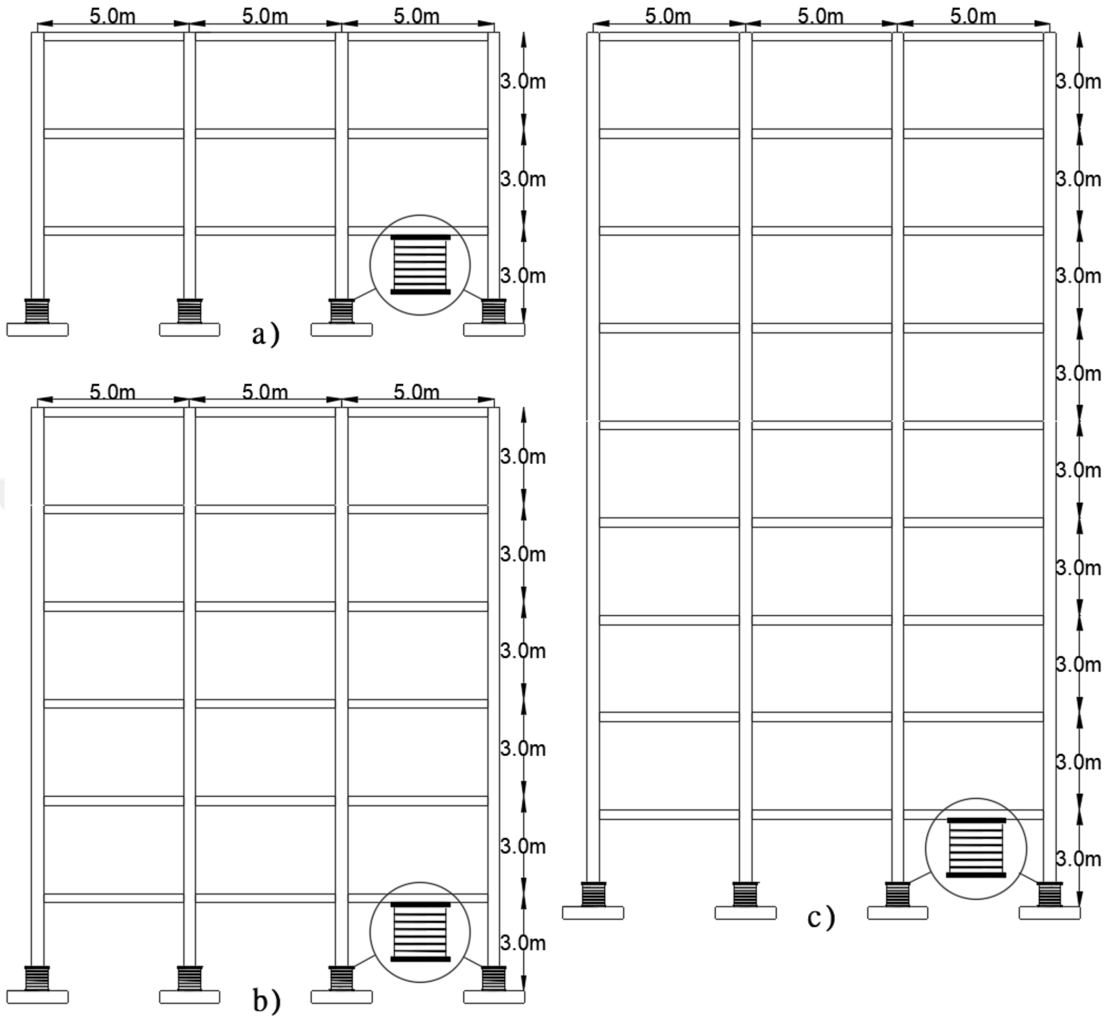

Figure 3.6 Elevation views of a) 3-storey, b) 6-storey, and c) 9-storey SMRF with HDRB under investigation

Figure 2.15(a) shows the cross-sectional view and hysteretic behaviour of HDRB [76]. Eighteen different base-isolated frame models are implemented in nonlinear frame analysis by software SAP 2000 [118] that is enabled to describe the nonlinearity of HDRB isolator. For this, a common link element was considered as rubber isolator link element in the modeling of HDRB and it was used and assigned as a single joint element between the ground and the superstructure according to the study of Sarno et al. [125]. Both of the bearings (namely inner and outer) were separately developed for the analytical modelling of the isolated buildings in which HDRB placed between the foundation and the column of the buildings. The link property of the isolators considered as the rubber isolator link element utilized firstly by Park et al. [120]. In this way, a set of isolation systems have been modelled by means of HDRB considering different isolation properties such as isolation period T, effective damping ratio ß, and post-yield stiffness ratio λ. An iterative design procedure applied and then the isolation parameters of HDRB were determined using following equations in accordance with Naeim and Kelly [1]. Firstly, the maximum isolator displacement was assumed and just once neglecting the yield displacement, the iteration started and continued until the assumed and obtained values were almost the same. In the iterative procedure described in ASCE [14], the following equations were used. The assumed value of period T was then utilized to calculate the effective stiffness, k_{eff};

$$k_{eff} = \frac{W}{g} x (\frac{2x\pi}{T})^2 \quad (3.12)$$

hysteresis loop (the energy dissipated per cycle), W_D;

$$W_D = 2x\pi x k_{eff} x ß x D^2 \quad (3.13)$$

characteristics strength, Q;

$$Q = \frac{W_D}{4(D - D_y)} \quad (3.14)$$

post-yield stiffness of the isolator, k_2;

$$k_2 = k_{eff} - \frac{Q}{D} \quad (3.15)$$

yield displacement, D_y is given by;

$$D_y = \frac{Q}{(k_1 - k_2)} \quad (3.16)$$

effective period, T_{eff};

$$T_{eff} = 2\pi\sqrt{\frac{W}{k_{eff} \cdot g}} \quad (3.17)$$

damping reduction factor, B;

$$\frac{1}{B} = 0.25(1 - \ln ß_{eff}) \quad (3.18)$$

displacement of isolation, D;

$$D = \frac{g.S_a.T_{eff}^2}{B.4\pi^2} \tag{3.19}$$

and yield strength, F_y;

$$F_y = Q + k_d.D_y \tag{3.20}$$

where gravitational acceleration is g, Q is characteristic strength, T is target period, W is total weight on the isolator, g is gravitational force, B is damping reduction factor, D_y is yield displacement, ß is effective damping ratio, and S_a is spectral acceleration. The mechanical behaviour of the rubber bearing characterized in the study of Naeim and Kelly [1] regarding the equivalent damping ratio reaching to 0.25. Furthermore, the post yield stiffness ratio defined as the ratio of the post yield stiffness (k_2) to the initial stiffness (k_1), and considered as 3 and 6. In the study of Ryan and Chopra [121], it was suggested that the constant value of 5 mm for the yield displacement (D_y) was taken into account rather than fixing the post yield stiffness ratio.

Table 3.4 Properties of HDRB for the outer columns in 3-storey base-isolated frame

T (s)	ß (%)	λ	Fy (kN)	k_1 (kN/m)	Q (kN)	D (m)	k_{eff} (kN/m)	Isolation System
	5		7.2	575.6	4.8	0.278		T2ß5λ3
2	10	3	10.2	516.9	6.8	0.185	209.1	T2ß10λ3
	15		15.3	440.1	10.2	0.163		T2ß15λ3
	5		5.7	368.4	3.8	0.348		T2.5ß5λ3
2.5	10	3	8.2	330.8	5.5	0.232	133.8	T2.5ß10λ3
	15		12.3	281.6	8.2	0.205		T2.5ß15λ3
	5		3.2	255.8	3.2	0.417		T3ß5λ3
3	10	3	4.6	229.8	4.5	0.278	92.9	T3ß10λ3
	15		6.8	195.6	6.8	0.245		T3ß15λ3
	5		5.6	1154.1	4.6	0.278		T2ß5λ6
2	10	6	7.6	1049.4	6.3	0.185	209.1	T2ß10λ6
	15		10.4	937.5	8.7	0.163		T2ß15λ6
	5		4.5	738.6	3.7	0.348		T2.5ß5λ6
2.5	10	6	6.1	671.6	5.1	0.232	133.8	T2.5ß10λ6
	15		8.3	600.0	6.9	0.205		T2.5ß15λ6
	5		3.7	512.9	3.1	0.417		T3ß5λ6
3	10	6	5.1	466.4	4.2	0.278	92.9	T3ß10λ6
	15		6.9	416.7	5.7	0.245		T3ß15λ6

In this paper, as previously mentioned, a set of different base-isolated steel frame models have been generated to evaluate the isolator characteristics of HDRB that was considered as variety of storey number (3, 6, and 9-storey), isolation period (T = 2, 2.5, and 3 s), effective damping ratio (ß = 0.05, 0.10, and 0.15), and post-yield stiffness ratio (λ = 3 and 6). In the design of HDRB, the bi-linear hysteretic behavior was regarded as shown in Figure 2.15(a) [76]. Other mechanical properties of the isolators were computed by Eqs. 3.12-3.20 and presented in Table 3.4 for 3-storey frame. The generated base-isolated model of isolation systems was labeled depend on their isolation period (T), effective damping ratio (ß), and stiffness ratio ($k_1/k_2 = \lambda$) as to present in the tables and figures and in the rest of the paper. For instance, T3ß15λ6 stands for the isolation model of T = 3 s, ß = 15 %, and λ = 6.

3.5 Case-4 (FD, LRB, FPB, HDRB, and Combination of those)

The seismic performance of the ordinary moment frame (OMF) upgraded with FD as an energy dissipation device, LRB, FPB, HDRB as base isolation system (BIS), and combination of those were evaluated. To this aim, 5-storey steel OMF was considered as fixed base. FD is placed to mid bay and over the height of the case study frame regarding the effectiveness of the slip load. Then, each of the base isolation devices (namely LRB, FPB, and HDRB) designed with distinctive mechanical behaviour and installed underneath of the column. Finally, OMF is retrofitted by the combination of FD and BIS together (i.e., FD+LRB, FD+FPB, and FD+HDRB) to develop seismically more efficient isolated frames. The nonlinear responses of the fixed base and retrofitted frame models are comparatively evaluated through time-history dynamic analyses using seven ground motion records. The obtained analysis results were elaborately discussed.

3.5.1 Designing and Modelling of the Case Study Frames

In this case, the fixed based OMF was upgraded by considering various strategies to evaluate the overall effectiveness of the friction device (FD) and isolators (LRB, FPB, HDRB). For this, the bare frame with FD, LRB, FPB, HDRB, FD+LRB, FD+FPB, and FD+HDRB were taken into account as given in Figure 3.7(b) to (h). FD designed using the similar procedure given in Section 3.2.2. Hence, the slip load for each FD is given in Table 3.1. FD modelled herein using single diagonal brace (see Figure 3.7(b)) represented by Plastic Wen element in SAP2000 [118] simulated the elasto-plastic shear force displacement hysteresis with the post yield stiffness ratio of 0.0001 and yielding exponent of 10. In addition to the above, the lead rubber bearings (LRB), friction pendulum bearing(FPB), and high damping rubber bearing (HDRB) are employed for the base isolation of the case study frame. The typical layout and force-deformation relationship for considered isolators of LRB, FPB, and HDRB were presented in Figure 3.7(c-e). The elastomeric bearings (namely, LRB and HDRB) were modeled using the nonlinear link element of “Rubber Isolator” while “Friction Pendulum’’ adopted for the modelling of FPB according to Bouc-Wen hysteretic model in which elastic-plastic transition was perfectly represented [120]. Thus, both NLlink elements were employed to model the isolators using finite element program of SAP2000 [69]. The design parameters of the bearings were computed as underlined by Naeim and Kelly [1] proposed an iterative computational method. It is started after assuming the isolator displacement and omitting first yield displacement, and is to be continued up to a certain value equal to almost assumed one. For each of the elastomeric bearings (namely, LRB and HDRB), the target isolation period T and effective damping ratio ß are assumed as 3 s and 15 %, respectively. In addition, the elastic stiffness k_1 is taken as 15 and 6 times post-yield stiffness k_2 for LRB and HDRB, respectively [1]. Eventually, the design parameters of the base isolation models have been determined to construct the bilinear modeling of LRB, FPB, and HDRB (see Figure 2.15(d)).

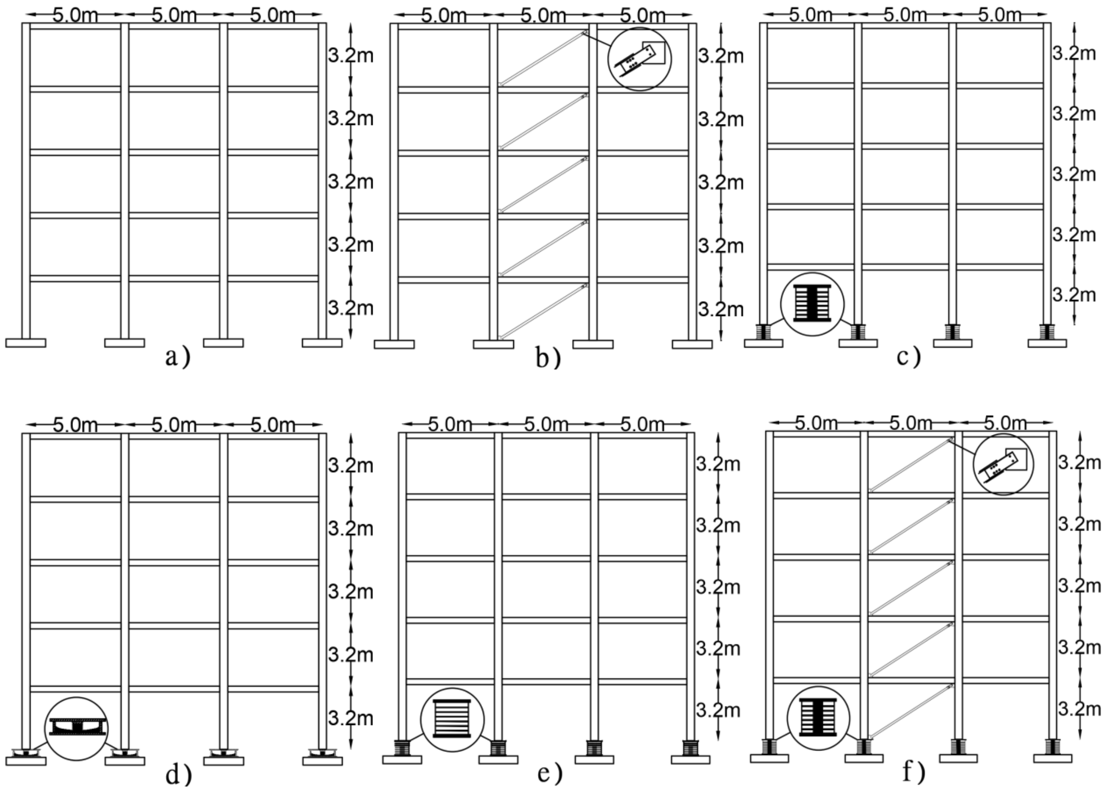

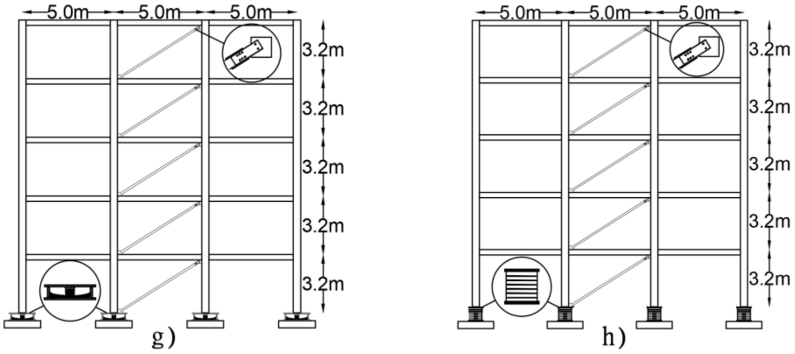

Figure 3.7 Elevation views of the case study bare frame: a) FB [110] and that with: b) FD, c) LRB, d) FPB, e) HDRB, f) FD+LRB, g) FD+FPB, and h) FD+HDRB

The most important design parameters of FPB are the friction coefficient and the radious of the curvature [126]. The former was selected as 0.05 for the sliding-based bearing of FPB according to the study of Jangid [77] while the latter was attained as 2.24 m corresponded to the isolation period of 3 s by Equation of 3.9. Furthermore, the elastic stiffness k_1 is to be 51 times the post-yield stiffness k_2 as recommended by Naeim and Kelly [1]. The equations of 3.7-3.11 were employed to compute the other isolation parameters. The load imparted to the isolator of the FPB is W, the radious of the curvature R, the horizontal displacement is D, and the friction coefficient is μ, then the resisting force F. The other properties of the isolation systems were calculated using Equations of 3.1-3.20 and illustrated in Table 3.5 for LRB, FPB, and HDRB.

Table 3.5 Properties of the isolators for the outer columns of 5-storey OMF

Isolation Systems	T (s)	$ß_{eff}$ (%)	W (kN)	k_1/k_2	Fy (kN)	k_2 (kN/m)	Q (kN)	k_1 (kN/m)	D (m)	k_{eff} (kN/m)
LRB	3	15	305.8	15	21.9	212.5	20.4	3187.9	0.302	280.0
FPB	3	15	305.8	51	28.1	280.1	27.6	14284.1	0.302	384.6
HDRB	3	15	305.8	6	25.7	209.3	21.4	1255.7	0.302	280.0

3.6 Nonlinear analysis of the Case Study Frames

SAP 2000 [118] was utilized for the analytical modelling of two-dimensional models of the case study frames (i.e., bare frame, friction damped, and isolated frames) through nonlinear time-history analyses including the direct integration method. Thus, the nonlinear responses of the considered case frames were computed for each of the earthquakes. It was known that PGA significantly characterizes the earthquake records thereby it was considered as an intensity measure. Seven earthquake records namely, Tabas (1978), Cape Mendocino (1992), Northridge (1994), Chi-Chi (1999) Gazlı, (1976), Superstition Hills (1987), and San Salvador (1986) were obtained by Pacific Earthquake Engineering Research Centre (PEER) [127] data bank to carry out the nonlinear time history analyses. More information on the earthquake records presented in Table 3.6.

Table 3.6 Characteristics of the ground motions used

Earthquake Record	Year	Magnitude (Mw)	R_{jb} (km)	R_{rup} (km)	V_{s30} (m/s)	PGA (g)	PGV (cm/s)	PGD (cm)
Tabas	1978	7.35	1.8	2.0	766.8	0.80	118.29	96.80
Cape M.	1992	7.01	0	8.2	712.8	0.61	81.87	25.48
Northridge	1994	6.69	0	5.3	251.2	0.79	93.29	53.29
Chi-Chi	1999	7.62	0.6	0.6	305.9	0.82	127.80	93.22
Gazlı	1976	6.8	3.9	5.5	659.6	0.59	69.64	24.18
S. Hills	1987	6.54	0.9	0.9	348.7	0.41	106.74	50.54
San Salvador	1986	5.8	2.1	6.3	545	0.84	62.23	10.01

Note: Mw: Moment magnitude; R_{jb}: Surface projection distance; R_{rup}: Rupture distance; V_{s30}: Mean shear velocity over the top 30 m; PGA: Peak ground acceleration; PGV: Peak ground velocity; PGD: Peak ground displacement

5 % damped acceleration response spectra of the ground motions are also illustrated in Figure 3.8. The signals of the ground motions are scaled in accordance with ASCE 7-10 [14] standard in which the scaled records should not be lower than the design spectrum over the period range from 0.2T to 1.5T where T is the fundamental vibration period of the building being designed.

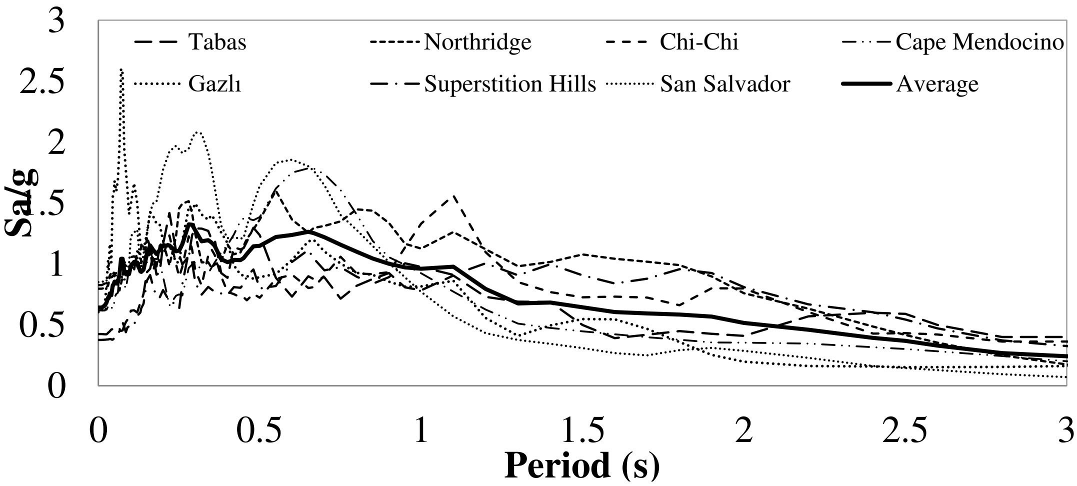

Figure 3.8 Elastic acceleration response spectra of the eartqhuake ground motions used

CHAPTER 4

RESULTS AND DISCUSSION

4.1. Introduction

In this chapter, the nonlinear responses of the case study frames are given in terms of the storey displacement, bearing displacement, relative displacement, roof drift, interstorey-drift ratio, absolute acceleration, base shear, base moment, hysteretic curve, and energy dissipation. They were obtained for all cases through nonlinear time-history analyses. The effectiveness of the seismic protective systems characterized with various design parameters was evaluated. In addition, the seismic performances of two sets of steel buildings with and without the seismic protective systems were comparatively discussed in four different cases.

4.2 Case-1 (FD, LRB, and FD with LRB)

The present study assessed the dynamic characteristic and seismic response of three 5-storey frames as OMF, IMF, SMF and two 10-storey frames as IMF and SMF upgraded with FD, LRB, and combination of those (i.e., FD+LRB). The inelastic seismic response of the frames with and without the structural protective systems have been examined in terms of roof drift, roof absolute acceleration, relative displacement, interstorey drift ratio, base shear, top storey moment obtained by means of the time history analyses.

4.2.1 Roof Drift Ratio

The roof drift ratio calculated as the roof displacement of the examined frames divided by the total height of the buildings. The roof drift ratios for all frames under seven ground motions were given in Figure 4.1. The corresponding reductions in the roof drift ratio values with respect to the original frame were given in Tables 4.1 and 4.2. As it was observed, the structures equipped with FDs experienced the lowest roof drift demand independent of the earthquake characteristic. For instance, for frames with FDs, corresponding average reduction percentages in the roof drift ratio were 65.6, 73.9, 75.5 % for 5-storey OMF, IMF, SMF and 47.6 and 47.5 % for 10-storey IMF and SMF, respectively. In addition, the greatest roof drift ratio was observed as 4.90 when 10 SMF was equipped with LRB under Chi-Chi earthquake while it was mitigated by FD and FD with LRB up to the roof drift ratios of 0.83 and 4.61 (see Figure 4.1(e)), respectively. The lowest roof drift ratio was experienced as 0.25 for 5 SMF with FD when subjected to Gazlı earthquake (see Figure 4.1(c)). As expected, the roof drift ratios of the frames with LRB, both FDs and LRB were generally greater than those of the original frames due to the low lateral stiffness of the isolators. When the structures changed from SMF towards IMF and OMF the roof drift demand reduced due to the increase in stiffness of the frames, originally.

Table 4.1 Reduction of the obtained maximum values for five storey frames (expressed as percentage)

Avg. Values	Structural Configurations								
	5 OMF FD	5 OMF LRB	5 OMF FD+LRB	5 IMF FD	5 IMF LRB	5 IMF FD+LRB	5 SMF FD	5 SMF LRB	5 SMF FD+LRB
R. Drift*	65.6	-72.0	-64.9	73.9	-59.3	-51.8	75.5	-61.3	-52.2
R. A. Ac.	42.5	81.6	88.1	58.4	85.3	87.8	60.1	80.4	87.5
R. Disp.	64.3	81.6	90.4	72.3	81.3	91.7	76.2	80.4	92.8
B. Shear	43.9	81.7	81.1	44.8	81.9	81.2	41.6	80.1	79.2
Top M.	60.8	78.5	83.4	70.6	77.9	82.3	66.1	69.9	77.1
Ints. Drf.	68.4	76.2	80.8	74.4	76.8	82.0	77.0	76.7	83.2

*R. Drift: Roof Drift Ratio; R. A. Ac.: Roof Absolute Acceleration; R. Disp.: Relative Displacement; B. Shear: Base Shear; Top M.: Top Storey Moment; Ints. Drf.: Interstorey Drift Ratio

Key: Negative values show an increase of the maximum values

Table 4.2 Reduction of the obtained maximum values for ten storey frames (expressed as percentage)

Avg. Values	Structural Configurations					
	10 IMF FD	10 IMF LRB	10 IMF FD+LRB	10 SMF FD	10 SMF LRB	10 SMF FD+LRB
R. Drift	47.6	-39.6	-3.2	47.5	-40.7	-31.2
R. A. Ac.	48.2	81.6	84.3	48.6	80.6	86.3
R. Disp.	49.9	83.9	91.1	48.7	82.7	91.5
B. Shear	24.6	75.2	70.4	23.2	71.7	71.1
Top M.	55.7	69.8	69.5	48.9	62.8	60.6
Ints. Drf.	53.5	79.4	82.6	54.7	78.5	84.8

Key: Negative values show an increase of the maximum values

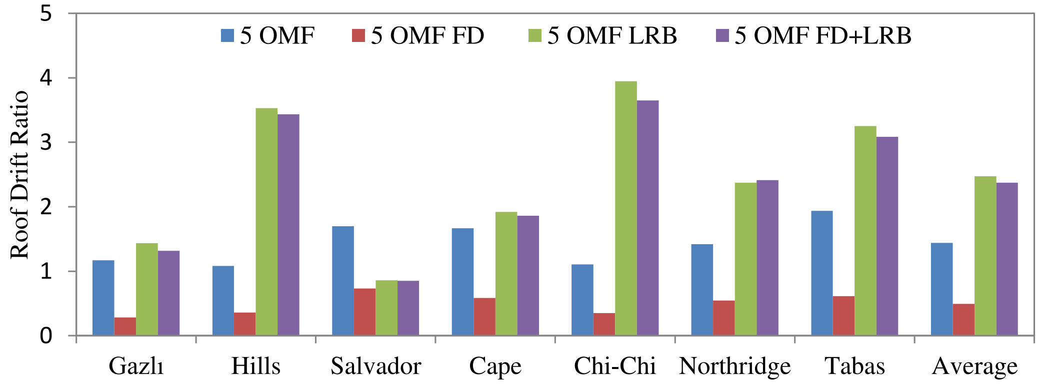
5 OMF
5 OMF FD
5 OMF LRB
5 OMF FD+LRB
Roof Drift Ratio
0
1
2
3
4
5
Gazlı
Hills
Salvador
Cape
Chi-Chi
Northridge
Tabas
Average

a)

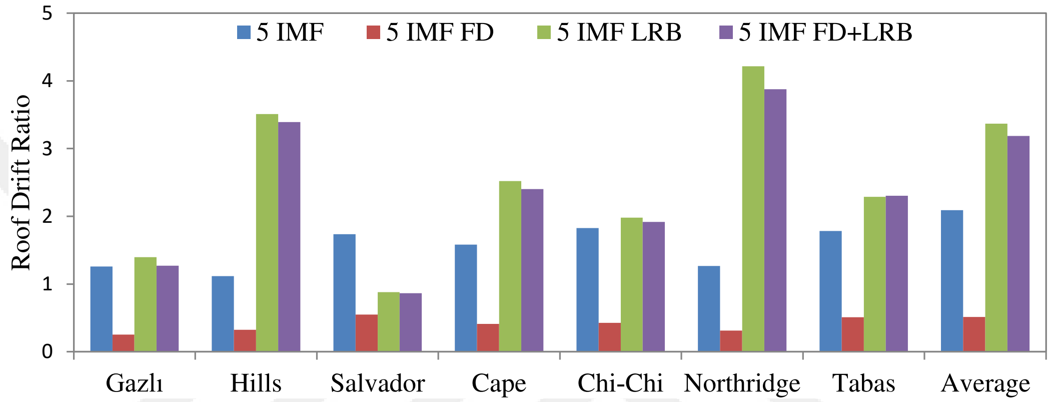
5 IMF
5 IMF FD
5 IMF LRB
5 IMF FD+LRB
Roof Drift Ratio
0
1
2
3
4
5
Gazlı
Hills
Salvador
Cape
Chi-Chi
Northridge
Tabas
Average

b)

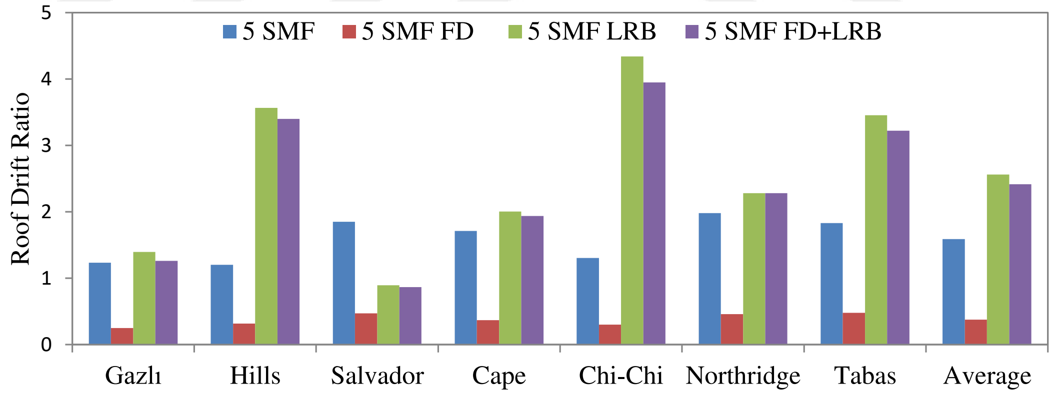
5 SMF
5 SMF FD
5 SMF LRB
5 SMF FD+LRB
Roof Drift Ratio
0
1
2
3
4
5
Gazlı
Hills
Salvador
Cape
Chi-Chi
Northridge
Tabas
Average

c)

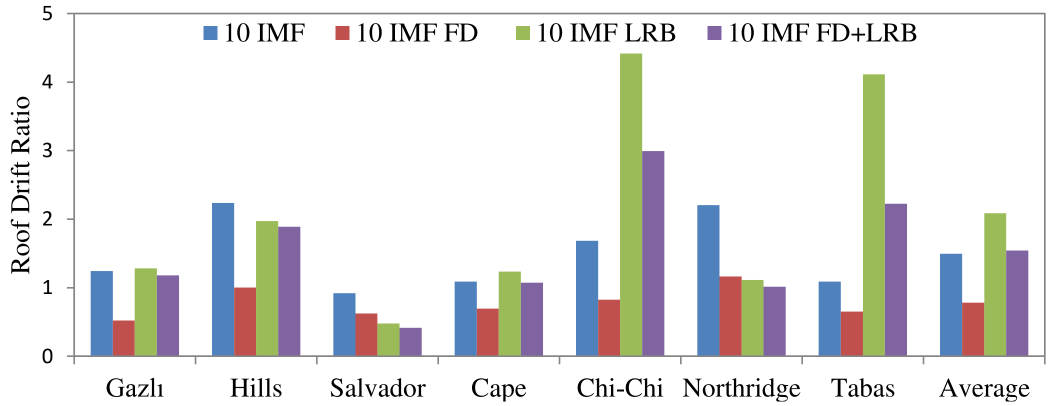
10 IMF
10 IMF FD
10 IMF LRB
10 IMF FD+LRB
Roof Drift Ratio
0
1
2
3
4
5
Gazlı
Hills
Salvador
Cape
Chi-Chi
Northridge
Tabas
Average

d)

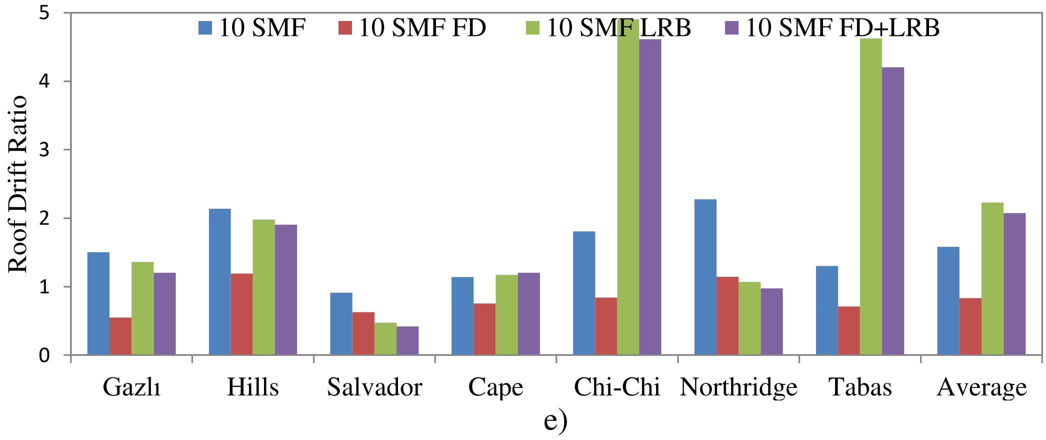

e)

Figure 4.1 The roof drift ratio of 5 and 10-storey frames

Figure 4.2 showed the time history response of the roof drift ratio for the case study frames with and without structural protective systems under Cape earthquakes. The results of the displayed response histories proved the supremacy of utilization of FDs in reducing the lateral displacement. As respect to other structural protective systems, use of FDs remarkably mitigated fluctuations on the drift during the earthquake records. For instance, significant residual drifts are observed especially for 5-storey frames; the residual drift for 5 SMF with FD was observed as 0.37, while the maximum roof drift ratio of 2 was computed for 5 SMF with LRB.

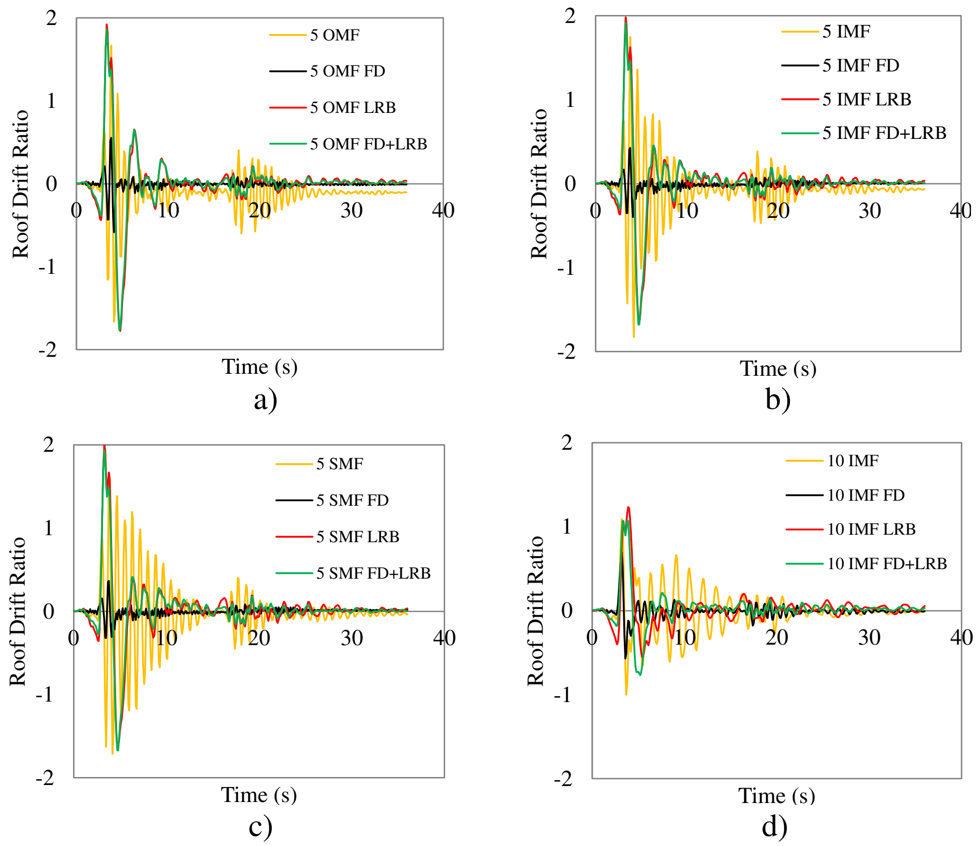

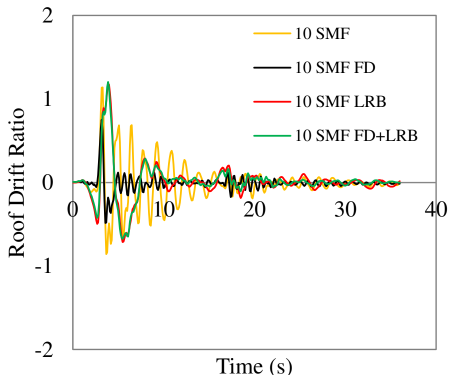

e)

Figure 4.2 Time history response of roof drift ratio under Cape earthquake

4.2.2 Roof Absolute Acceleration

The maximum roof absolute accelerations were plotted in Figure 4.3. It is clearly shown that application of all structural protective systems remarkably reduced the roof absolute acceleration, especially combined use of FDs and LRB led to nearly 88% average reduction. In addition, when subjected to Salvador earthquake 5 IMF caused the greatest absolute acceleration of 22.53 m/s^2, it was remarkably reduced up to 1.47 m/s^2 by means of the utilization of FD with LRB. All, corresponding reductions in the roof absolute acceleration values with respect to the original frame were given in Tables 4.1 and 4.2. Considering these reductions, it was observed that the enhancement in response of SMF and IMF was nearly identical, in turn, for 5-storey OMF with FDs and LRB succeed as 94.4% reduction under Salvador earthquake as displayed in Figure 4.3(a). It was pointed out that the number of storey of the buildings had not significant effect on the reduction of the maximum roof accelerations.

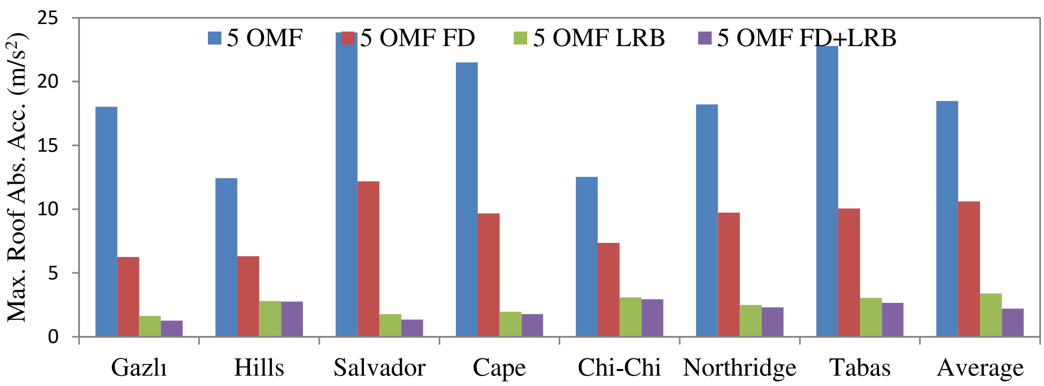

a)

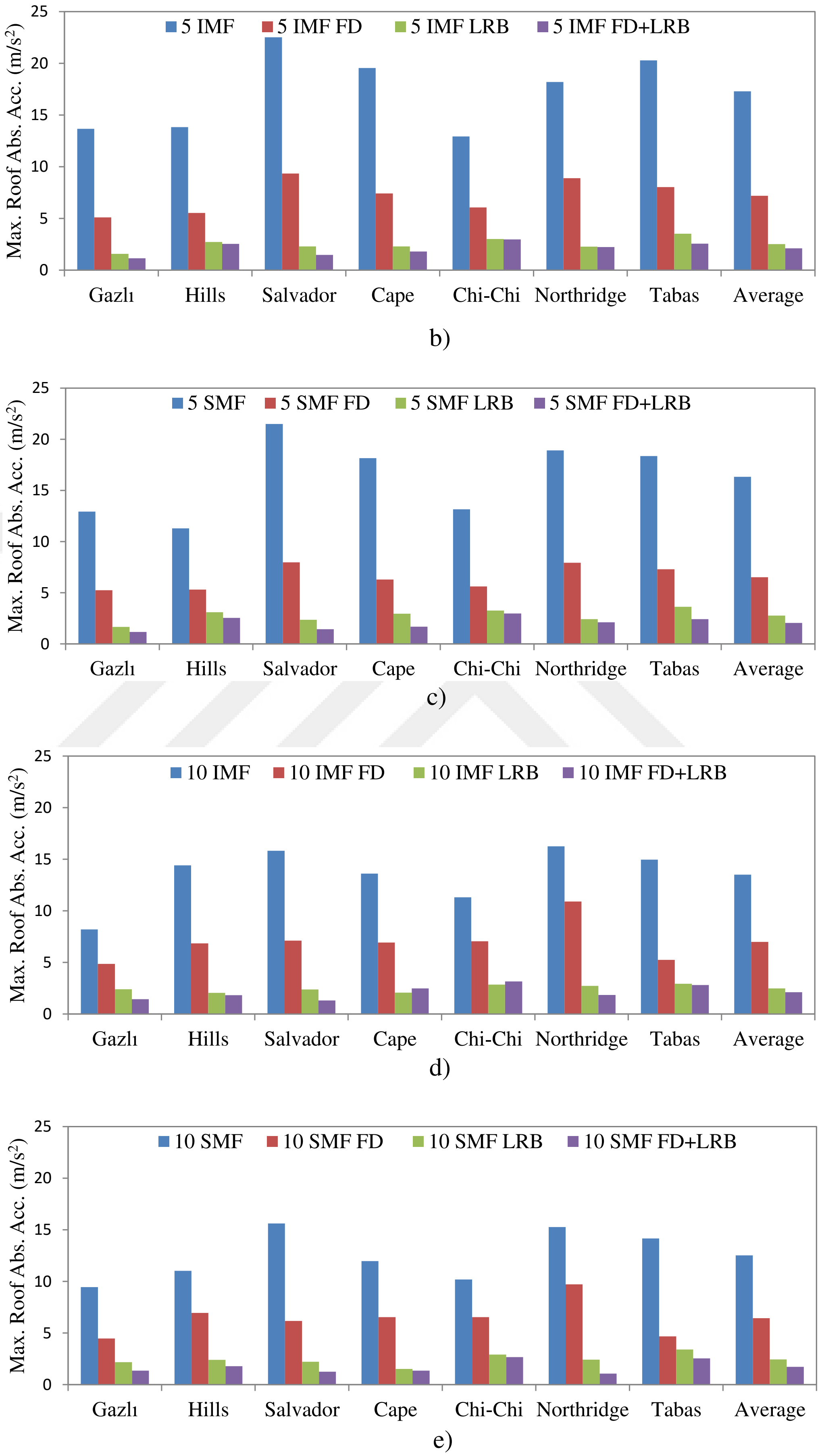

Figure 4.3 Maximum roof absolute accelerations of 5 and 10 storey frames

4.2.3 Relative Displacement

The relative displacement is computed by subtracting the displacement of the corresponded storey from the base displacement. The maximum relative displacement is normalized by corresponding building height and obtained normalized maximum relative displacement ratios are given in Figure 4.4. As explained previously, since the stiffness of the rubber was low, it provided horizontally flexibility and allowed to lateral movement at the base, therefore LRB and combined case FD+LRB had smaller values than FDs and original frames. The lowest normalized maximum relative displacement was experienced as 0.12 (see Figure 4.4(b)) in case of 5-storey IMF equipped with the combination of FD with LRB that was correspondence to reduction as 91.8 % with respect to 5-storey IMF. It was seen that on average the relative displacement ratio of 5-storey OMF equipped with FD was only reduced by 64.3%, while that of SMF was reduced significantly by 76.2%, and that of IMF reduced by 72.3% as shown in Table 4.1 and Figure 4.4.

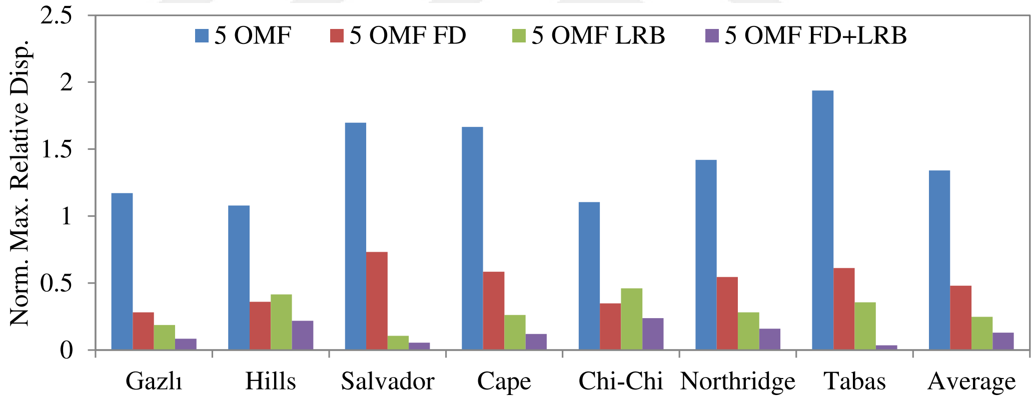

a)

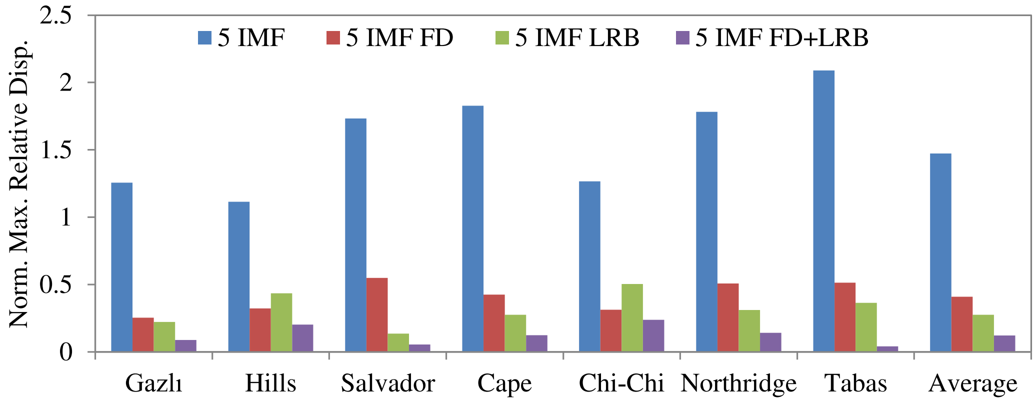

b)

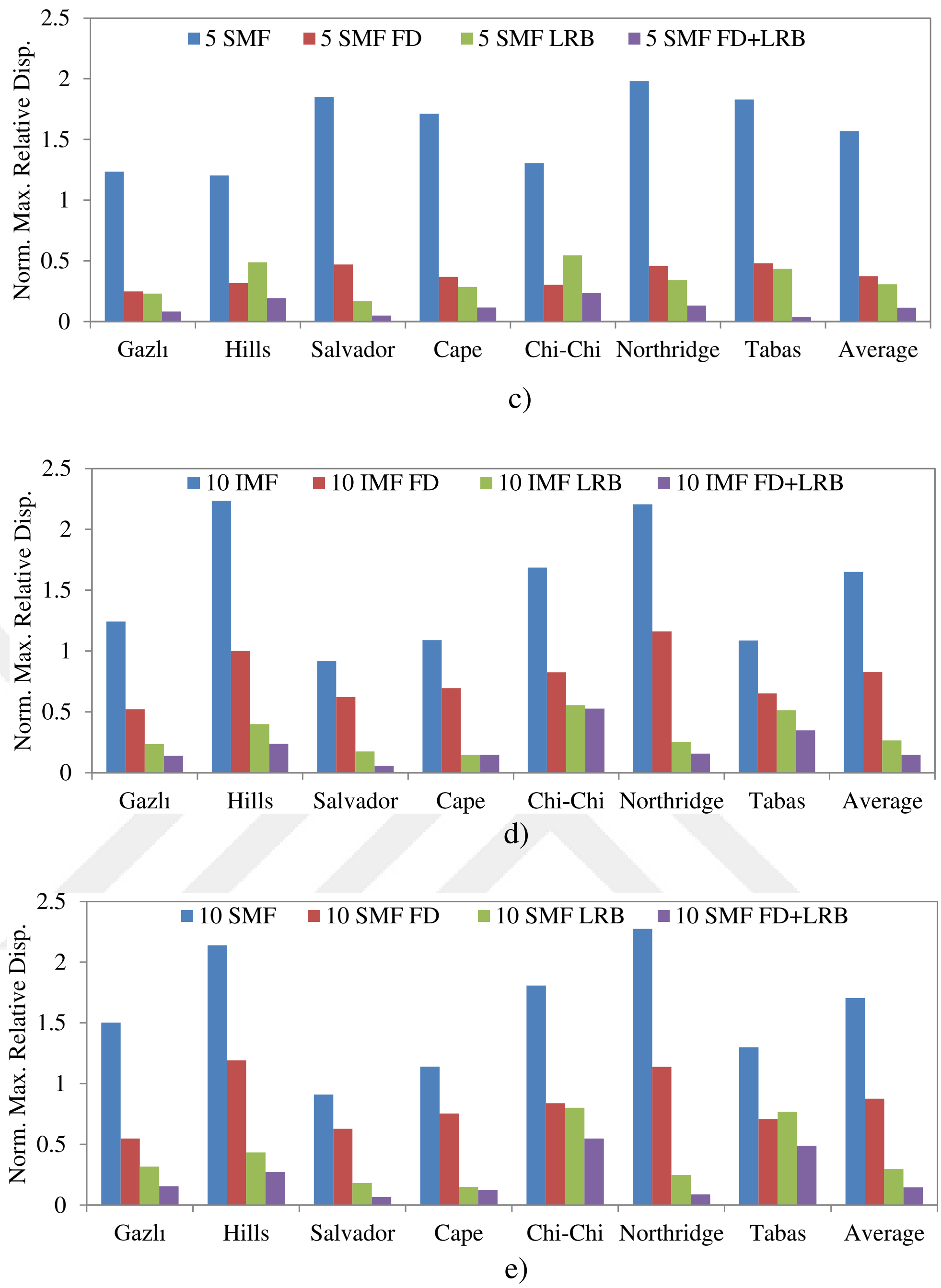

Figure 4.4 Normalized maximum relative displacement ratio of 5 and 10 storey frames

In addition, it was clearly observed that instead of implementing of the isolation systems one by one the use of FD with LRB together provided significant improvement on the maximum relative displacement demand of each examined case study frames. For example, for 10-storey SMF, corresponding average reduction percentages in the maximum relative displacement were 48.7, 82.7 and 91.5% for FD, LRB and FD+LRB, respectively, as shown in Figure 4.4 and Tables 4.2. The variation of the relative displacements with storey height under Northridge earthquake was given in Figure 4.5. These results proved that use of FDs with LRB were very effective in reducing the lateral displacement demand especially in SMF. For instance, 5-storey OMF, IMF and SMF, 10-storey IMF and SMF equipped with FD+LRB subjected to Northridge earthquake that is enabled to greatest reduction percentage in the maximum relative displacement were 88.8, 92.1, 93.4, 92.8 and 96.1% (see Figure 4.4) for FD, LRB and FD+LRB, respectively. Furthermore, as it was observed from Figure 4.5, the use of FDs with LRB in 10-storey SMF tended to distribute the relative displacement demand more uniformly than other cases, especially under Northridge earthquake.

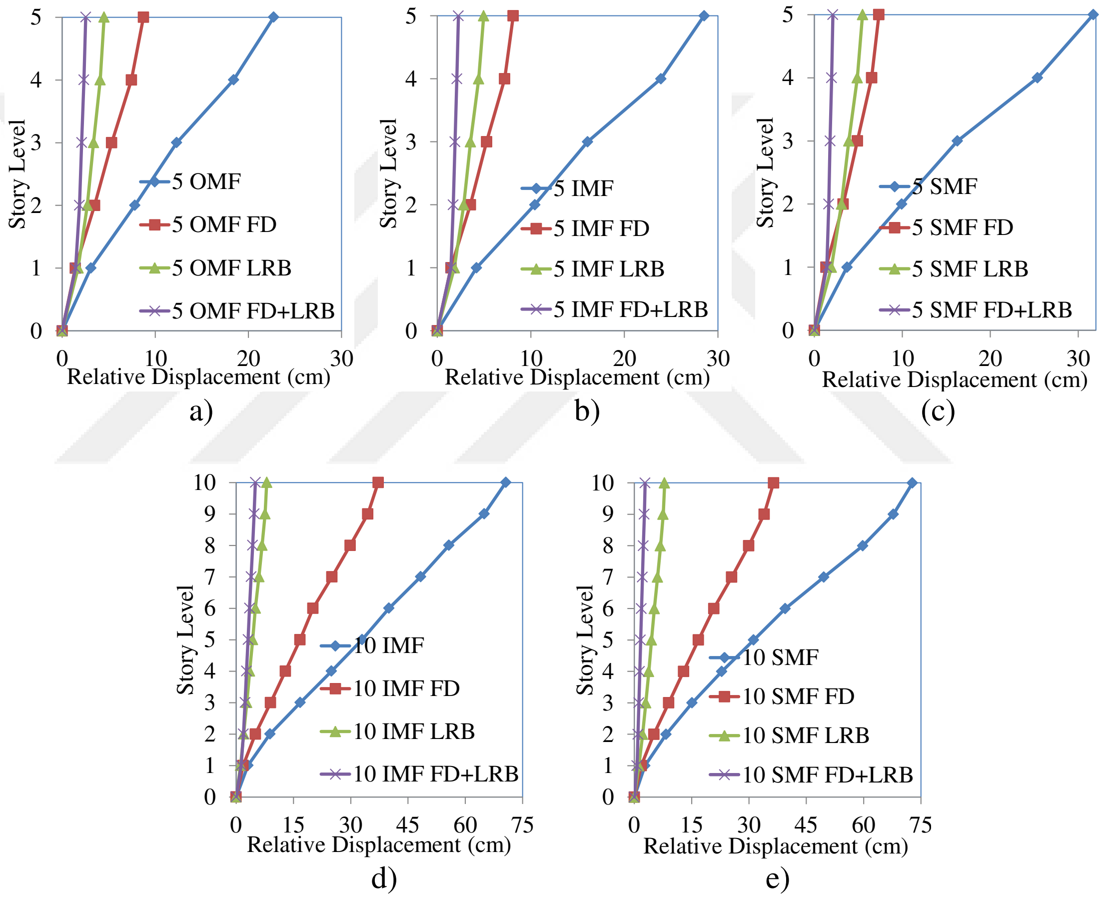

Figure 4.5 The variation of the relative displacements with storey height under Northridge earthquake

4.2.4 Interstorey Drift Ratio

The interstorey drift ratio was computed as the difference between displacements of the two consecutive storeys and divided by the corresponding storey height (3.2 m). The interstorey drift ratio was a significant parameter and used on the assessment of the seismic performance of civil engineering structures [128]. It was directly related to level of structural damage that may be observed in a structure. For the structural performance evaluation; fully operational, FO, operational, OP, life safety, LS, and near collapse, NC limit states are considered, which are denoted by SP1, SP2, SP3 and SP4, respectively. Those are in compliance with seismic provisions by SEAOC [129], and given in Table 4.3. Since limited information about limit state of IMF, it was linearly interpolated between the values of OMF and SMF [110]. The maximum interstorey drift ratios (i.e., in percentage, %) for each examined frame subjected to seven different earthquakes and average of those were given in Figure 4.6.

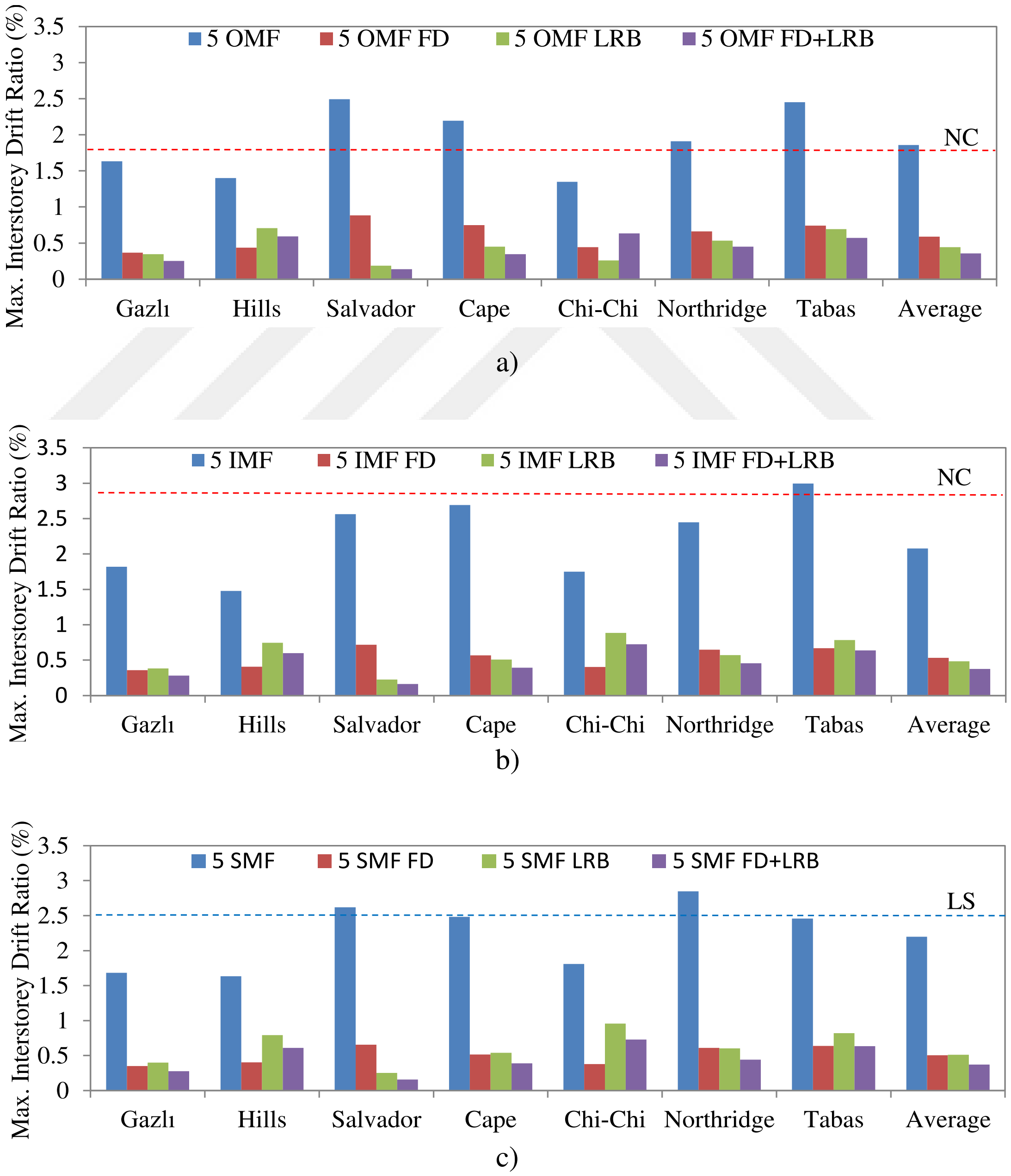

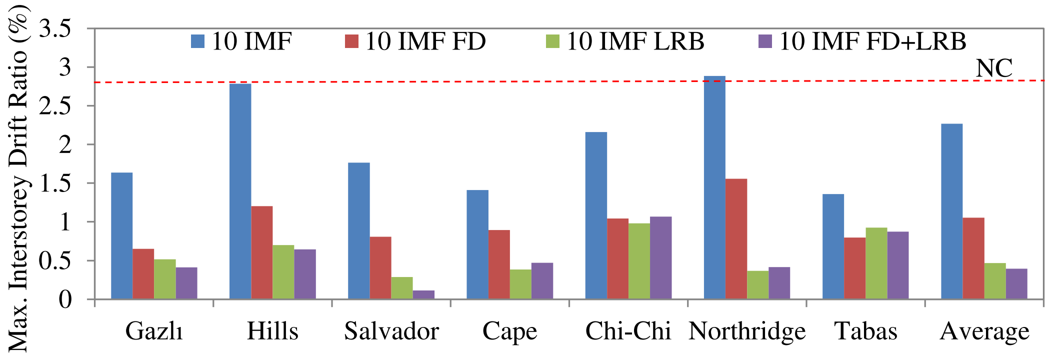

d)

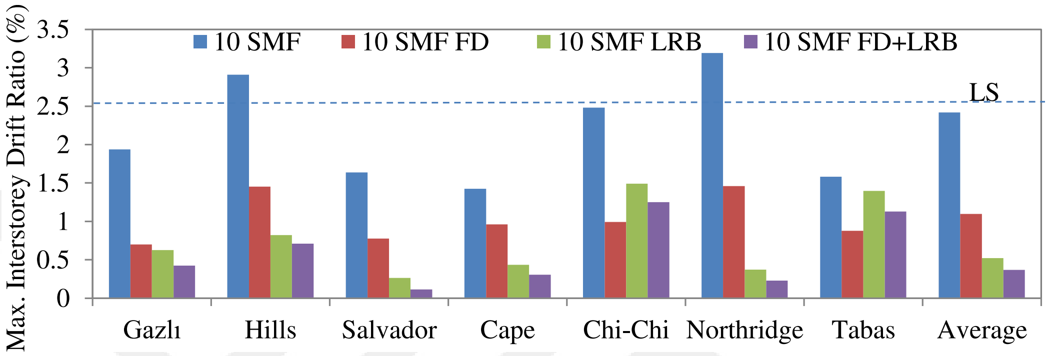

e)

Figure 4.6 Maximum interstorey drift ratio of 5 and 10 storey frames

FDs, LRB and use of both together provided remarkable reduction as shown in Tables 4.1 and 4.2. The frames upgraded with FDs and LRB together witnessed to lowest interstorey drift ratio independently of the type of the frames and number of storey. For example, the maximum interstorey drift reduction of 94.5% was observed when 5-storey OMF was hit by Salvador earthquake as shown in Figure 4.6(a). The frames with protective systems exhibited lower drift than corresponding life safety limit; furthermore, each of them also met SP2 limit state for only Northridge and Gazlı earthquakes. The drift ratio of the upgraded frames was generally satisfied with the SP2 limit state for each earthquake record, in turn, SP1 limit state was valid only for 5-storey upgraded frames under Gazlı earthquake. Figures 4.6 and 4.7 described the maximum interstorey drift ratio of 5-storey SMF was obtained as 2.85% exceed the LS limit, while SMF with either FDs or LRB satisfied the requirement of SP2, on the other hand SMF with FDs and LRB together was below SP1 limit state which obstruct the loss of structural functionality as shown in Figures 4.6 and 4.7(c). The variation of drift reductions depends on predefined slip load of FDs and design period of the LRB; hence the effectiveness of the protective systems can be tuned by means of these parameters. For each structural protective system, SMF experienced greater interstorey drift reduction than OMF and IMF since SMF has higher ductility demand than other frames [110]. It was seen that use of FDs with LRB had the lowest drift demand. For example, on average maximum interstorey drift ratio of 5-storey IMF equipped with the FDs and LRB were reduced by 82%. Similarly, the maximum interstorey drift demand on average for 10-storey IMF and SMF equipped with FDs and LRB was reduced by 82.6 and 84.8%, respectively. As an example, the variation of the interstorey drift ratio versus storey height under Northridge earthquake was given in Figure 4.7. It was observed that the use of FDs with LRB led to more uniform distribution along the height of the frames especially in SMF.

Table 4.3 Recommended drift limits by structural performance levels [129].

	Performance Levels			
Frames	SP1 (%) Fully Operational	SP2 (%) Operational	SP3 (%) Life safety	SP4 (%) Near collapse
SMF	0.5	1.5	2.5	3.8
OMF	0.4	0.8	1.2	1.8

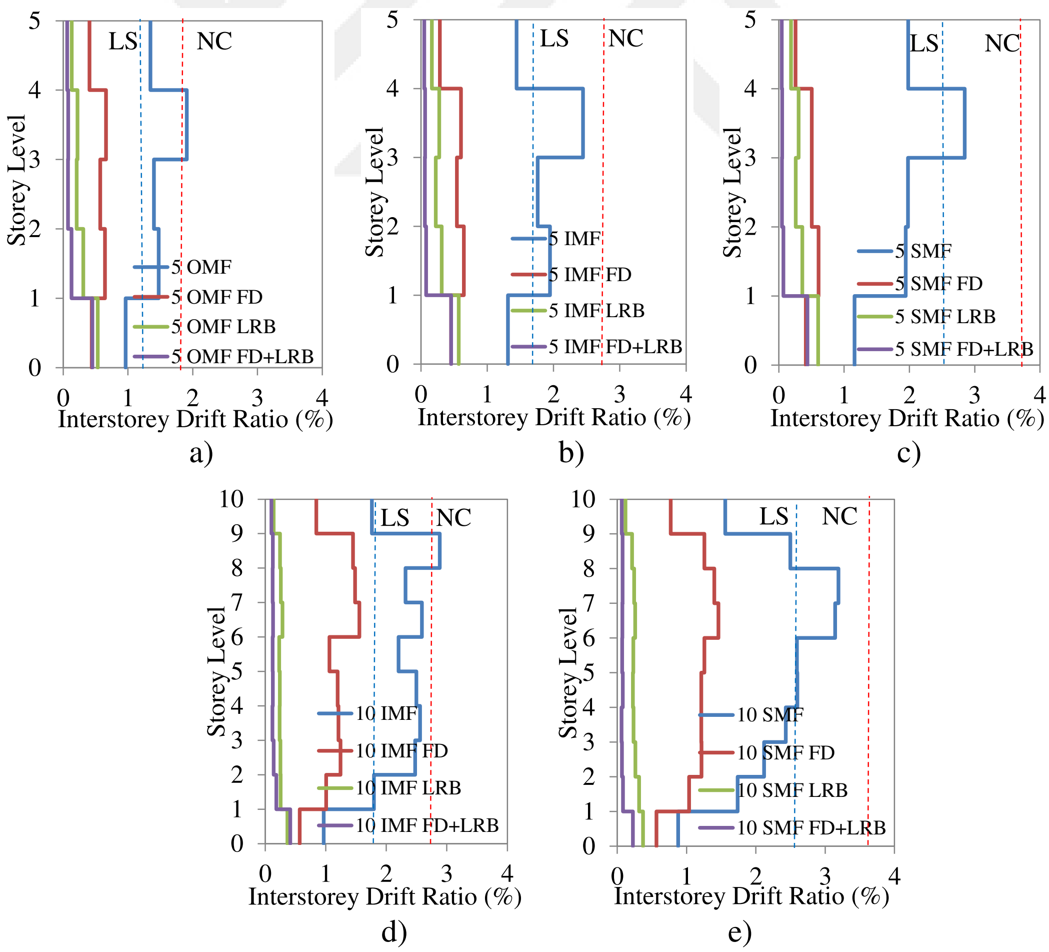

Figure 4.7 Interstorey drift ratio of 5 and 10 storey frames under Northridge earthquake. Key: LS=Life Safety, NC=Near Collapse

4.2.6 Base Shear

The base shear of the examined frames normalized by corresponding weight and it was depicted in Figure 4.8. The use of FDs slightly reduced the base shear especially 10-storey frames. For example, the lowest normalized base shear was obtained as 0.036 (142.1 kN) in case of 10 SMF with LRB under Salvador earthquake that was equal to 91.1 % reduction with respect to 10 SMF as shown in Figure 4.8(e). In addition, the reduction was about 5 % for 10-storey SMF with FD subjected to Hills and Tabas earthquakes.

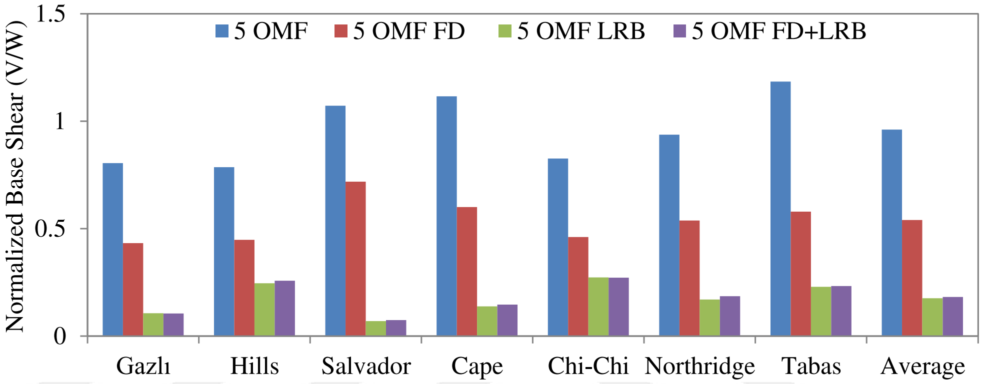

a)

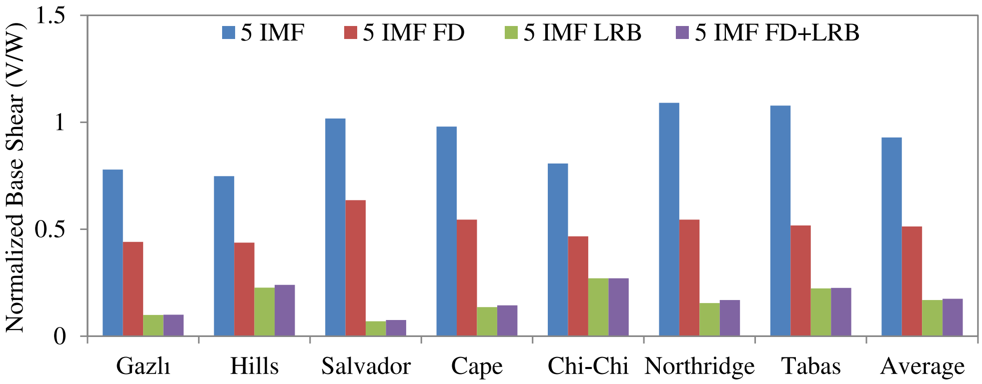

b)

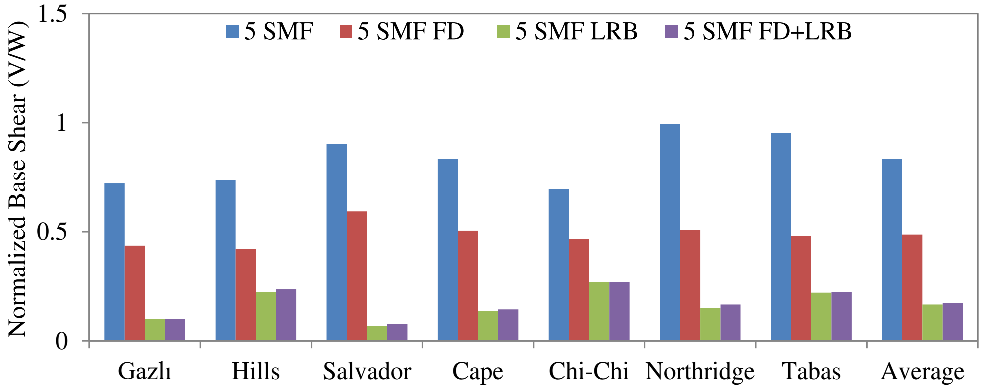

c)

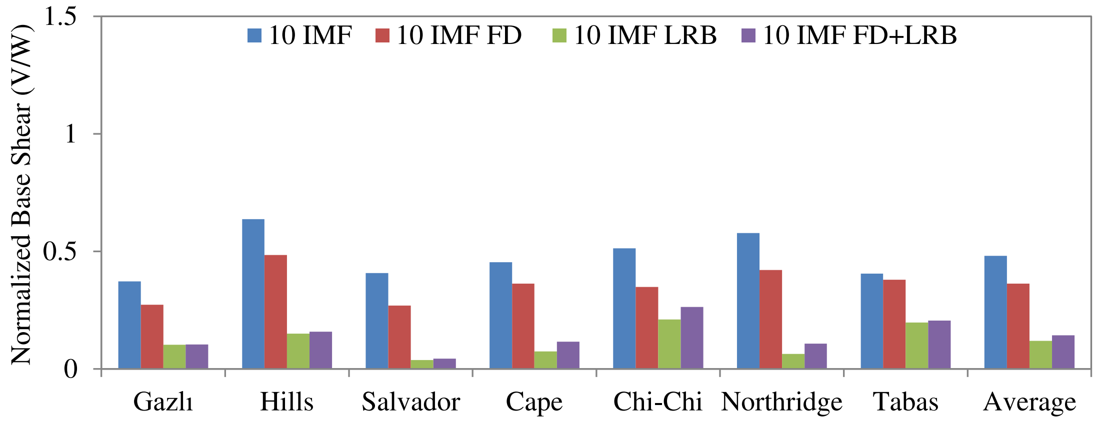

d)

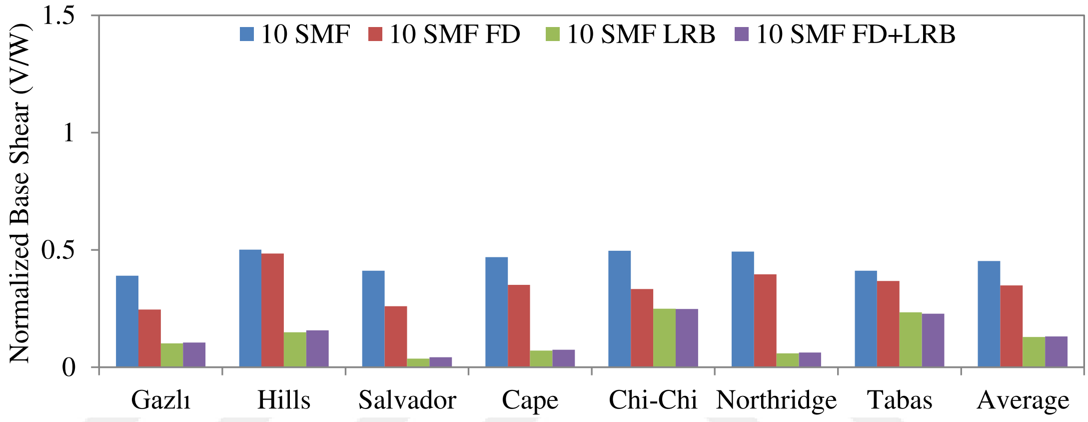

e)

Figure 4.8 Maximum base shears of 5 and 10 storey frames

On the other hand, the maximum base shear demand reduction for the frames with LRB and for the frames with both LRB and FD were more pronounced such that as seen in Tables 4.2 and 4.3; on average the reduction in the maximum base shear of 5-storey OMF equipped with both LRB and FD was 81.1%, and that of 5-storey OMF equipped with LRB was 81.7%. Similarly, for 10-storey IMF equipped with both LRB and FD, the reduction was 70.4%; and for the frame with LRB it was 75.2%; while the reduction was 71.1 and 71.7% for the SMF with both LRB and FD; and only LRB, respectively. When the base shear demand of the frames with protective systems were compared, as expected there was a great reduction in the base shear demand of the frames with LRB. As explained previously, LRB is designed to eliminate the horizontal earthquake forces by providing a layer with low horizontal stiffness, and also the attained stiffness of LRB would be less than FD. Due to this property, the combined use of FD with LRB led to similar base shear reduction with respect to LRB while the LRB dominated the base shear demand.

4.2.7 Top Storey Moment

The maximum top storey moment of all frames were given in Figure 4.9. It is clearly shown that installation of the energy dissipation systems into the original frames led to remarkable reduction on the top storey moment in each case. Indeed, the response of the top storey moment changed with the building type rather than the earthquake characteristic, number of the storey and type of the energy dissipation systems. For example, the lowest base moment was obtained as 17.47 kNm in case of 5 SMF with FD and LRB under Salvador earthquake that was equal to 85.2% reduction with respect to 10 SMF as shown in Figure 4.9(c). In addition to description of Figure 4.9, Tables 4.1 and 4.2 also showed that FDs, LRB and the combined case decreased the top storey moment as 55.7, 69.8, and 69.5% for 10-storey IMF, while 48.9, 62.8 and 60.6% for 10-storey SMF, respectively. Furthermore, it can be inferred that the response of IMF and SMF was almost same and OMF had the least moment reduction capacity.

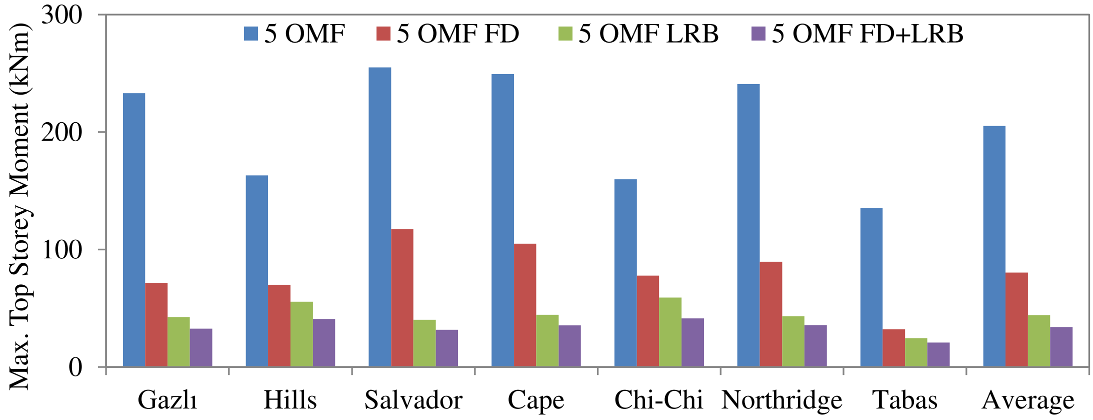

a)

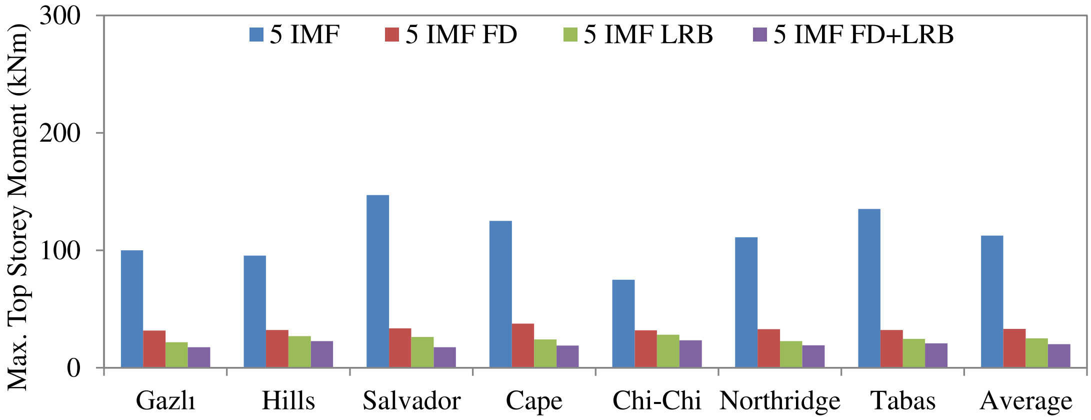

b)

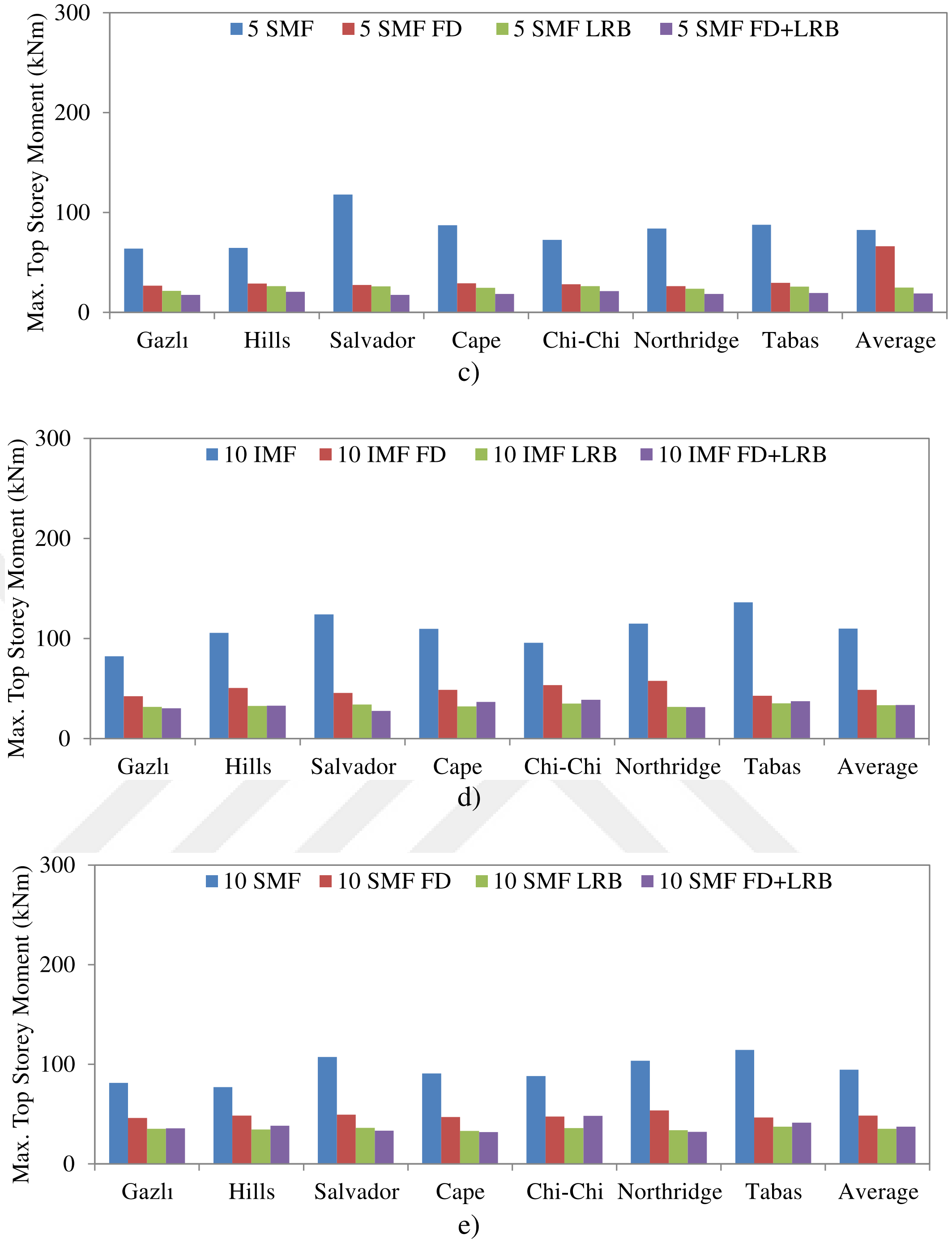

Figure 4.9 Maximum top storey moments of 5 and 10 storey frames.

4.3 Case-2 (FPB)

In this case, the seismic response of 3, 6, and 9-storey steel frames equipped with FPB systems having various properties of isolation period, (T,) effective damping ratio (ß), and yield strength to weight ratio, (Fy/W) were studied. In this regard, the behaviour of the base isolated frames were evaluated and discussed in terms of the engineering demand parameters such as isolator displacement, interstorey drift ratio, roof drift, relative displacement, absolute acceleration, base shear, base moment, hysteretic curve, and dissipated energy.

4.3.1 Isolator Displacement

The maximum isolator displacement of 3, 6, and 9-storey base isolated frames were computed in accordance with the corresponding earthquakes through the nonlinear analyses and plotted as shown in Figures 4.10, 4.11, and 4.12, respectively. It could be clearly observed that the variation of the isolation parameters had remarkably influence on the isolator displacement of the FPB by providing lateral movement demand of the base isolated frames. The isolation system having greater isolation period and effective damping ratio with the lowest yield strength ratio enabled to increase the isolator displacement demand since the lower yield strength ratio (Fy/W) produced smaller elastic stiffness (see Table 3.3).

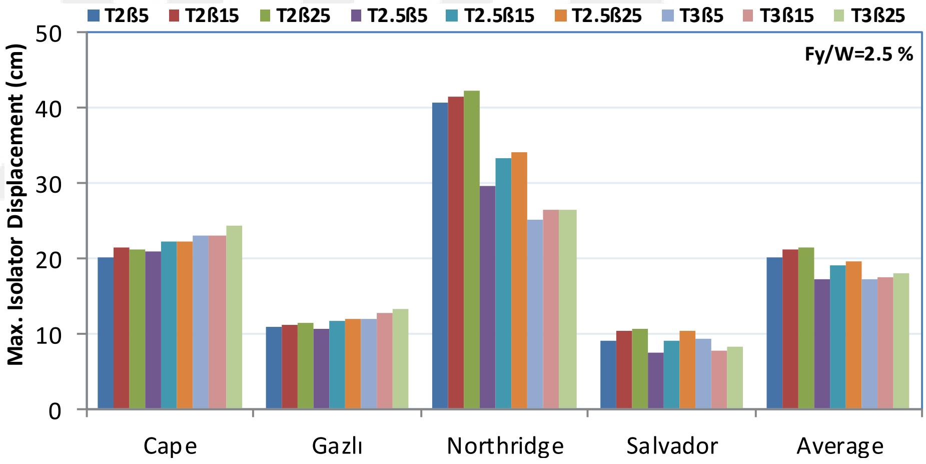

a)

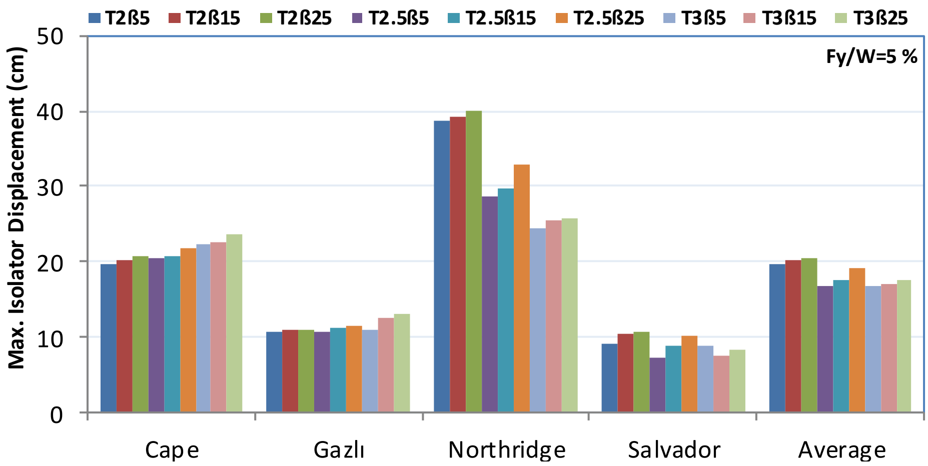

b)

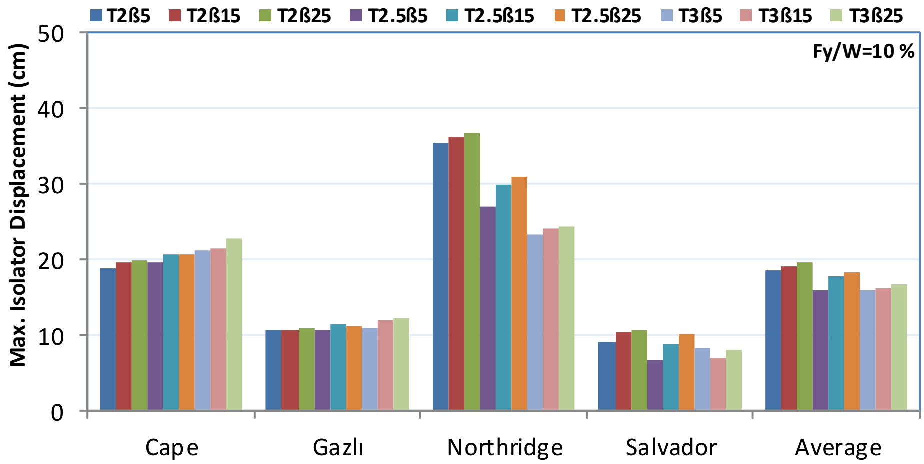

c)

Figure 4.10 Maximum isolator displacement of 3-storey frames

The greater isolation period was capable of higher flexibility on the bearing. 3-storey isolated frame was more effective than 6-storey isolated frame for the isolator displacement demand as shown in Figures 4.10 and 4.11. For example, when 3, 6, and 9-storey isolated frames were hit by Cape, Gazlı, and again Cape earthquakes, the isolation system of T3ß25FyW2.5 produced the maximum isolator displacement as 24.35, 13.76, and 22.02 cm, respectively. The effect of the isolation period on the isolator displacement can be monitored in Figures 4.10-4.12. The greatest isolation period was more favorable for 9-storey isolated frames than the other frames. The average value of the maximum isolator displacement was observed in the isolation system of T3ß5FyW2.5 as 14.12 cm. As for 3-storey base isolated frames, the isolation system having the greatest isolation period (T = 3 s) experienced the maximum isolator displacement when subjected to Cape and Gazlı earthquakes, but it was not valid for Northridge and Salvador earthquakes.

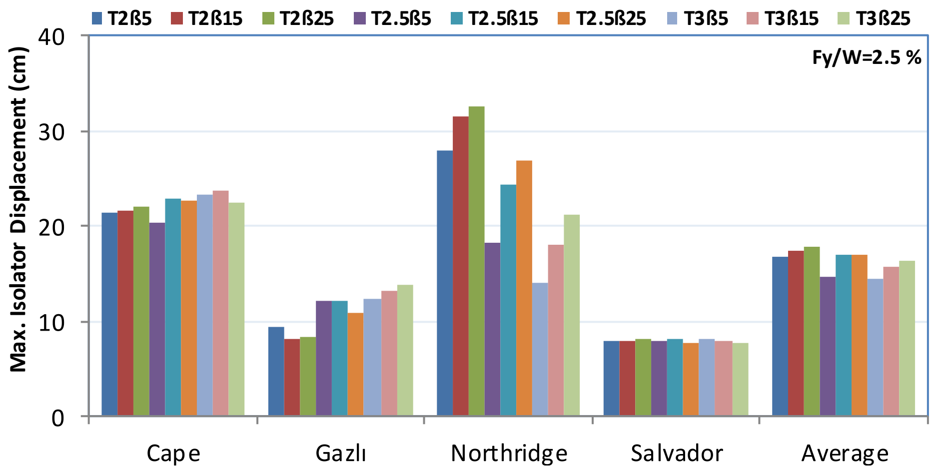

a)

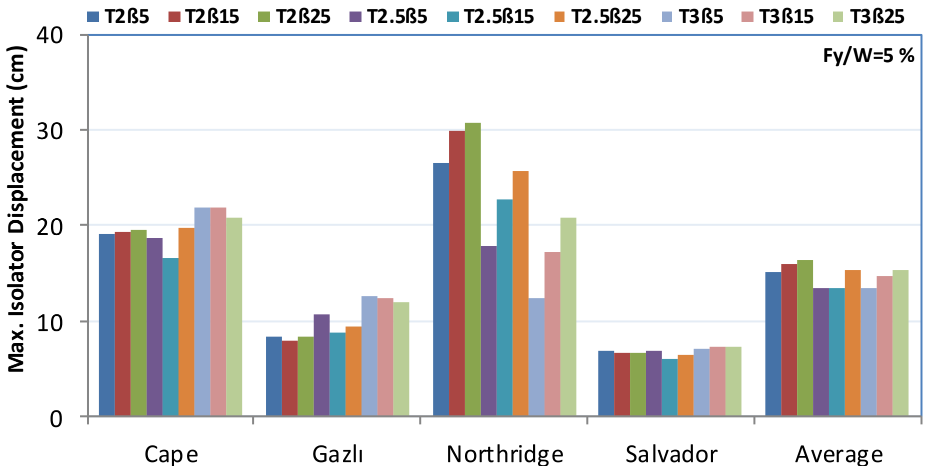

b)

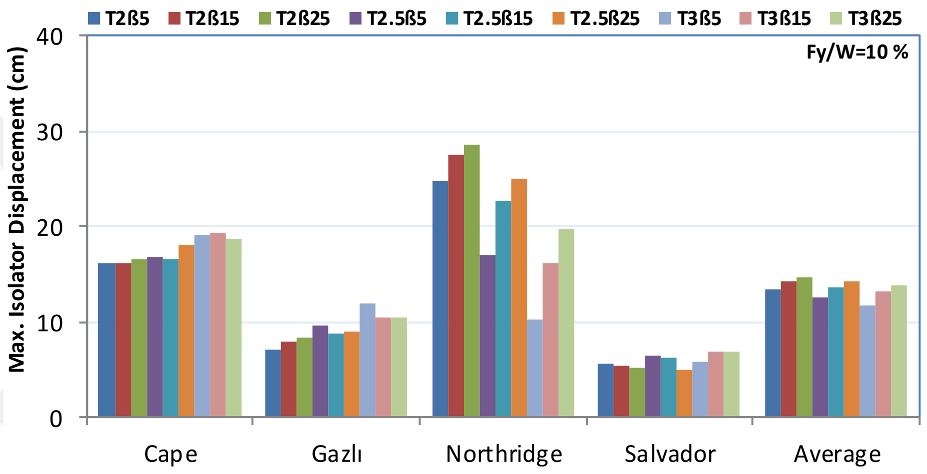

c)

Figure 4.11 Maximum isolator displacement of 6-storey storey frames

Moreover, 6 and 9-storey frames equipped with the isolation system to be found within the greatest isolation period (namely T = 3 s) that was generated the maximum isolator displacement. For example, the isolation system of T3ß15FyW2.5 and T3ß25FyW2.5 presented the maximum isolator displacement as 23.76 and 13.76 for 6-storey isolated frame under Cape and Gazlı earthquakes, respectively (see Figure 4.11(a)). Similarly, T3ß5FyW2.5 and T3ß25FyW2.5 caused the value of the maximum isolator displacement as 16.9 and 22.02 cm for 9-storey isolated frame under Gazlı and Cape earthquakes (see Figure 4.12(a)), respectively. The greater effective damping ratio generally presented the more isolator displacement, especially for 3 and 6-storey isolated frames subjected to Cape, Gazlı, and Northridge earthquakes. For example, when the effective damping ratio reached to 25 %, the maximum isolator displacement of the isolation system of T3ß25FyW2.5 occurred as 24.35 and 13.25 cm, T2ß25FyW2.5 as 42.22 cm, and T2ß25FyW5 as

10.73 cm for 3-storey isolated frame under Cape, Gazlı, Northridge, and Salvador earthquakes, respectively.

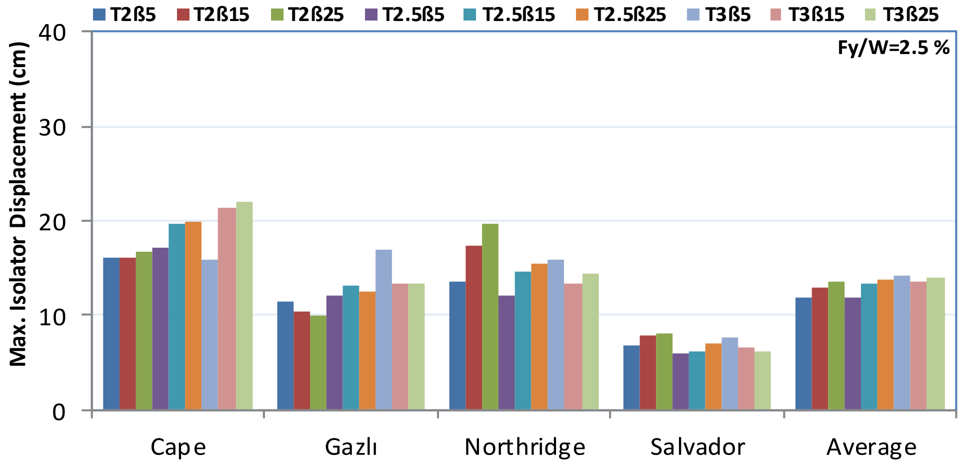

a)

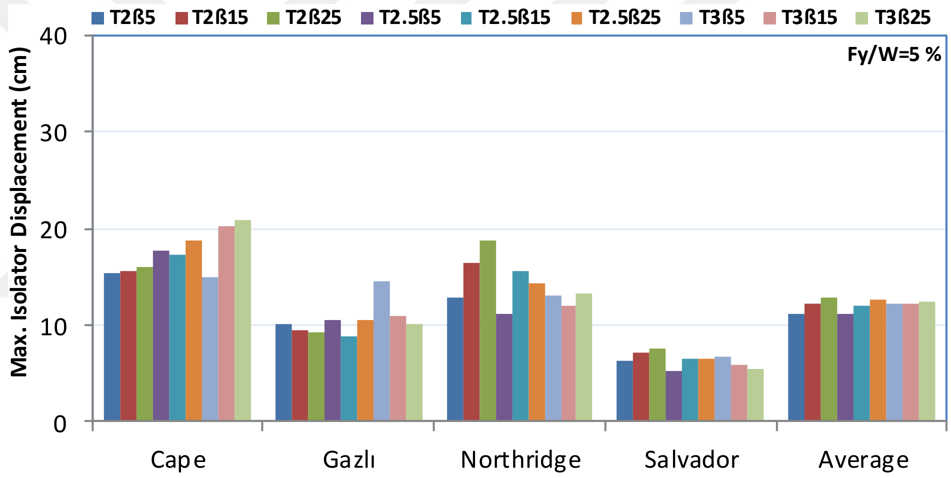

b)

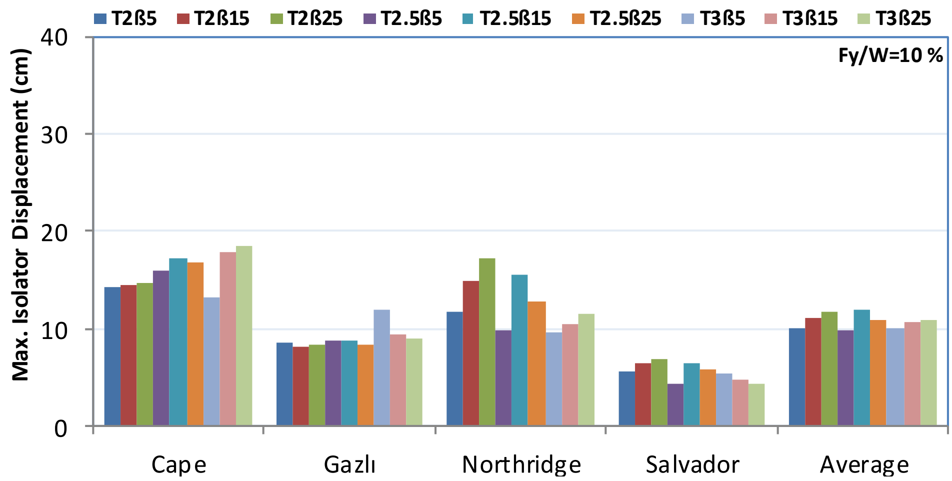

c)

Figure 4.12 Maximum isolator displacement of 9-storey storey frames

As for 6-storey isolated frame, it was occurred as 13.76 cm (T3ß25FyW2.5), 32.6 cm (T2ß25FyW2.5) under Gazlı and Northridge earthquakes, respectively. The maximum isolator displacement of 9-storey isolated frame was as 22.02 cm (T3ß25FyW2.5), 19.74 and 8.18 cm (T2ß25FyW2.5) under Cape, Northridge, and Salvador earthquakes, respectively. The moderate effective damping ratio, (namely ß = 15 %) also succeed the maximum isolator displacement as 23.76 cm (T3ß15FyW2.5) and 8.22 cm (T2.5ß15FyW2.5) for 6-storey isolated frame subjected to Cape and Salvador earthquakes, respectively. Furthermore, it was observed as 22.02 cm (T3ß25FyW2.5) for 9-storey isolated frame under Cape earthquake (see Figure 4.12(a)). Conversely, when the yield strength ratio reached to 0.10, the minimum isolator displacement was reported as 6.81 and 4.36 cm (T2.5ß5FyW10), 4.93 cm (T2.5ß25FyW10) for 3, 9, and 6-storey seismically isolated frames subjected to Salvador earthquake (see Figures 4.10(c), 4.11(c), and 4.12(c)), respectively. Among the isolation models, the average value of the maximum isolator displacement was occurred in case of Fy/W = 0.025 as 21.22 cm(T2ß15FyW2.5), 16.30 and 13.98 cm (T3ß25FyW2.5) for 3, 6, and 9-storey seismically isolated frames, respectively. Similar trend of the Fy/W on the maximum isolator displacement was observed under all earthquakes.

4.3.2 Interstorey Drift Ratio

The interstorey drift ratio is a key parameter related to the structural damage level that might be seen in a structure. Interstorey drift is calculated as the difference between displacements of the two consecutive storeys normalized by the corresponding storey height. The maximum interstorey drift ratio of the 3, 6, and 9-storey isolated frames with corresponding isolation period, effective damping ratio, and yield strength ratio under four ground motions were computed and given in Figures 4.13, 4.14, and 4.15, respectively. The variation of interstorey drift ratio under Salvador earthquake was illustrated in Figures 4.16-4.18, regarding the isolation parameters (i.e., isolation period, effective damping ratio, and yield strength ratio). Firstly, increasing the isolation period seemed to reduce the maximum interstorey drift ratio of each isolation system especially for 3 and 6-storey isolated frames (see Figures 4.13 and 4.14). For example, when the isolation period of 2 reached to 3 s and the other isolation parameters keep constant (namely, ß = 5 and

Fy/W = 2.5 %), the maximum interstorey drift ratio of 3, 6, and 9-storey isolated frames reduced from 0.92, 1.07, and 0.95 % (T2ß5FyW2.5) to 0.84, 0.62, and 0.66 % (T3ß5FyW2.5) under Salvador earthquake, respectively. The lowest value of the maximum interstorey drift ratio was observed in the isolation system of T3ß25FyW10, T2.5ß15FyW5, and T3ß5FyW2.5 as 0.67, 0.53, and 0.66 % for 3, 6, and 9-storey isolated frames under Gazlı, again Gazlı, and Salvador earthquakes, respectively (see Figures 4.13(c), 4.14(b), and 4.15(a)). Secondly, the use of the greater effective damping ratio (as 15 and 25 %) typically resulted in lower interstorey drift ratio. For example, the lowest interstorey drift ratio was occurred as 0.78 % in the isolation system of T3ß25FyW5 (under Cape earthquake), as 0.67 % T2ß25FyW10 (under Salvador earthquake), as 0.67 % T3ß25FyW10 (under Gazlı earthquake) for 3-storey isolated frame as shown in Figure 4.13.

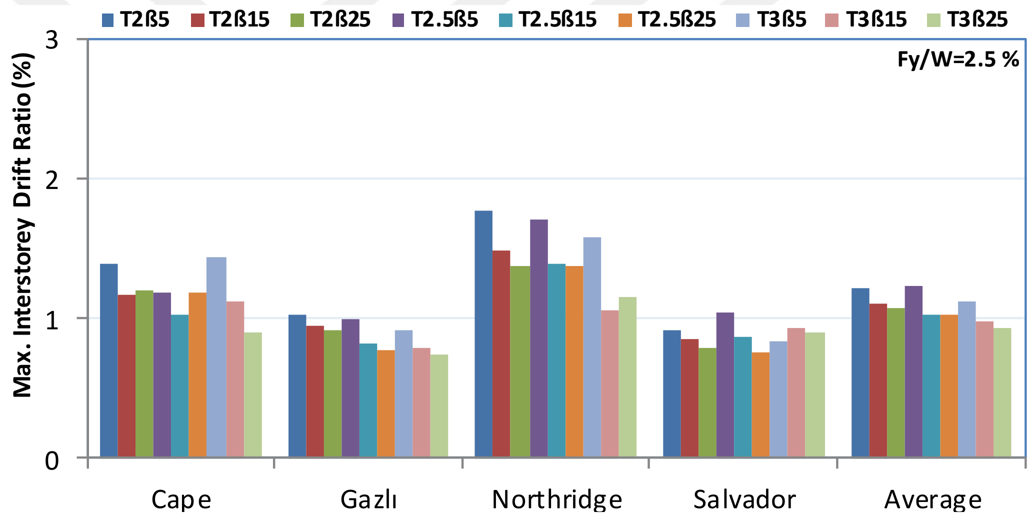

a)

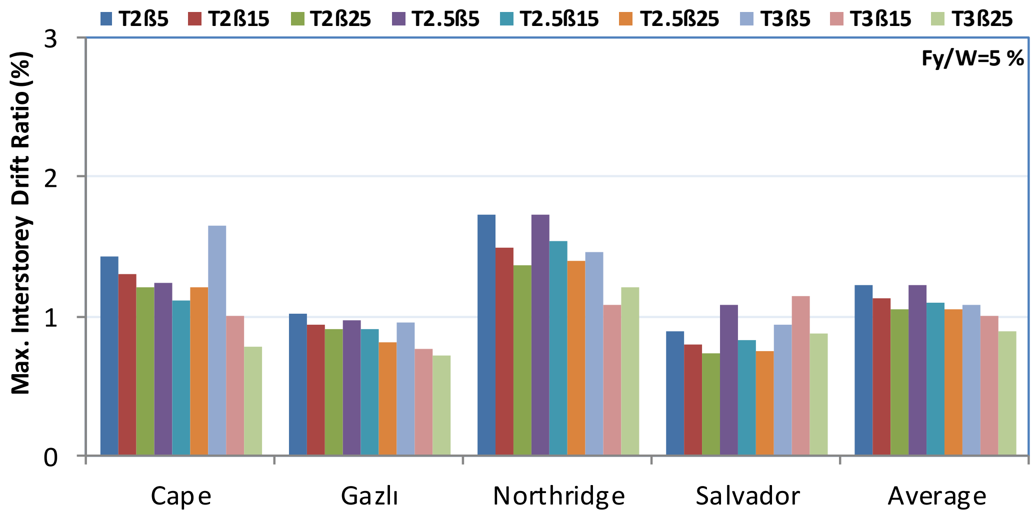

b)

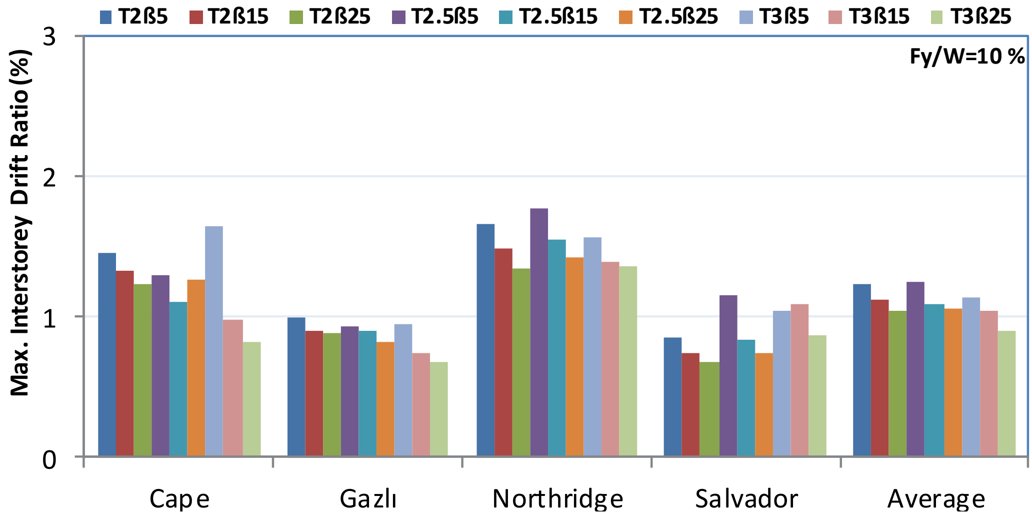

c)

Figure 4.13 Maximum interstorey drift ratio of 3-storey storey frames

As for 6-storey isolated frame, the isolation system having the greater effective damping ratio achieved the lowest interstorey drift ratio as 1.08 % T2.5ß25FyW2.5 (under Cape earthquake), 0.53 % T2.5ß15FyW5 (under Gazlı earthquake), 1.52 % T3ß25FyW5 (under Northridge earthquake) as shown in Figure 4.14. In the isolation system of T3ß15FyW2.5 (under Cape earthquake), T2ß25FyW10 (under Gazlı earthquake), T2.5ß25FyW2.5 (under Northridge earthquake) obtained the lowest interstorey drift ratio as 1.21, 0.83, and 1.71 % for 9-storey isolated frame as shown in Figure 4.15. An example of exception is ß = 5 % isolation system of T3ß5FyW2.5 which resulted in slightly the lowest interstorey drift ratio as 0.62 and 0.66 % for 6 and 9-storey isolated frames under Salvador earthquake (see Figures 4.14(a) and 4.15(a)).

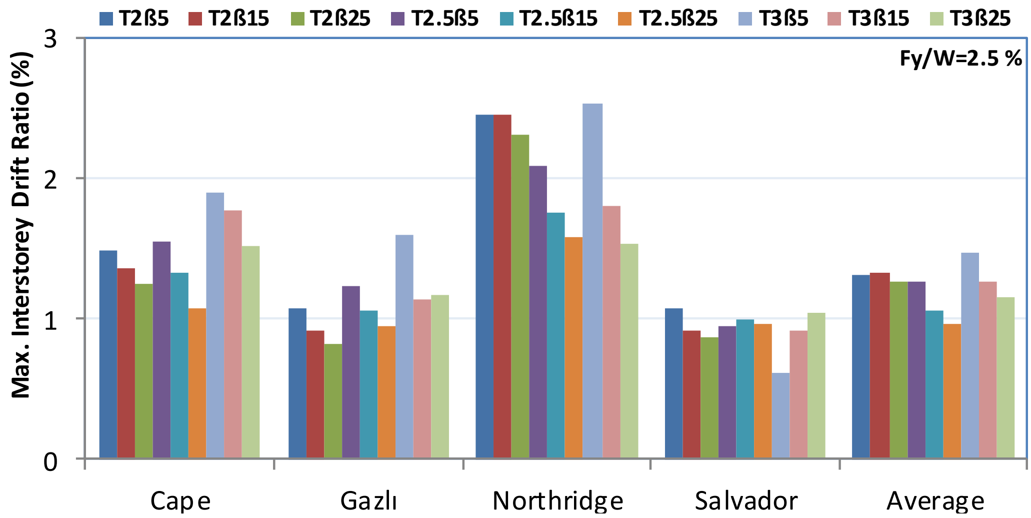

a)

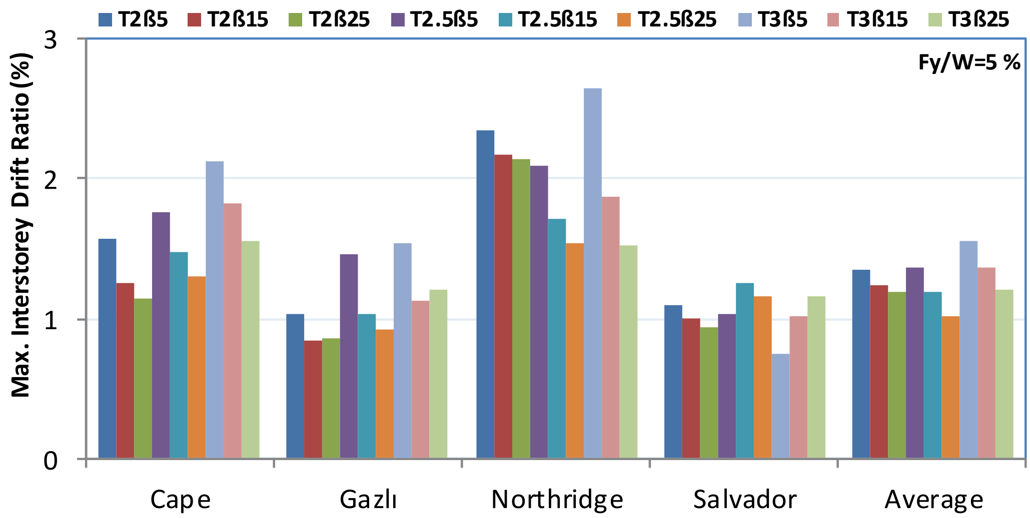

b)

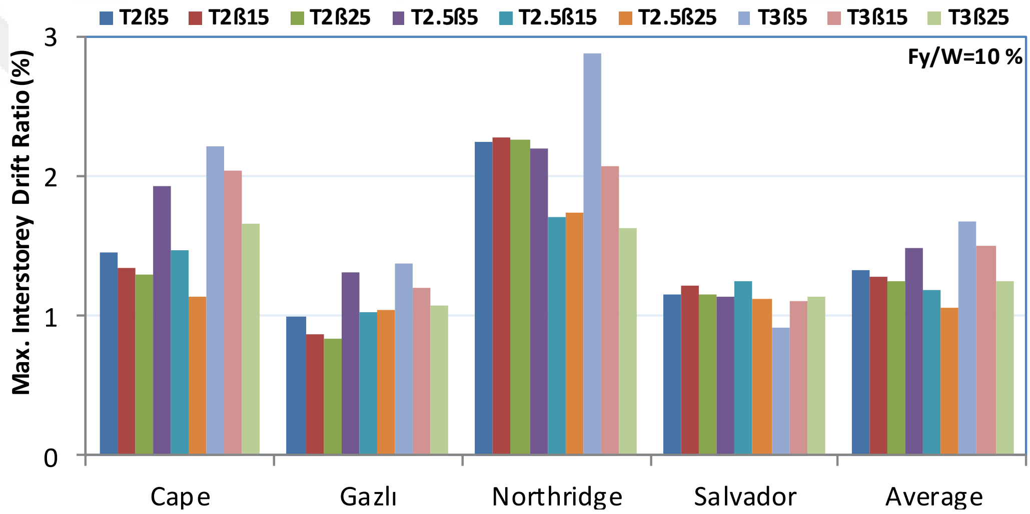

c)

Figure 4.14 Maximum interstorey drift ratio of 6-storey frames

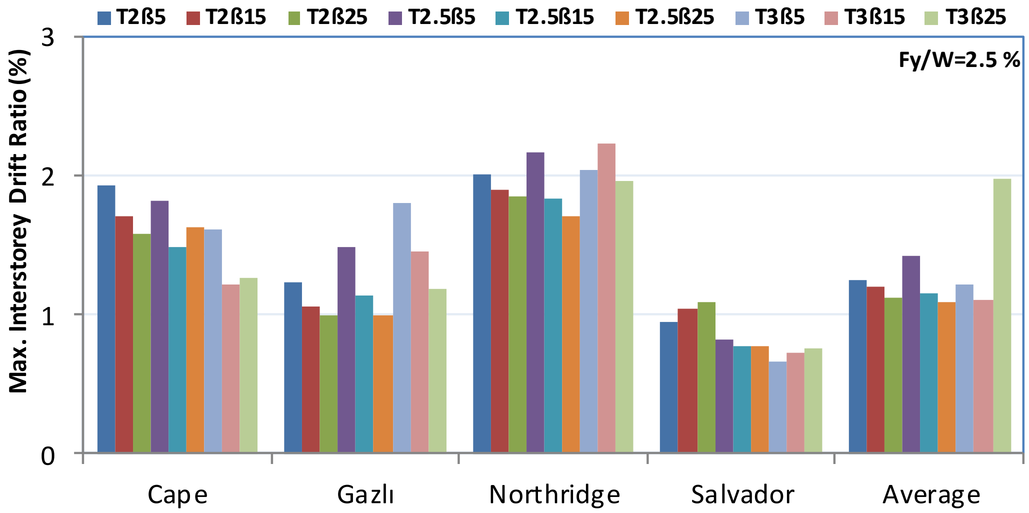

a)

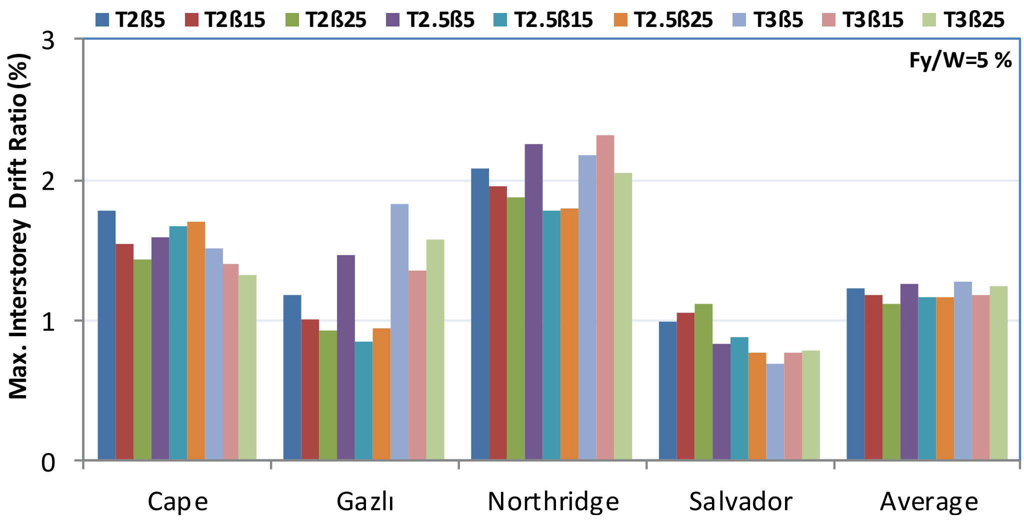

b)

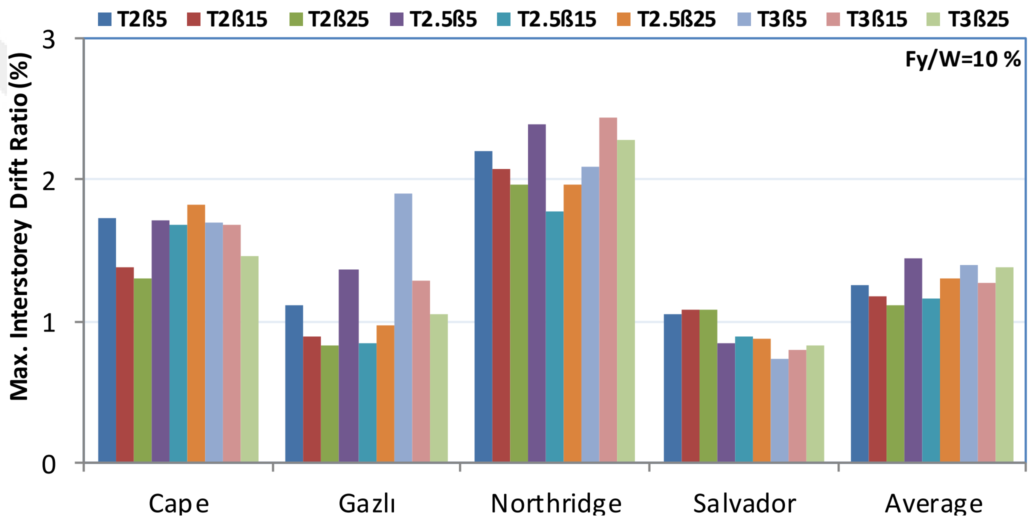

c)

Figure 4.15 Maximum interstorey drift ratio of 9- storey frames

Moreover, the isolation systems having moderate and the greatest effective damping ratio tended to more uniform interstorey drift ratio distribution especially when Fy/W = 2.5 (see Figures 4.16-4.18). Similarly, it occurred as 0.83 % (T2ß25FyW10) in case of the greatest Fy/W ratio for 9-storey isolated frame subjected to Gazlı earthquake (see Figure 4.15(c)), whereas 1.21 % (T3ß15FyW2.5), 1.71 % (T2.5ß25FyW2.5), and 0.66 % (T3ß5FyW2.5) in case of the lowest Fy/W ratio for 9-storey isolated frame subjected to Cape, Northridge, and Salvador earthquakes, respectively as shown in Figure 4.15(c). The most uniform interstorey drift ratio distribution observed when 9-storey frame equipped with the isolation system having the greatest isolation period and greater effective damping ratio as shown in Figures 4.16-4.18. Furthermore, the greatest, lowest, and again lowest level of Fy/W (namely, 10 and 2.5 %) presented the most uniform distribution for 9-storey isolated frames (see Figures 4.16-4.18), respectively. When compared to other isolation systems, the lowest interstorey drift ratios were achieved in Figures 4.16(a), 4.17(a), and 4.18(a) for 9-storey isolated frames.

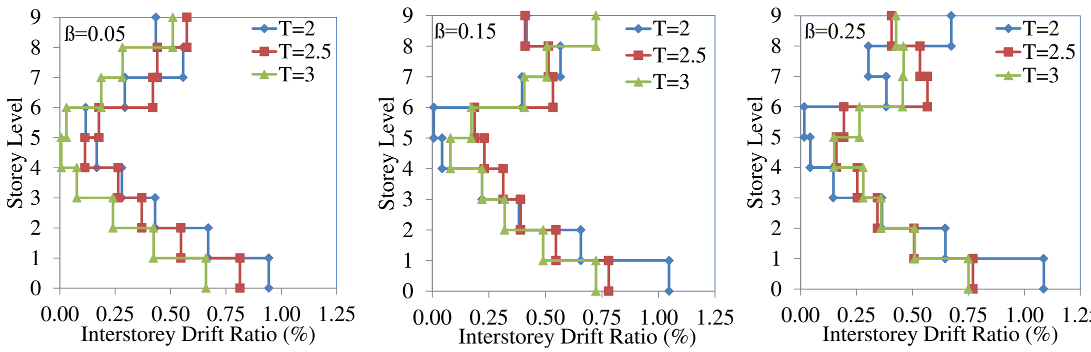

a) b) c)

Figure 4.16 Variation of the interstorey drift ratio against storey height of 9-storey isolated frames under Salvador earthquake for Fy/W=0.025

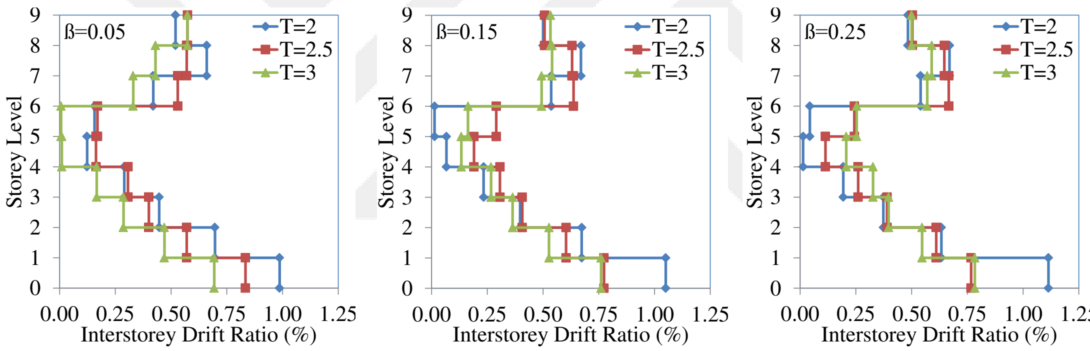

a) b) c)

Figure 4.17 Variation of the interstorey drift ratio against storey height of 9-storey isolated frames under Salvador earthquake for Fy/W=0.05

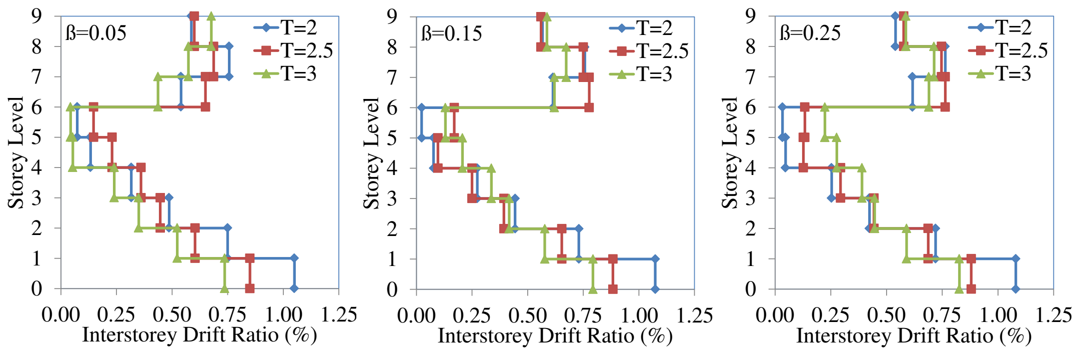

a) b) c)

Figure 4.18 Variation of the interstorey drift ratio against storey height of 9-storey isolated frames under Salvador earthquake for Fy/W=0.10

4.3.3 Roof Drift Ratio

The maximum roof displacement demand of the 3, 6, and 9-storey base isolated frames under four ground motions were determined and normalized by the building height so the effect of the shape factor was removed. The obtained roof drift ratios of 3, 6, and 9-storey isolated frames subjected to four earthquakes and average of them were given in Figures 4.19, 4.20, and 4.21, respectively. It could be clearly seen that the frames supported with the FPB having different isolation parameters (i.e., the isolation period T, effective damping ratio ß, and yield strength parameters ratio Fy/W) had successfully reduced the roof drift demand, but ß and Fy/W were more decisive than T. In addition to isolation parameters, the characteristic of the earthquakes and number of storeys had notable effect on the variation of the roof drift ratio. For example, the greater isolation period was convenient for reduction of the roof drift ratio, but an example of exception testified under Northridge earthquake. The isolation system of T2.5ß25FyW10 and T3ß25FyW10 presented the lowest roof drift as 1.75 and 3.72 under Gazlı and Northridge earthquakes for 3-storey isolated frame (see Figure 4.19(c)), respectively. It was for T2.5ß25FyW10 as 1.95 and 2.45 (under Cape and Northridge earthquakes), T3ß5FyW2.5 as 0.90 (under Salvador earthquake) for 6-storey isolated frame (see Figure 4.20(c) and 4.20(a)), furthermore, T3ß15FyW2.5 as 1.69 (under Cape earthquake) and T3ß5FyW2.5 as 1.68 and 0.55 (under Northridge and Salvador earthquakes) for 9-storey isolated frame (see Figure 4.21(c)). Conversely, the isolation systems having the lowest isolation period with the greatest yield strength ratio and effective damping ratio rarely, if ever, introduced the lowest roof drift. For instance, T2ß25FyW10 had as 3.06 and 1.65 for 3-storey isolated frame under Cape and Salvador earthquakes (see Figure 4.19(c)) and as 0.92 for 9-storey isolated frame under Gazlı earthquake (see Figure 4.21(c)). T2ß25FyW2.5 had as 1.02 for 6-storey isolated frame under Gazlı earthquake (see Figure 4.20(a)). The greater effective damping ratio provided remarkable reduction on the maximum roof drift, irrespective of building storey and characteristic of the earthquakes. For example, when the effective damping ratio increased from 5 to 25 %, (keep the other parameters constant, as T = 2.5 s and Fy/W = 10 %), the roof drift ratio decreased from 1.92 to 1.75 for 3-storey isolated from under Gazlı earthquake (see Figure 4.19(c)).

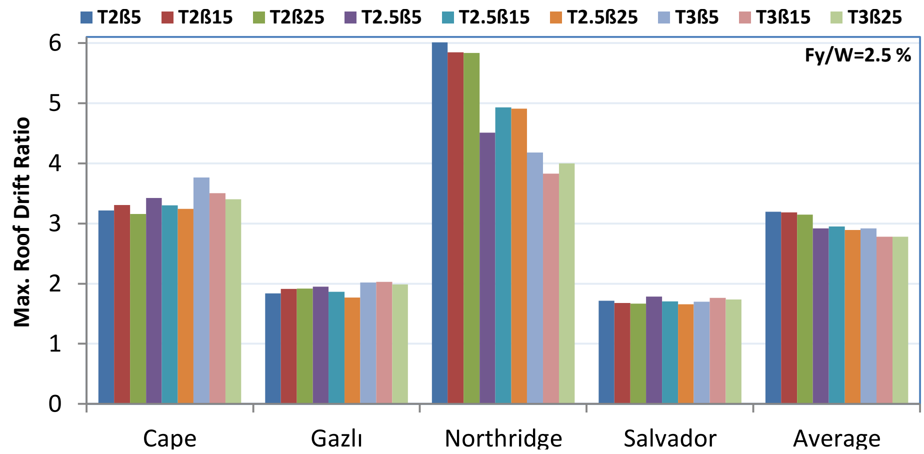

a)

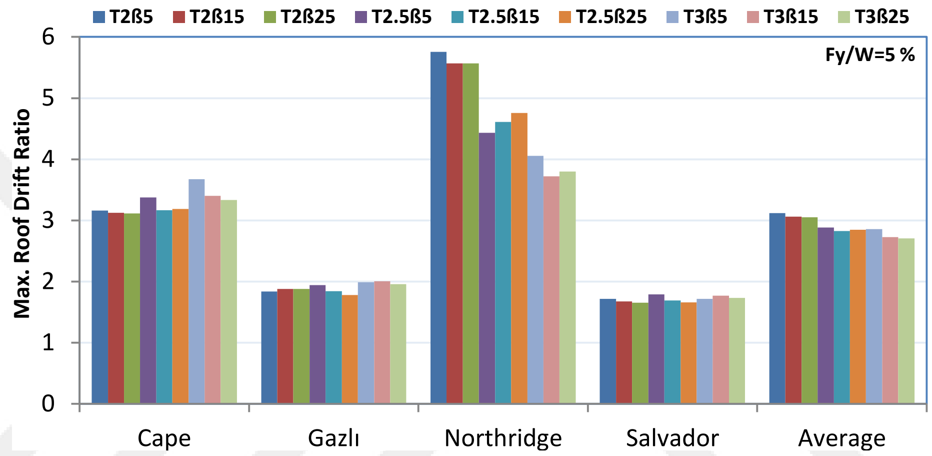

b)

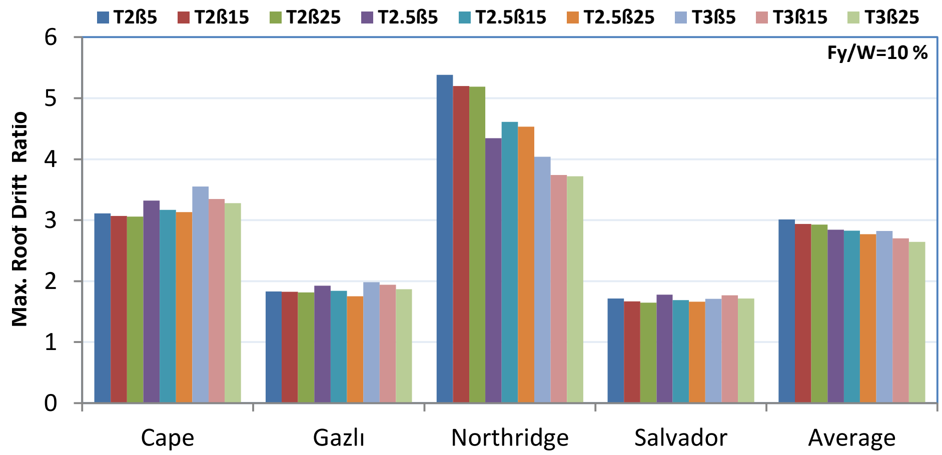

c)

Figure 4.19 Maximum roof drift ratio of 3-storey frames

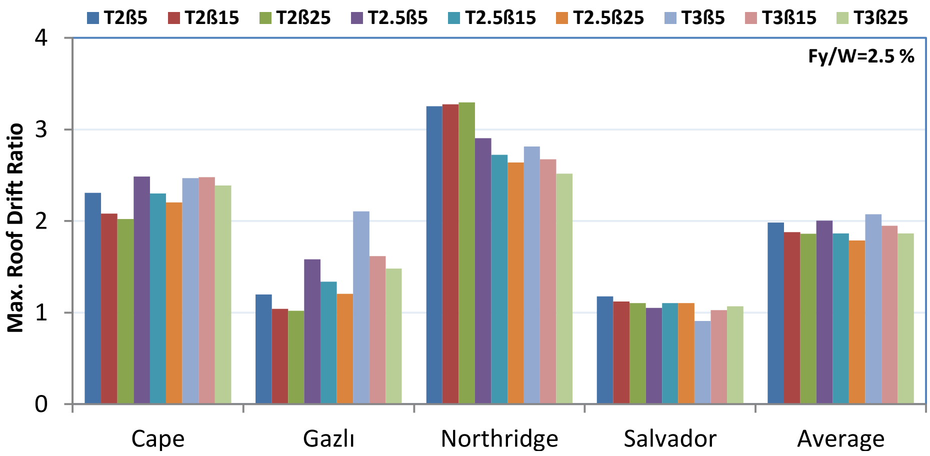

a)

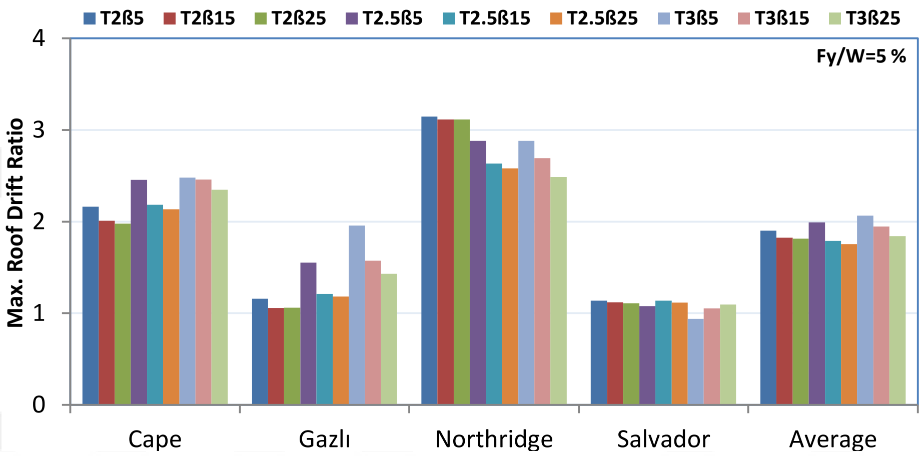

b)

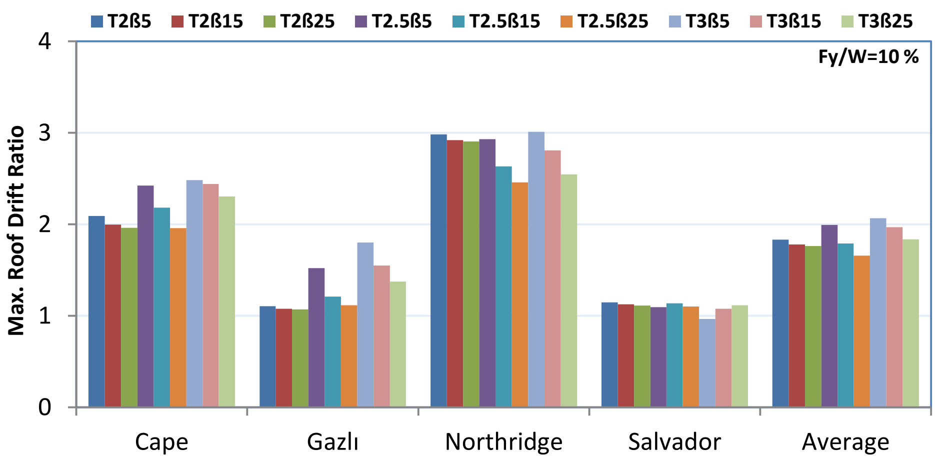

c)

Figure 4.20 Maximum roof drift ratio of 6-storey frames

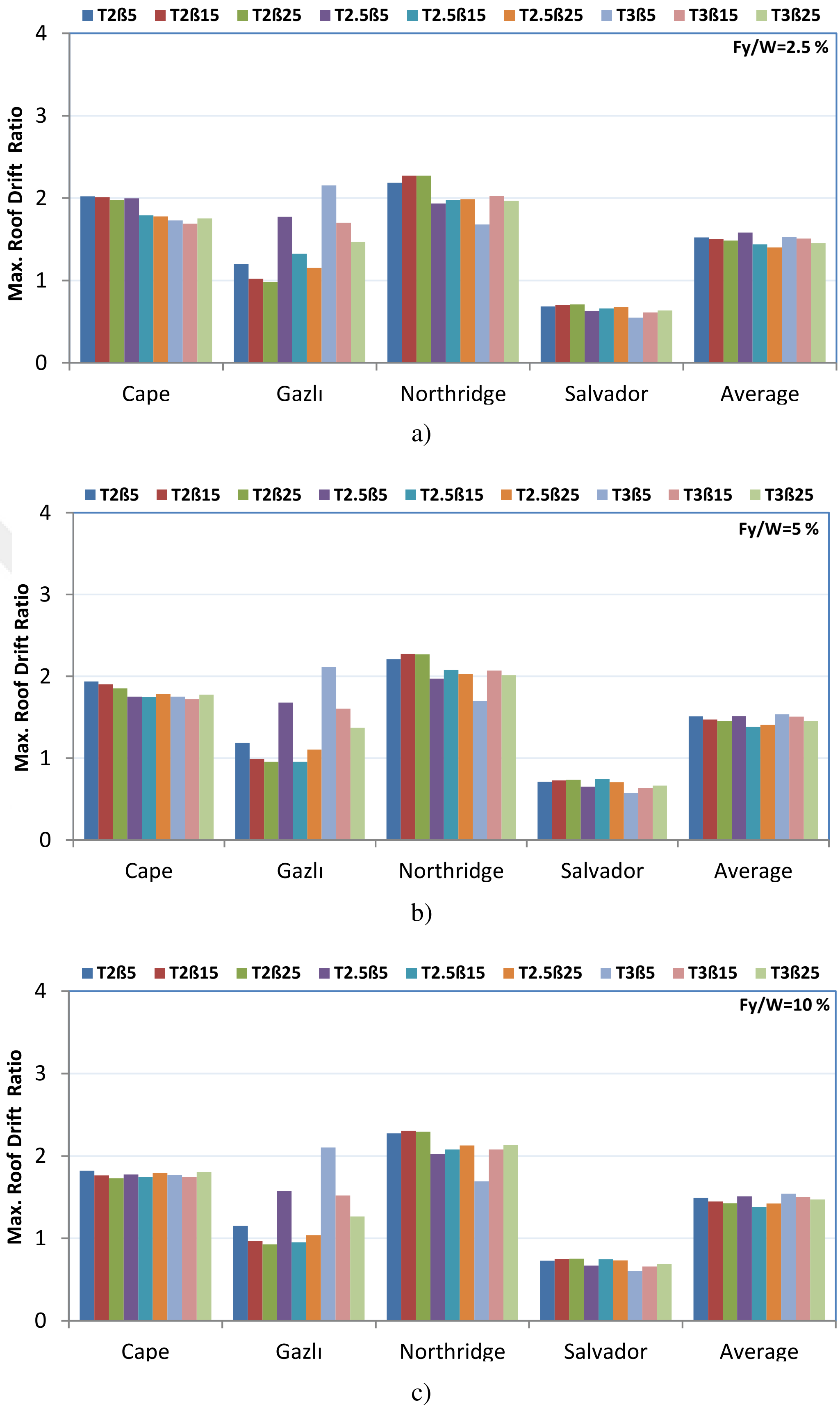

Figure 4.21 Maximum roof drift rati of 9-storey frames

Similarly, the roof drift decreased from 2.43 to 1.96, and 2.93 to 2.45 for 6-storey isolated from under Cape and Northridge earthquakes (see Figure 4.20(c)), respectively. Moreover, the lowest average roof drift of 2.65, 1.66, and 1.38 experienced in the isolation system of T3ß25FyW10, T2.5ß25FyW10, and T2.5ß15FyW10 for 3, 6, and 9-storey isolated frames (see Figure 4.19(c), 4.20(c), and 4.21(c)), respectively. The isolation system having greater yield strength ratio had lower roof drift demand, especially for 3-storey isolated frame demand, irrespective of the characteristic of earthquakes (see Figure 4.19(c)). For example, when 3-storey frame equipped with T3ß25FyW10 instead of T3ß25FyW2.5 and subjected to Northridge earthquake, it was decreased the roof drift from 4.0 to 3.72. As for 6-storey isolated frame, the isolation system of T2.5ß25FyW10 enabled to reduce the roof drift from 2.20 to 1.96 with respect to T2.5ß25FyW2.5 under Cape earthquake. However, the lowest yield strength ratio is also effective only for 9-storey isolated frame subjected to Cape, Northridge, and Salvador earthquakes for the isolation system of T3ß15FyW2.5, T3ß5FyW2.5, and again T3ß5FyW2.5, respectively (see Figure 4.21(a)).

4.3.4 Relative Displacement

The relative displacements can be determined as the difference between the roof and base displacement of frames, therefore it can be accepted as appreciable parameter in the seismic response evaluation of the frames. The maximum relative displacements of 3, 6, and 9-storey base isolated frames were computed accordance with the corresponding earthquakes through the nonlinear analysis (see Figures 4.22, 4.23, and 4.24). It could be clearly observed that the base isolated frames with different isolation parameters had remarkably improved the relative displacement. Since the assigned stiffness of the isolator is low, the model having greater period and lower Fy/W easily enables to horizontal flexibility and provides also lateral movement of the structure (see Table 3.3), thus FPB effectively reduced the relative displacement. The increase of the isolation period (namely from 2 to 2.5 and 3 s) effectively culminated in mitigation of the maximum relative displacement. For example, when the effective damping ratio and yield strength ratio were constant (namely 15 and 5 %, respectively) and the isolation period increased from 2 to 3 s, the relative displacement decreased from 10.78 to 7.99 cm, 26.16 to 17.71 cm for 3 and 6-storey isolated frame under Northridge earthquake (see Figures 4.22(b) and 4.23(b)), respectively.

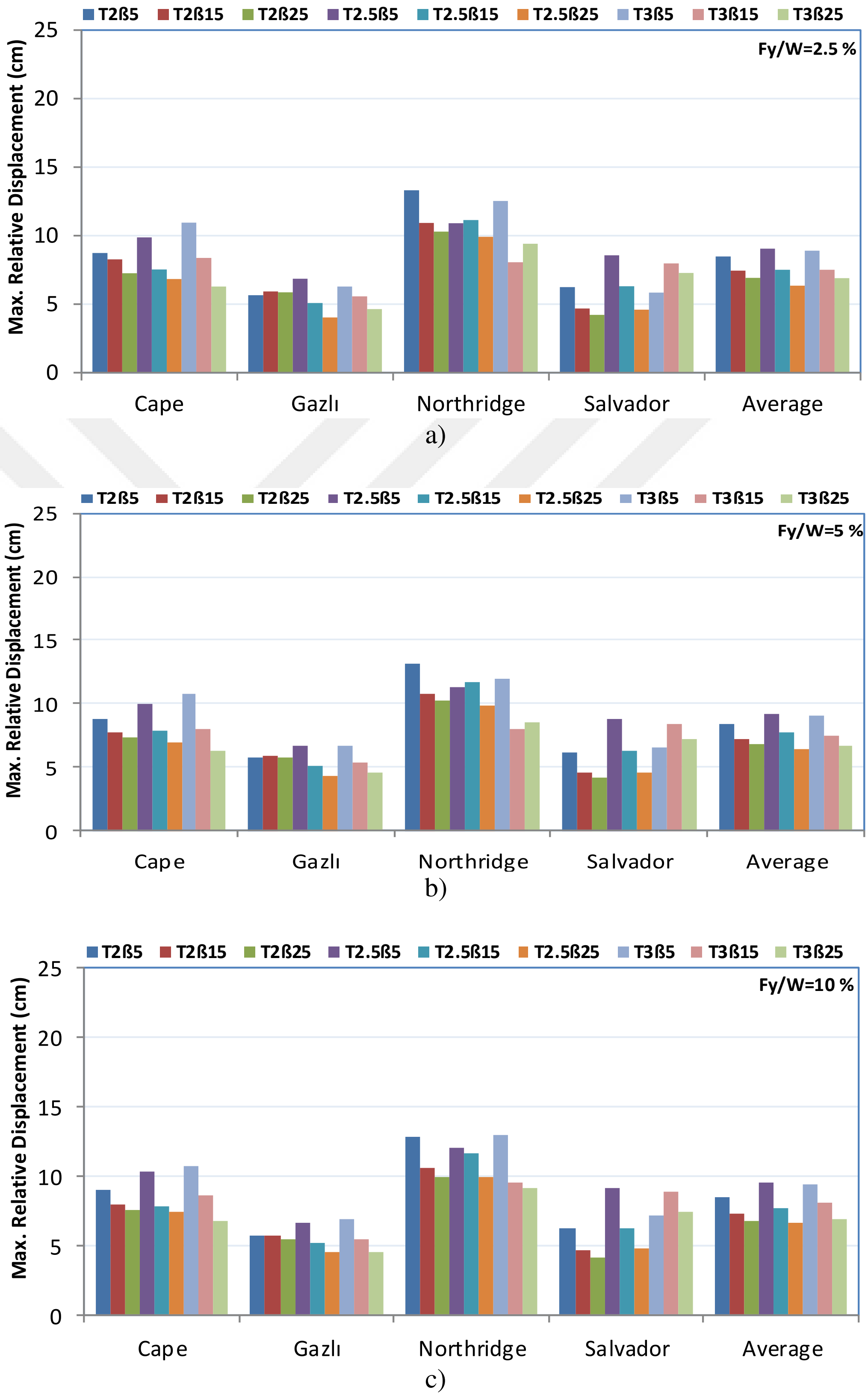

Figure 4.22 Maximum relative displacements of 3-storey frames

Similarly, the increase of the isolation period from 2 to 3 s decreased the maximum relative displacement from 37.12 to 27.22 cm (see Figure 4.24(a)) for 9-storey isolated frame under Northridge earthquake when the effective damping and yield strength ratios were constant (as 5, 2.5 %, respectively). The variation of the effective damping ratio remarkably affected the relative displacement demand especially a certain value that was also steady on the reduction of the relative displacement. For example, 25 % of ß is very effective for the reduction of the relative displacement demand of 3-storey isolated frame under Cape, Gazlı, Northridge, and Salvador earthquakes, 6 and 9-storey isolated frames under Cape and Gazlı earthquakes as well. 15 % of ß was decisive for 3 and 6-storey isolated frames under Northridge earthquakes, and 5 % of ß can be only esteemed for 9-storey isolated frame under Northridge and Salvador earthquakes.

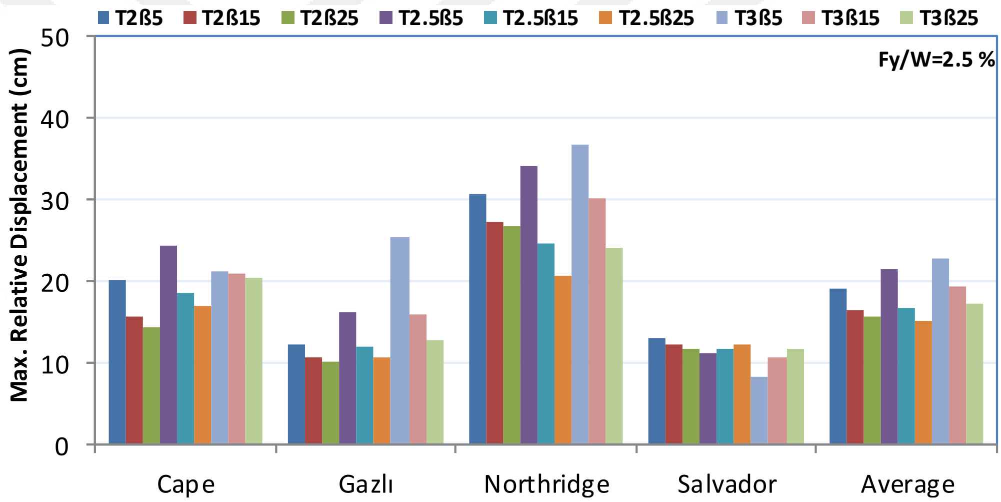

a)

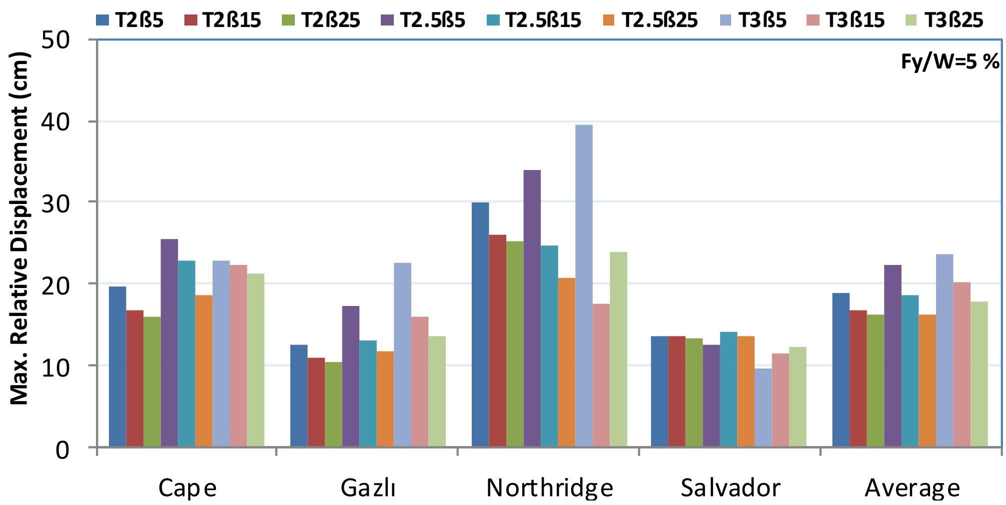

b)

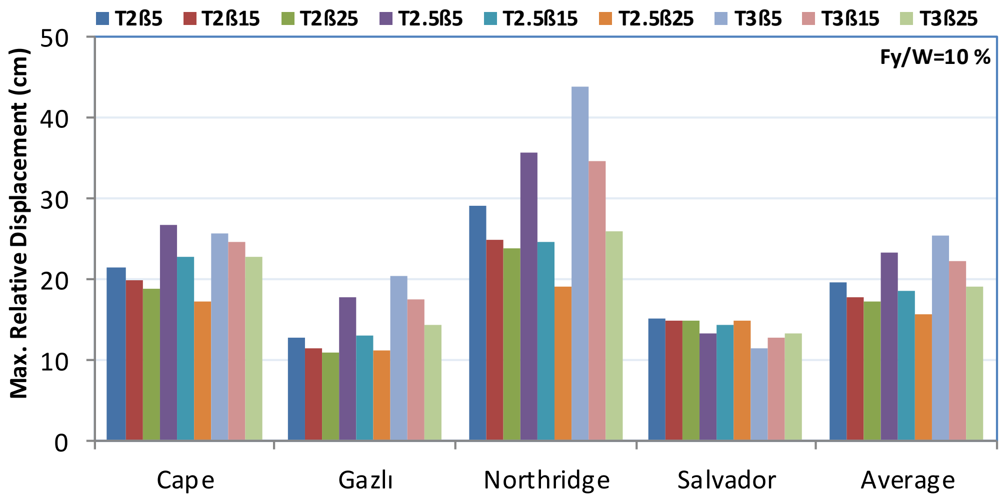

c)

Figure 4.23 Maximum relative displacements of 6-storey frames

Hence, the utilization of the greater value of the effective damping ratio in the isolation systems contributed to the relative displacement reduction as 6.81, 15.13, and 35.05 cm that can be monitored in the average maximum relative displacement of 3, 6, and 9-storey frames with T2ß25FyW10, T2.5ß25FyW2.5, and T2.5ß15FyW10, respectively (see Figures 4.22(c), 4.23(a), and 4.24(c)). The effect of the yield strength ratio on the relative displacement can be observed in Figures 4.22-4.24. The isolation system of T3ß25FyW5, T3ß15FyW5, and T2ß25FyW5 having moderate yield strength ratio (namely 5 %) emphasized the relative displacement as 6.24, 7.99, and 4.15 cm for 3-storey isolated frame under Cape, Northridge and Salvador earthquakes (see Figure 4.22(b)).

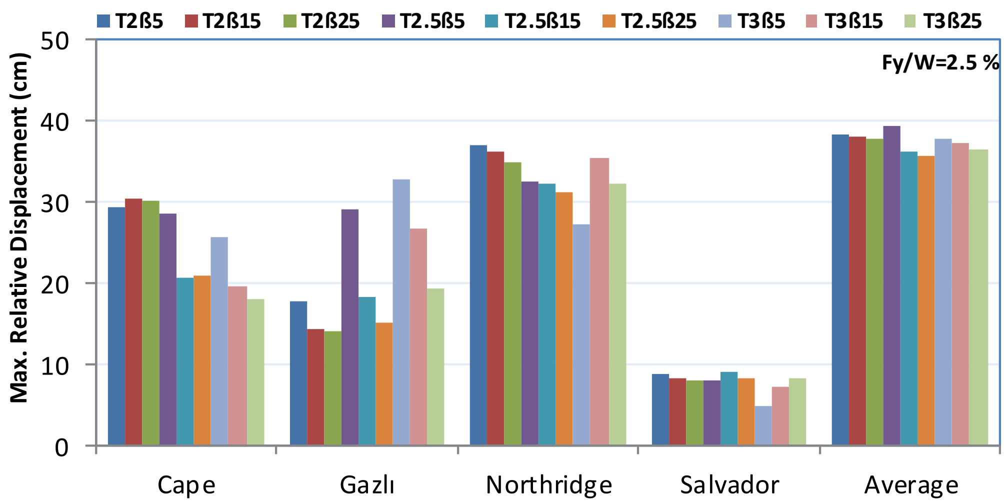

a)

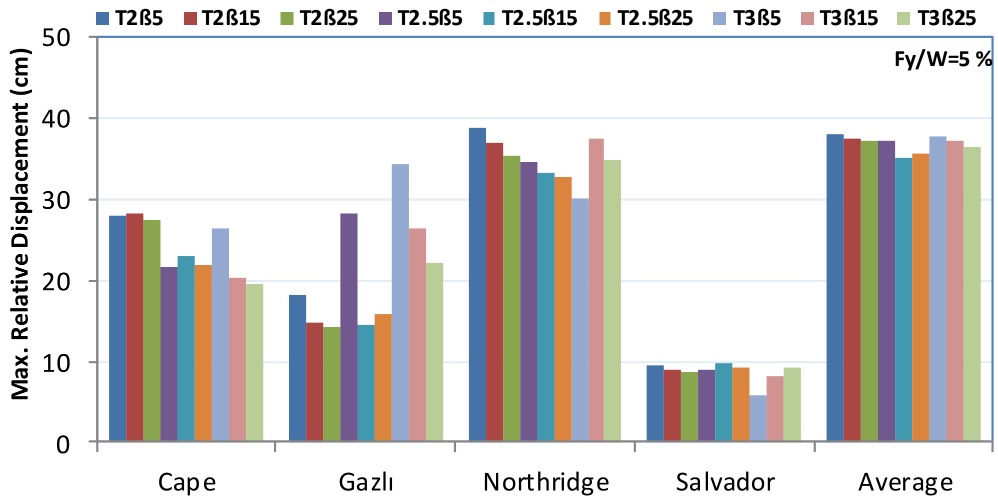

b)

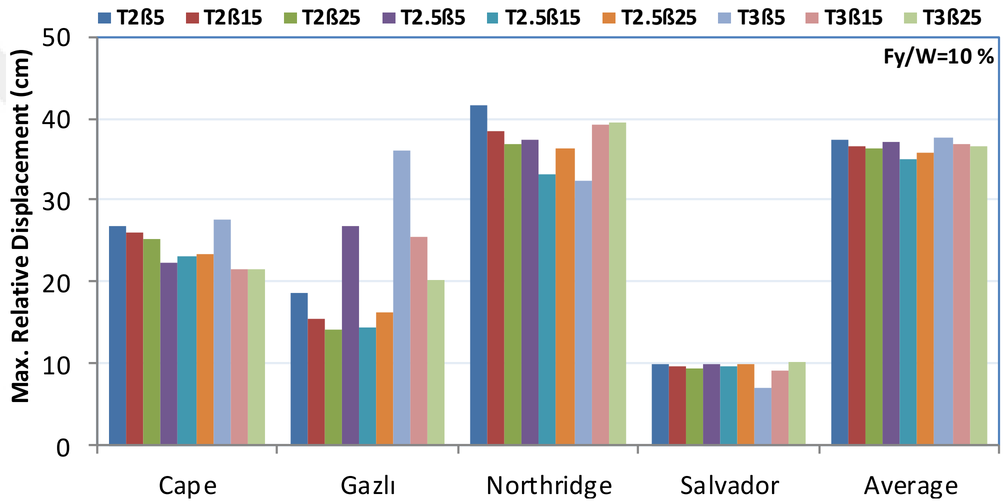

c)

Figure 4.24 Maximum relative displacements of 9-storey frames

As for 6 and 9-storey isolated frame, the lower yield strength ratio exhibited the lowest relative displacement for all earthquakes. For example, the isolation system having the yield strength ratio of 2.5 % (Cape, Gazlı, and Salvador earthquakes) and 5 % (Northridge earthquake) for 6-storey isolated frame, furthermore, 2.5 % for 9-storey isolated frame under all earthquakes provided the lowest relative displacement (see Figures 4.23 and 4.24).

4.3.5 Absolute Acceleration

The corresponding maximum absolute acceleration values of the frames with the isolation system for all earthquakes can be observed in Figures 4.25-4.27. In addition, the variations of the absolute accelerations versus storey height under Salvador earthquake were illustrated in Figures 4.28-4.30. The absolute acceleration was affected by the variation of the isolation parameters. Firstly, the moderate and greatest isolation period (namely 2.5 and 3 s) successfully exhibited the lowest absolute acceleration for nearly whole isolation systems of 3, 6, and 9-storey frames under all earthquakes. The isolation system of T3ß25FyW2.5 presented the lowest value of the maximum absolute acceleration of 2.43 m/s^2 for 3-storey isolated frame under Gazlı earthquake, 3.36 and 3.01 m/s^2 for 6-storey isolated frame under Cape and Northridge earthquakes, (see Figures 4.25(a) and 4.26(a)), respectively. The lowest value of the maximum absolute acceleration of 9-storey isolated frame under Gazlı earthquake reported as 2.85 m/s^2 for the isolation system of T2.5ß25FyW2.5 (see Figures 4.27(a)).

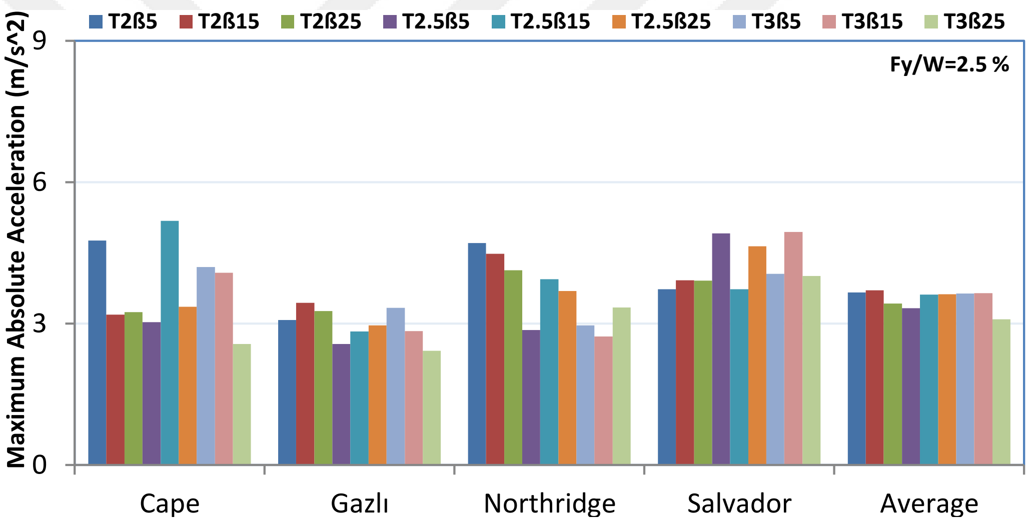

a)

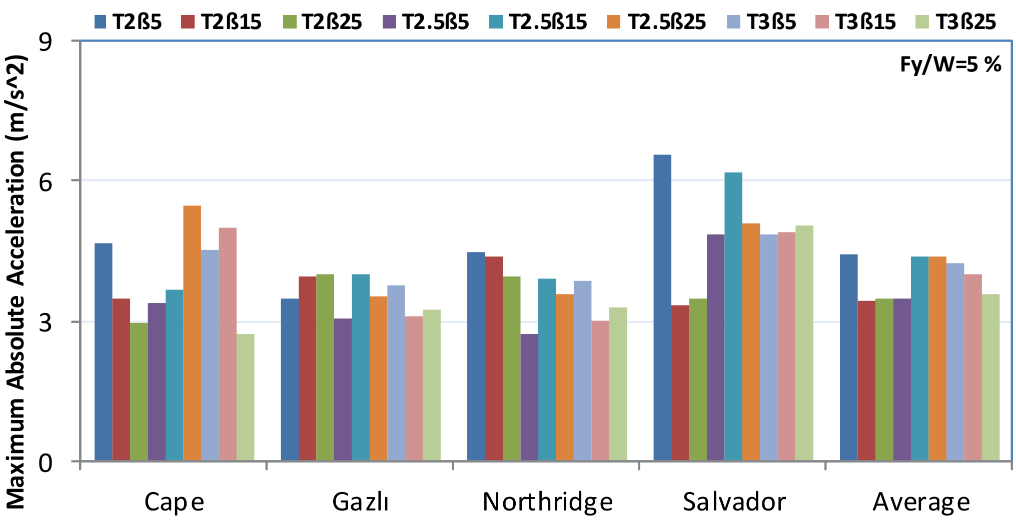

b)

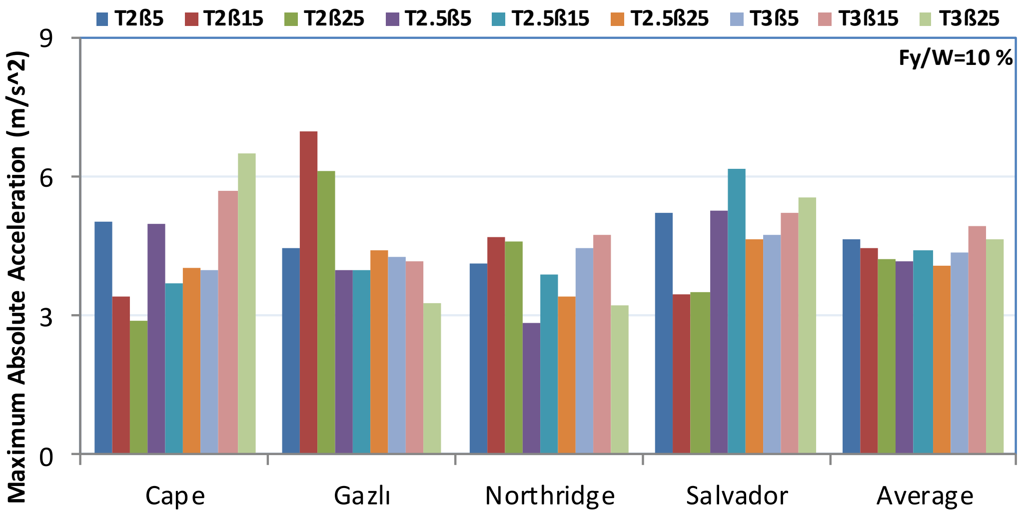

c)

Figure 4.25 Maximum absolute accelarations of 3-storey frames

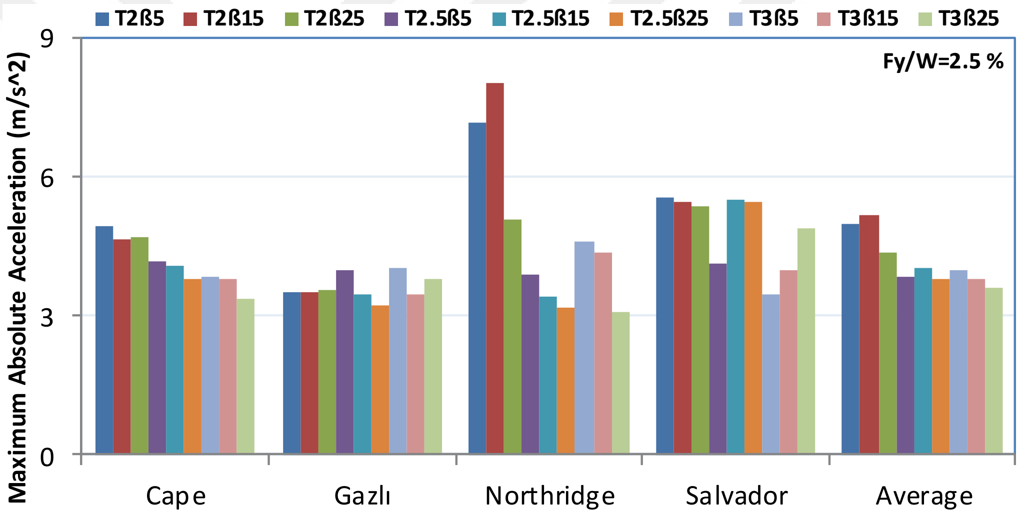

a)

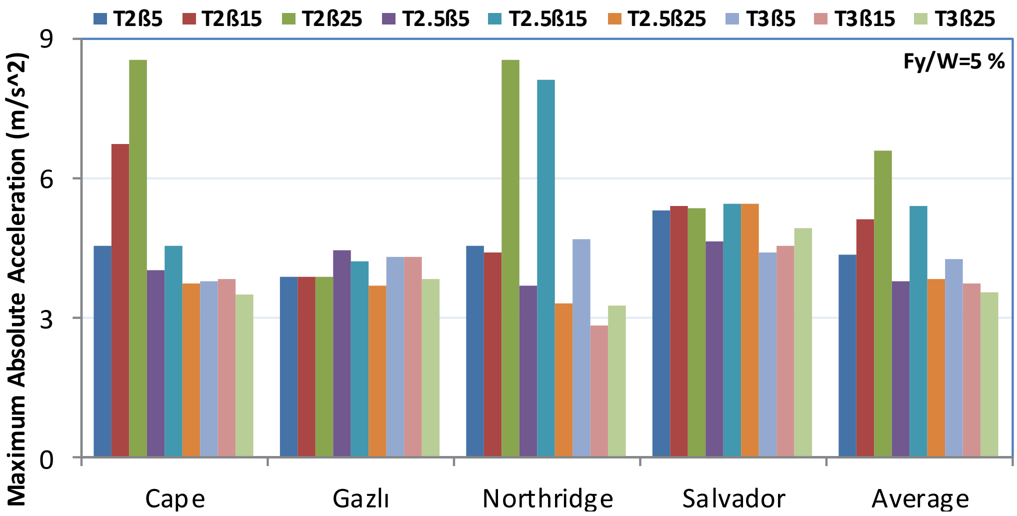

b)

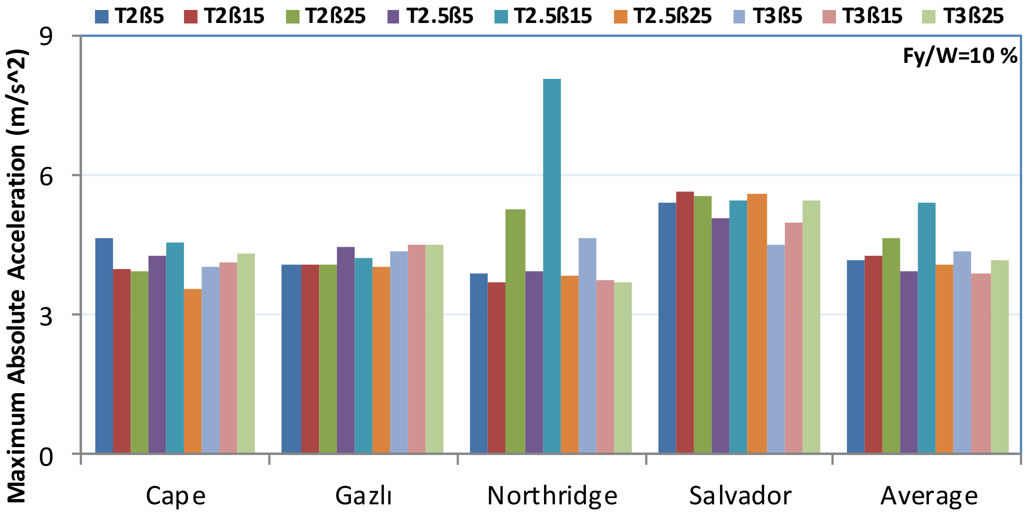

c)

Figure 4.26 Maximum absolute accelarations of 6-storey frames

The lowest average values of the maximum absolute acceleration as 3.33, 3.56, and 2.58 m/s^2 observed in the isolation system of T2.5ß5FyW2.5, T3ß25FyW5, and T3ß25FyW2.5 for 3, 6, and 9-storey isolated frames, respectively. Moreover, the isolation system having greater isolation period exhibited the most uniform absolute acceleration distribution with respect to the other isolation systems. For example, when the ß and Fy/W remained constant as 5 % and the isolation period increased from 2 to 3 s, the absolute acceleration of 9-storey isolated frame under Salvador earthquake at uppermost was decreased from 4.77 to 3.52 m/s^2 as shown in Figure 4.29(a). Secondly, when the variation of the absolute acceleration assessed in terms of the effective damping ratio, it was clearly observed that the greater effective damping ratio (namely, 15 and 25 %) was mostly decisive for mitigating the storey absolute acceleration also obtaining the lowest roof absolute acceleration for the isolated frames. For example, the utilization of the effective damping ratio as 25 % instead of 15 % that was reduced the roof absolute acceleration as 10.75 % when the isolation period and yield strength ratio were constant (namely, T = 2.5 s, Fy/W = 10 %) for 9-storey isolated frame under Salvador earthquake as shown in Figures 4.30(b) and 4.30(c). The isolation system of T2.5ß15FyW5, T3ß25FyW2.5, and T2.5ß15FyW5 yielded the lowest value of the maximum absolute acceleration as 2.57, 3.36, and 4.18 m/s^2 for 3, 6, and 9-storey isolated frames under Cape earthquake (see Figures 4.25(b), 4.26(a), 4.27(b)), respectively. Thirdly, at a glance it was noted that the mitigation of the yield strength ratio enabled the maximum absolute acceleration to reduce in all examined frames.

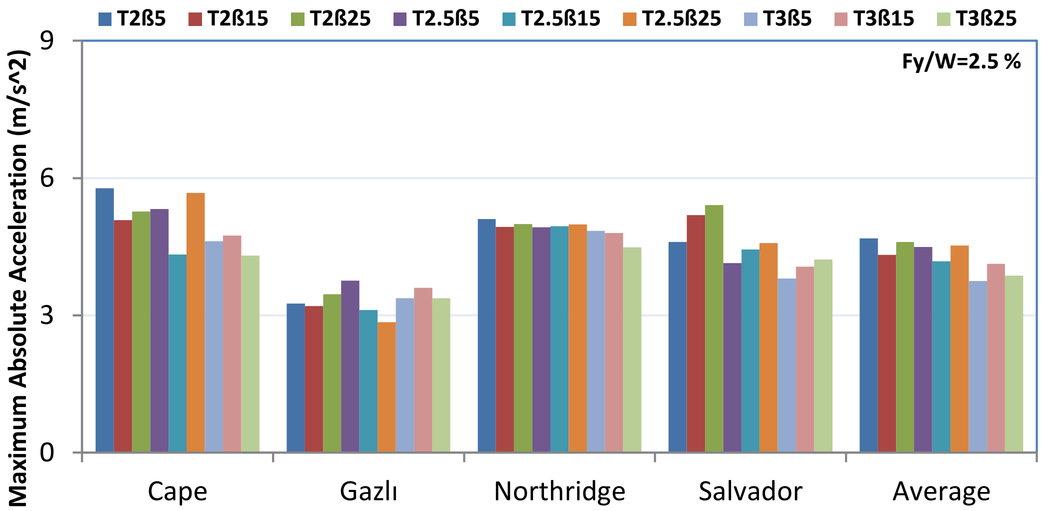

a)

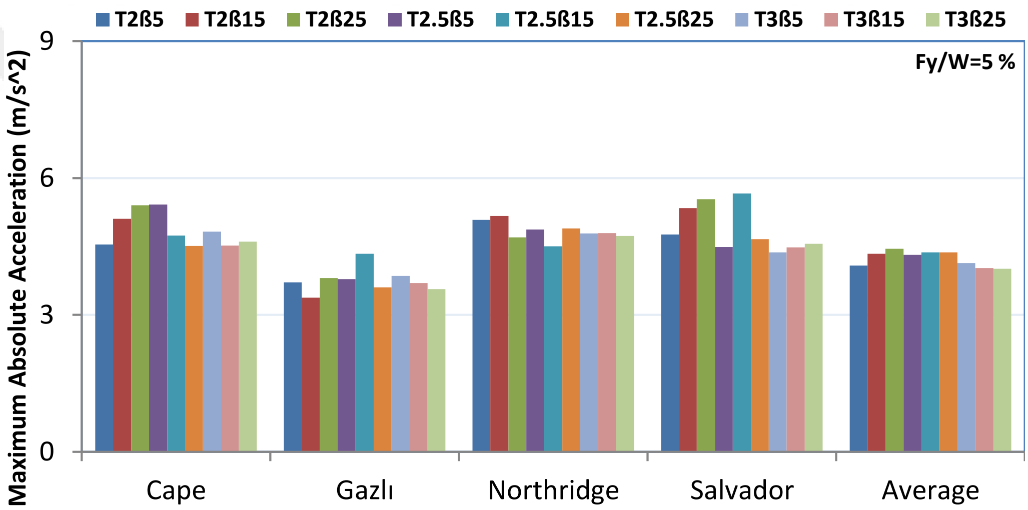

b)

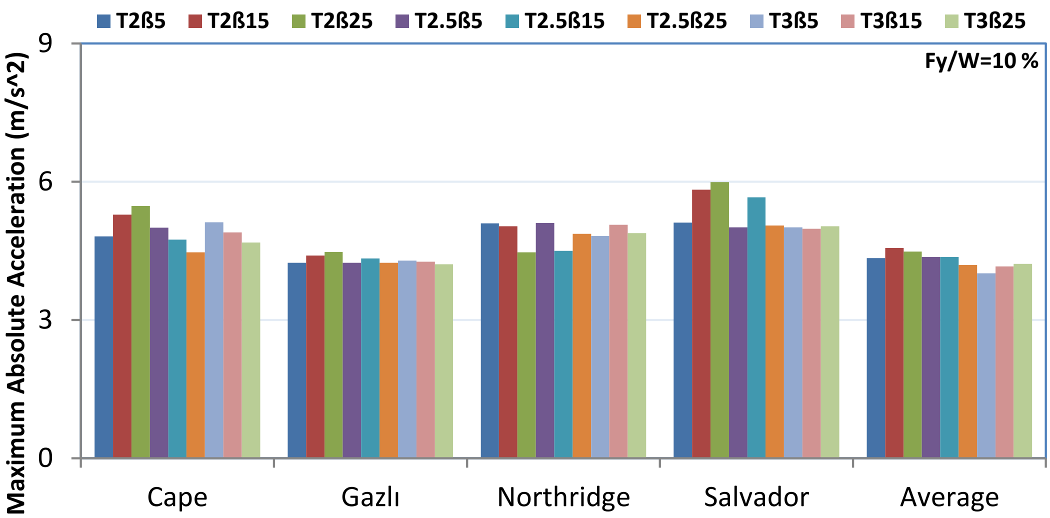

c)

Figure 4.27 Maximum absolute accelarations of 9-storey frames

In other words, the absolute acceleration demand of the isolation system including the lower yield strength ratios such as 2.5 and 5 % was substantially lower than yield strength ratio of 10 %. For example, the isolation system of T2.5ß15FyW5, T3ß25FyW2.5, T2.5ß5FyW5, and T2ß15FyW5 having the lower yield strength ratio succeeded the lowest absolute acceleration as 2.57, 2.43, 2.73, and 3.33 m/s^2 for 3-storey isolated frame under Cape, Gazlı, Northridge, and Salvador earthquakes, respectively as shown in Figure 4.25. Similarly, the isolation system of T3ß25FyW2.5 testified the lowest absolute acceleration as 3.36 and 3.01 m/s^2 for 6-storey isolated frame under Cape and Northridge earthquakes (see Figure 4.26(a)). As for 9-storey isolated frame, the reduction of the yield strength ratio from 10 to 2.5 % mitigated the average absolute acceleration from 4.21 to 3.87 m/s^2 when the isolation period and effective damping ratio constant as T = 3 s, ß = 25 % (see Figures 4.27(a) and 4.27(c)).

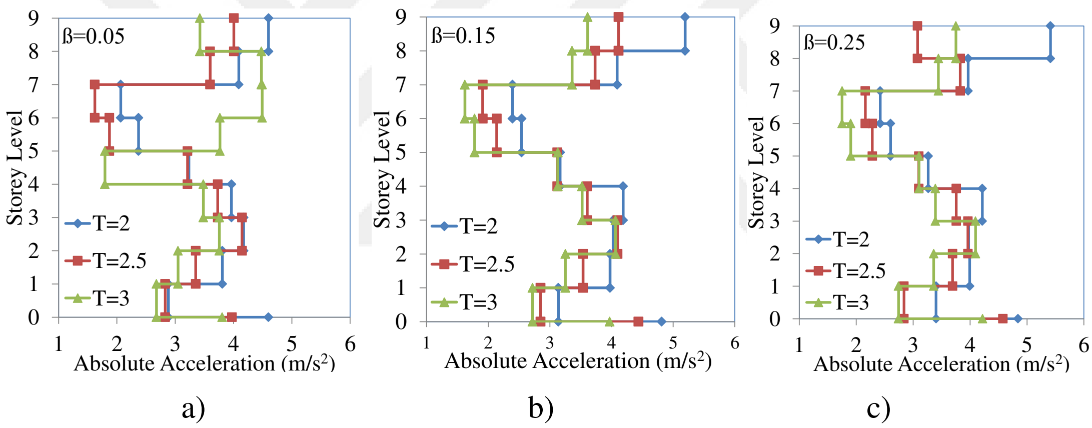

Figure 4.28 Variation of the absolute accelaration against storey height of 9-storey isolated frames under Salvador earthquake for Fy/W=0.025

The variation of the absolute acceleration against height of the examined frames considering the isolation parameters (isolation period, effective damping ratio, and yield strength ratio) was presented in Figures 4.28, 4.29, and 4.30. It was shown that the reduction of the effective damping ratio and yield strength ratio provided the distribution of absolute acceleration uniformly tended as well as the increase of the isolation period. For example, the use of T3ß15FyW2.5 instead of T3ß15FyW10 reduced the roof absolute acceleration as 12.80 % (namely from 4.14 to 3.61 m/s^2) as shown in Figure 4.28(b) and 4.230(b), respectively. As the effective damping ratio decreased from 25 to 15 and then 5 % reduced the roof absolute acceleration from

4.43 (see Figure 4.30(c)) to 4.14 (see Figure 4.30(b)) and then 3.96 m/s^2 (see Figure 4.30(a)) in the isolation system of T3ß25FyW10, T3ß15FyW10, and T3ß5FyW10, respectively.

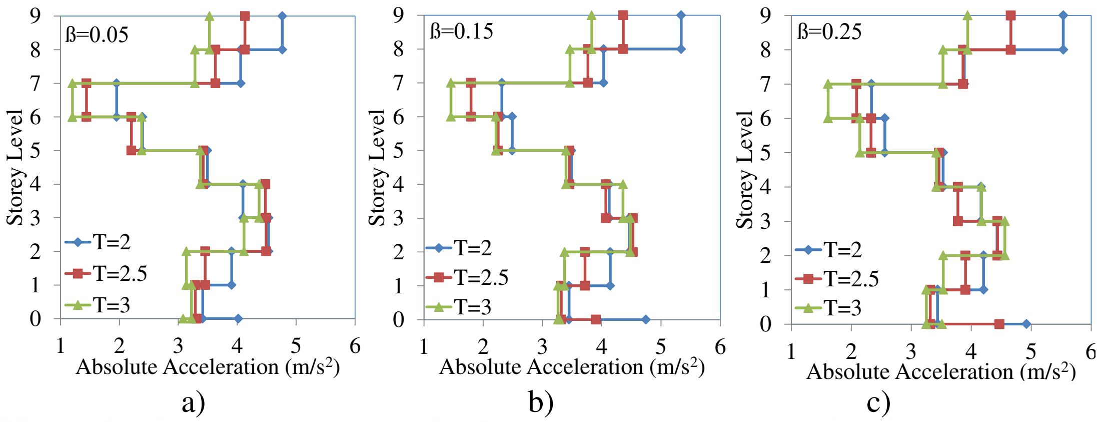

Figure 4.29 Variation of the absolute accelaration against storey height of 9-storey isolated frames under Salvador earthquake for Fy/W=0.05

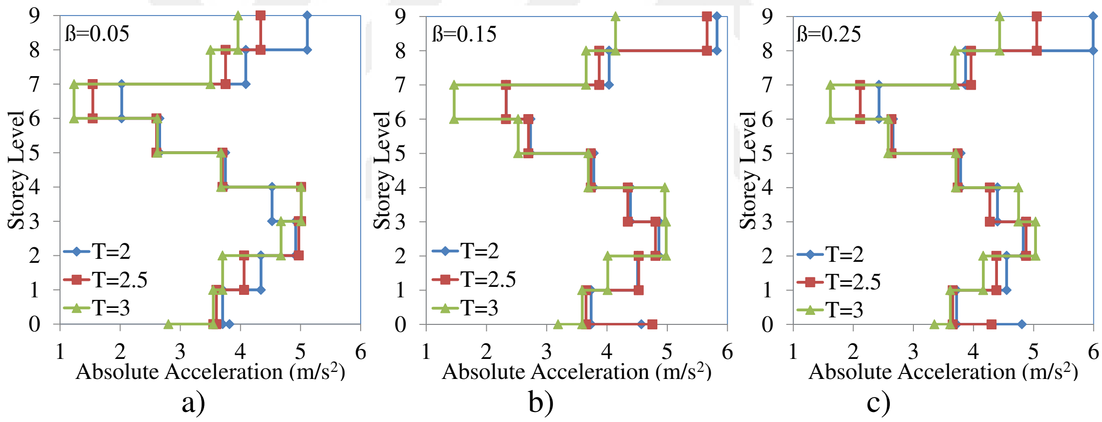

Figure 4.30 Variation of the absolute accelaration against storey height of 9-storey isolated frames under Salvador earthquake for Fy/W=0.10

4.3.6 Base Shear

For the 3, 6, and 9-storey frames equipped with various isolation systems of FPB subjected to different real ground motions, the maximum base shear demand values were computed and plotted in Figures 4.31, 4.32, and 4.33, respectively. The use of FPB considerably reduced the base shear demand especially for 6-storey frame. To evaluate the effectiveness of the isolation parameters and earthquake characteristic on the base shear demand that was normalized by the building weight (namely 1290, 2540, and 3686 kN). The normalized base shears were varied between 0.068-0.347 in all frames and depicted in Figures 4.31-4.33. Besides the variation of the yield strength ratio from 0.025 to 0.10, shifting the isolation period from 2 to 3 s also caused steady reduction on the maximum base shear of the 3, 6, and 9-storey isolated frames.

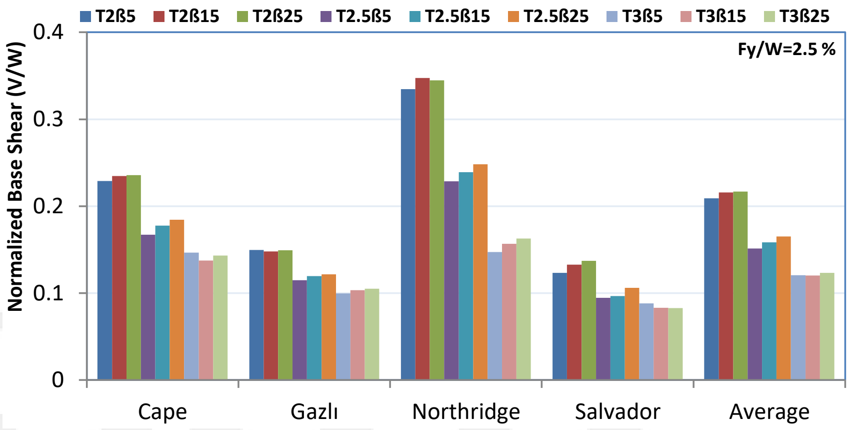

a)

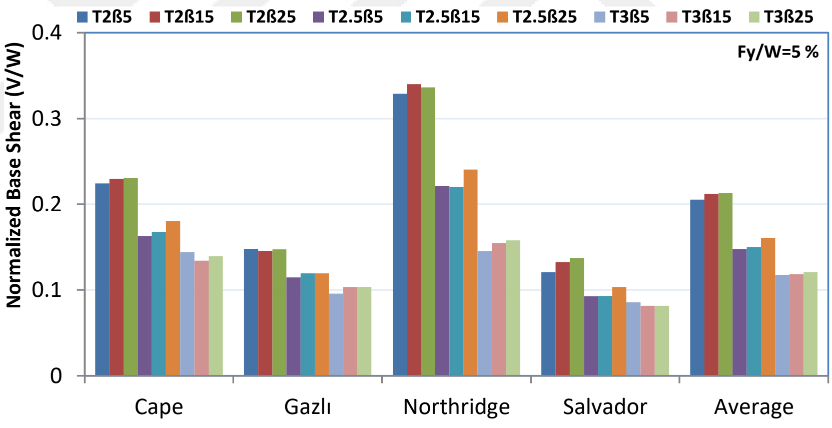

b)

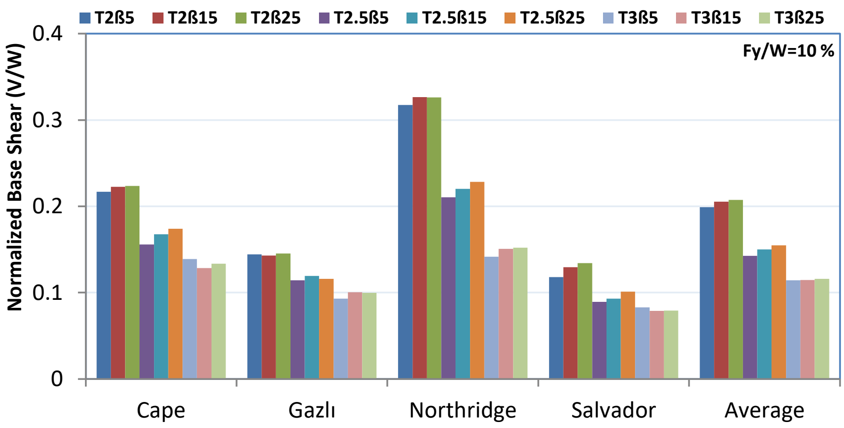

c)

Figure 4.31 Normalized Base Shears of 3-storey frames

When T3ß5FyW10 containing the greatest yield strength ratio was implemented for 3, 6, and 9-storey frames as isolation system subjected to Northridge earthquake that ensured the lowest base shear demand (as 0.141, 0.082, and 0.085) with respect to the other isolation systems, as shown in Figures 4.31(c), 4.32(c), and 4.33(c), respectively. Furthermore, the isolation system of T3ß25FyW10 having the maximum yield strength ratio presented the lowest base shear demand as 0.099, 0.110, and 0.086 (see Figures 4.31(c), 4.32(c), and 4.33(c)) for 3, 6, and 9-storey isolated frames under Gazlı, Cape, and again Gazlı earthquakes, respectively. The lowest value of the effective damping ratio as 5 % can be accepted as dramatically determinative isolation parameters for the assessment of the base shear demand since it exhibited the lowest base shear.

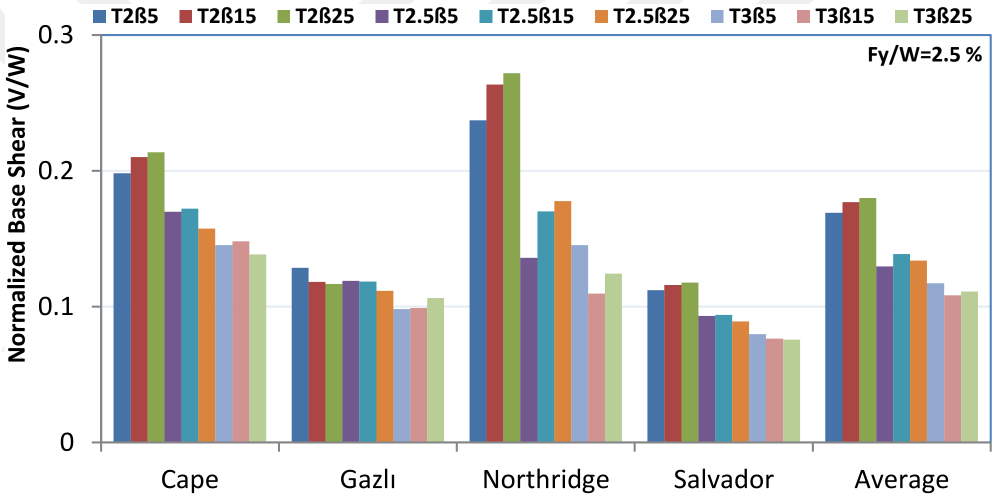

a)

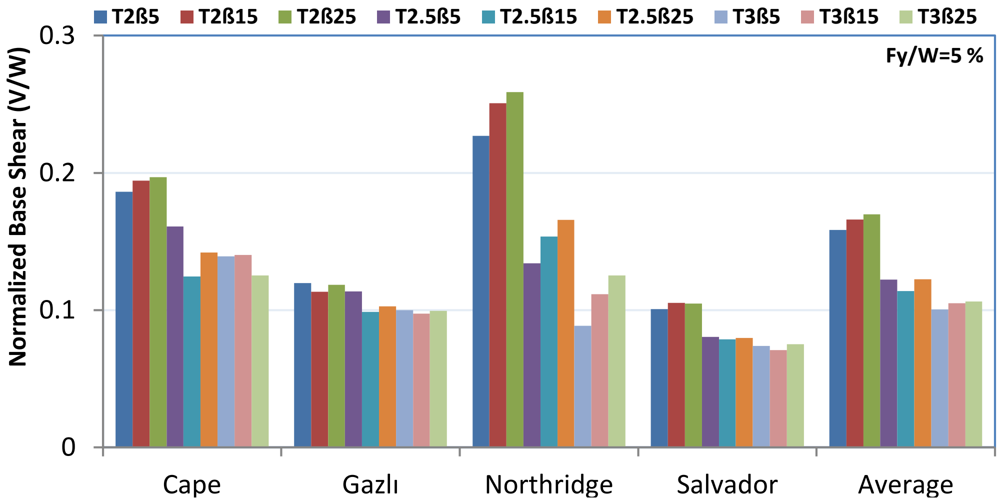

b)

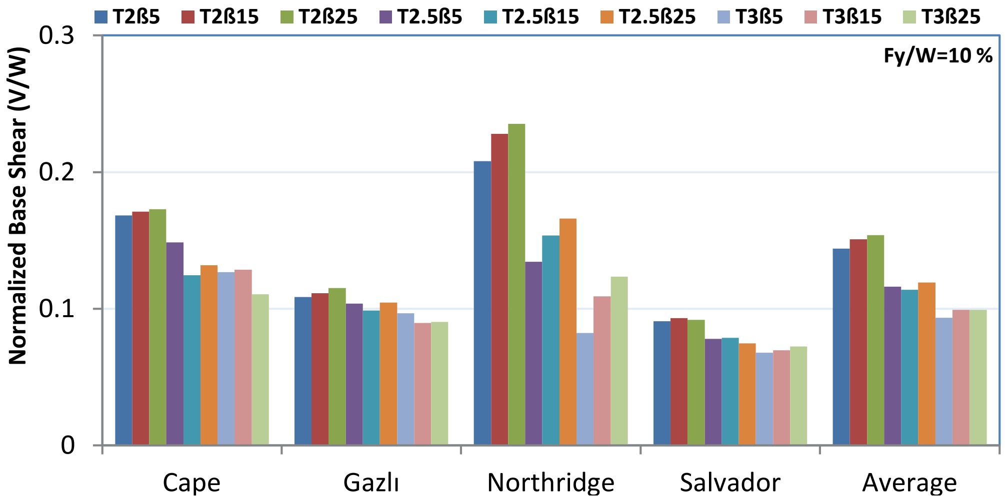

c)

Figure 4.32 Normalized Base Shears of 6-storey frames

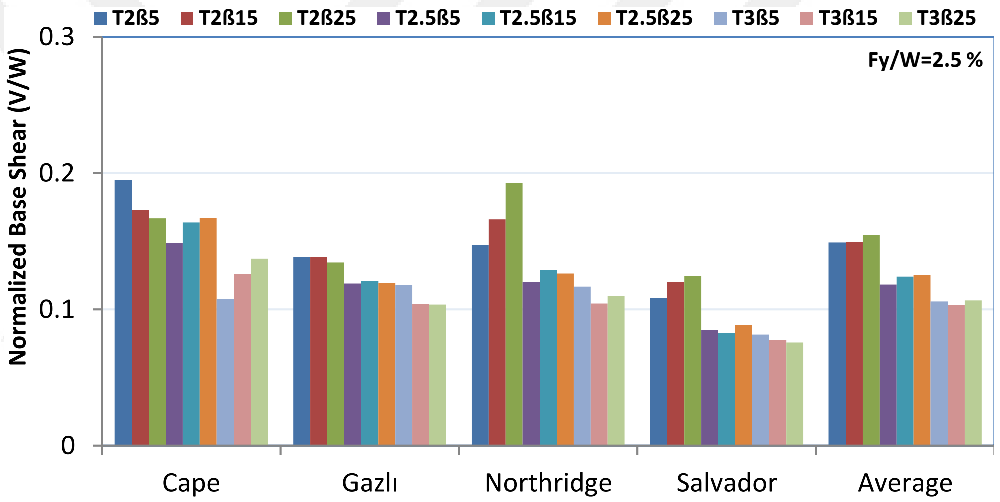

a)

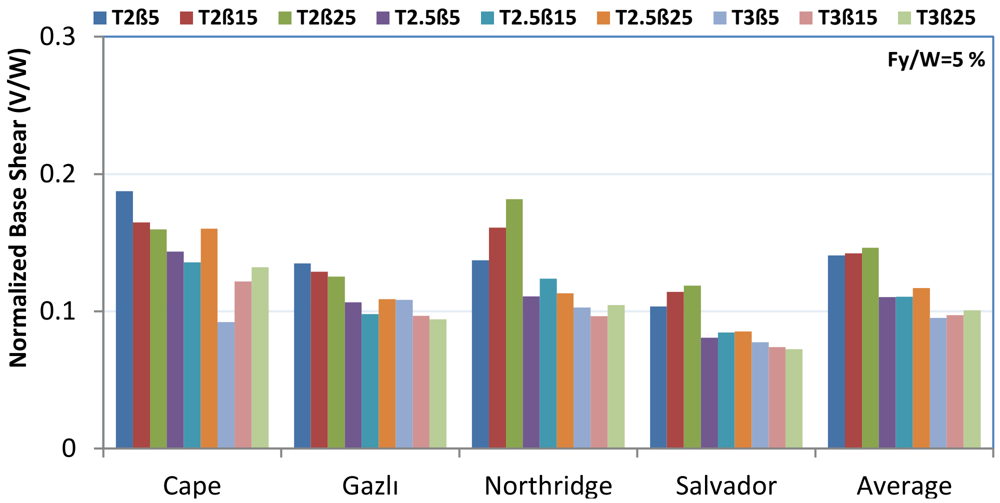

b)

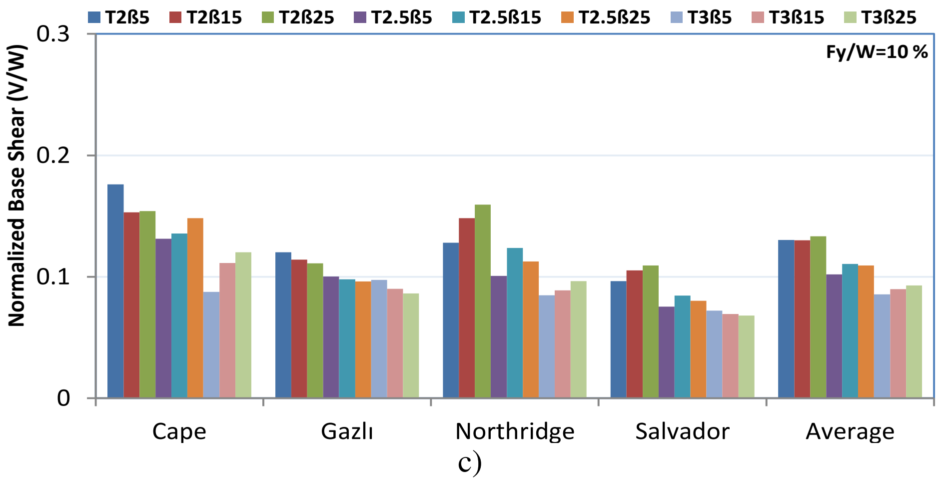

Figure 4.33 Normalized Base Shears of 9-storey frames

For instance, the lowest normalized base shear as 0.141 obtained thanks to the isolation system of T3ß5FyW10 for 3-storey isolated frame under Northridge earthquake, 0.082 and 0.067 for 6-storey isolated frame under Northridge and Salvador earthquakes. Similarly, the lowest normalized base shear as 0.087 and 0.084 for 9-storey isolated frame under Cape and Northridge earthquakes, (see Figures 4.31(c), 4.32(c), and 4.33(c)) respectively.

4.3.7 Base Moment

The variation of the maximum base moment demand in the 3, 6, and 9-storey frames equipped with twenty-seven different isolation systems for four different earthquake records was plotted in Figures 4.34, 4.35, and 4.36, respectively. It was clearly pointed out that the utilization of FPB effectively diminished the base moment. Similar to the base shear demand, the enhancement of the isolation periods significantly decreased the base moment of 3, 6, and 9-storey isolated frames, regardless of the earthquake characteristics. For instance, when the isolation period increased from 2 to 3 s in case of ß5FyW2.5, the base moment decreased from 3139 to 1446 kNm, 7783 to 5378 kNm, 12850 to 5474 kNm for 3, 6, and 9-storey isolated frames under Northridge earthquake (see Figures 4.34(a), 4.35(a), and 4.36(a)), respectively. The lower effective damping ratio produced the lower base moment for 3-storey isolated frame. The isolation system of T3ß5FyW5 having the lowest effective damping ratio gave the lowest value of the maximum base moment as 1374 kNm for 3-storey isolated frame subjected to Northridge earthquake (see Figure 4.34(b)).

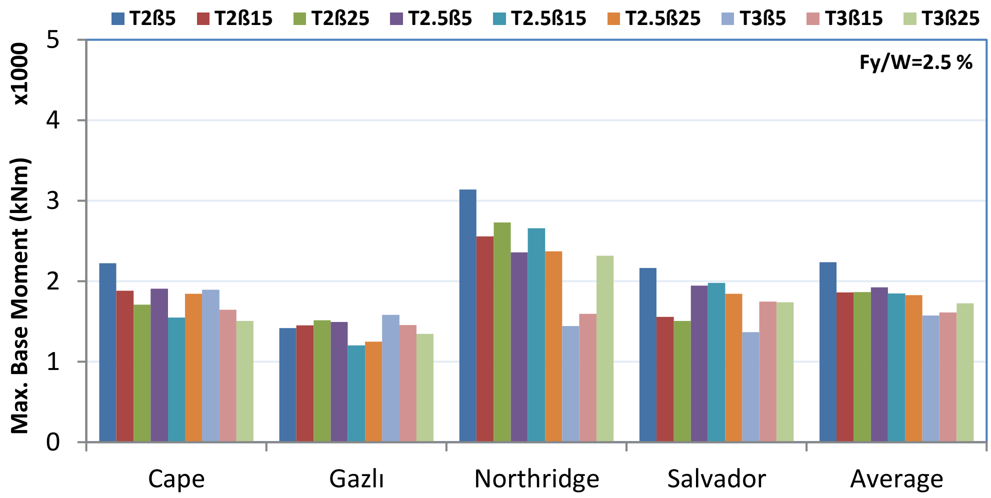

a)

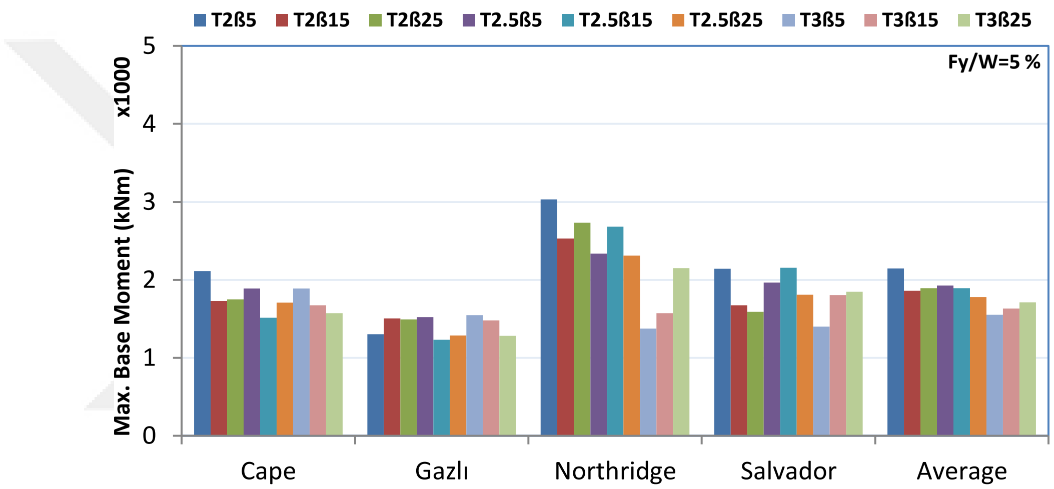

b)

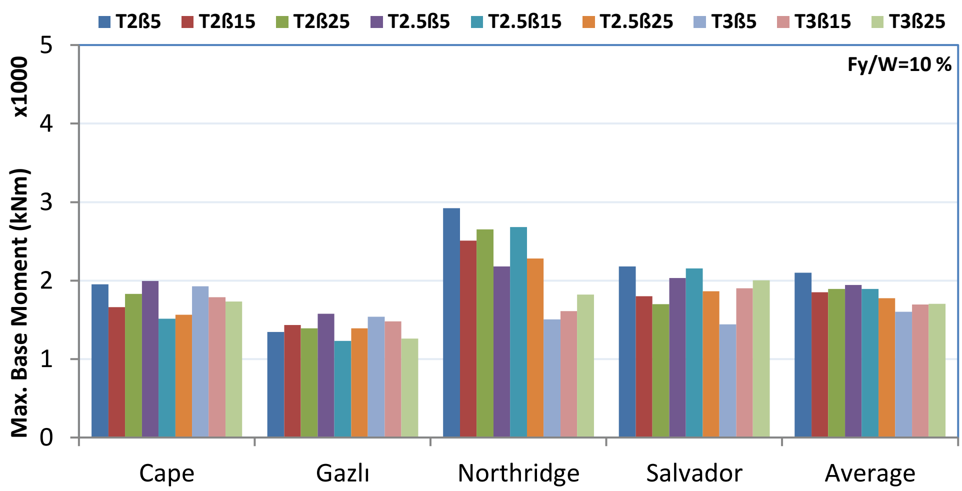

c)

Figure 4.34 Normalized Base Moments of 3-storey frames

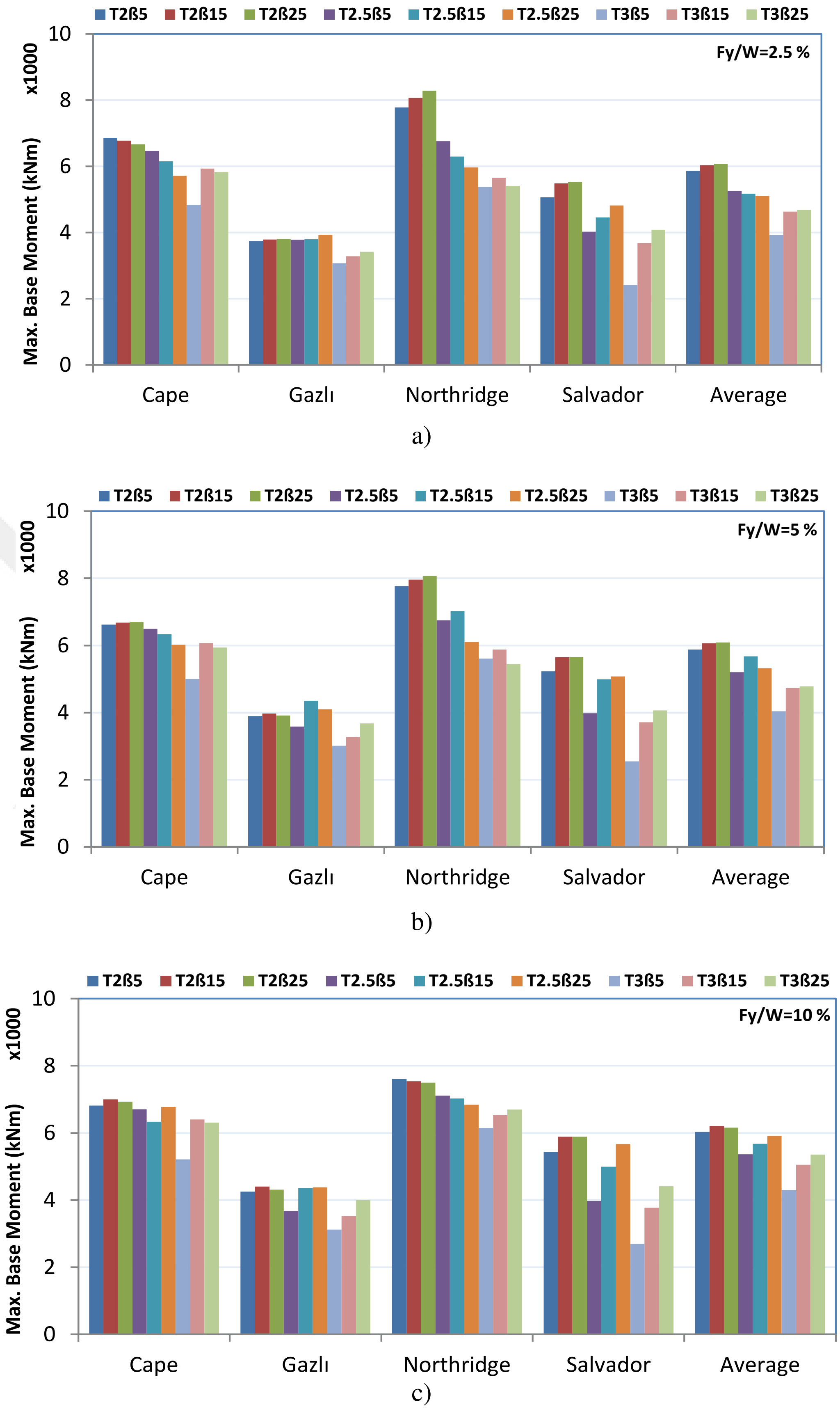

Figure 4.35 Normalized Base Moments of 6-storey frames

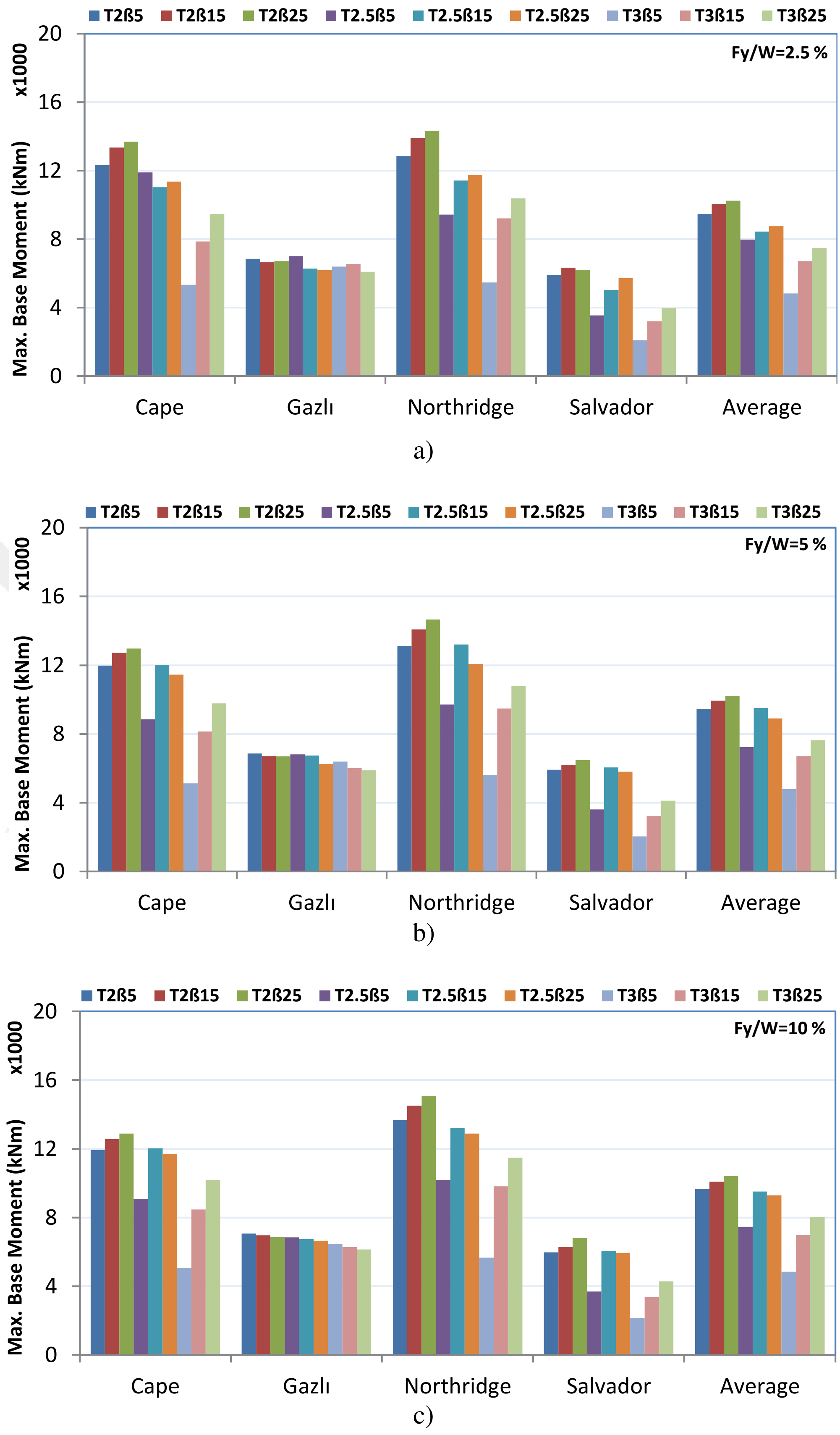

Figure 4.36 Normalized Base Moments of 9-storey frames

Accordingly, it was computed as 3011 kNm for 6-storey isolated frame subjected to Gazlı earthquake (see Figure 4.35(b)). Moreover, the base moment of 2033 kNm was recorded for 9-storey isolated frame subjected to Salvador earthquake (see Figure 4.36(b)). T3ß5FyW5 case caused significant reduction on the average value of the maximum base moment as 9.37, 15.47, and 37.33 % with respect to the isolation system of T3ß25FyW5 for 3, 6, and 9-storey isolated frames, respectively. The moderate and lowest yield strength ratios were capable of reducing the base moment of 3, 6, and 9-storey isolated frames. For instance, the utilization of T3ß5FyW2.5 yielded the lowest base moment as 1369 kNm (see Figure 4.34(a)) for 3-storey isolated frame under Salvador earthquake. Accordingly it was estimated as 4834, 5378, and 2426 kNm for 6-storey isolated frame under Cape, Northridge, and Salvador earthquakes (see Figure 4.35(a)). Furthermore, the lowest base moment testified as 5474 kNm for 9-storey isolated frame under Northridge earthquake as shown in Figures 4.36(a).

4.3.7 Hysteretic Behaviour and Energy Dissipation

The hysteretic curves of 3, 6, and 9-storey frames subjected to Gazlı earthquake was illustrated in Figures A1, A2, and A3, respectively. The obtained curves were in agreement with the bi-linear force-deformation as shown in Figure 2.15(c) [76]. When the isolation parameters were computed in the light of the Eqns. 3.7-3.11, the twenty-seven different isolation systems were obtained and also the position of the hysteretic curve shifted while it abided by the original force-deformation curve. Among the isolation systems, it was observed that when the yield strength ratio was fixed, the dissipated energy by the isolators enhanced with the increase of the isolation period, irrespective of the effective damping ratio and yield strength ratio. On the other hand, it decreased with the increase of the yield strength ratio in case of the isolation period remained constant. Moreover, the isolation period of 2 and 3 s had the smallest and largest hysteresis curves, further the other isolation period remained between them as shown in Figures A1-A3. The utilization of the lower yield strength ratio in the isolation system culminated in expansion on the hysteretic curve. In addition, the isolation system having the greatest isolation period and the lowest yield strength ratio (as 3 s and 2.5 %) remarkably obtained the largest hysteretic curve. For example, the isolation system of T3ß25FyW2.5 associated the largest hysteretic curve as shown in Figures A1(a) and A2(a) for 3 and 6-storey isolated frames under Gazlı earthquake, respectively. Similarly, 9-storey isolated frame reached to the largest hysteretic curve in case of T3ß25FyW2.5, as shown in Figure A3(a). When the influence of the effective damping ratio on the hysteretic curve evaluated, it was observed that the isolation system including greater effective damping ratio mitigated the area of the hysteretic curves for 3 and 6-storey isolated frames (see Figures A1 and A2). Nevertheless, 9-storey frame equipped with the isolation system having the lower effective damping ratio is very capable for the enlargement of the hysteretic curves (see Figure A3). The amount of the dissipated energy by the isolators could be computed by Equation 4.1 [130].

$$E_{loop} = 4(D_{max}F_y - F_{max}D_y) \tag{4.1}$$

where E_{loop}, D_{max}, Fy, F_{max}, and D_y are the amount of the dissipated energy, maximum displacement, yield force, maximum force, and yield displacement of the isolator, respectively. By using Equation 4.1, the amount of the dissipated hysteresis energy of each isolation systems computed and presented in Table 4.4.

Table 4.4 Total dissipated energy Eloop (kJ) with isolation systems for 3, 6, and 9-storey frames under Gazlı earthquake

Isolation Systems	Frames: 3-storey			6-storey			9-storey		
	FyW 2.5	FyW 5	FyW 10	FyW 2.5	FyW 5	FyW 10	FyW 2.5	FyW 5	FyW 10
T2ß5	7.59	7.49	7.37	6.70	5.97	5.09	7.33	6.49	5.38
T2ß15	7.67	8.44	7.24	5.81	5.32	5.28	6.81	6.04	5.31
T2ß25	7.75	7.54	7.37	5.58	5.64	5.49	6.56	5.64	5.47
T2.5ß5	7.69	7.68	7.59	9.21	8.45	7.24	8.19	6.96	6.06
T2.5ß15	8.44	8.44	8.23	8.99	7.75	6.47	8.88	7.44	6.06
T2.5ß25	8.55	8.39	8.08	8.13	7.00	7.07	8.52	7.16	5.66
T3ß5	8.85	8.25	7.88	9.26	9.34	8.71	12.80	10.90	8.93
T3ß15	9.22	9.20	8.72	10.10	9.49	7.98	9.48	8.19	7.02
T3ß25	9.68	9.49	8.91	10.90	9.63	8.91	9.36	7.82	6.33

It was observed that the higher isolation period and lower yield strength ratio effectively gave the maximum energy dissipation. As for the effective damping ratio, the greater effective damping ratio presented the higher dissipation energy for 3 and 6-storey isolated frame as shown in Table 4.4. Conversely, the lower effective damping ratio generally caused the higher dissipation energy for 9-storey isolated frame. For example, the greatest dissipated energies as 9.68 and 10.90 kNm were experienced in the isolation system of T3ß25FyW2.5 for 3 and 6-storey isolated frames under Gazlı earthquake. Similarly, T3ß5FyW2.5 case testified the greatest dissipation energy as 12.80 kNm for 9-storey isolated frame under Gazlı earthquake. Ultimately, the effectiveness of the isolation systems of FPB for low and mid-rise buildings could be very easily tuned by conducting the suitable isolation parameters (namely the isolation period, effective damping ratio, and yield strength ratio).

4.4 Case-3 (HDRB)

In this case, the seismic performance of 3, 6, and 9-storey steel frames equipped with HDRB having various design properties such as the isolation period T, effective damping ratio ß, and post-yield stiffness ratio λ were examined. Thus, the nonlinear response of the base isolated frames were assessed through isolator displacement, interstorey drift ratio, relative displacement, absolute acceleration, base shear, base moment, hysteretic curve, and energy dissipation.

4.4.1 Isolator Displacement

When 3, 6, and 9-storey frames were hit by five different earthquakes, the isolator displacements of those were determined using nonlinear time history analyses and then presented in Figure 4.37-4.39. Moreover, in order to better investigate the effectiveness of HDRB having different design properties, the variation of average percent values of isolator displacement of 3-storey frame with each isolation system with respect to that of the case T2ß5λ3 are given in Table 4.5. It can be obviously shown that the changing of the design characteristic of the isolator had significantly varied the isolator displacement demand of HDRB by ensuring horizontal displacement of case study isolated frame structures. As post-yield stiffness ratio λ gets lower, initial stiffness k_1 become less, and utilization of T as 2.5 and 3 s produced more flexible bearing as well (see Table 3.4). Furthermore, the maximum isolator displacement increased in case of the isolation models consisted of the greater ß and T with less λ.

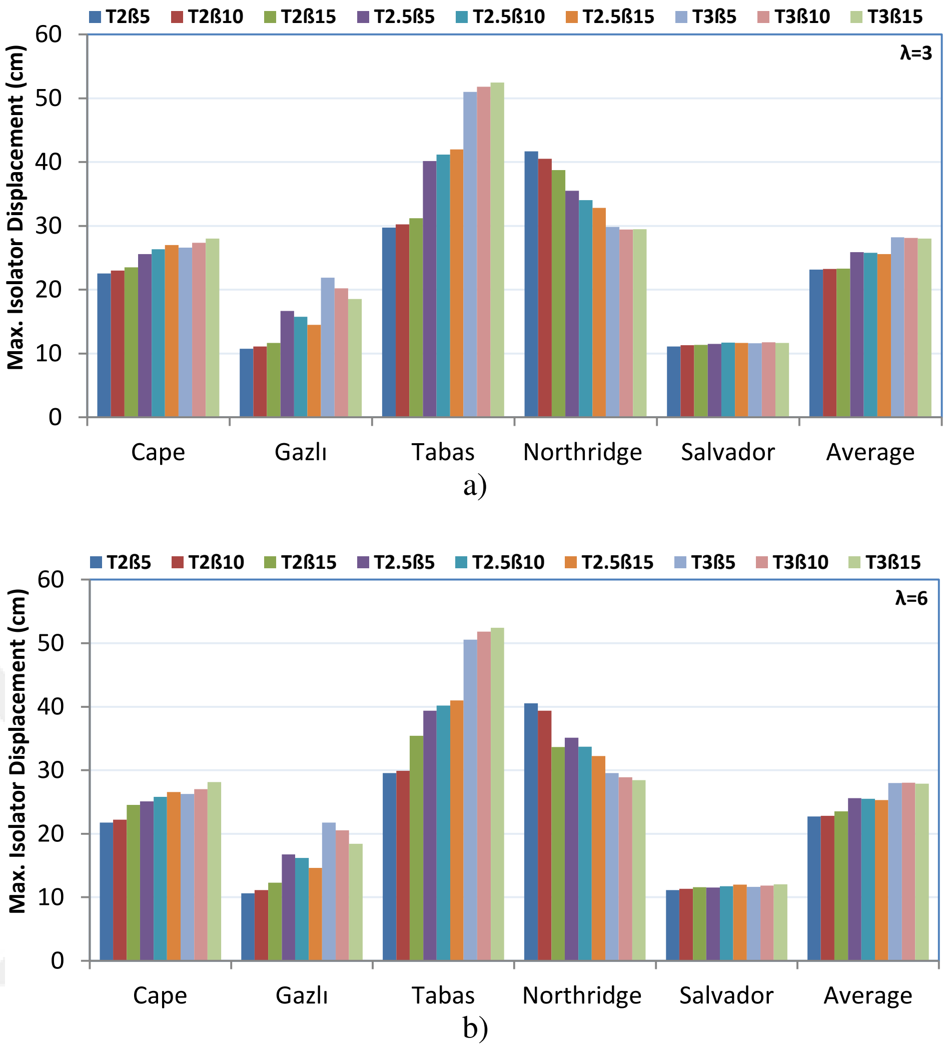

Figure 4.37 Maximum isolator displacement of 3-storey frames

The isolation period of T as 3 s definitely became favourable in terms of the isolator displacement independently height of the building and active earthquakes. When ß and λ are fixed to comprehend the effect of T on the isolator displacement, and it was observed that the use of T3ß15λ6 instead of T2ß15λ6 enhanced the isolator displacement from 24.52 to 28.15 cm (see Figure 4.37(b)), 21.19 to 27.49 cm (see Figure 4.38(b)), 18.57 to 28.48 cm (see Figure 4.39(b)) for 3, 6, and 9-storey frames subjected to Cape earthquake, respectively. When the isolator displacement of the case study frames were evaluated considering the effect of the damping ratio it was noticed that the use of ß (namely 10 and 15 %) increased the isolator displacement. For instance, the increase of the effective damping ratio from 5 to 15 % in the isolation system of T = 3 s and λ = 6 enhanced 3-storey base-isolated frames' isolator displacement from 11.62 to 12.05, 26.27 to 28.15 cm, 50.58 to 52.45 cm under Salvador, Cape, and Tabas earthquakes, respectively as shown in Figure 4.37(b).

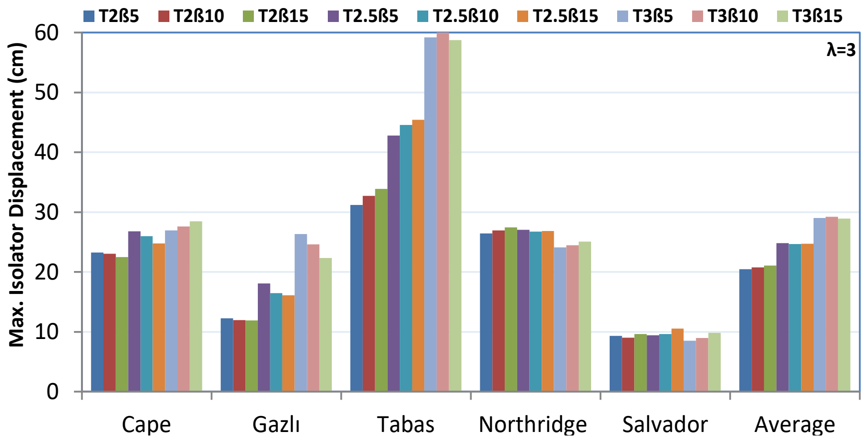

a)

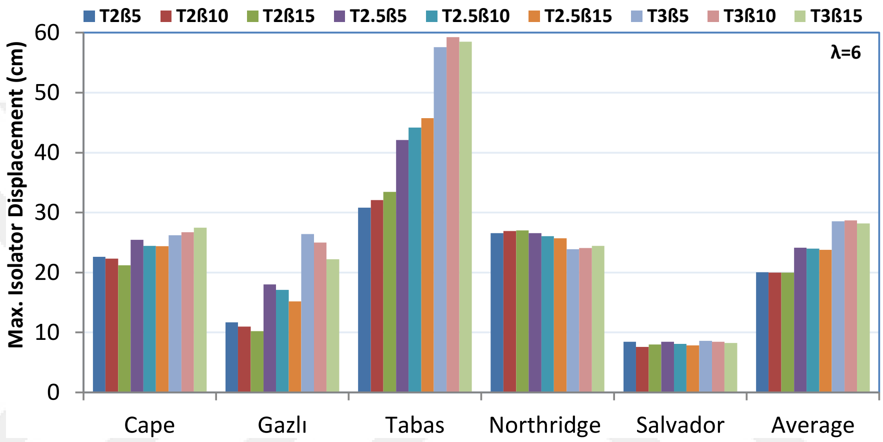

b)

Figure 4.38 Maximum isolator displacement of 6-storey frames

The moderate value of ß as 10 % also satisfied the maximum isolator displacement of 6-storey isolated frame with T3ß10λ3 as 60.39 cm under Tabas earthquake (see Figure 4.38(a)). The maximum average isolator displacement of 28.34 cm was experienced for 9-storey frame with T3ß15λ3 that has the greatest effective damping ratio as 15 % (see Figure 4.39(a)).

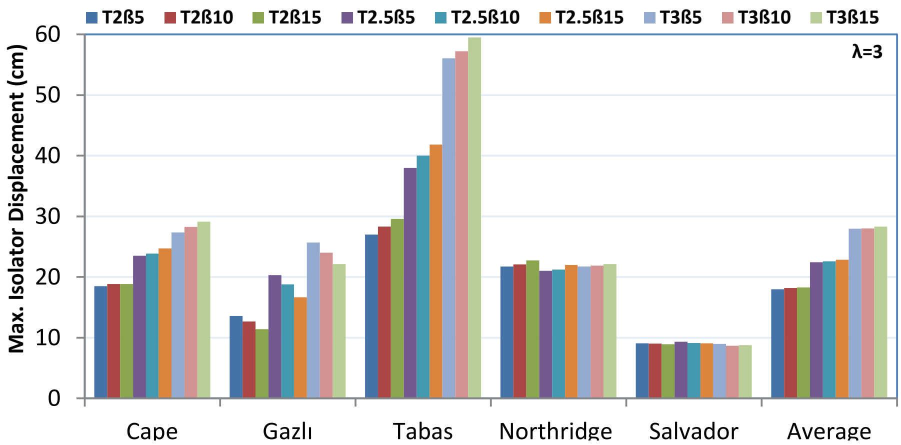

a)

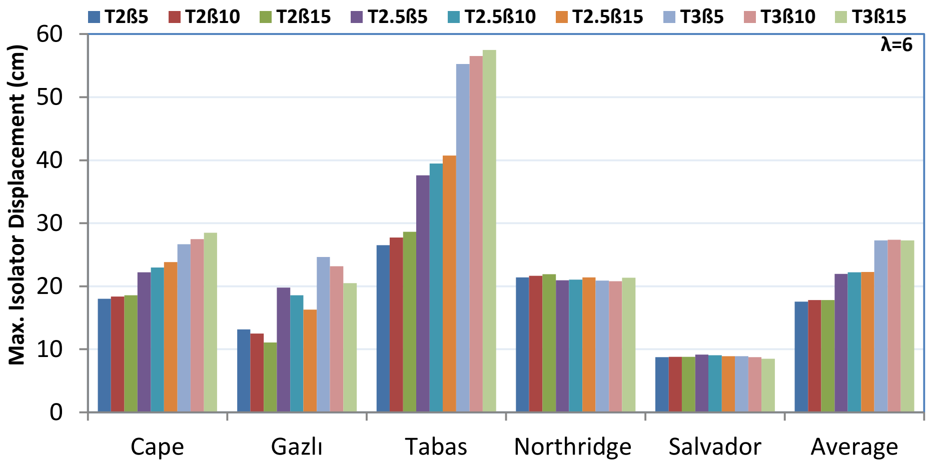

b)

Figure 4.39 Maximum isolator displacement of 9-storey frames

Table 4.5 Variation of the average seismic demand values in percentage based on the case T2ß5λ3 in 3-storey frames

Isolation System	Iso. Disp. (%)	Int. Str. Drift R. (%)	Roof. Drift R. (%)	Rel. Disp. (%)	Abs. Acc. (%)	Base Shear (%)	Base Moment (%)
T2ß5λ3	0	0	0	0	0	0	0
T2ß10λ3	0.4	-7.9	-1.7	-8.4	-0.2	-3.0	-5.2
T2ß15λ3	0.6	-14.4	-3.2	-15.5	-5.9	-6.0	-11.3
T2.5ß5λ3	11.8	-34.1	1.6	-31.4	-22.1	-26.1	-25.5
T2.5ß10λ3	11.4	-37.6	0.6	-34.6	-24.5	-29.3	-28.8
T2.5ß15λ3	10.4	-44.3	-0.8	-37.4	-23.4	-32.7	-31.1
T3ß5λ3	21.7	-50.8	5.4	-47.8	-37.8	-49.5	-42.5
T3ß10λ3	21.4	-53.3	4.6	-50.2	-35.9	-44.4	-44.1
T3ß15λ3	21	-55.3	3.9	-51.7	-37.3	-46.5	-45.4
T2ß5λ6	-1.9	-3.5	-2.2	-3.0	11.9	-1.9	-1.9
T2ß10λ6	-1.6	-9.7	-3.2	-8.5	0.9	-4.4	-4.7
T2ß15λ6	1.4	-23.8	-5.0	-25.8	-1.1	-23.6	-24.4
T2.5ß5λ6	10.4	-38.2	-0.3	-35.0	-8.7	-27.1	-27.4
T2.5ß10λ6	10.1	-41.4	-1.2	-37.8	-16.1	-30.1	-30.4
T2.5ß15λ6	9.1	-46.1	-2.9	-42.0	-12.4	-32.6	-31.1
T3ß5λ6	20.7	-53.5	4.1	-49.6	-18.8	-44.4	-44.0
T3ß10λ6	20.9	-55.2	3.9	-51.6	-31.8	-46.2	-45.1
T3ß15λ6	20.4	-57.7	3.1	-53.5	-28.9	-47.6	-45.2

Key: Negative values show an decrease of the maximum average values

The less post-yield stiffness ratio, λ generally presented more isolator displacement than the isolation system including highest value of λ. For instance, when λ decreased to 3, the maximum isolator displacements of 21.89 and 25.67 cm occurred for 3 and 9-storey frames equipped with T3ß5λ3 under Gazlı earthquake, 52.5 and

59.53 cm obtained for 3 and 9-storey frames with T3ß15λ3 under Tabas earthquake as depicted in Figure 4.37(a) and 4.39(a), 27.45 and 22.76 cm acquired for 6 and 9-storey frames with T2ß15λ3 under Northridge earthquake as depicted in Figure 4.38(a) and 4.39(a), respectively. Furthermore, the isolation systems of T3ß5λ3, T3ß10λ3, T3ß15λ3 have the lowest post-yield stiffness ratio (namely λ = 3) also succeeded the average maximum increment on the isolator displacement percentage as 21.7, 42.6, 57.7 % versus T2ß5λ3 for 3, 6, and 9-storey base-isolated frames as shown in Figures 4.37(a), 4.38(a), and 4.39(a), respectively.

4.4.2 Interstorey Drift Ratio

The interstorey drift ratio can be admitted as an engineering demand parameter (EDP) to meet the limiting criteria of structural and non-structural members that are restricted in accordance with SEAOC included Operational (SP-1) as 0.5 %, Occupiable (SP-2) as 1.8 %, Life Safety (SP-3) as 3.2 %, and Near Collapse (SP-4) as 4 % [129]. İnterstorey drift could be calculated as the translational displacement of successive storey over associated storey height. The maximum interstorey drift ratios were computed for the isolated frames with various isolation systems under five earthquakes and plotted in Figures 4.40-4.42. In addition, the interstorey drift ratio against height of the base-isolated frames with different isolation systems under Northridge earthquake was presented in Figures 4.43 and 4.44. The effectiveness of the proposed isolation systems was evaluated whether the corresponding performance levels was satisfied or not. First, the increase of T mitigated the maximum interstorey drift ratio of the isolated frames (see Figures 4.40-4.42).

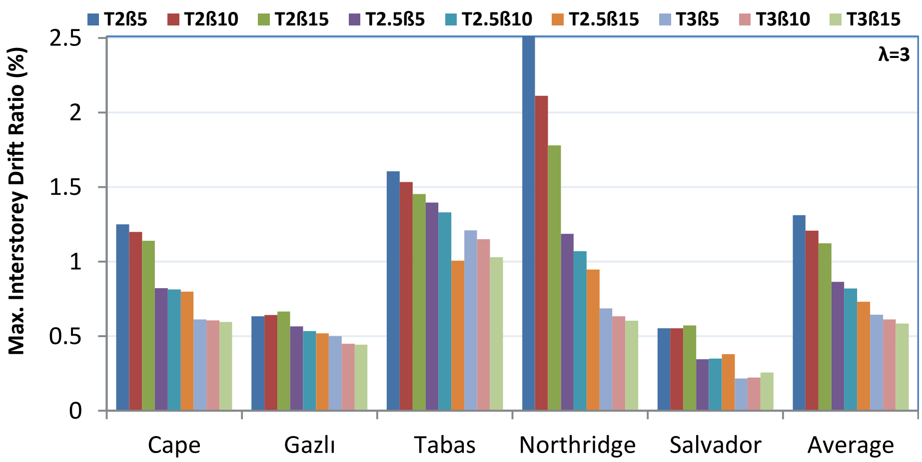

a)

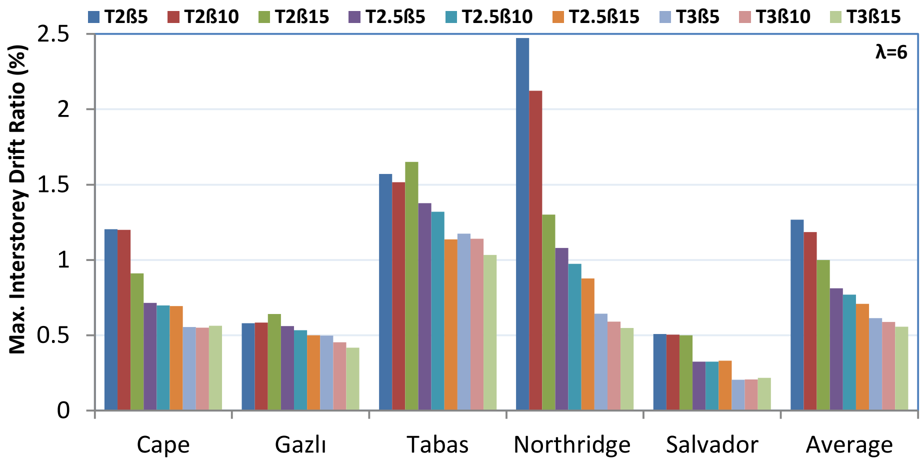

b)

Figure 4.40 Maximum interstorey drift ratio of 3-storey frames

When T reached to 3 s, ß and λ fixed as 5 % and 3, the maximum interstorey drift ratios of 2.52, 3.03, and 2.54 % (T2ß5λ3) dropped to 0.69, 0.99, and 0.90 % (T3ß5λ3) which met the limiting criteria of SP-2 for 3, 6, and 9-storey base-isolated frames under Northridge earthquake, as described in Figures 4.40(a), 4.41(a), and 4.42(a), respectively. Similarly, the utilization of T3ß5λ6 instead of T2ß5λ6 mitigated the interstorey drift ratios from 2.47 to 0.64 % (see Figure 4.40(b)), 2.96 to 0.96 % (see Figure 4.41(b)), 2.46 to 0.85 % (see Figure 4.42(b)) for 3, 6, and 9-storey isolated frames under Northridge earthquake, respectively, the reduced interstorey drift ratios met the limiting criteria of SP-2. The Operational performance level of SP-1 was observed if only 3-storey frame with the isolation period of 3 s under Gazlı and Salvador earthquakes (see Figures 4.40(a, b)). It was also valid for 6 and 9-storey isolated frame buildings under Salvador earthquake as show in Figures 4.41 and 4.42.

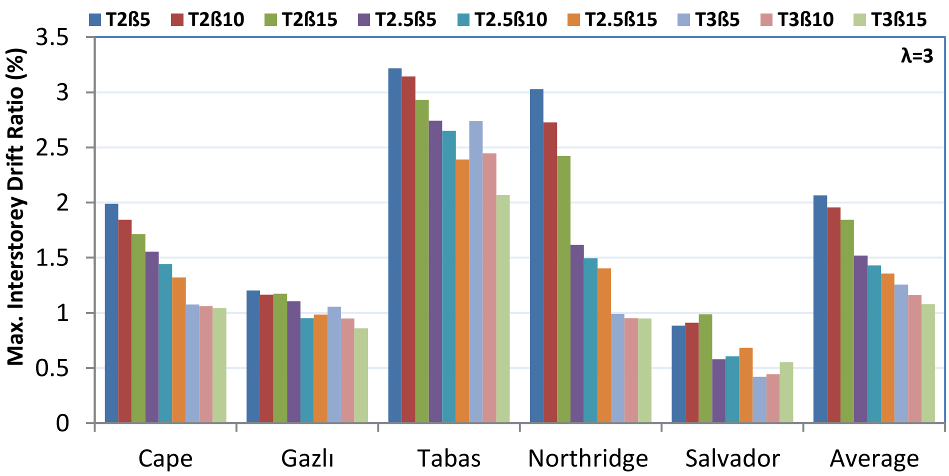

a)

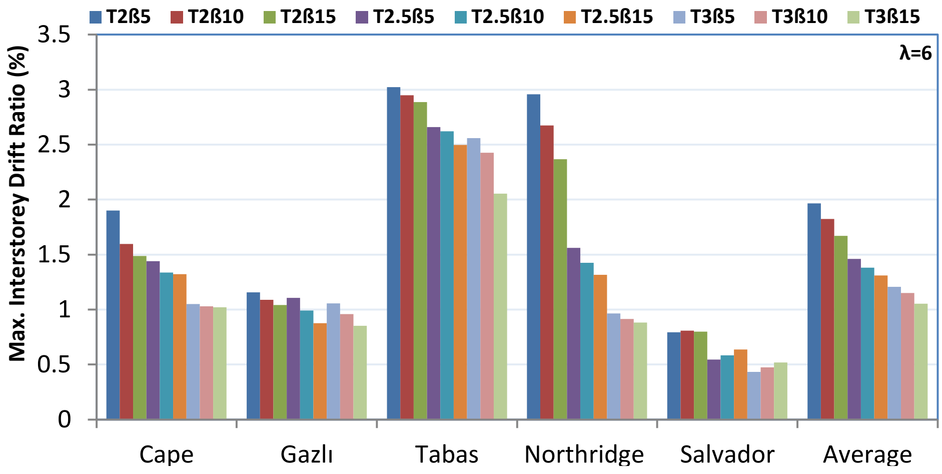

b)

Figure 4.41 Maximum interstorey drift ratio of 6-storey frames

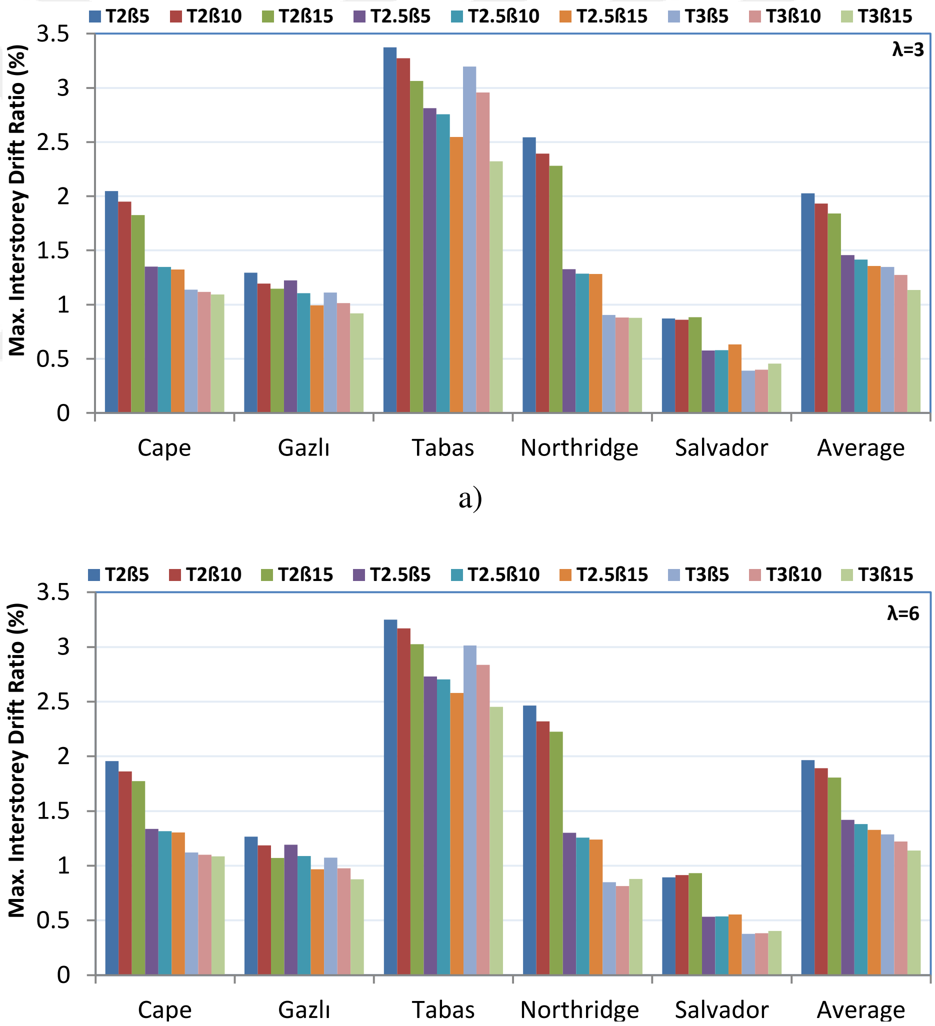

Figure 4.42 Maximum interstorey drift ratio of 9-storey frames

The isolation systems having greater isolation period represented more uniform drift distribution, and also lower interstorey drift ratio under Northridge earthquake as shown in Figures 4.43 and 4.44. Secondly, the greater effective damping ratios (as 10 and 15 %) significantly produced less interstorey drift ratios. For instance, the minimum interstorey drift ratios of 0.42, 0.55, 0.54 % were acquired for 3-storey frame with T3ß15λ6, T3ß10λ6, T3ß15λ6 (see Figure 4.40(b)) under Gazlı, Cape, Northridge, respectively. It was as 1.00 % by T2.5ß15λ3 (see Figure 4.40(a)) under Tabas earthquakes thereby the performance level of SP-1 and SP-2 satisfied.

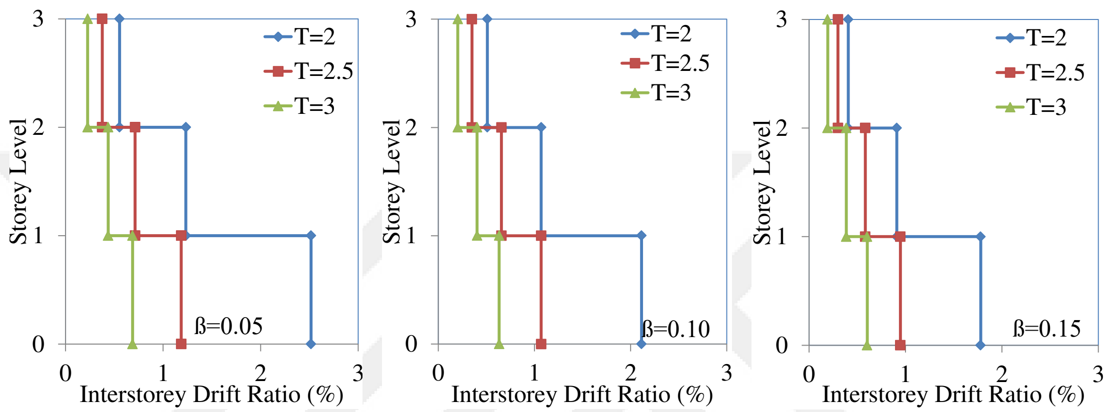

a) b) c)

Figure 4.43 Variation of the interstorey drift ratio against storey height of 3-storey isolated frames under Northridge earthquake for λ = 3

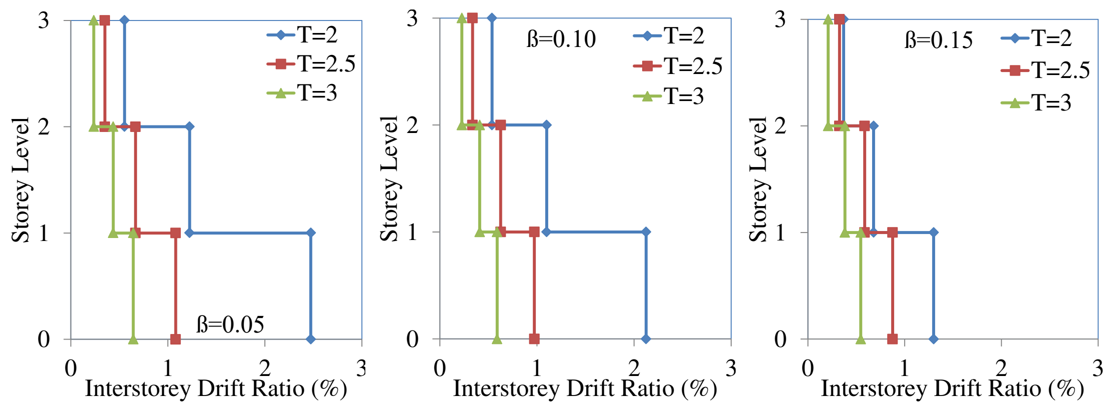

a) b) c)

Figure 4.44 Variation of the interstorey drift ratio against storey height of 3-storey isolated frames under Northridge earthquake for λ = 6

When subjected to Cape, Gazlı, Tabas, and Northridge earthquakes, 6-storey frame with T3ß15λ6 provided the minimum interstorey drift ratios of 1.02, 0.85, 2.05, 0.88 %, respectively, as shown in Figure 4.41(b). Similarly, when 9-storey base-isolated frame equipped with T3ß15λ6 and hit by Cape and Gazlı earthquakes the minimum interstorey drift ratios of 1.08 and 0.87 % obtained (see Figure 4.42(b)) and they are in convenient with SP-2. Figures 4.43 and 4.44 described that the use of the effective damping ratios of 10 and 15 % not only mitigated the interstorey drift but also provided more uniform drift distribution. For instance, when subjected to Northridge earthquake the interstorey drift ratios at roof storey of the corresponding 3-storey base-isolated frames experienced as 0.55 % for the isolation system of T2ß5λ3 (see Figure 4.43(a)), which are decreased up to 0.51 % for the isolation system of T2ß10λ3 (see Figure 4.43(b)), and 0.40 % for T2ß15λ3 (see Figure 4.43(c)). Furthermore, compared to T2ß5λ3, the average value of the maximum interstorey drift ratio reduction of 3, 6, and 9-storey base-isolated frames with T2ß10λ3 occurred as 7.9, 5.2, 4.5 %, and T2ß15λ3 ensured as 14.4, 10.6, 9.2 % (see Table 4.5). Thirdly, the increase of the post-yield stiffness ratio λ decreased the interstorey drift particularly 3 and 6-storey frame (see Figures 4.40 and 4.41). For instance, when subjected to Cape earthquake, 3, 6, and 9-storey base-isolated frames with T2.5ß10λ3 produced the interstorey drift ratios as 0.81, 1.44, and 1.35 %, whereas T2.5ß10λ6 caused as 0.69, 1.33, and 1.31 %, respectively. In addition, the lowest average value of the maximum interstorey drift ratios of 3 and 6-storey frames with T3ß15λ6 computed as 0.56 and 1.05 %, respectively, whereas it was as 1.13 % for 9-storey frame with T3ß15λ3. Moreover, the use of greater λ exhibited the more uniform interstorey drift distribution and reduced it as well, as clearly shown in Figure 4.44(c).

4.4.3 Relative Displacement

The relative displacement can be found by subtracting the top storey displacement from the bearing displacement, and it can also be used as one of the most influential EDP for the seismic performance assessment. After subjecting a set of earthquakes the maximum relative displacements were computed, and given in Figures 4.45-4.47. The increase of the isolation period considerably mitigated the relative displacements. For instance, when subjected to Cape, Gazlı, Tabas, Northridge, and Salvador earthquakes, the lowest relative displacements were obtained as 3.33, 2.58, 5.71, 3.42, and 1.18 cm for 3-storey frame with T3ß5λ6, T3ß15λ6, T3ß15λ3, T3ß15λ6, and again T3ß15λ6, respectively, as shown in Figure 4.45. Moreover, the lowest average value was as 3.31 cm for 3-storey frame with T3ß15λ6 provided 53.5 % relative displacement reduction with respect to T2ß5λ3 as shown in Figure 4.45(b) and Table 4.5. When considered 6-storey frame, the lowest relative displacements of 7.45, 6.33, 16.86, 7.21, and 6.50 cm were actualized for the isolation systems of T3ß5λ6, T3ß15λ3, T2.5ß15λ6, T3ß15λ3, and T3ß10λ3 (see Figure 4.46). As an example of 9-storey building with T3ß15λ3, T2.5ß15λ3, T3ß15λ3, T3ß5λ3, and T3ß15λ3 provided the lowest relative displacements as 8.79, 10.75, 26.46, 11.65, and 5.45 cm for 9-storey building, respectively, (see Figure 4.47). The maximum relative displacement decreased and also behaved more uniform distribution over the storey height in the case of HDRB designed by the greater isolation period as shown in Figures 4.48 and 4.49.

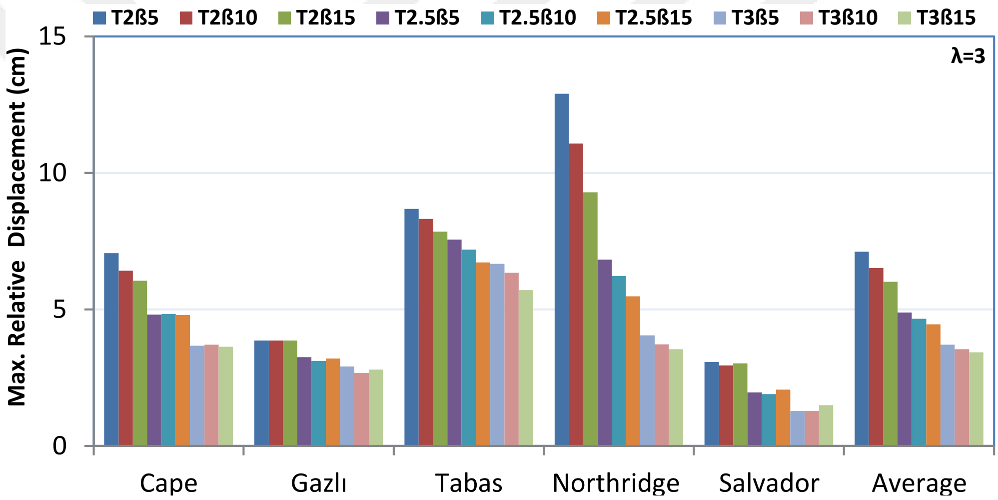

a)

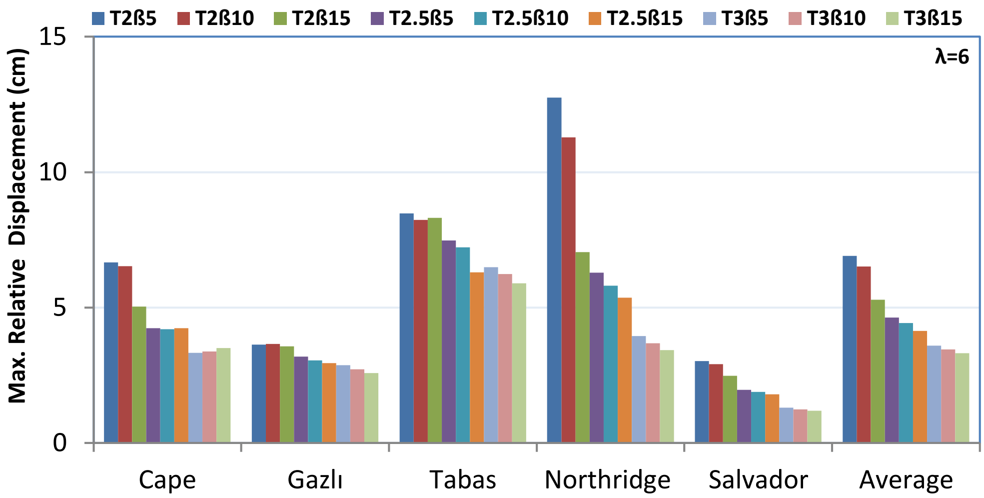

b)

Figure 4.45 Maximum relative displacement of 3-storey frames

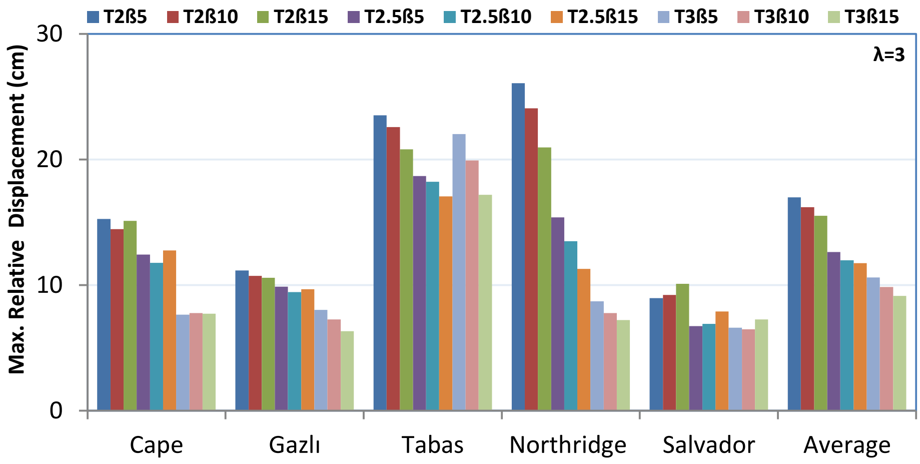

a)

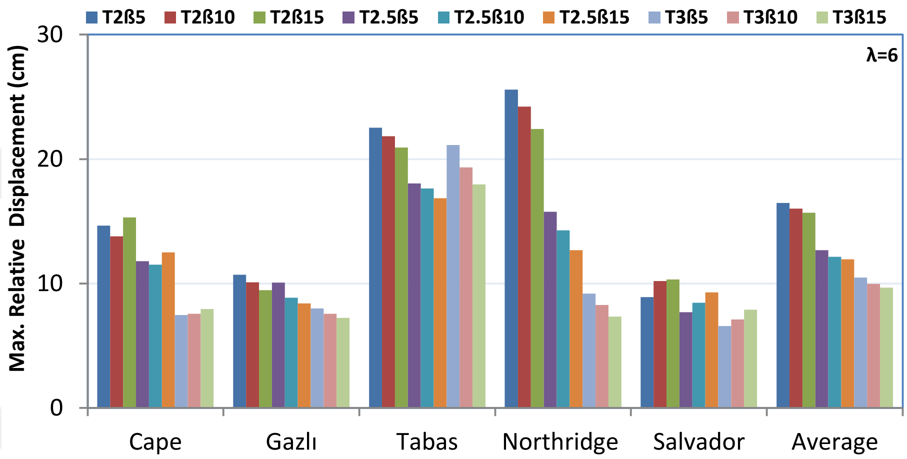

b)

Figure 4.46 Maximum relative displacement of 6-storey frames

When it enhanced from 2 to 3 s and the others are fixed (namely, ß = 10 % and λ = 3), compared to T2ß10λ3, the utilization of T3ß10λ3 provided the greatest relative displacement reduction as 67.7 % at roof storey level of 6-storey building (see Figure 4.48(b)).

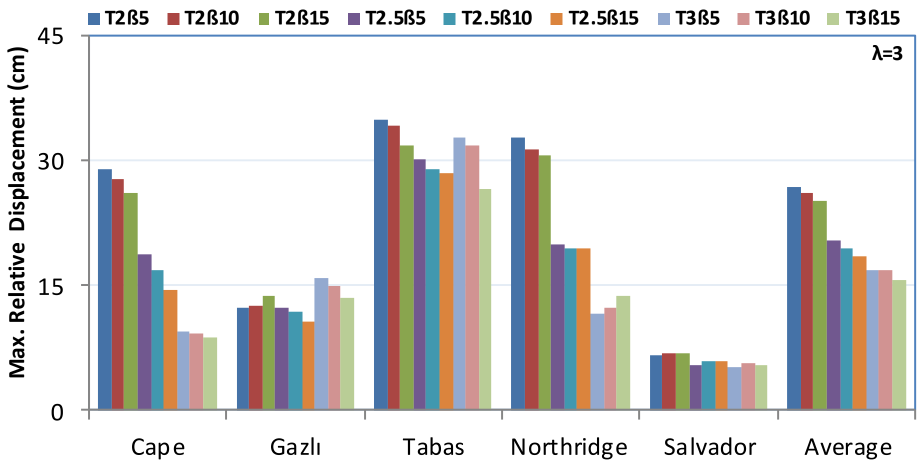

a)

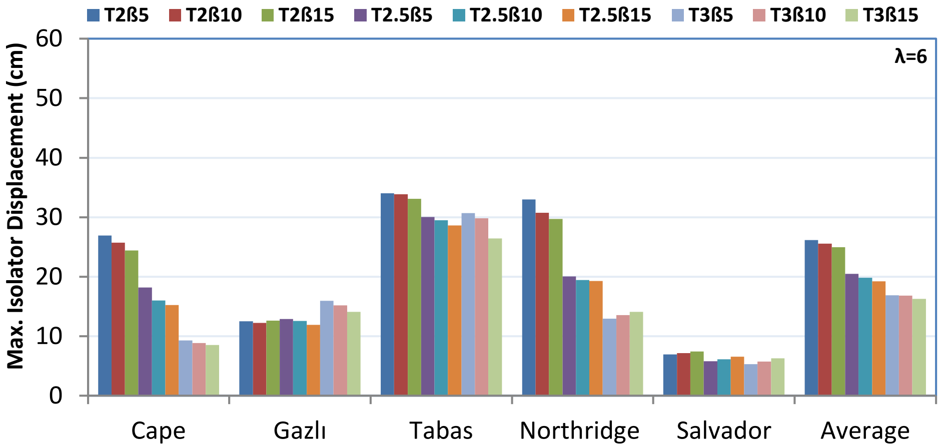

b)

Figure 4.47 Maximum relative displacement of 9-storey frames

The performance of the isolated frames with the greatest effective damping ratio was found to be superior to that of the low and moderate effective damping ratio. The isolation system of T3ß15λ3 succeeded the lowest relative displacements of 5.71 cm in the event of 3-storey frame hit by Tabas earthquake (see Figure 4.45(a)), it was as 7.21 and 6.33 cm for 6-storey building hit by Northridge and Gazlı earthquakes (see Figure 4.46(a)), 5.45, 8.79, and 26.46 cm for 9-storey building under Salvador, Cape, and Tabas earthquakes (see Figure 4.47(a)), respectively.

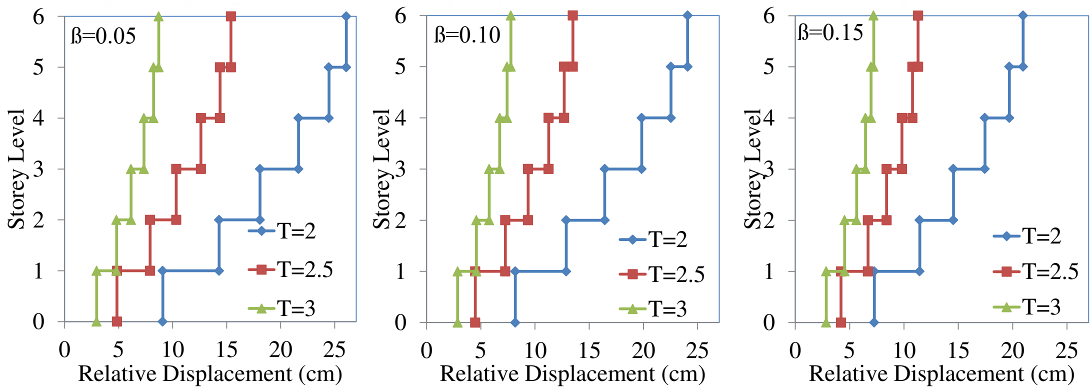

a) b) c)

Figure 4.48 Variation of the relative displacement against storey height of 6-storey isolated frames under Northridge earthquake for λ = 3.

Furthermore, the utilization of the moderate and greatest value of ß provided more uniform relative displacement distribution with storey level. For instance, when ß of 5 reached to 10, and then 15 %, keep the other isolation parameters constant (namely, T = 2 s and λ = 6), the maximum relative displacement at roof storey mitigated from 25.59 to 24.21, and then 22.43 cm for 6-storey frame hit by Northridge earthquake, as shown in Figure 4.49 (a, b, and c), respectively. The greatest average relative displacement reductions occurred as 46.2 and 41.1 % when 6 and 9-storey frame with T3ß15λ3 respectively, as 53.5 % for 3-storey frame with T3ß15λ6 (see Table 4.5). A set of λ (as 3, 6) had been proposed to characterize the response of the examined frames with HDRB. T3ß15λ6 including λ as 6 which provided the lowest average value of the maximum relative displacements as 3.31 cm for 3-storey frame (see Figure 4.45(b)). However, it was obtained as 9.15 and 15.72 cm for 6 and 9-storey frame with T3ß15λ3 as shown in Figure 4.46(a) and 4.47(a), respectively. The use of less λ proved the relative displacement reduction for 6-storey frame and assisted to ensure more uniform relative displacement distribution as shown in Figure 4.48(c).

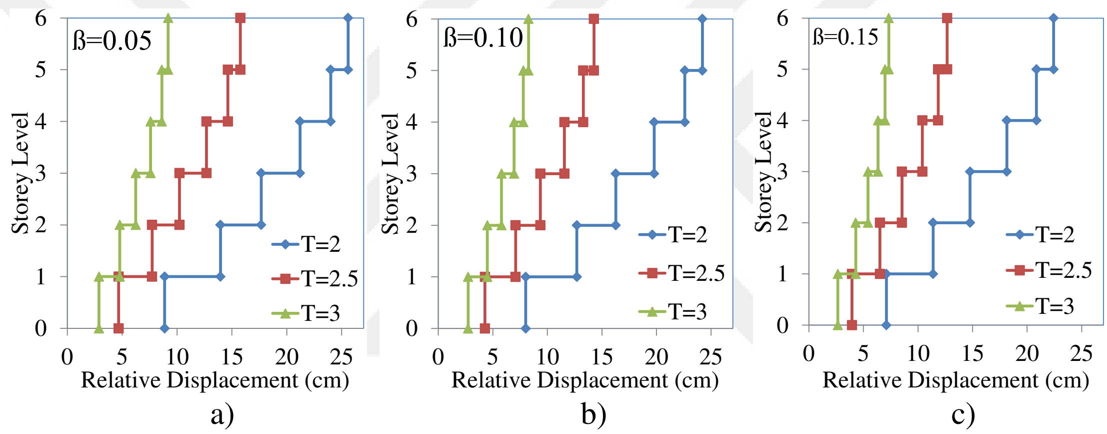

Figure 4.49 Variation of the relative displacement against storey height of 6-storey isolated frames under Northridge earthquake for λ = 6

4.4.4 Absolute Acceleration

The case study frames with HDRB subjected to a set of earthquakes and then the maximum absolute accelerations computed and plotted in Figures 4.50-4.52. Furthermore, the change of one storey to another is described for 9-storey frame in Figures 4.53 and 4.54. Firstly, it was generally provided the lowest absolute accelerations when 2.5 and 3 s utilized as the isolation period independently height of the buildings and active earthquakes as well. When subjected to Cape and Tabas earthquakes, the lowest maximum absolute accelerations of 1.65 and 2.29 m/s^2 for 3-storey frame with T3ß10λ6 were achieved (see Figure 4.50(b)), respectively.

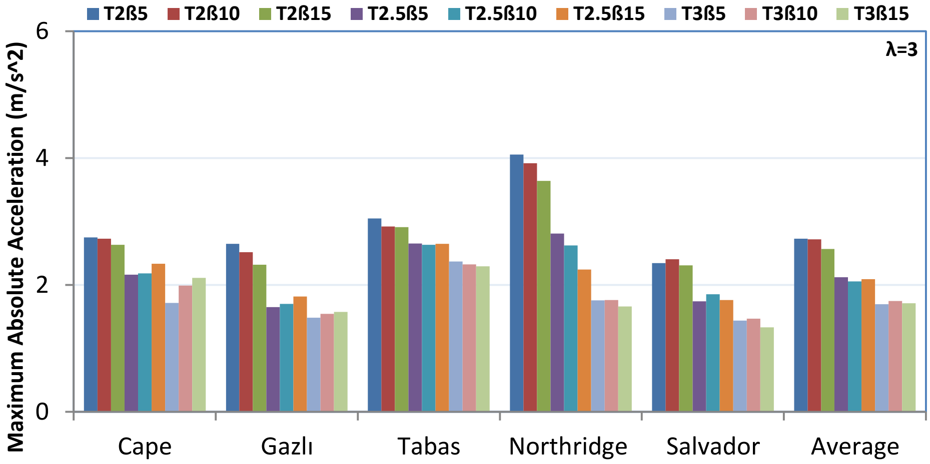

a)

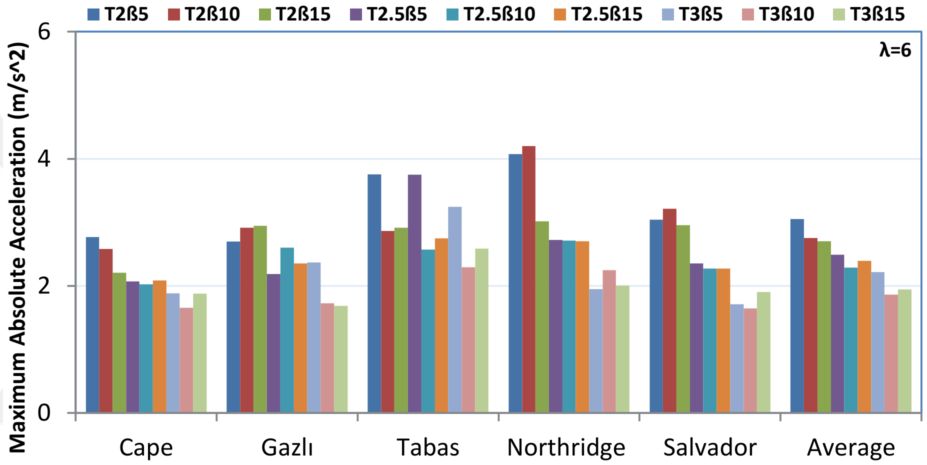

b)

Figure 4.50 Maximum absolute acceleration of 3-storey frames

T3ß5λ3 also introduced the lowest absolute acceleration as 2.30 and 2.78 m/s^2 when 6-storey frame hit by Cape and Salvador earthquakes (see Figure 4.51(a)). When subjected to Gazlı and Tabas earthquakes, the lowest maximum absolute accelerations occurred as 2.08 and 3.39 m/s^2 for 9-storey frame with T3ß15λ3 as seen in Figure 4.52(a), respectively. The use of the isolation periods of 2.5 and 3 s not only decreased the absolute acceleration but also was capable of uniform absolute acceleration distribution as shown in Figure 4.53 and 4.54. 3, 6, and 9-storey base-isolated frames with T3ß5λ3, T3ß15λ3, and T3ß5λ6 introduced the greatest value of average absolute acceleration reduction as 37.8, 36.4, and 32.6 %, respectively. The lower effective damping ratio reduced the maximum absolute acceleration especially in 6 and 9-storey frames. When ß reached to greatest value of 15 %, T3ß15λ3 yielded the lowest maximum absolute accelerations as 1.66 and 1.33

m/s^2 for 3-storey frame hit by Northridge and Salvador earthquakes (see Figure 4.50(a, b)), 1.85, 2.55 m/s^2 for 6-storey frame (see Figure 4.51(a, b)), 2.08 and 3.39 m/s^2 for 9-storey frame hit by Gazlı and Tabas earthquakes (see Figure 4.52(a, b)), respectively. When 6 and 9-storey frames with T3ß10λ3 under Northridge earthquake, the lowest absolute acceleration obtained as 2.29 and 2.73 m/s^2 as seen in Figures 4.51(a) and 4.52(a), respectively. Thirdly, when used less post-yield stiffness ratio in the design of HDRB that mitigated the maximum absolute acceleration. For instance, when T and ß regarded as 2 s and 10 %, and λ decreased from 6 to 3, the maximum absolute accelerations were diminished from 4.20 to 3.92, 3.77 to 3.59, 3.87 to 3.72 m/s^2 (see Figures 4.50, 4.51, and 4.52 for 3, 6, and 9-storey frames hit by Northridge earthquake, respectively.

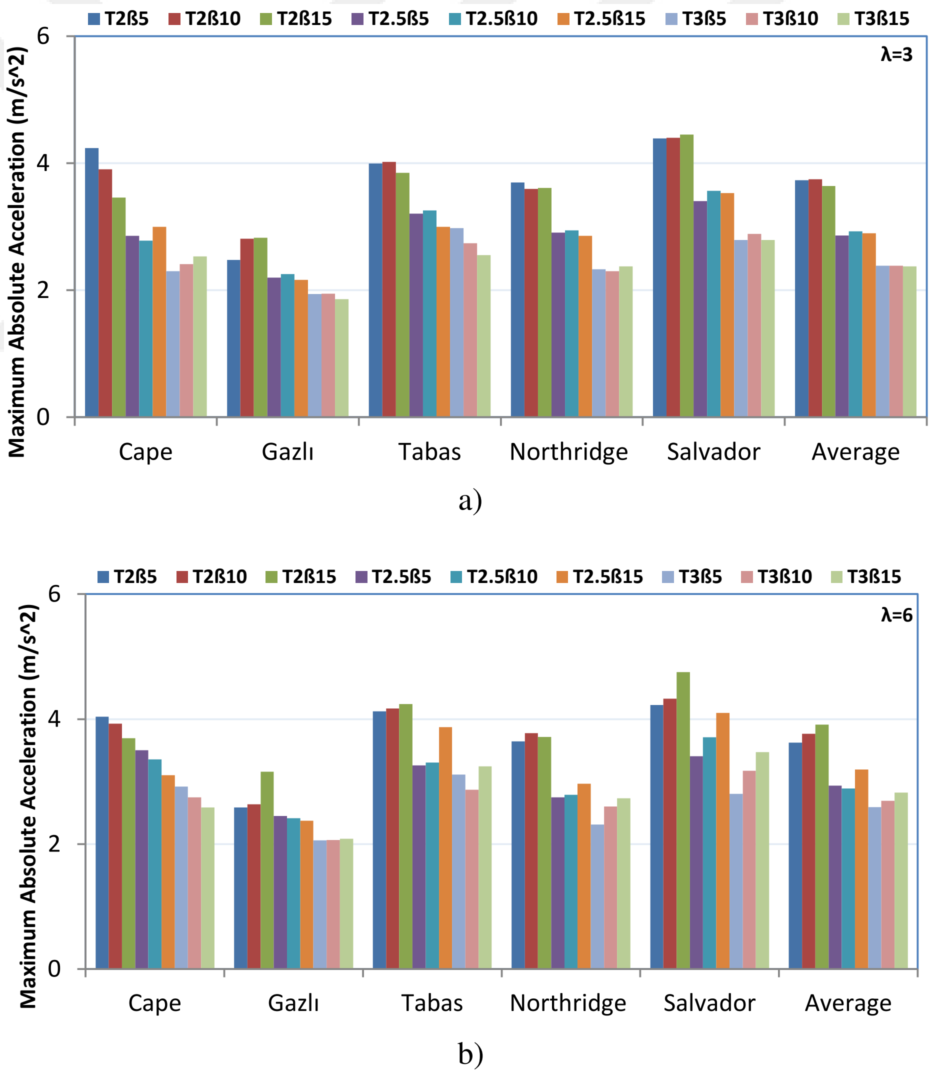

Figure 4.51 Maximum absolute acceleration of 6-storey frames

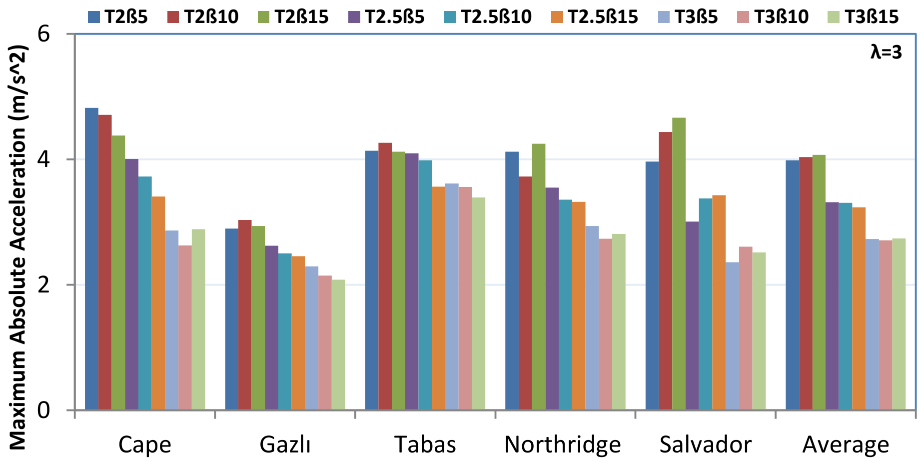

a)

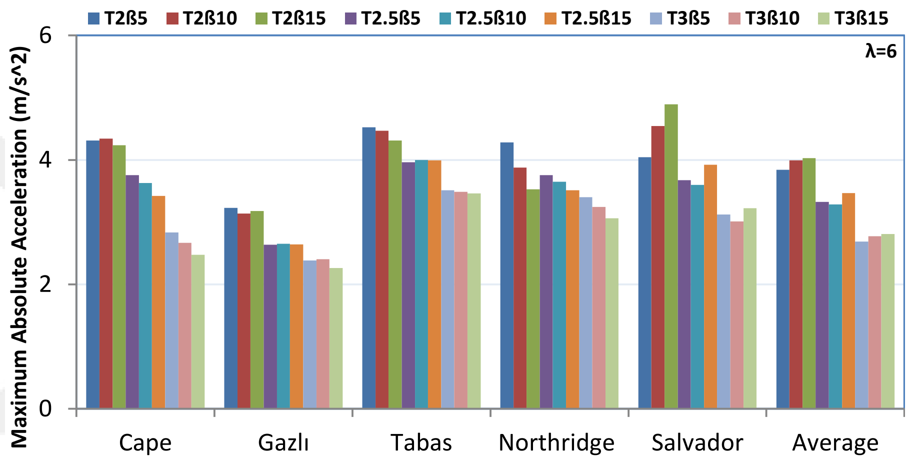

b)

Figure 4.52 Maximum absolute acceleration of 9-storey frames

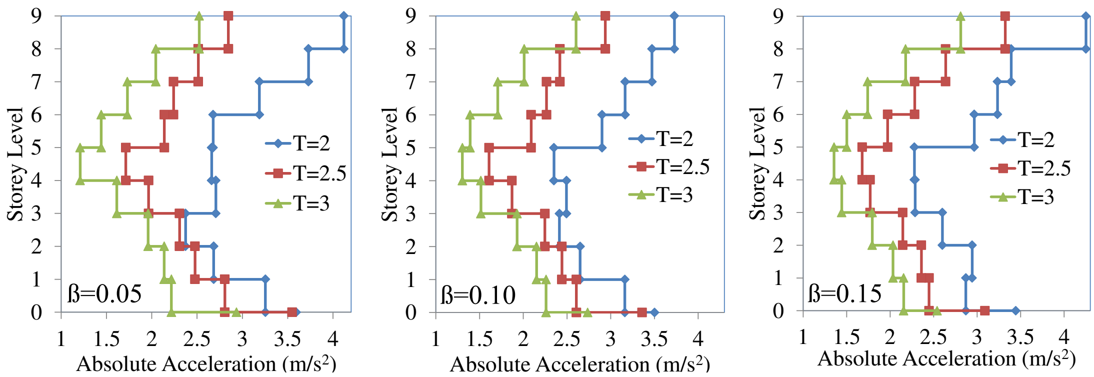

a) b) c)

Figure 4.53 Variation of the absolute acceleration against storey height of 9-storey isolated frames under Northridge earthquake for λ = 3

Furthermore, 9-storey with T3ß10λ3 under Northridge earthquake provided the lowest absolute acceleration as 2.73 m/s^2 (see Figure 4.52(a)) and more uniform distribution as shown in Figure 4.53(b). In addition, the roof absolulte acceleration was experienced as 3.87 m/s^2 for 9-storey isolated frame with the isolation system of T2ß10λ6 (see Figure 4.54(b)) while it was reduced to 3.73 m/s^2 in the isolation system of T2ß10λ3 (see Figure 4.53(b)). Similarly, the lowest roof absolute acceleration was obtained as 2.34 m/s^2 for 9-storey isolated frame with the isolation system of T3ß5λ6 (see Figure 4.54(a)).

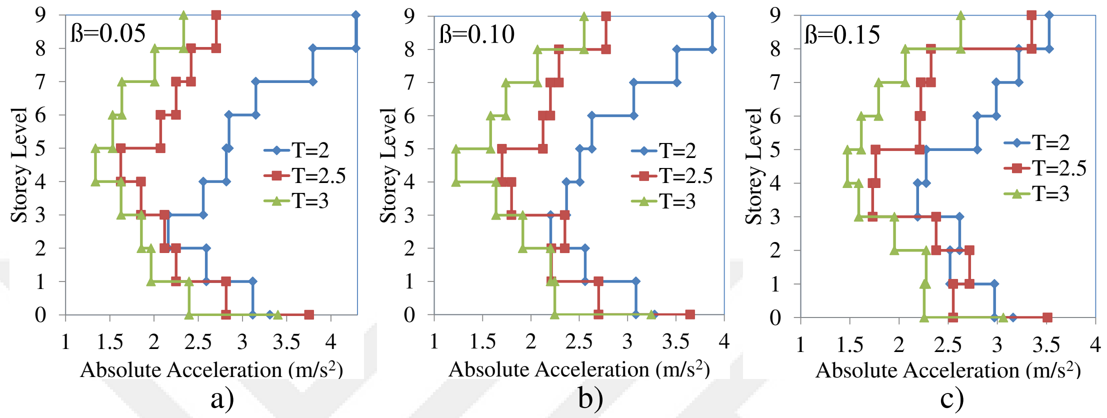

Figure 4.54 Variation of the absolute acceleration against storey height of 9-storey isolated frames under Northridge earthquake for λ = 6

4.4.4 Base Shear

The effectiveness of HDRB having different design properties was assessed through nonlinear analyses in which 3, 6, and 9-storey buildings hit by a series of earthquakes, and then the base shear demands of those were computed. The base shear demands of those were divided by corresponding total weights of 1290, 2540, and 3686 kN to compare the significance of the isolation systems of HDRB regarding the earthquake characteristics. The base shear ratios were in the range of 0.045-0.354 in all frames and depicted in Figures 4.55-4.57 where can be seen the use of HDRB substantially mitigated the base shear demand, depending on the number of storey of the structures. Compared to the lower isolation period, the greatest isolation period remarkably mitigated the base shear, irrespective of the earthquake characteristics. For instance, when Gazlı and Northridge earthquakes hit the 3-storey frame with T3ß15λ6 the lowest normalized base shears of 0.085 and 0.108 were obtained as shown in Figure 4.55(b).

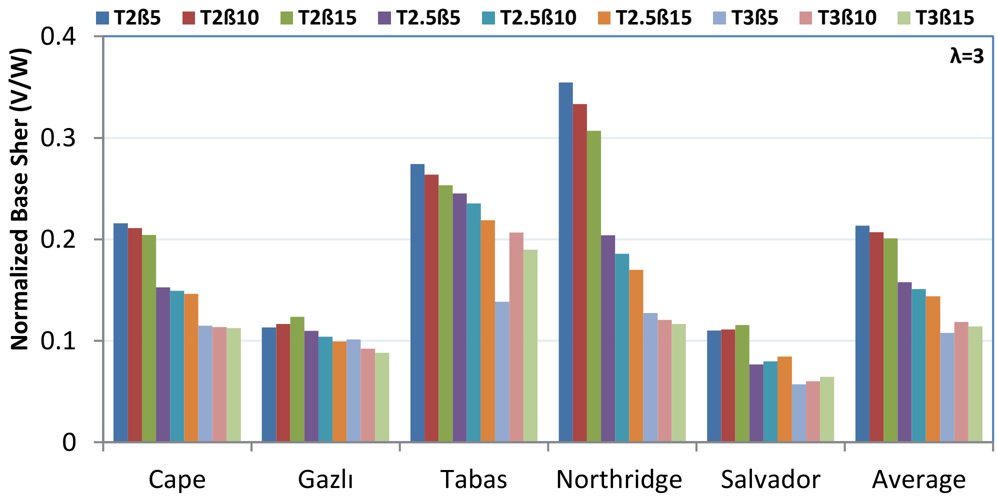

a)

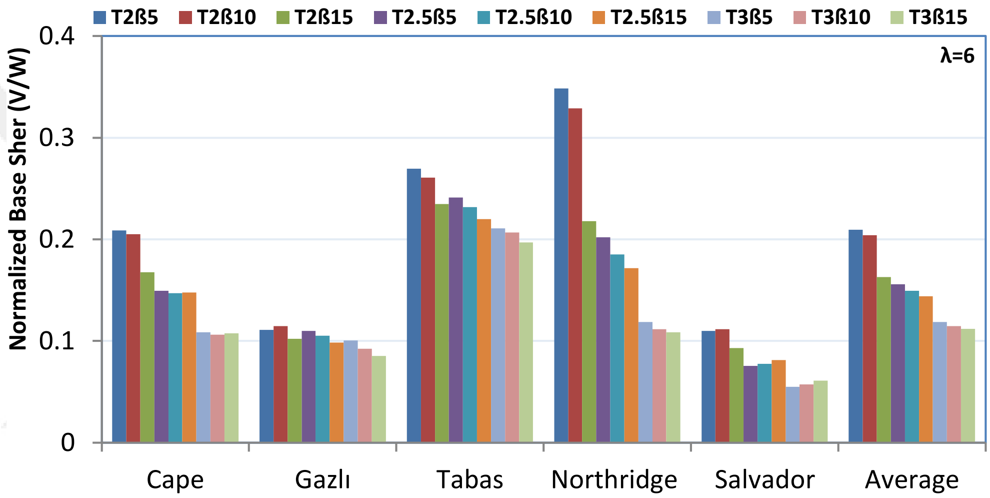

b)

Figure 4.55 Maximum base shear of 3-storey frames

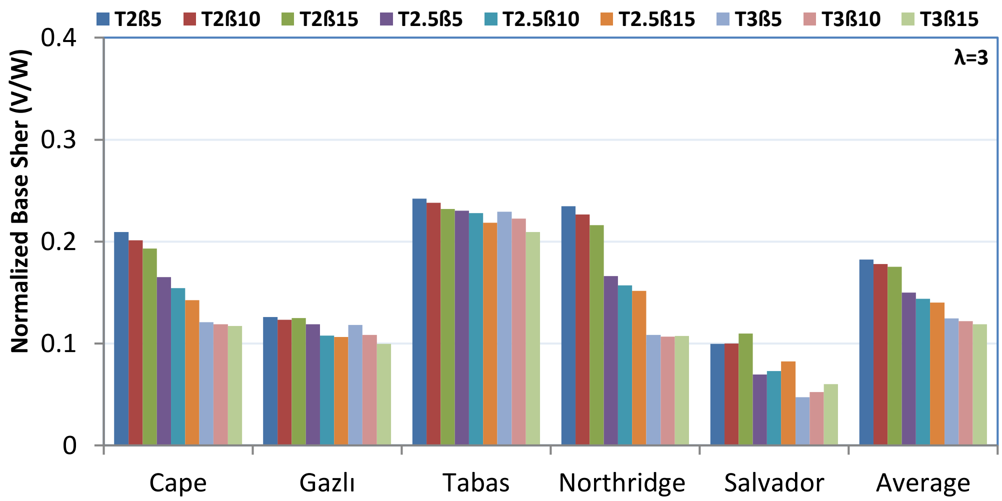

a)

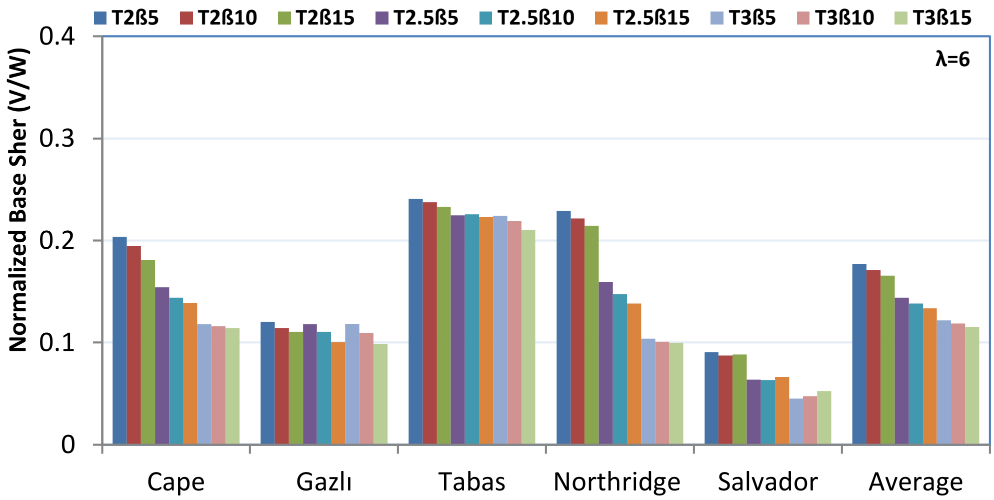

b)

Figure 4.56 Maximum base shear of 6-storey frames

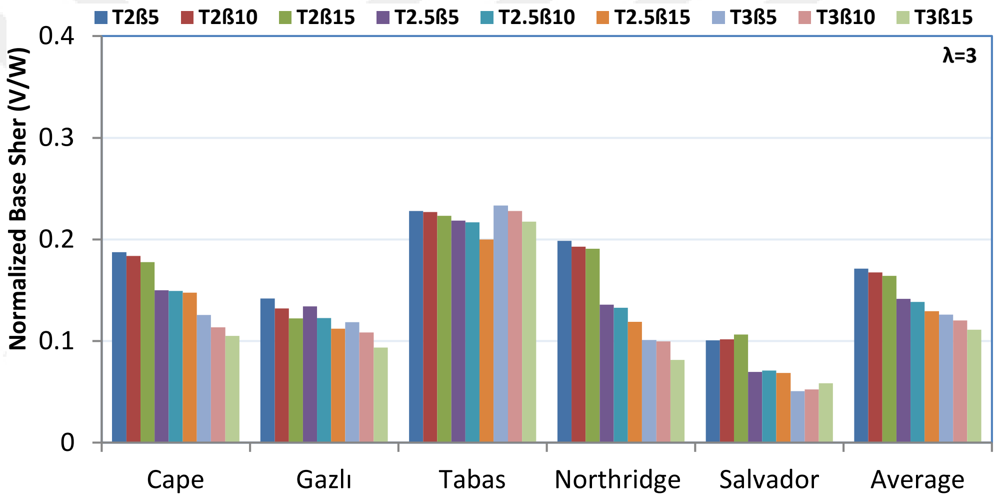

a)

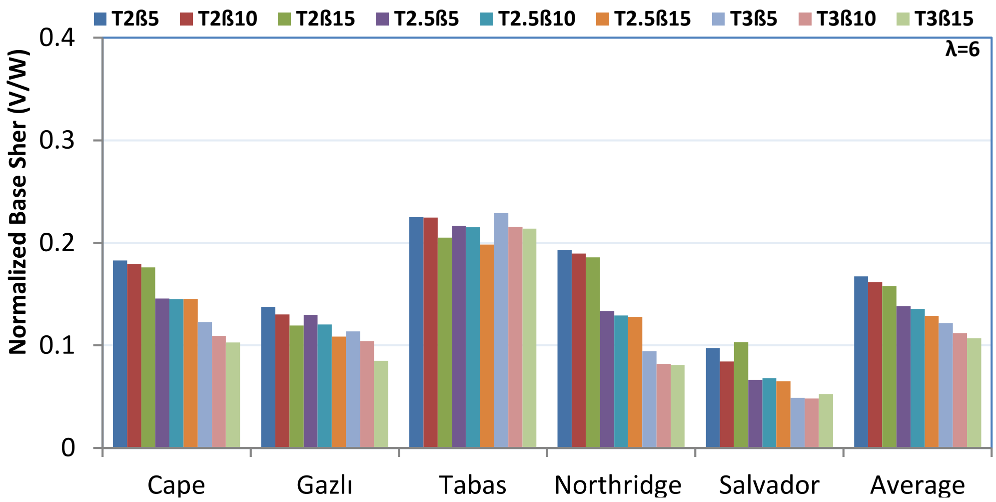

b)

Figure 4.57 Maximum base shear of 9-storey frames

Similarly, when subjected to Cape, Gazlı and Northridge earthquakes, it was as 0.114, 0.098, and 0.099 for 6-storey frame (see Figure 4.56(b)), 0.102, 0.084, and 0.081 for 9-storey frame (see Figure 4.57(b)), respectively. The use of ß as 10 and 15 % reduced the base shear demand. For instance, when increased ß from 5 to 10 % in the isolation of 3, 6, and 9-storey frames with T2ß5λ3 and hit by Cape earthquake, the normalized base shear mitigated from 0.215 to 0.210 (see Figure 4.55(a)), 0.209 to 0.201(see Figure 4.56(a)), and 0.187 to 0.183 (see Figure 4.57(a), respectively. The greater post-yield stiffness ratio of 6 was more decisive on the base shear demand as shown in Figures 4.55-4.57. When subjected to Cape earthquake the normalized base shear of 3, 6, and 9-storey frames with T3ß15λ3 introduced as 0.112, 0.117, and 0.105 while T3ß15λ6 case reduced it up to 0.107, 0.114, and 0.102 (see Figures 4.55-4.57). Similar trend can also be testified in Tables 4.5 where the average base shear reductions of the isolation systems are given in comparision with T2ß5λ3. The use of λ as 6 in the isolation models such as T3ß15λ6 reduced the average base shear as 47.6 % for 3-storey frame as shown in Table 4.5.

4.4.4 Base Moment

The base moment demands of the examined structures were plotted in Figures 4.58-4.60. Moreover, the average value of the maximum base moment reductions was given in Table 4.5. It was evidently proved that the base moments of the frames with HDRB fluctuated depending on the isolation parameters. HDRB sufficiently reduced the base moment in case of T enhanced to 2.5 and then 3 s. The lowest maximum base moment of 3-storey frame with T3ß15λ3 was introduced as 1513 and 957.8 kNm (see Figure 4.58(a)) under Tabas and Northridge earthquakes, it was as 5632 and 3337 kNm for 6-storey frame (see Figure 4.59(a)), respectively. The isolation systems having greater effective damping ratio mitigated the base moment. For example, 3, 6, and 9-storey frame with T3ß15λ3, T3ß15λ6, and T3ß10λ6 provided the average value of the minimum base moment as 962.8, 3737.2, and 7175.2 kNm, respectively. The influence of λ on the base moment demand could be monitored in Figures 4.58-4.60. Compared to T2ß5λ3, T2ß5λ6 reduced the maximum base moment from 1821 to 1722, 6000 to 5824, 14520 to 14100 kNm in case of 3, 6, and 9-storey frame hit by Cape earthquake, respectively, as shown in Figures 4.58-4.60.

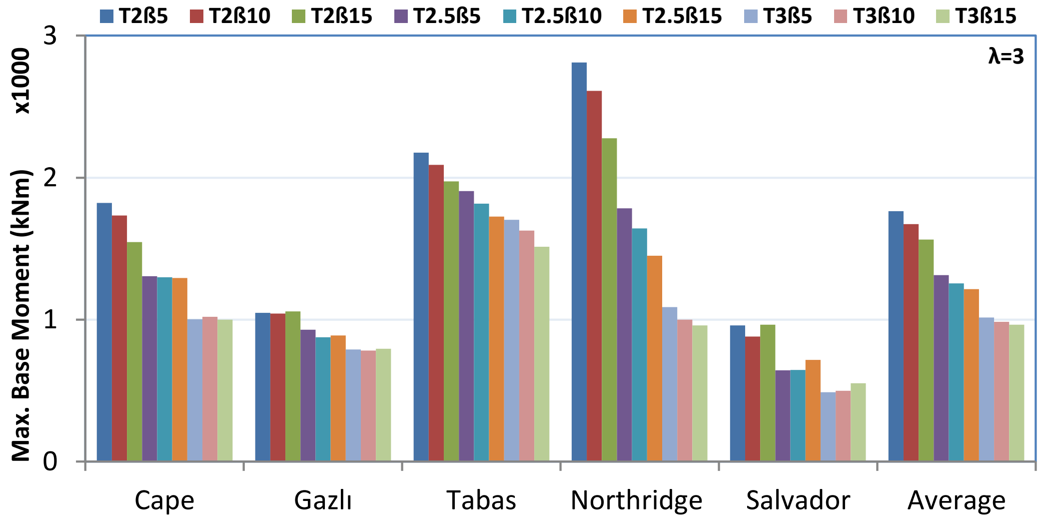

a)

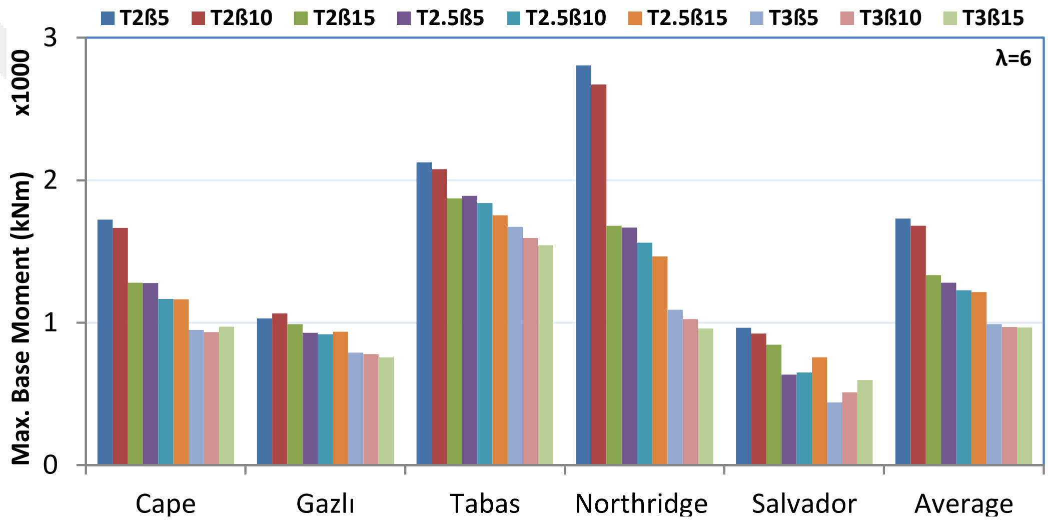

b)

Figure 4.58 Maximum base moment of 3-storey frames

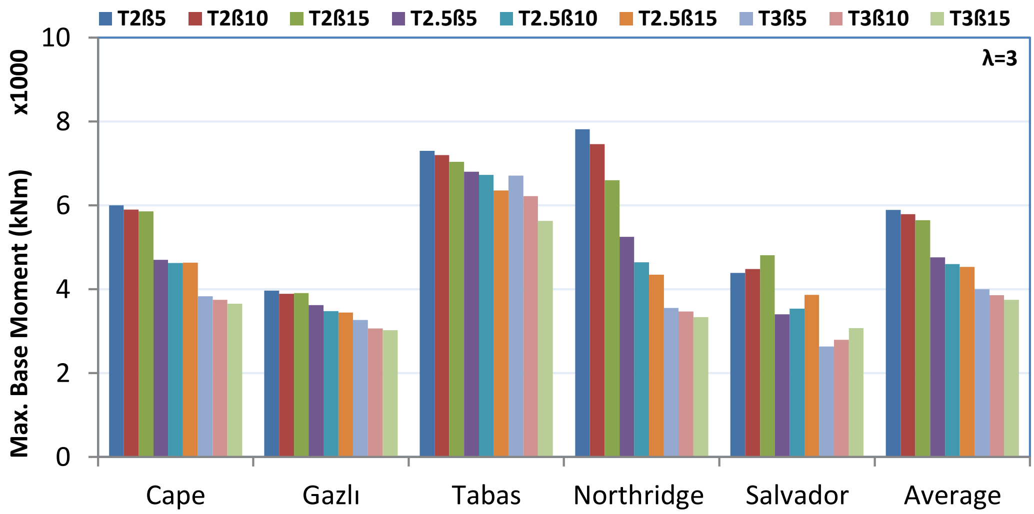

a)

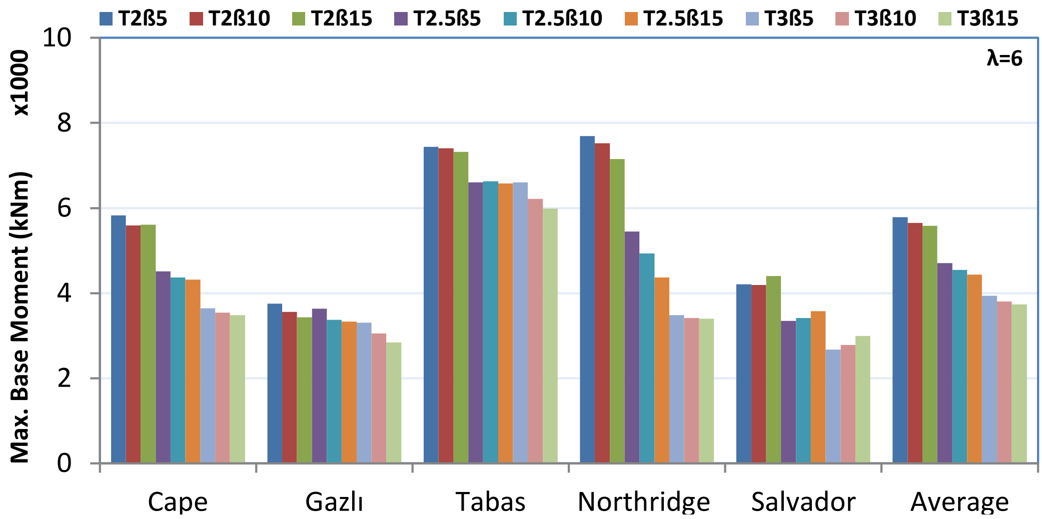

b)

Figure 4.59 Maximum base moment of 6-storey frames

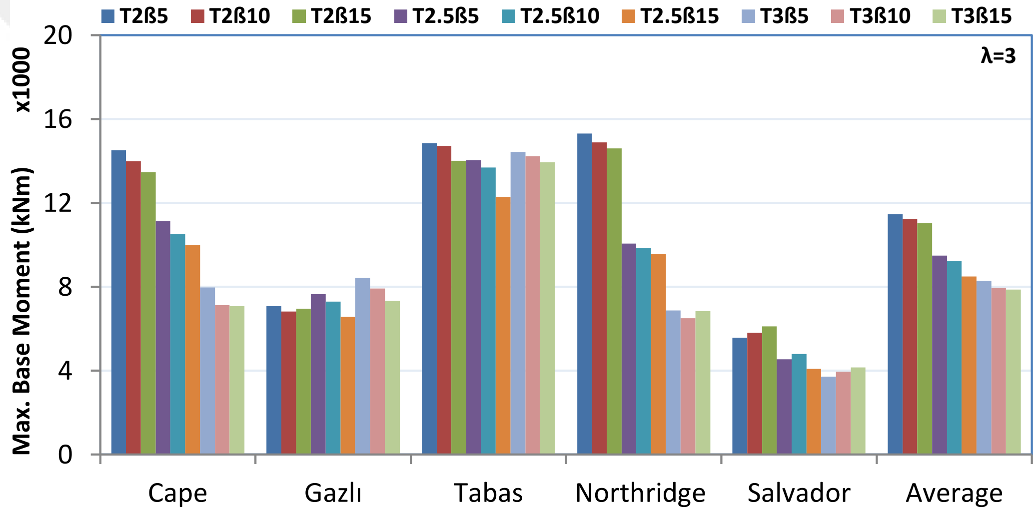

a)

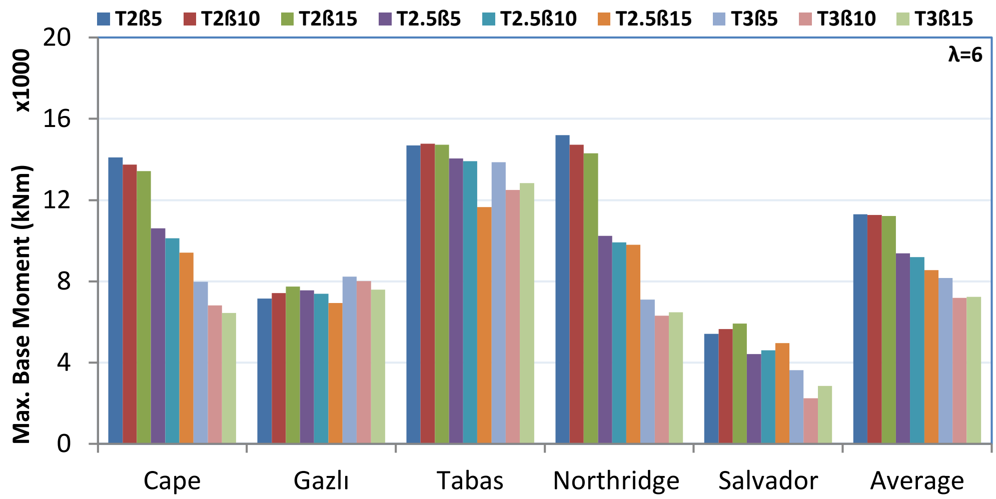

b)

Figure 4.60 Maximum base moment of 9-storey frames

In addition, the greatest average base moment reductions recorded as 45.4, 36.6, and 37.5 % when designed 3, 6, and 9-storey frames with T3ß15λ3, T3ß15λ6, and T3ß10λ6 cases as shown in Table 4.5, respectively. The isolation systems having greater isolation period and effective damping ratio provided the lowest maximum base moments which was also obtained both value of λ (i.e., 3 and 6). Therefore, it can be said that λ was less decisive than the T and ß as shown in Figures 4.58-4.60.

4.4.5 Hysteretic Behaviour and Energy Dissipation

When subjected to Gazlı earthquake the hysteretic curves of 3, 6, and 9-storey frames with eighteen various HDRB obtained and given in Figure B1. Those hysteretic curves were compatible with the typical bi-linear hysteretic force-displacement relationship (see Figure 2.15(a)) [76]. The isolation parameters significantly influenced the hysteretic characteristics of 3, 6, and 9-storey frames depending on the characteristics of ground motions. The utilization of the greater isolation period not only enlarged the area of the curves and also changed those behaviours. When ß and λ were fixed, the minimum and maximum oblique hysteretic curves were plotted for T of 2 and 3 s, respectively. The hysteretic curves including moderate value of T (namely, 2.5 s) located between them (see Figure B1). Furthermore, when HDRB designed with T = 3 s and ß = 5 %, T3ß5λ3 was remarkably enlarged the hysteretic curves reached to the strains of 0.206 m, 0.240, and 0.245 m corresponded to the forces of 43.12, 90.91, and 142.10 kN for 3, 6, and 9-storey buildings under Gazlı earthquake, respectively, as shown in Figure B1. The less ß tended to be depicted the larger hysteretic curve independently height of the buildings in case of T and λ were fixed. Similarly, the larger hysteretic curves obtained when the examined isolated frames designed with less λ as seen in Figure B1 (a, c, and e). For instance, 9-storey frame with T2.5ß5λ3 instead of T2.5ß5λ6 that was increased the displacement and force of the hysteretic curve from 0.185 to 0.190 m and 155.74 to 160.74 kN as shown in Figure B1(e, f). In addition, the reduction of λ made the hysteretic curve described linear behaviour while the shape of the hysteretic curve seemed to have been angular in case of λ enhanced to 6. For 3, 6, and 9-storey frames equipped with HDRB and hit by Gazlı earthquake, the amount of the dissipated energy computed by Equation 4.1 [130], and given in Table 4.6.

Table 4.6 Total dissipated energy Eloop (kJ) with isolation systems for 3, 6, and 9-storey frames under Gazlı earthquake

Isolation System	3-Storey Frame $\lambda = 3$	3-Storey Frame $\lambda = 6$	6-Storey Frame $\lambda = 3$	6-Storey Frame $\lambda = 6$	9-Storey Frame $\lambda = 3$	9-Storey Frame $\lambda = 6$
T2ß5	2.74	2.09	6.22	4.61	10.70	8.04
T2ß10	4.03	2.98	8.66	5.87	14.10	10.40
T2ß15	6.27	4.88	12.80	7.37	19.00	12.50
T2.5ß5	3.52	2.76	7.70	5.97	13.20	10.00
T2.5ß10	4.75	3.64	9.98	7.71	17.50	12.90
T2.5ß15	6.49	4.46	14.60	9.29	23.20	15.30
T3ß5	3.94	3.04	9.59	7.49	14.20	10.60
T3ß10	5.21	3.94	12.80	9.67	19.00	13.60
T3ß15	7.09	4.80	17.40	11.70	26.20	16.40

The utilization of both greater T and ß with less λ was necessary to obtain more and more energy dissipation as shown in Table 4.6. Firstly, compared to the isolation system of T2ß5λ3, it was observed that T2.5ß5λ3 and T3ß5λ3 cases increased the dissipated energy as 28.5 and 43.8 % for 3-storey frame, 23.8 and 54.2 % for 6-storey frame, and 23.4 and 32.7 % for 9-storey frame, respectively. The influence of ß on the amount of the dissipated energy can be evaluated by Table 4.6 For instance, when 3, 6, and 9-storey frames hit by Gazlı earthquake T3ß15λ3 ensured the maximum dissipated energies as 7.09, 17.40, and 26.20 kJ, respectively. The use of less λ let the dissipated energy to be increased as shown in Table 4.6.

4.5 Case-4 (FD, LRB, FPB, HDRB, and Combination of those)

Evaluating the effectiveness of the isolator characteristics of LRB, FPB, HDRB and slip load of FD in Cases 1, 2, and 3, as a final part, Case 4 was introduced. In this case, single and combine uses of energy dissipation devices (i.e., FD) and base isolation devices (i.e., LRB, FPB, HDRB) were adopted to examine the overall performance of the seismic protective systems. The most favourable isolation parameters of the isolators and slip load of FD were used to design more efficient protective systems. For this, the nonlinear seismic response of the considered case study frame (i.e., 5 OMF) with and without the seismic protective systems have been evaluated through time-history analyses in terms of displacements (i.e., storey, bearing and relative displacements), roof drift, interstorey drift ratio, absolute acceleration, base shear, base moment, hysteretic curve, and dissipated energy. They were comparatively discussed below.

4.5.1 Displacement

When the case study frame equipped with a series of passive protective systems and hit by seven different earthquakes through nonlinear time-history analyses, the storey displacements of those were determined and then presented in Figures 4.61 and 4.62. The former presented the maximum displacement demand of the case study frame with and without the protective systems for all earthquakes while the latter described the distribution of the displacement against height of the building for all earthquakes. In addition, the variation of the average percent values of the displacements for each of the protective systems with respect to that of the fixed base frame are given in Table 4.7 where can be easily followed the effectiveness of the proposed seismic protective systems.

Table 4.7 Variation of average local and global deformations for the frames with protective sysytems

Protective System	Disp. (%)	Rel. Disp. (%)	Roof Drift (%)	Int. S. Drift Ratio (%)	Abs. Acc. (%)	Base Shear (%)	Base Moment (%)
FD	-65.6	-65.6	-65.6	-68.9	-52.4	-43.9	-27.0
LRB	67.0	-84.3	67.0	-79.2	-86.4	-84.7	-50.8
FPB	39.9	-71.1	39.9	-69.2	-78.1	-83.5	-47.3
HDRB	74.5	-82.9	74.5	-76.8	-86.5	-84.1	-50.7
FD+LRB	60.0	-93.1	60.0	-84.5	-88.4	-84.3	-51.1
FD+FPB	29.2	-81.9	29.2	-78.7	-80.0	-83.2	-47.7
FD+HDRB	67.7	-92.4	67.7	-83.1	-89.6	-83.8	-50.9

It was observed that the protective systems remarkably differentiated the displacement demand of the case study frame. Firstly, the sudden drop in the maximum displacement demand rooted in the utilization of FD, and what is more, it is valid for all earthquake responses as shown in Figure 4.61. For example, the case frame structure was equipped with FD and then subjected to Gazlı earthquake, the greatest displacement reduction was observed as 76.0 % that meant the maximum displacement mitigated from 18.73 to 4.50 cm as shown in Figures 4.61 and 4.62(e). Each of the storey displacements were gradually rehabilitated by FD, and also distribution of the displacement became more uniform compared to the fixed-base frame as shown in Figure 4.62(a-h). In addition, the average displacement reduction was recorded as 65.6 % (see Table 4.7). Secondly, the use of the base isolation devices increased the maximum displacement demands of the case study frame structure (see Figure 4.61). Compared to FPB, the elastomeric bearing isolators (i.e., LRB and HDRB) produced much more displacement demands.

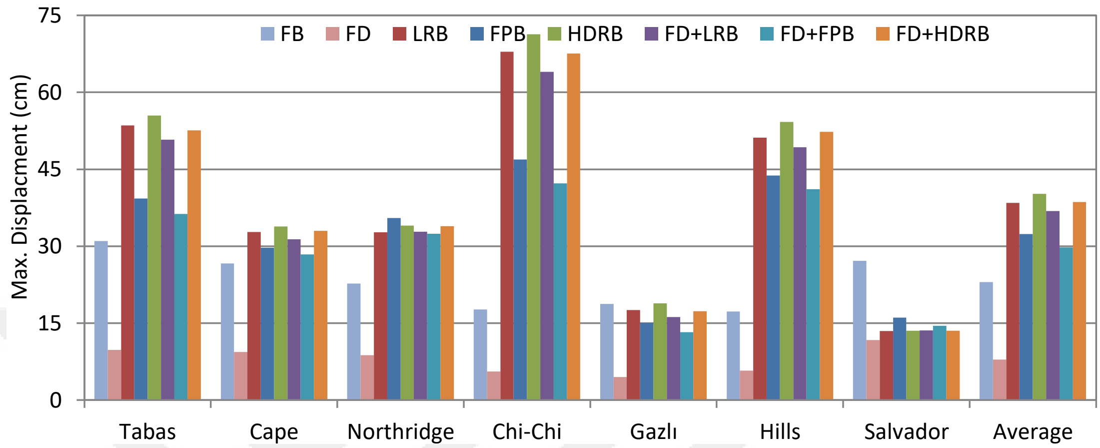

Figure 4.61 Maximum displacements for the frames with and without protective sysytems

When subjected to Chi-Chi earthquake, FPB, LRB, and HDRB introduced the greatest value of the maximum displacement as 45.96, 67.94, and 71.34 cm, respectively, as shown in Figures 4.61 and 4.62(d). The similar trend almost can be monitored for the other earthquake responses. As a matter of fact that the average values of the maximum displacement percentages of 39.9, 67.0, and 74.5 % (see Table 4.7) were obtained for FPB, LRB, and HDRB whose influences on the enhancement of the displacement demand were proved.

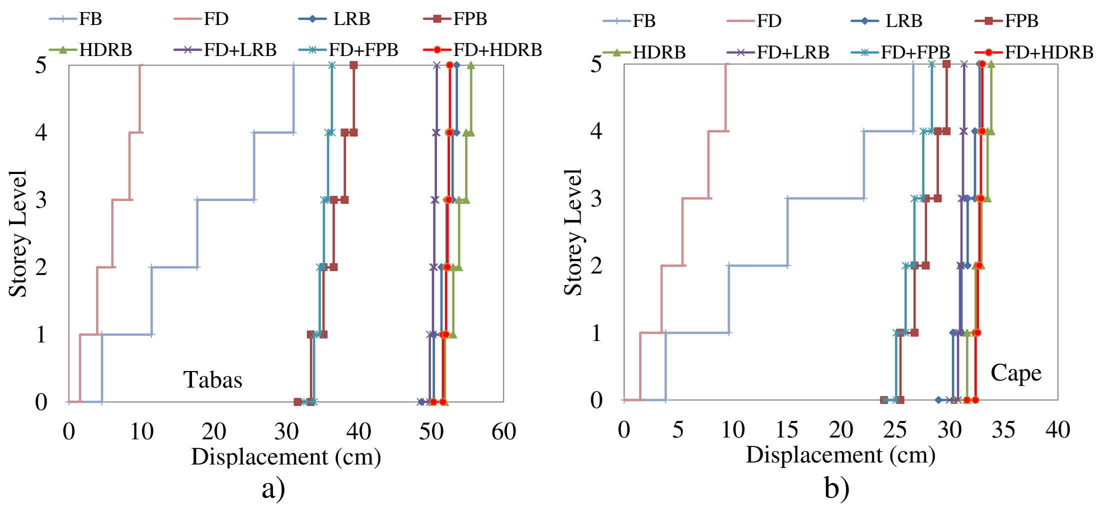

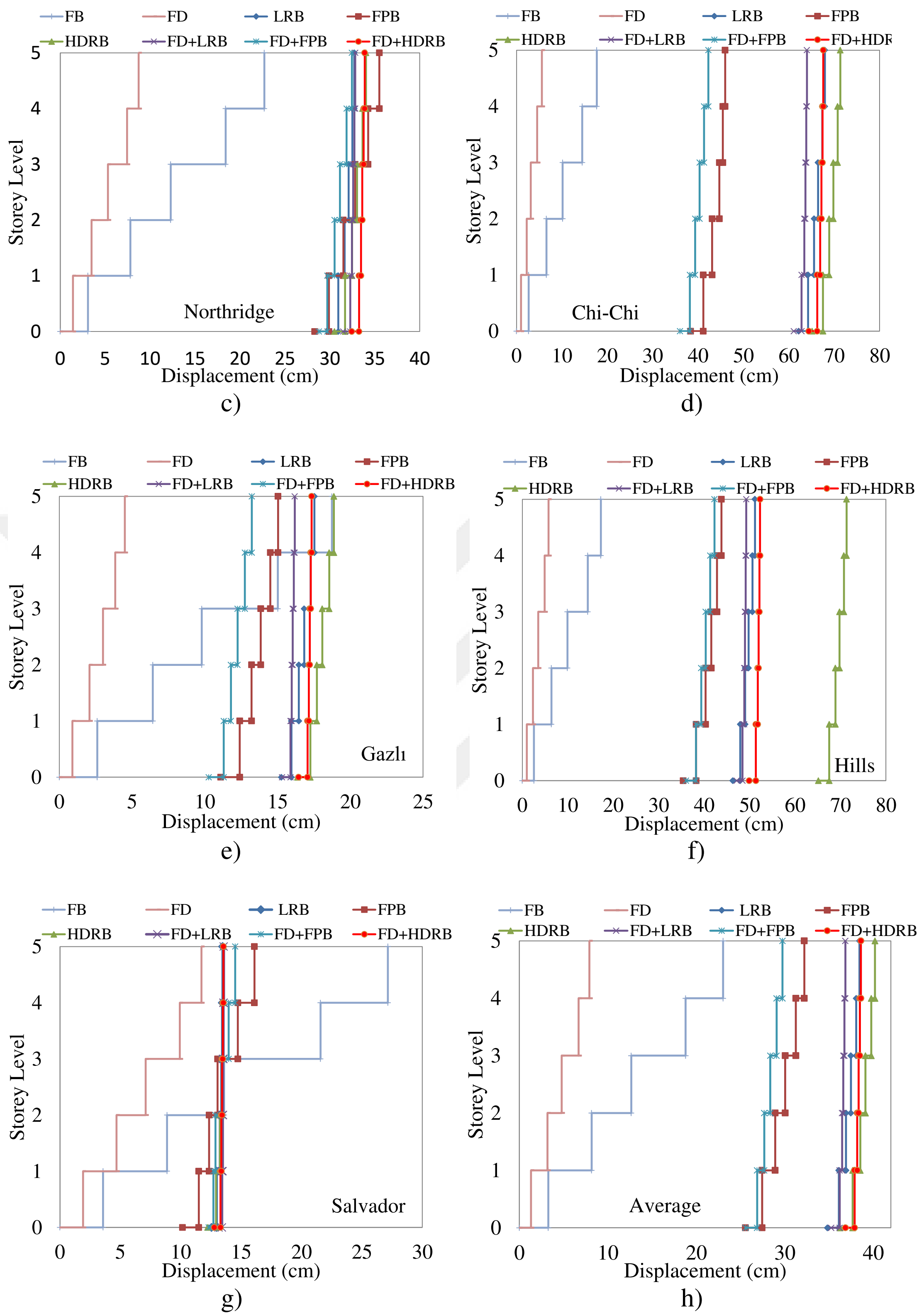

Figure 4.62 Variation of the displacement against storey height

In addition, the elastomeric bearings especially LRB were much more susceptible to exhibiting more uniform storey displacement demand than friction-based devices (i.e., FD and FPB) as shown in Figure 4.62(a-h). Thirdly, when examined the displacement demand considering the combined case, it was observed that the utilization of the FD with the elastomeric bearings not only increased the displacement but also exhibited much more uniform distribution than FD, FPB, and combination of those together as FD+FPB as shown in Figure 4.62. For instance, the average percentage of the maximum displacement enhancement recognized as 60.0 and 67.7 % for FD+LRB and FD+HDRB, respectively. However, it was as 39.9 and 29.2 % for FPB and FD+FPB, respectively, as shown in Table 4.7. The maximum bearing displacements induced by the isolation systems are depicted in Figure 4.63. Since the stiffness of the friction-based isolator was much more than the elastic bearings (see Table 3.5) the latter was much more prone to lateral movement. Thus, the greatest bearing displacement was observed when implemented the elastomeric isolation systems, on the other hand friction-based protective systems introduced the lowest bearing displacement. For example, the considered case study frame equipped with FPB and then subjected to Tabas, Cape, Northridge, Salvador earthquakes the lowest bearing displacements obtained as 31.60, 23.97, 28.31, 10.14 cm, furthermore, it was as 36.02, 10.27, 35.16 cm for FD+FPB under Chi-Chi, Gazlı, Hills earthquakes, respectively. The greatest bearing displacements testified as 65.15, 11.13, and 50.36 cm cm for HDRB, FD+LRB, and FD+HDRB under Chi-Chi, Salvador, and Tabas earthquakes, as hown in Figure 4.63.

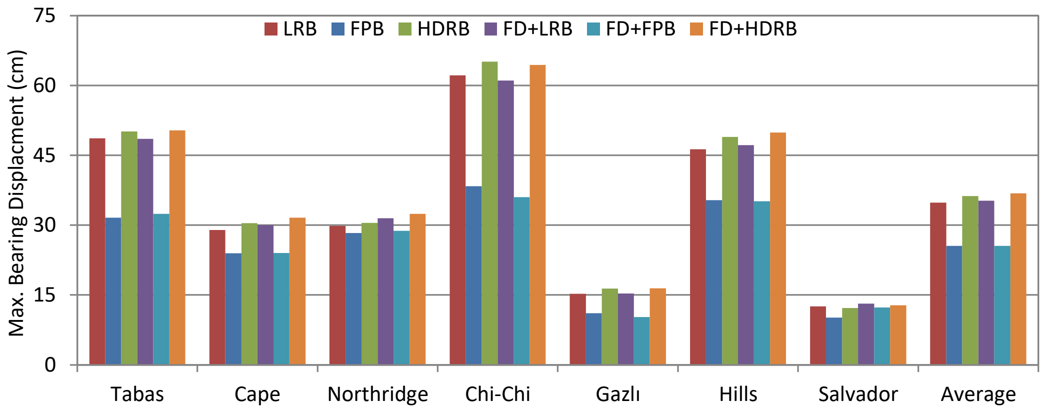

Figure 4.63 Maximum bearing displacements for the frames with protective sysytems

4.5.2 Relative Displacement

The displacement of a point on the structure respect to the ground level adopted as the relative displacement and acknowledged one of the most reliable seismic performance evaluation parameters [131]. The variation of the maximum relative displacements was presented in Figure 4.64. The equipment of the protective systems reduced the relative displacement of the considered case study frame structure. When subjected to Gazlı earthquake the use of FD mitigated the relative displacement from 18.73 to 4.49 cm, it was as 0.87, 0.90, 2.96, 2.27, 2.50, and 3.94 cm in case of FD+LRB, FD+HDRB, FD+FPB, LRB, HDRB, and FPB. In addition, the lowest relative displacements were presented as 1.34, 2.89, 2.10, and 0.43 cm under Cape, Chi-Chi, Hills, and Salvador earthquakes, respectively, as shown in Figure 4.64. Compared to the single use of the protective systems, the effectiveness of the combine protectives systems was proved by the average relative displacement demand. For example, the relative displacement was observed as 3.62, 3.94, and 6.66 cm for LRB, HDRB, and FPB while it was as 1.60, 1.75, and 4.18 for FD+LRB, FD+HDRB, and FD+FPB, respectively.

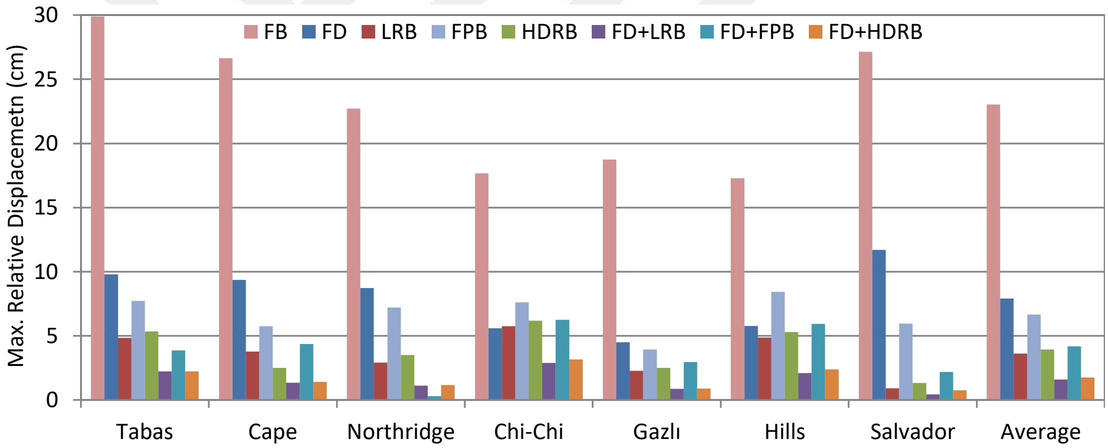

Figure 4.64 Maximum relative displacements for the frames with and without protective sysytems

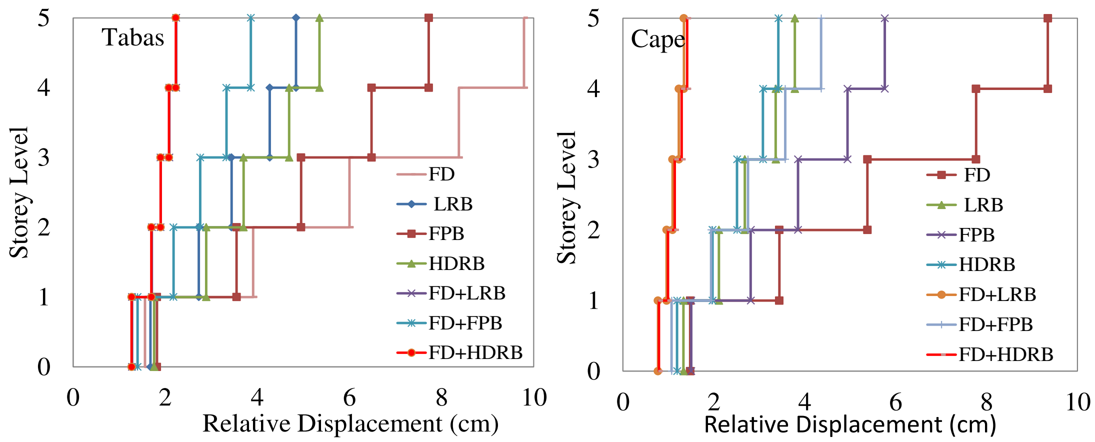

a) b)

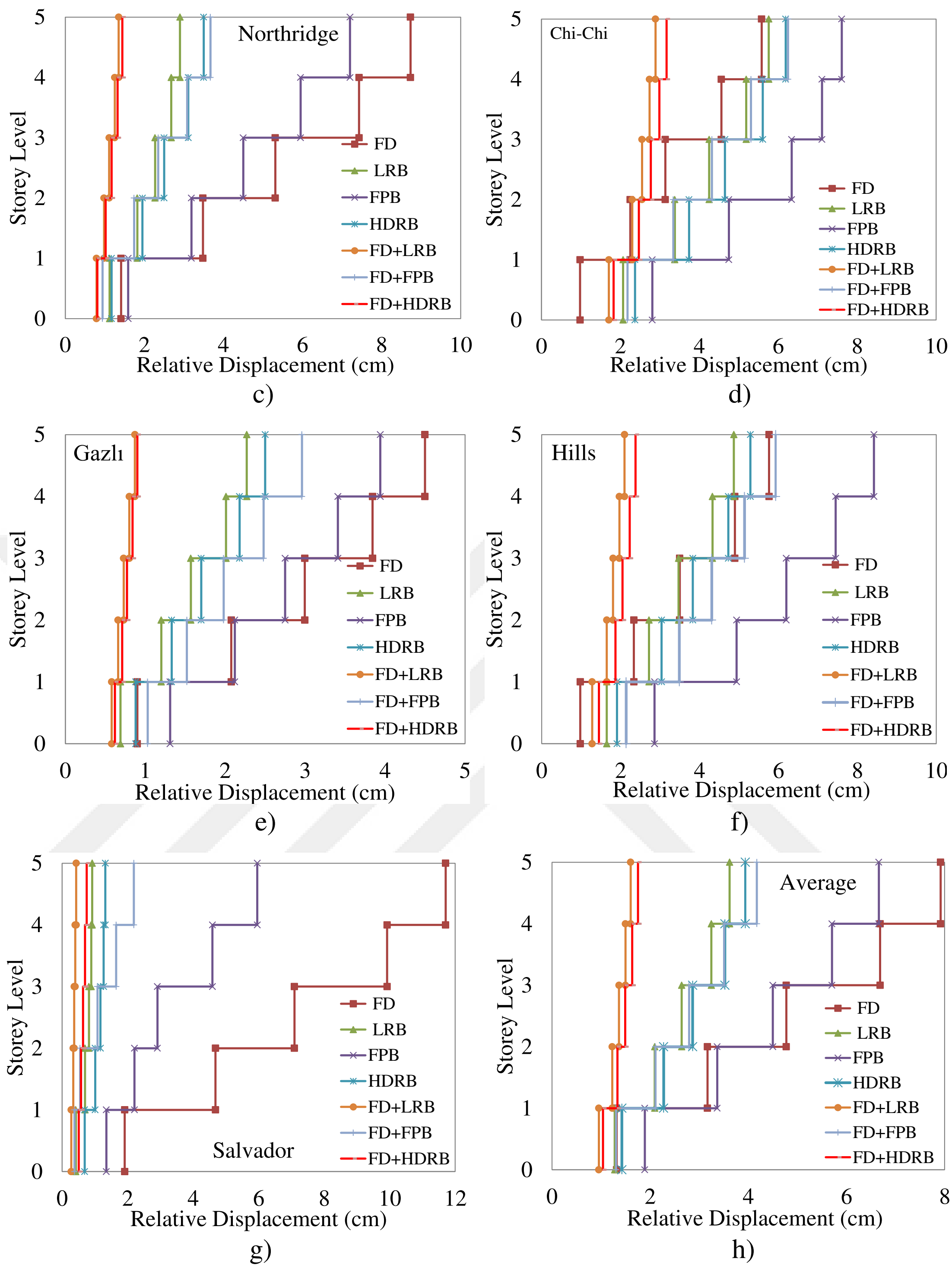

Figure 4.65 Variation of the relative displacement against storey height

The variation of the relative displacement demands over the height of the case study frames were given in Figure 4.65 for all earthquakes. The utilization of FD with the base isolation systems together not only mitigated the relative displacement of the fixed-base frame but also perfectly regulated the non-uniform distribution as given in Figures 4.65(a-h). For example, the protective systems of FD+LRB and FD+HDRB subjected Salvador earthquake, mitigated the top storey relative displacement of the fixed base frame from 27.1 cm to 0.43 and 0.75 cm, respectively, as shown in Figure 4.65(g). Furthermore, the greatest average relative displacement reductions carried out by FD+LRB, FD+HDRB, LRB, and HDRB as 93.1, 92.4, 84.3, and 82.9 %, respectively, presented in Table 4.7. Compared to the friction-based protective systems (FD, FPB, FD+FPB), the success of the elastomeric bearings on the relative displacement reduction proved by Figures 4.64 and 4.65.

4.5.3 Roof Drift Ratio

The roof displacement divided by the height of the buildings, and called as roof drift ratio used for the evaluation of the structural damage [132]. The maximum roof drift ratios of the investigated frames were computed for all earthquakes and presented in Figure 4.66 where can be observed that the braking effect of FD led to experience the lowest roof drift under each of the earthquakes. Similarly, both of FPB and FD+FPB exhibited the lower roof drift. Compared to the friction-based protective systems, the others caused the greater roof drift as they had lower stiffness than FPB (see Table 3.5). For example, the roof drift of 1.94 was obtained when the case study frame structure subjected to Tabas earthquake while it was reduced up to 0.61, 2.27, 2.46 for FD, FD+FPB, FPB, conversely it was enhanced to 3.17, 3.29, 3.35, 3.47 for FD+LRB, FD+HDRB, LRB, and HDRB, respectively.

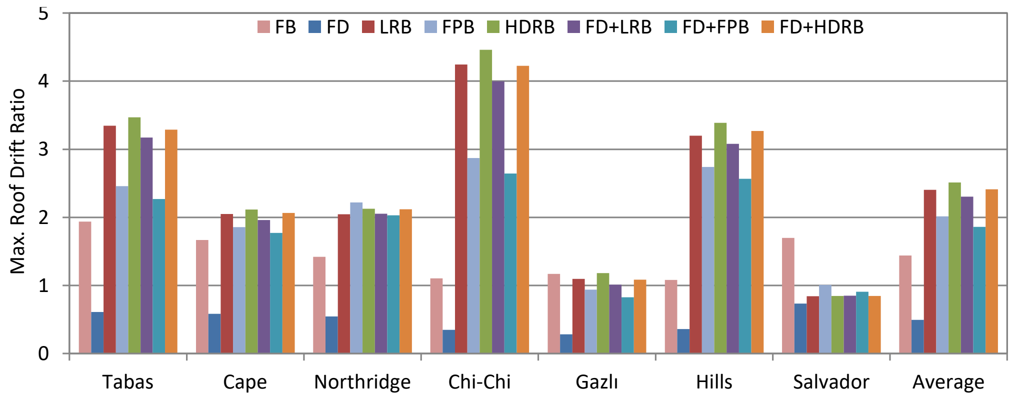

Figure 4.66 Maximum roof drift ratio for the frames with and without protective sysytems

The lowest roof drift of 0.28 for FD under Gazlı earthquake were acquired while the greatest roof drift was as 4.45 for HDRB under Chi-Chi earthquake as displayed in Figure 4.66. Similarly, the lowest average roof drift reduction was occurred as 65.6

% in case of FD while HDRB caused the greatest average roof drift ratio increase as 74.5 %. FPB induced the average roof drift reduction as 39.9 % while it was as 29.2 % for FD+FPB as listed in Table 4.7. The time-history responses of the roof drift for the case study frame with and without the protective systems under Northridge earthquake are given in Figure 4.67.

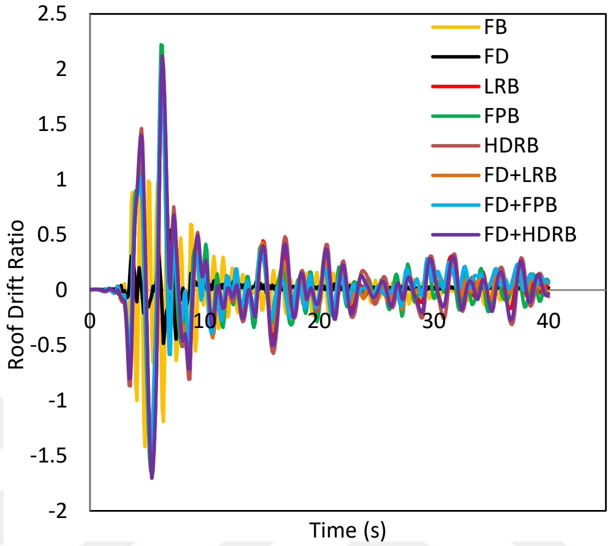

Figure 4.67 Time-history response of the roof drift ratio for the case frames with and without protective sysytems under Northridge earthquake

The use of FD not only reduced the roof drift but also restricted the fluctuation of the roof drift under Northridge earthquake. In other words, the response of the roof drift for the fixed base frame was fluctuated between -1.42 and 1.10, and it was ranged from -0.48 to 0.54 by FD while it was between -1.63 and 2.05 (LRB), -1.64 and 2.22 (FPB), -1.70 and 2.13 (HDRB), -1.61 and 2.05 (FD+LRB), -1.45 and 2.03 (FD+FPB), -1.70 and 2.12 (FD+HDRB as shown in Figure 4.67.

4.5.4 Interstorey Drift Ratio

The interstorey drift ratio was defined as the displacement difference of the adjacent storey normalized by the corresponded storey height. It is well associated with the assessment of the structural damage level [133]. The maximum interstorey drift ratios were computed for all the frames under earthquakes, and presented in Figure 4.68. In addition, the interstorey drift ratios against storey height of the considered case study frame with and without the protective systems under all earthquakes were plotted in Figure 4.69(a-h).

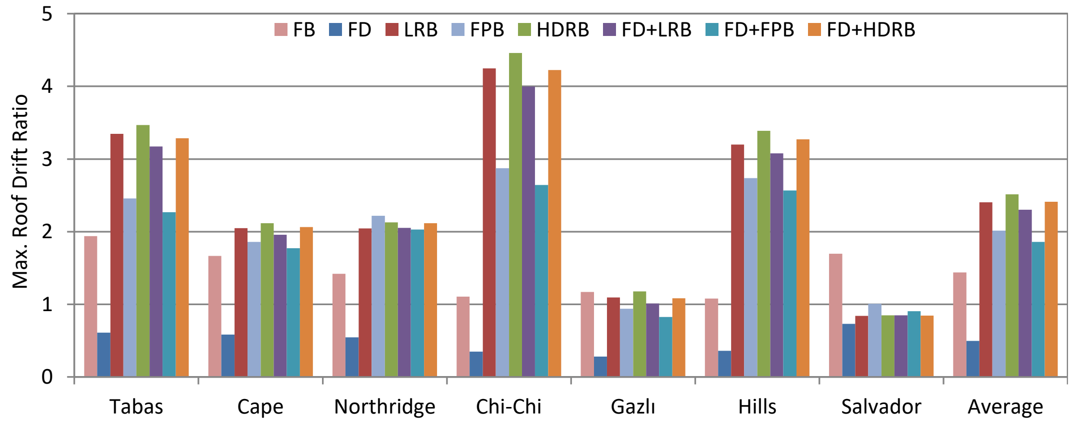

Figure 4.68 Maximum interstorey drift for the frames with and without protective sysytems

When subjected to all earthquakes the considered case frame produced immense interstorey drift ratios were generally beyond the near collapse damage state of 1.8 %, fortunately it was decreased up to the operational limit damage state of 0.8 % in case of the utilization of FD under all earthquakes. However, one exception was witnessed for Salvador earthquakes as revealed in Figure 4.68. As for the base isolation systems, LRB reached the lower interstorey drift ratios and satisfied the operational limit, even the fully operational limit with 0.35, 0.22, 0.13 % under Northridge, Gazlı, Salvador earthquakes, respectively. The operational limit was almost obtained for FPB under all earthquakes, but the earthquakes of Chi-Chi and Hills caused to the life safety damage level due to introducing 0.88 and 0.89 % interstorey drift. HDRB succeeded the fully operational limit under Cape, Northridge, Gazlı, and Salvador earthquakes as shown in Figure 4.68. The combination cases substantially provided the fully operational limit. For instance, when subjected to Northridge earthquake, the maximum interstorey drift ratio of the case study frame was 1.91 % corresponded to the near collapse damage state while it was reached to fully operational limit of 0.24, 0.29, 0.25 % by virtue of FD+LRB, FD+FPB, FD+HDRB, respectively, as displayed in Figure 4.68. In addition, the lowest average maximum interstorey drift ratio was observed as 0.29 % in case of the combination of FD with LRB together. The exertion of the isolation devices to reduce the interstorey drift over the height of the frame can be observed in Figure 4.69(a-h). FD mitigated the interstorey drift ratio to a certain extent, but it could not describe prominent interstorey drift distribution (see Figure 4.69(a, g)) where FD could not afford to satisfy the fully operational limit. Fortunately, each of the elastomeric bearings provided both uniformly distribution and mitigation of the interstorey drift. FPB depicted the most uniform interstorey drift distribution under Cape and Northridge earthquake (see Figure 4.69(b, c)) where the fully operational damage state achieved. As seen in Figure 4.69(b), compared to FD, the utilization of the elastomeric bearings or the combination of FD with the base isolation systems remarkably arranged the interstorey drift distribution and also achieved the damage state of the fully operational. It should be noted that the combined protective systems especially FD+LRB and FD+HDRB exhibited better interstorey drift response regardless of the earthquake records. The average values of the maximum interstorey drift ratio reductions are presented in Table 4.7 whereby the performance of the proposed protective systems can be evaluated. Compared to the friction-based systems of FD and FPB, the elastomeric bearings of LRB and HDRB introduced the greater reductions as 79.2 and 76.8 %, respectively, but the greatest average reductions of 84.5 and 83.1 % were governed by FD+LRB and FD+HDRB, respectively.

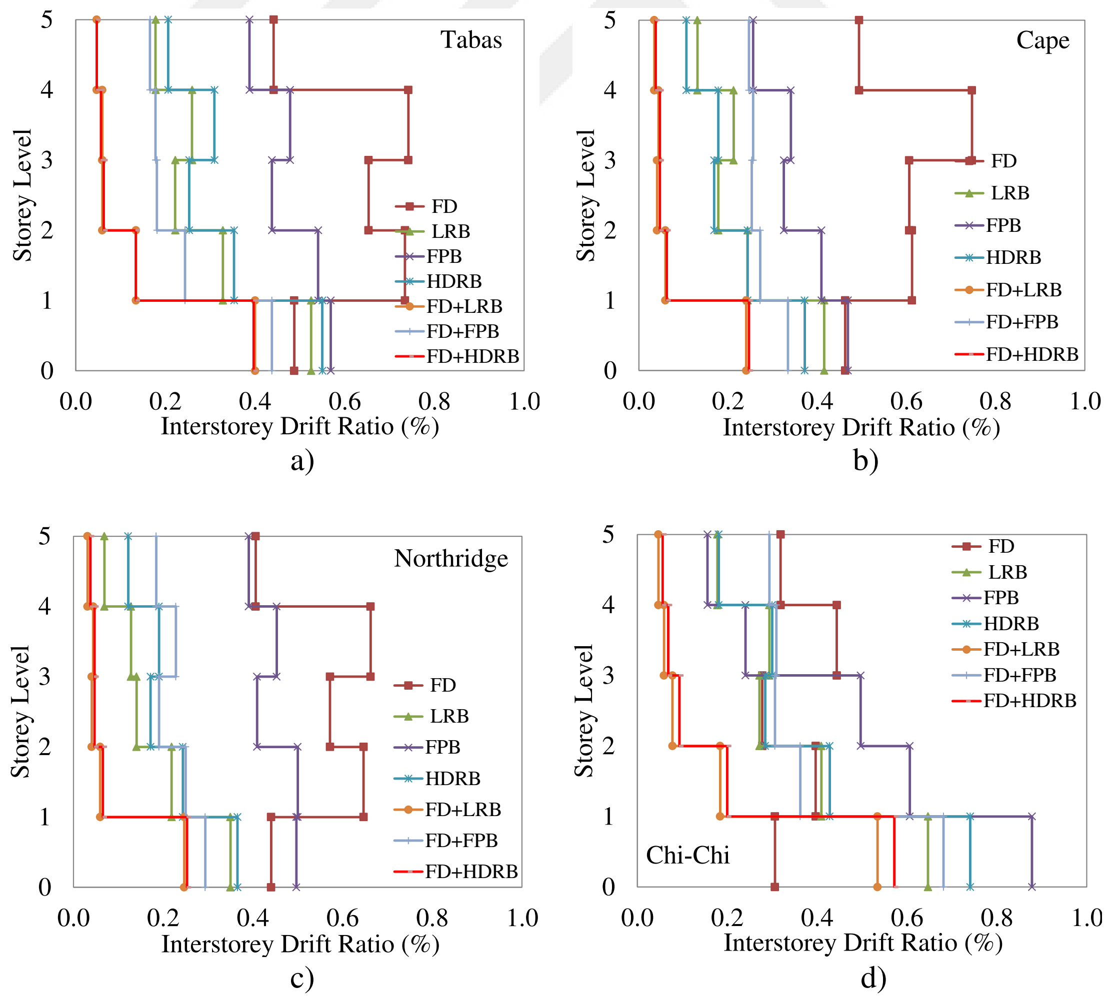

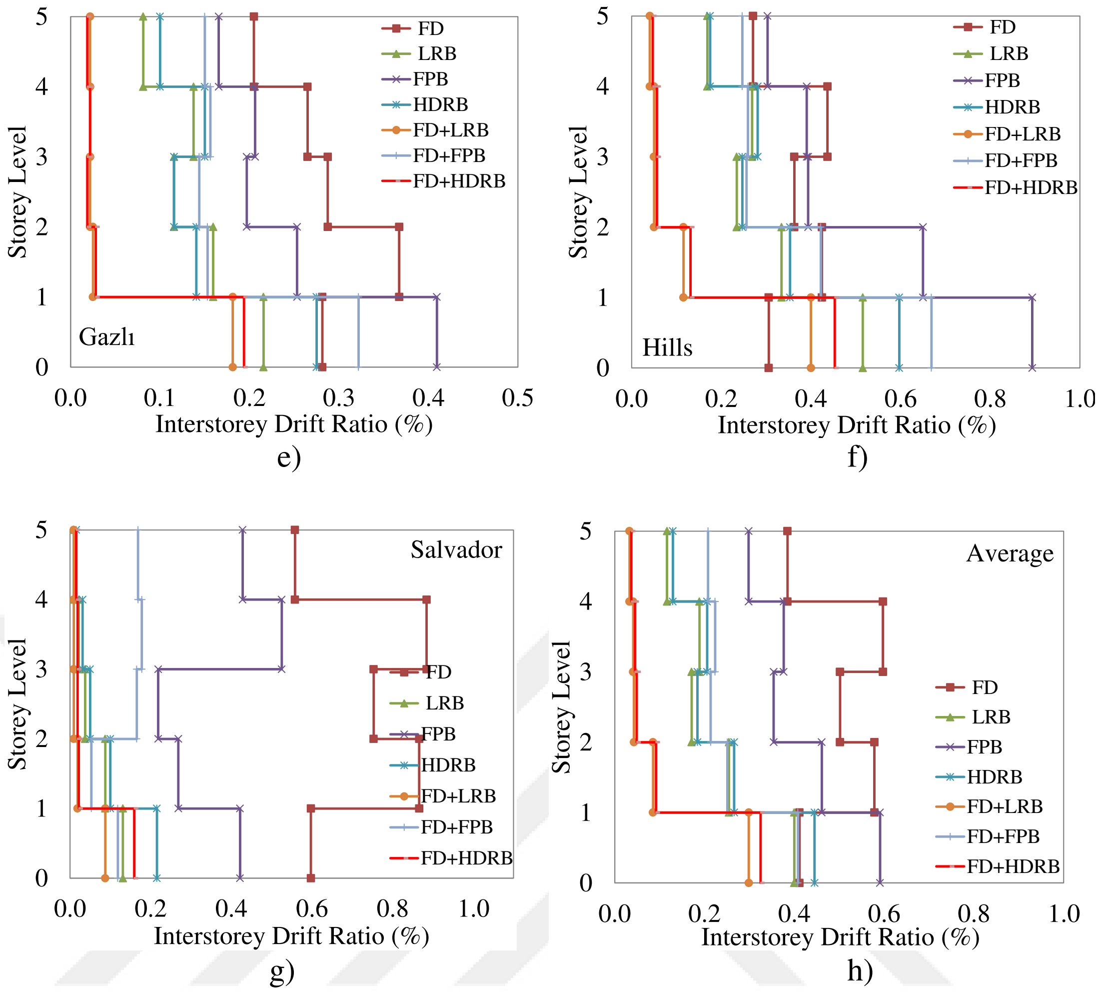

Figure 4.69 Variation of the interstorey drift ratio against storey height

4.5.5 Absolute Acceleration

The maximum absolute accelerations were computed for the case study frame with and without the protective systems under seven earthquakes and presented in Figure 4.70. When the considered case study frame subjected to the seven earthquake records, the average maximum absolute acceleration of 1.88 g recorded for the fixed base frame. The equipment of FD almost reduced by half of the maximum absolute acceleration independently active earthquakes. For example, Hills and Salvador earthquakes caused the maximum absolute accelerations of 1.27 and 2.43 g while they were mitigated up to 0.64 and 0.90 g thanks to FD (see Figure 4.70), respectively. The elastomeric base isolation systems were much more effective in reducing the absolute acceleration than the other systems. It was observed that LRB and HDRB performed the dramatic absolute accelerations as 0.34 and 0.30 g, they were as 1.02 and 0.80 g for FD and FPB, similarly, 0.28, 0.43, 0.23 g introduced by

FD+LRB, FD+FPB, and FD+HDRB under Tabas earthquake, respectively. Therefore, the combined cases were much more favourable in terms of the absolute acceleration mitigation. Among them, the lowest maximum absolute accelerations were recorded by FD+LRB under Chi-Chi, Gazlı, Hills earthquakes, FD+HDRB under Tabas, Cape, Nortridge and Salvador earthquakes as depicted in Figure 4.70. In addition, the variation of the absolute acceleration over the height of the frame plotted in Figure 4.71. When the response of the protective systems compared in terms of the storey absolute acceleration demands, it was observed that the frames equipped with FD and the base isolation systems together were much more protective than the other protective systems. In addition, the protective systems except the friction-based ones sharply reduced the absolute acceleration. For example, FD mitigated the roof absolute acceleration of FB from 2.34 to 1.02 g under Tabas earthquake (see Figure 4.71(a)) while it was as 0.34, 0.80, 0.30 g for LRB, FPB, HDRB, respectively. By the way, it was as 0.28, 0.43, 0.23 g for FD+LRB, FD+FPB, FD+HDRB, respectively.

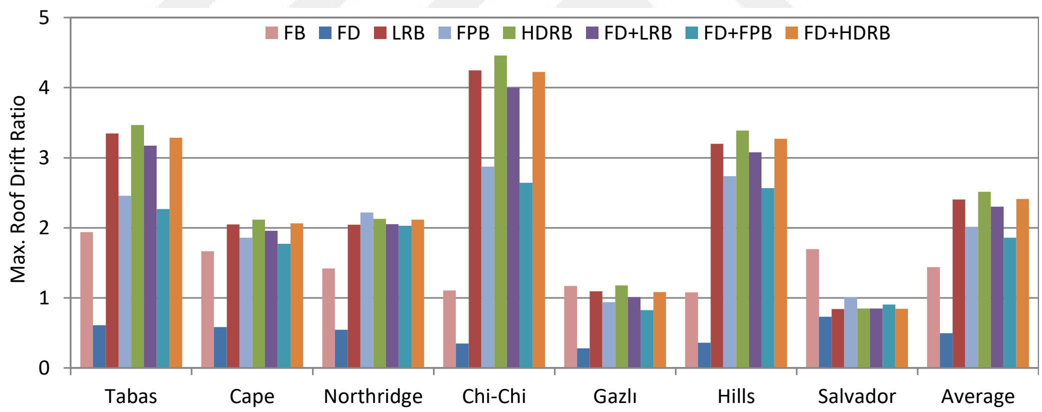

Figure 4.70 Maximum absolute acceleration for the frames with and without protective sysytems

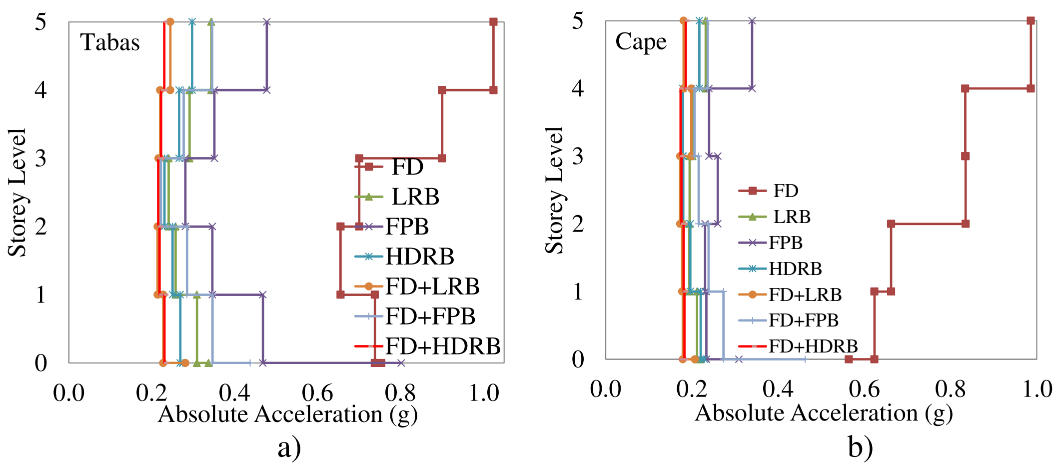

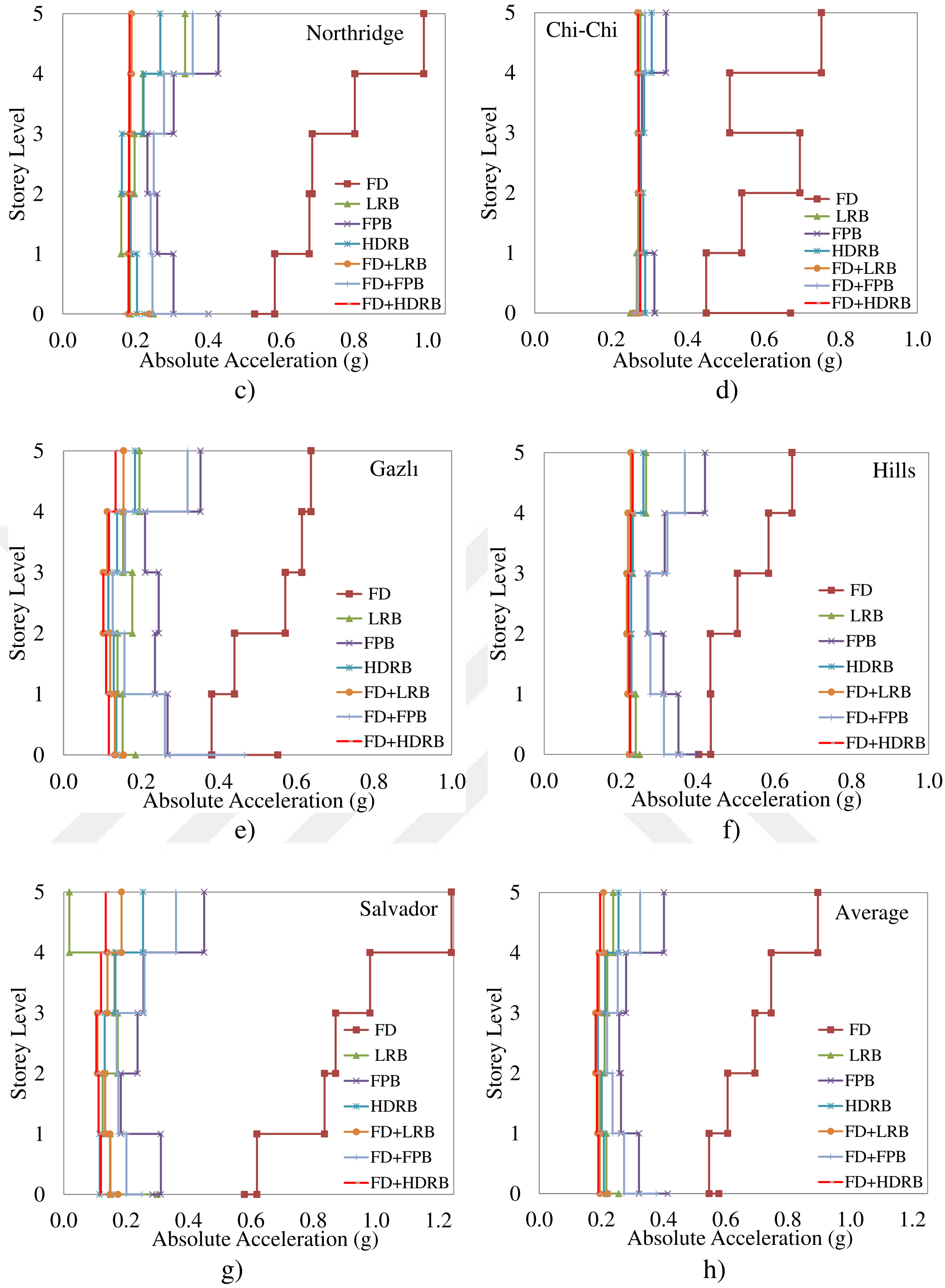

Figure 4.71 Variation of the absolute acceleration against storey height.

The poor response of FD was also observed on the variation of the absolute acceleration over the height of the case study frames which mostly tended to non-uniform distribution as shown in Figure 4.71(a-h). Although the combined cases exhibited similar trend against the height of the frame for all earthquakes, the most uniform absolute accelerations plotted for FD+HDRB and FD+LRB. The percentage of the average values of the maximum absolute acceleration reductions was computed and presented in Table 4.7 whereby the effectiveness of the combined cases on the absolute acceleration reductions were proved. For example, FD+HDRB presented the greatest reduction percentage as 89.6 %, it was as 88.4 and 80.0 % for FD+LRB and FD+FPB, respectively. In addition, the contribution of the elastomeric bearings of LRB, HDRB on the absolute acceleration mitigations were as 86.4 and 86.5 %, respectively. As stated before, FD had the lowest reduction percentage as 52.4 % over the proposed protective systems. It was also worthy to note that each of the proposed protective systems comparatively advocated the seismic response of the case study frame. However, compared to the friction-based protective systems of FD, FD+FPB, the elastomeric isolation systems of FD+LRB and FD+HDRB were much more favourable since they remarkably improved the interstorey drift mitigation and distribution, at the same time effectively limited the absolute acceleration. For example, the average maximum interstorey drift ratios of 0.60, 0.59, and 0.40 % were experienced by FD, FPB, FD+FPB (see Figure 4.68), also witnessed the average maximum absolute acceleration of 0.90, 0.41, and 0.38 g (see Figure 4.70), respectively. However, FD+LRB and FD+HDRB provided the average maximum interstorey drift ratios of 0.30 and 0.33 % (see Figure 4.68), also produced the average maximum absolute acceleration of 0.22 and 0.20 g (see Figure 4.70), respectively. Eventually, it was shown that the friction-based protective systems could not overcome the absolute acceleration and interstorey drift as much as the elastomeric bearings.

4.5.6 Base Shear

The base shears of the case study frame with and without the protective systems were computed for each of the ground motions and then the obtained maximum base shears divided by the building weight of 1865.3 kN and corresponding normalized maximum base shears were presented in Figure 4.72. The normalized base shear value of 0.937 (1747.2 kN) for the case study frame reduced up to 0.538 (1003.1 kN) by means of FD under Northridge earthquake. It was as 0.132 (246.7 kN), 0.166 (309.6 kN), and 0.135 (251.0 kN) for LRB, FPB, and HDRB, furthermore, FD+LRB, FD+FPB, FD+HDRB as 0.139 (259.4 kN), 0.170 (317.3 kN), 0.142 (265.2 kN), respectively, as shown in Figure 4.72. The lowest normalized base shears of 0.130, 0.132, 0.083, 0.186, and 0.069 were testified for the protective system of LRB under Cape, Northridge, Gazlı, Hills, and Salvador earthquakes, respectively. Furthermore, it was as 0.186 and 0.213 for FPB and FD+FPB under Tabas and Chi-Chi earthquakes, respectively. Among the earthquakes, Salvador caused the greatest base shear reductions with respect to the FB. For instance, LRB, FPB, HDRB, FD+LRB, FD+FPB, and FD+HDRB were provided as 93.6, 92.0, 93.4, 93.2, 90.7, and 93.1 %, respectively. The average lowest normalized base shear was obtained as 0.147 for the protective system of LRB. The greatest reduction percentages of 84.7, 84.3, 84.1 % were computed for LRB, FD+LRB, HDRB while they were as 83.8, 83.5, 83.2 % for FD+HDRB, FPB, FD+FPB, respectively, as shown in Table 4.7.

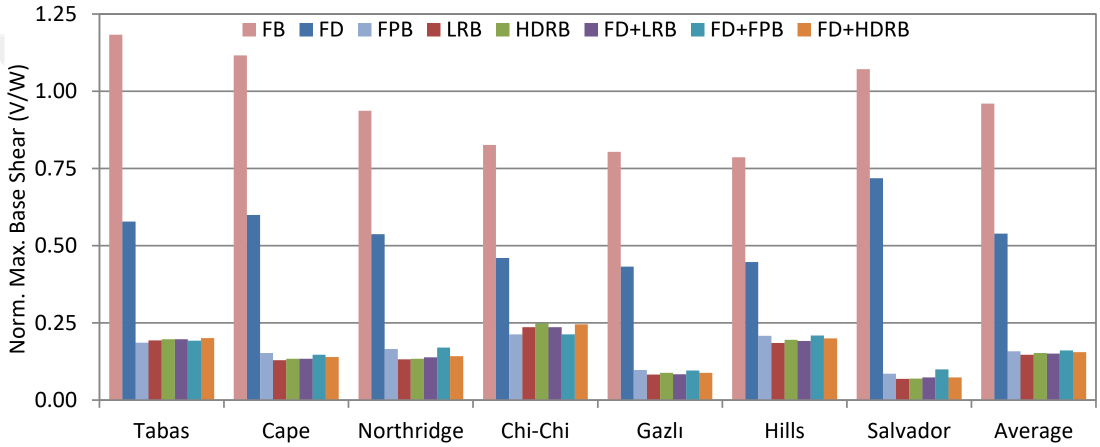

Figure 4.72 Normalized maximum base shear for the frames with and without protective sysytems

4.5.7 Base Moment

The maximum base moments for each of the protective systems were obtained through the time history analyses using seven earthquake records and presented in Figure 4.73. Similar to the response of the base shear, the equipment of the protective systems substantially mitigated the base moment of FB. The friction-based protective systems of FD, FPB, and FD+FPB produced moderate reduction percentage for the base moment as 14.0, 38.8, and 40.3 % while the reductions were boosted by the elastomeric bearings of LRB and HDRB as 45.5 and 45.0 %, it was reached to 45.7 and 45.4 % by FD+LRB, FD+HDRB under Northridge earthquake, respectively, as shown in Figure 4.73. The protective system of HDRB produced the lowest maximum base moments as 16460 kNm under Cape earthquake corresponded to 56.1 % reduction of the base moment of FB. Similarly, FD+LRB provided the lowest base moments of 16450, 15420, 16490 kNm, the reductions of 45.7, 50.4, 46.1 % under Northridge, Gazlı, Hills earthquake. FD+HDRB ensured the reductions as 50.8, 46.3, 59.7 % equivalent to the maximum moments of 17450, 16650, 14950 kNm under Tabas, Chi-Chi, Salvador earthquakes, respectively. Indeed, the lowest average base moment was witnessed by means of FD+LRB as 16301 kNm. The base moment reductions of the protective systems with respect to FB under earthquakes were computed and given in Table 4.7. The average reduction percentages of the base moment for the protective systems of FD, FPB, and FD+FPB were obtained as 27, 47.3, and 47.7 %, on the other hand the greatest reductions were recorded through elastomeric bearings namely LRB, HDRB, FD+LRB, and FD+HDRB as 50.8, 50.7, 51.1, and 50.9 %, respectively.

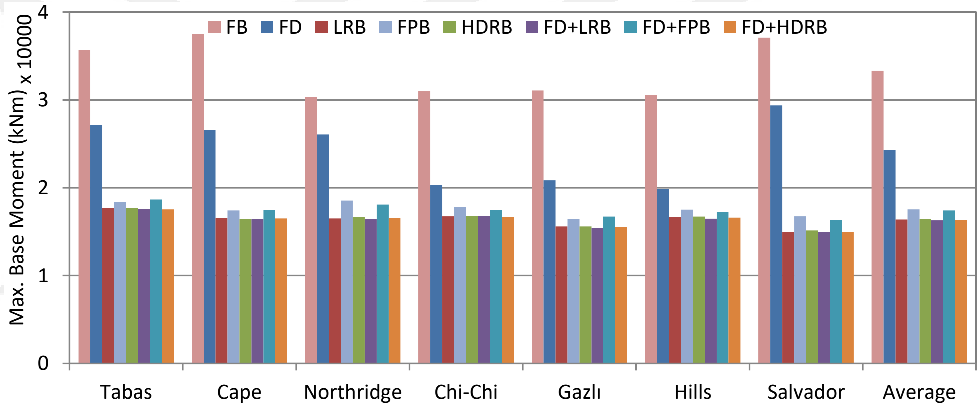

Figure 4.73 Maximum base moment for the frames with and without protective sysytems

4.5.8 Hysteretic Behaviour and Energy Dissipation

A series of protective systems was offered to retrofit the poor steel moment frame and then performed nonlinear time-history analyses using seven different earthquake records. In the analyses results, the hysteretic cycles of the protective systems were generated for all earthquakes, but herein the hysteretic cycles induced by Cape earthquake are only presented in Figures C1 and C2. It can be observed that the obtained hysteretic cycles represented similar responses to the force-deformation behaviour of the each protective system described in Figures 2.10 and 2.15. The hysteretic cycles were constructed for FD almost described rectangular shape. It was shown that the hysteretic cycles precisely obeyed to the maximum force of FD governed by the attained slip loads of 300, 279, 240, 180, and 111 kN as shown in Figure C1, respectively. In addition, 1st, 2nd, 3rd, 4th, and 5th storey link element of FD produced the maximum displacements as 7.6, 9.5, 8.1, 11.0, and 8.3 mm, respectively. The hysteric cycles of HDRB, LRB, and FPB presented in Figure C2(c, a, and b), those were similar to Figure 2.15(a, b, and c), respectively. In other words, the shape of the hysteretic cycles for the friction-based protective systems of FD and FPB described the rectangular shape while the elastomeric bearings of LRB and HDRB exhibited the angular shape and linear behaviour, respectively. The displacement ranged between -0.174 and 0.290 m for LRB, -0.117 and 0.189 m for FPB, and -0.174 and 0.302 m for HDRB, respectively. Moreover, FD+LRB, FD+FPB, and FD+HDRB provided the greatest displacements of 0.298, 0.240, and 0.313 m, respectively, as shown in Figure C2(d, e, and f). Note that the maximum amplitudes of the elastomeric bearings were almost equivalent to the design displacement of 0.302 m as shown in Table 3.5.

Table 4.8 Total dissipated energy Eloop (kJ) for the frames with protective systems under all earthquakes

Protective System	Tabas	Cape	Northridge	Chi-Chi	Gazlı	Hills	Salvador
LRB	19.08	11.28	11.54	24.54	5.81	18.20	4.77
FPB	17.84	10.00	12.15	19.05	5.78	17.17	3.37
HDRB	20.07	11.79	11.82	26.46	6.05	19.67	4.43
FD+LRB	18.96	11.59	12.18	24.12	5.88	18.53	4.99
FD+FPB	17.10	12.88	15.34	18.51	5.33	18.56	6.44
FD+HDRB	20.10	12.24	12.59	26.16	6.08	20.06	4.62

When OMF equipped with the protective systems and hit by all earthquakes, the amount of the dissipated energy could be computed by Equation 4.1 [130], and given in Table 4.8. The largest energy dissipations were experienced in case of the utilization of the elastomeric bearings namely, LRB and HDRB under Tabas, Cape, Chi-Chi, Gazlı, Hills, and Salvador earthquakes. When subjected to Tabas, Chi-Chi, Gazlı, and Hills earthquakes, FD+HDRB provided the maximum energy dissipations as 20.10, 26.16, 6.08, 20.06 kJ, respectively. In addition, FD+FPB dissipated the greatest seismic energy as 12.88, 15.34, 6.44 kJ by Cape, Northridge, and Salvador earthquakes, respectively.

CHAPTER 5

CONCLUSIONS

In this study, the effectiveness of the seismic protective systems was investigated considering various design parameters. The characterized protective systems (i.e., FD, LRB, FPB, HDRB, FD+LRB, FD+FPB, and FD+HDRB) were utilized to retrofit the case study frames. Two sets of steel buildings were considered as the benchmark buildings. Each of the upgrading techniques was applied to such building, and evaluated by means of several engineering demand parameters through the nonlinear time-history analyses under different ground motion records. The following conclusions are presented below:

- Case-1 provided that the utilization of LRB increased the lateral displacement demand due to the minor stiffness of the bearing, while use of FDs significantly reduced because of having major stiffness of the friction device.
- The use of LRB and FD together was very effective in diminishing the absolute acceleration. When compared to other models, in 5-storey OMF with FD and LRB together led to greatest reduction about 88.1 %.
- Given that LRB lateral movement demand and the braking effect of the FD simultaneously it was observed that combined use of LRB and FD caused the greatest relative displacement reduction that of 5-storey SMF with FD and LRB together was reduced by 92.8%.
- When the interstorey drift and relative displacement demand of the frames was compared, it was seen that the use of FD and LRB together exhibited more uniform drift distribution along the height of the frames.
- In particular, 10-storey SMF with FD and LRB had provided greatest interstorey drift reduction with respect to the original frame about 84.8 %.

- The greatest interstorey drift ratio of the case study frames was observed in the middle stories that led to excess the SP3 and SP4 limit state, while utilization of the structural protective systems eliminated these sudden drift enhancements and the occurrence of structural damage.

- The results showed that the use of only LRB and combined use of FD with LRB generated minimum base shear demand with respect to the other case.

- It was observed that when upgraded with the structural protective systems, the case study frames would be in the elastic range of the deformation thus they had structural reliability, otherwise they could not satisfied the requirement of SP1, SP2 and SP3 limit state.

- Case-2 reported that the maximum isolator displacement was observed when the isolation period and effective damping ratio reached to the greatest value with the lowest yield strength ratio (i.e., T3ß25FyW2.5).

- The isolation system of T3ß25FyW5 yielded the most uniform drift distribution along the storey height, especially for 6-storey isolated frame under Salvador earthquake.

- The isolation system of T3ß25FyW10, T2.5ß25FyW10, and T2.5ß15FyW10 gave the lowest value of the average roof drift for 3, 6, and 9-storey isolated frames, respectively.

- The isolation system having moderate values of isolation parameters (namely T2.5ß15FyW5) exhibited significant reduction on the relative displacement, especially for 6-storey isolated frame under all earthquakes.

- The isolation system of T2.5ß15FyW5 having moderate isolation parameters exhibited the lowest absolute acceleration as 2.58 and 4.18 m/s^2 for 3 and 9-storey isolated frames subjected to Cape earthquake, respectively.

- The lowest base shear was obtained in the isolation system of T3ß5FyW10 for 3, 6, and 9-storey isolated frames under Northridge earthquake.

- The lower effective damping ratio and yield strength ratio were substantially capable of reducing the base moment in case of the greatest isolation period, especially in 6 and 9-storey frames equipped with the isolation system of T3ß5FyW5.

- The use of appropriate isolation systems remarkably caused the largest hysteretic curves and also the greatest dissipation of the hysteresis earthquake energy, especially for 6-storey frames.

- The greater values of isolation parameters generally seemed to be more favorable when the seismic performance of the isolated frames was compared in terms of the displacement and drift demands.

- Case-3 pointed out that the isolation system composed of the greater T and ß with λ (i.e., T3ß15λ3 and T3ß10λ3) was more prone to produce the greater isolator displacement with respect to other isolation models.

- The isolation system of T3ß15λ6 provided the lowest interstorey drift ratio and also behaved more uniform distribution over the building height.

- T3ß15λ6 gave the most uniform relative displacement distribution over building height. The lowest value of the average relative displacement proved as 3.31 cm for 3-storey frame with T3ß15λ6 while it was found as 9.15 and 15.71 cm for 6 and 9-storey frames with T3ß15λ3, respectively.

- 3, 6, and 9-storey frames with T3ß5λ3, T3ß15λ3, and T3ß5λ6 succeeded the lowest value of the average absolute acceleration, respectively. Moreover, use of greater isolation parameters ensured the more uniform absolute acceleration distribution over the height of the structures.

- The lowest normalized base shear of 0.108, 0.099, and 0.081 were obtained when 3, 6, and 9-storey frames with T3ß15λ6 hit by Northridge earthquake.

- The use of appropriate HDRB models noticeably provided not only maximum energy dissipation but also the largest hysteretic curves, furthermore aforementioned isolation system was liable to typical hysteretic curve of HDRB.

- Case-4 proved that the utilization of FD caused the greatest average displacement reduction as 65.6 %. On the contrary, LRB and HDRB provided the greatest average displacement increments as 67 and 74.5 %, respectively.

- The greatest relative displacement reductions of 93.1, 81.9, and 92.4 % were experienced in the combined cases of FD+LRB, FD+FPB, and FD+HDRB, respectively.

- It was shown that FD reduced the average roof drift as 65.6 % while it was increased as 67.0 and 74.5 % by LRB and HDRB because of the horizontal displacement demand of the elastomeric bearings, respectively.

- Although each of the protective systems enhanced the poor seismic performance of OMF, the fully operational damage state was only satisfied by the combined cases, which also exhibited the most uniform drift distribution along the height of the frame.

- The success of the combined cases also proved by their absolute acceleration demands. In particular, FD+HDRB provided the greatest average absolute acceleration reduction about 89.6 %.

- Although the friction-based protective systems of FD, FPB, and FD+FPB substantially limited the interstorey drift ratio, they could not restrain the absolute accelerations as much as FD+LRB and FD+HDRB.

- LRB and FD+LRB, both of them performed the greatest average base shear reductions about 84 % which was much more than the single implementation of FD as 43.9 %.

- At the end of the nonlinear analyses, FD, LRB, FPB, and HDRB obtained the hysteretic cycles being similar to the bilinear model of the protective systems.

- The largest energy dissipations of 20.10, 6.08, and 20.06 kJ were recognized under Tabas, Gazlı, and Hills earthquakes thanks to the protective system of FD+HDRB, respectively.

REFERENCES

[1] Naeim, F., Kelly, J. M. (1999). *Design of Seismic Isolated Structures, From Theory to Practice*. John Wiley & Sons, New York, NY, USA.

[2] Sezen, H., Whittaker, A. S., Elwood, K. J., Mosalam, K. M. (2003). Performance of reinforced concrete buildings during the August 17, 1999 Kocaeli, Turkey earthquake, and seismic design and construction practise in Turkey, Turkey, *Engineering Structures*. **25**, 103-114.

[3] Erdik, M., Demircioğlu, M., Sesetyan, K., Durukal, E., Siyahi, B. (2004). Earthquake hazard in Marmara Region, Turkey, *Soil Dynamics and Earthquake Engineering*. **24 (8)**, 605-631.

[4] Shang, Q., Wang, T., Li, J. (2019). Seismic fragility of flexible pipeline connections in a base isolated medical building, *Earthquake Engineering and Engineering Vibration*. **18**, 903-916.

[5] Skinner, R. I., Robinson, W. H., McVerry, G. H. (1999). *An Introduction to Seismic Isolation.* New York, John Wiley and Sons Ltd.

[6] Spencer Jr, B. F., Nagarajaiah, S. (2003). State of the art of structural control, *Journal of Structural Engineering*. **129,** 845–856.

[7] Soong, T. T., Dargush, G. F. (1997). *Passive energy dissipation systems in structural engineering.* Chichester, John Wiley and Sons Ltd.

[8] Moon, K. H., Han, S. W., Lee, C. S. (2017). Seismic retrofit design method using friction damping systems for old low- and mid-rise regular reinforced concrete buildings, *Engineering Structures*. **146**, 105-117.

[9] Tafakori, E., Banazadeh, M., Jalali, S. A., Tehranizadah, M. (1982). Risk-based optimal retrofit of a tall steel building by using friction dampers, *Structural Design of Tall and Special Buildings*. **22**, 700-717.

[10] Soong, T. T., Dargush, G. F. (1999). *Passive Energy Dissipation and active control.* Structural Engineering Handbook. CRS Press LLC, Boca Raton.

[11] Pall, A. S., Marsh, C. (1982). Response of friction damped braced frames, *Journal of Structural Engineering.* **108(6),** 1313–23.

[12] Hassan, W. M. (2020). Assessment of ASCE 7–16 Seismic Isolation Bearing Torsional Displacement, *International Journal of Civil Engineering.* **18,** 351-366.

[13] Erdik, M., Ülker, Ö., Şadan, B., Tüzün, C. (2018). Seismic isolation code developments and significant applications in Turkey, *Soil Dynamics and Earthquake Engineering.* **115,** 413-437.

[14] American Society of Civil Engineers, ASCE. 2010. *Minimum design loads for buildings and other structures.* ASCE/SEI 7-10, Reston, VA.

[15] Eurocode, EN 1998-1 Eurocode 8. 2004. *Design of structures for earthquake resistance, European Committee for Standardization.* CEN, Brussels.

[16] TSCB. 2018. *Turkish Seismic Code for Buildings.* The Disaster and Emergency Management Presidency of Turkey, Ankara.

[17] Skinner, R. I., Robinson, W. H., McVerry, G. H. (1993). *Introduction to Seismic Isolation.* New York, John Wiley and Sons Ltd.

[18] Khoshnudian, F., Motamedi, D. (2013). Seismic Response of Asymmetric Steel Isolated Structures Considering Vertical Component of Earthquakes, *KSCE Journal of Civil Engineering.* **17(6),** 1333-1347.

[19] Lin, Y. Y., Tsai, M. H., Hwang, J. S., Chang, K. C. (2003). Direct displacement-based design for building with passive energy dissipation systems, *Engineering Structures.* **25,** 25-37.

[20] Güneyisi, E. M., Deringöl, A. H. (2018). Seismic response of friction damped and base-isolated frames considering serviceability limit state, *Journal of Constructional Steel Research.* **148,** 639-657.

[21] Constantinou, M. C., Symans, M. D. (1993). Seismic response of structures with supplemental damping, *The Structural Design of Tall Buildings*. **2,** 77–92.

[22] Domenico, D. De., Ricciardi, G., Takewaki, I. (2019). Design strategies of viscous dampers for seismic protection of building structures: A review, *Soil Dynamics and Earthquake Engineering*. **118,** 144-165.

[23] Güneyisi, E. M., Altay, G. (2008). Seismic fragility assessment of effectiveness of viscous dampers in R/C buildings under scenario earthquakes, *Structural Safety*. **30,** 461-480

[24] Zhou, Y., Lu, X., Weng, D., Zhang, R. (2012). A practical design method for reinforced concrete structures with viscous dampers, *Engineering Structures.* **39,** 187-198.

[25] Tabar, A. M. (2019). Linearization of seismic response of structures equipped with nonlinear viscous dampers using perturbation technique, *Engineering Structures.* **184,** 459-468.

[26] Dicleli, M., Mehta, A. (2007). Seismic performance of chevron braced steel frames with and without viscous fluid dampers as a function of ground motion and damper characteristics, *Journal of Constructional Steel Research.* **63,** 1102-1115.

[27] Landi, L., Conti, F., Diotallevi, P. P. (2015). Effectiveness of different distributions of viscous damping coefficients for the seismic retrofit of regular and irregular RC frames, *Engineering Structures.* **100,** 79-93.

[28] Kim, J., Lee, J., Kang, H. (2016). Seismic retrofit of special truss moment frames using viscous dampers, *Journal of Constructional Steel Research.* **123,** 53-67.

[29] Sullivan, T. J., Lago, A. (2012). Towards a simplified Direct DBD procedure for the seismic design of moment resisting frames with viscous dampers, *Engineering Structures*. **35,** 140-148.

[30] Jamshidiha, H. R., Yakhchalian, M., Mohebi, B. (2018). Advanced scalar intensity measures for collapse capacity prediction of steel moment resisting frames with fluid viscous dampers, *Soil Dynamics and Earthquake Engineering*. **109,** 102-118.

[31] Samali, B., Kwok, K. C. S. (1995). Use of viscoelastic dampers in reducing wind- and earthquake-induced motion of building structures, *Engineering Structures.* **17(9),** 639-654.

[32] Guo, A. X., Xu, Y. L., Wu, B. (2002). Seismic reliability analysis of hysteretic structure with viscoelastic dampers, *Engineering Structures.* **24,** 373-383.

[33] Kim, J., Bang, S. (2002). Optimum distribution of added viscoelastic dampers for mitigation of torsional responses of plan-wise asymmetric structures, *Engineering Structures*. **24,** 1257-1269.

[34] Min, K-W., Kim, J., Lee, S-H. (2004). Vibration tests of 5-storey steel frame with viscoelastic dampers, *Engineering Structures.* **26,** 831-839.

[35] Zhang, L., Su, M., Zhang, C., Shen, H., Islam, M. M., Zhang, R. (2019). A design method of viscoelastic damper parameters based on the elastic-plastic response reduction curve, *Engineering Structures*. **117**, 149-163.

[36] Shu, Z., Ning, B., Li, S., Li, Z., Gan, Z., Xie, Y. (2020). Experimental and numerical investigations of replaceable moment-resisting viscoelastic damper for steel frames, *Journal of Constructional Research.* **170,** 106100.

[37] Alam, Z., Zhang, C., Samali, B. (2020). The role of viscoelastic damping on retrofi tting seismic performance of asymmetric reinforced concrete structures, *Earthquake Engineering and Engineering Vibration.* **19(1),** 223-237.

[38] Xie, L., Zhang, Li., Pan, C., Zhang, R., Chen, T. (2020). Uniform damping ratio-based design method for seismic retrofitting of elastoplastic RC structures using viscoelastic dampers, *Soil Dynamics and Earthquake Engineering.* **128,** 105866.

[39] Ghotb, M. R., Toopchi-Nezhad, H. (2019). A feasibility study on pre-compressed partially bonded viscoelastic dampers, *Engineering Structures.* **201,** 109796.

[40] Kang, Y-J., Peng, L-Y. (2019). Optimisation Design and Damping Effect Analysis of Large Mass Ratio Tuned Mass Dampers, *Shock and Vibration.* **8376781.**

[41] Kang, Y-J., Peng, L-Y. (2019). A Novel Hybrid Semi-Active Mass Damper Configuration for Structural Applications, *Applied Sciences.* **6(12),** 10.3390/app6120397.

[42] Pinkaew, T., Lukkunaprasit , P., Chatupote, P. (2003). Seismic effectiveness of tuned mass dampers for damage reduction of structures, Engineering Structures. **25,** 39-46.

[43] Taniguchi, T., Kiureghian, A. D., Melkumyan, M. (2008). Effect of tuned mass damper on displacement demand of base-isolated structures, *Engineering Structures.* **30,** 3478-3488.

[44] Greco, R., Marano, G. C. (2013). Optimum design of Tuned Mass Dampers by displacement and energy perspectives, *Soil Dynamics and Earthquake Engineering.* **49,** 243-253.

[45] Petrini, F., Giaralis, A., Wang, Z. (2020). Optimal tuned mass-damper-inerter (TMDI) design in wind-excited tall buildings for occupants' comfort serviceability performance and energy harvesting, *Engineering Structures.* **204,** 109904.

[46] Ghabraie, K., Chan, R., Huang, X., Xie, Y. M. (2010). Shape optimization of metallic yielding devices for passive mitigation of seismic energy, *Engineering Structures.* **32,** 2258-2267.

[47] Aliakbari, F., Garivani, S., Aghakouchak, A. A. (2020). An energy based method for seismic design of frame structures equipped with metallic yielding dampers considering uniform inter-story drift concept, *Engineering* Structures. **205,** 110114.

[48] Sahoo, D. R., Singhal, T., Taraithia, S. S., Saini, A. (2015). Cyclic behavior of shear-and-flexural yielding metallic dampers, *Journal of Constructional Research*. **114**, 247-257.

[49] Li, Z., Shu, G., Huang, Z. (2019). Development and cyclic testing of an innovative shear-bending combined metallic damper, *Journal of Constructional Research*. **158**, 28-40.

[50] Pall, A.S., Marsh, C., Fazio, P. (1980). Friction Joints for Seismic Control of Large Panel Structures, *Journal of Prestressed Concrete Institute.* **6(25)**, 38-61.

[51] Filiatrault, A,. Cherry, S. (1990). Seismic design spectra for friction damped structures, *Journal of Structural Division. ASCE*. **16,** 1334-55.

[52] Pasquin, C., Leboeuf, N., Pall, R., Pall, A. (2004). *Friction Dampers for Seismic Rehabilitation of Eaton's Building, Montreal*. 13th World Conference on Earthquake Engineering, Vancouver, B.C., Canada. 1949.

[53] Moon KH, Han SW, Lee CS. (2017). Seismic retrofit design method using friction damping systems for old low- and mid-rise regular reinforced concrete buildings, *Engineering Structures.* **146,** 105-117.

[54] Pall, A.S., Marsh, C. (1982). Response of friction damped braced frames, *Journal of Structural Engineering*. **108(6),** 1313–23.

[55] Lian, Y., Xunan, Z., Cherry, S. (2007). Damping characteristics of friction damped braced frame and its effectiveness in the mega-sub controlled structure system, *Earthquake Engineering and Engineering Vibration*. **6(2),** 171–181.

[56] Montuori, R., Nastri, E., Piluso, V. (2014). Theory of plastic mechanism control for the seismic design of braced frames equipped with friction dampers, *Mechanics Research Communications.* **58,** 112-123.

[57] Nabid, N., Hajirasouliha, I., Petkovski, M. (2019). Simplified Method for Optimal Design of Friction Damper Slip Loads by Considering Near-Field

and Far-Field Ground Motions, *Journal of Earthquake Engineering*. DOI: 10.1080/13632469.2019.1605316.

[58] Lee, C. H., Ryu, J., Oh, J., Yoo, C. H., Ju, Y. K. (2016). Friction between a new low-steel composite material and milled steel for SAFE Dampers, *Engineering Structures.* **122,** 279-295.

[59] Lu, L.Y. (2004). Semi-active modal control for seismic structures with variable friction dampers, *Engineering Structures.* **26,** 437-454.

[60] Armali, M., Damerji, H., Hallal, J., Fakih, M. (2019). Effectiveness of friction dampers on the seismic behavior of high rise building VS shear wall system, *Engineering Reports.* e12075. https://doi.org/10.1002/eng2.12075

[61] Amjadian, M., Agrawal, A. K. (2019). Seismic response control of multi-story base-isolated buildings using a smart electromagnetic friction damper with smooth hysteretic behavior, *Mechanical Systems and Signal Processing*. **130,** 409-432.

[62] Santos, A. F., Santiago, A., Latour, M., Rizzano, G. (2019). Analytical assessment of the friction dampers behaviour under different loading rates, *Journal of Constructional Steel Research.* **158,** 443-459.

[63] Quintana, H. C., Petkovski, M. (2018). Optimum performance of structural control with friction dampers, *Engineering Structures.* **172,** 154-162.

[64] Qu, Z., Ji, X., Shi, X., Wang, Y., Liu, H. (2020). Cyclic loading test of steel coupling beams with mid-span friction dampers and RC slabs, *Engineering Structures.* **203,** 109876.

[65] Ontiveros-Pérez, S. P., Miguel, L. F. F., Rieara, J. D. (2019). Reliability-based optimum design of passive friction dampers in buildings in seismic regions, *Engineering Structures.* **190,** 276-284.

[66] Dos Santos, M. B., Coelho, H. T. (2019). Assessment of semi-active friction dampers in auxiliary mass dampers' Suspension, *Engineering Structures.* **186,** 356-368.

[67] Piluso, V., Montuori, R., Nastri, E., Paciello, A. (2019). Seismic response of MRF-CBF dual systems equipped with low damage friction connections, *Journal of Constructional Steel Research.* **154,** 263–277.

[68] Nabid, N., Hajirasouliha, I., Petkovski, M. (2019). Adaptive low computational cost optimisation method for performance based seismic design of friction dampers, *Engineering Structures.* **198,** 109549.

[69] Bhuiyan, A.R., Okui, Y., Mitamura, H., Imai, T. (2009). A rheology model of high damping rubber bearings for seismic analysis: Identification of nonlinear viscosity, *International Journal of Solids and Structures*. **46(7-8),** 1778-1792.

[70] Tubaldi, E., Mitoulis, S. A., Ahmadi, H. (2018). Modeling of high damping rubber bearings under bidirectional shear loading, *Soil Dynamics and Earthquake Engineering*. **104**, 329-345.

[71] Clemente, P., Martelli, A. (2019). Seismically isolated buildings in Italy: State-of-the-art review and applications, *Soil Dynamics and Earthquake Engineering*. **119,** 471-487.

[72] Gjorgjiev, I., Garevski, M. (2013). A polynomial analytical model of rubber bearings based on series of tests, *Engineering Structures.* **56**, 600-609.

[73] Madera Sierra, I. E., Losanno, D., Strano, S., Marulanda, J., Thomson, P. (2019). Development and experimental behavior of HDR seismic isolators for low-rise residential buildings, *Engineering Structures.* **183,** 894–906.

[74] Pant, D. R. (2017). Influence of scaling of different types of ground motions on analysis of code-compliant four-story reinforced concrete buildings isolated with elastomeric bearings, *Engineering Structures.* **135,** 53-67.

[75] Burtscher SL and Dorfmann A. (2004). Compression andshear tests of anisotropic high damping rubber bearings, *Engineering Structures.* **26,** 1979-1991.

[76] Zhang, J., Huo, Y. (2009). Evaluating effectiveness and optimum design of isolation devices for highway bridges using the fragility function method, *Engineering Structures.* **31,** 1648-1660.

[77] Jangid, R. S. (2005). Optimum friction pendulum system for near-fault motions, *Engineering Structures*. **27,** 349–359.

[78] Jangid, R. S. (2000). Optimum frictional elements in sliding isolation system, Computers and Structures. **76,** 651-661.

[79] Deringol, A. H., Guneyisi, E. M. (2019). Effect of friction pendulum bearing properties on behaviour of buildings subjected to seismic loads, *Soil Dynamics and Earthquake Engineering*. **125,** 105746.

[80] Xu, Z., Du, X., Xu, C., Han, R. (2020). Numerical analyses of seismic performance of underground and aboveground structures with friction pendulum bearings, *Soil Dynamics and Earthquake Engineering*. **130,** 105967.

[81] Ren, X., Lu, W., Mosalam, K. M., Xu, W. (2019). Similitude theory for scaled friction pendulum bearings for shaking table experiments, *Soil Dynamics and Earthquake Engineering.* **121**, 399-404.

[82] Bao, Y., Becker, T. (2019). Three-dimensional double friction pendulum bearing model including uplift and impact behavior: Formulation and numerical example, *Engineering Structures.* **199,** 109579.

[83] Calhoun, S. J., Harvey, Jr. PS. (2019). Enhancing the teaching of seismic isolation using additive manufacturing, *Engineering Structures.* **167,** 494-503.

[84] Castaldo, P., Alfano, G. (2020). Seismic reliability-based design of hardening and softening structures isolated by double concave sliding devices, *Engineering Structures.* **129,** 105930.

[85] Shao, B., Mahin, S. A., Zayas, V. (2019). Achieving targeted levels of reliability for low-rise seismically isolated structures, *Soil Dynamics and Earthquake Engineering*. **125,** 105744.

[86] American Society of Civil Engineers (ASCE). *Minimum design loads for buildings and other structures.* ASCE standard ASCE/SEI 7-16. Reston, US: American Society of Civil Engineer; 2017.

[87] Domenico, D. D., Gandelli, E., Quaglini, V. (2020). Effective base isolation combining low-friction curved surface sliders and hysteretic gap dampers, *Soil Dynamics and Earthquake Engineering*. **130,** 105989.

[88] Bao, Y., Becker, T. C., Sone, T., Hamaguchi, H. (2018). To limit forces or displacements: Collapse study of steel frames isolated by sliding bearings with and without restraining rims, *Soil Dynamics and Earthquake Engineering*. **112,** 203-214.

[89] Habieb, A. B., Valente, M., Milani, G. (2019). Effectiveness of different base isolation systems for seismic protection: Numerical insights into an existing masonry bell tower, *Soil Dynamics and Earthquake Engineering*. **105752.**

[90] Castaldo, P., Palazzo, B., Vecchia, P. D. (2016). Life-cycle cost and seismic reliability analysis of 3D systems equipped with FPS for different isolation degrees, *Engineering Structures.* **125,** 349-363.

[91] Calabrese, A., Losanno, D., Spizzuoco, M., Strano, S., Terzo, M. (2019). Recycled Rubber Fiber Reinforced Bearings (RR-FRBs) as base isolators for residential buildings in developing countries: The demonstration building of Pasir Badak, Indonesia, *Engineering Structures.* **192,** 126-144.

[92] Alhan, C., Sahin, F. (2011). Protecting vibration-sensitive contents: an investigation of floor accelerations in seismically isolated buildings, *Bulletin of Earthquake Engineering*. **9,** 1203–1226.

[93] Moslemi, M., Kianoush, M. R. (2016). Application of seismic isolation technique to partially filled conical elevated tanks, *Engineering Structures.* **127,** 663-675.

[94] Alhan, C., Oncu-Davas, S. (2016). Performance limits of seismically isolated buildings under near-field earthquakes, *Engineering Structures.* **116**, 83-94.

[95] Mansouri, I., Amiri, G. G., Hu, J. W., Khoshkalam, M., Soori, S., Shahbazi, S. (2017). Seismic Fragility Estimates of LRB Base Isolated Frames Using Performance-Based Design, *Shock and Vibration.* **5184790,** https://doi.org/10.1155/2017/5184790

[96] Eröz, M., Desroches, R. (2013). A Comparative Assessment of Sliding and Elastomeric Seismic Isolation in a Typical Multi-Span Bridge, *Journal of Earthquake Engineering.* **17(5),** 637–657.

[97] Mazza, F. (2017). Residual seismic load capacity of fire-damaged rubber bearings of r.c. base-isolated buildings, *Engineering Failure Analysis.* **79,** 951–970.

[98] Kim, J. H., Kim, M. K., Choi, I. K. (2019). Experimental study on seismic behavior of lead-rubber bearing considering bi-directional horizontal input motions, *Engineering Structures.* **198,** 109529.

[99] Ahmadipour, M., Alam, M. S. (2017). Sensitivity analysis on mechanical characteristics of lead-core steel-reinforced elastomeric bearings under cyclic loading, *Engineering Structures.* **140,** 39-50.

[100] Kumar, M., Whittaker, A. (2018). Cross-platform implementation, verification and validation of advanced mathematical models of elastomeric seismic isolation bearings, *Engineering Structures.* **175,** 926-943.

[101] Markou, A. A., Stefanou, G., Manolis, G. D. (2019). Stochastic energy measures for hybrid base isolation systems, *Engineering Structures.* **172,** 629-643.

[102] Dao, N. D., Nguyen-Van, H., Nguyen, T. H. A., Chung, A. B. (2020). A new statistical equation for predicting nonlinear time history displacement of seismic isolation systems, *Structures.* **24,** 177-190.

[103] Wei, W., Tan, P., Yuan, Y., Zhu, H. (2019). Experimental and analytical investigation of the influence of compressive load on rate-dependent high-damping rubber bearings, *Construction and Building Materials.* **200,** 26-35.

[104] Cancellara, D., Angelis, F. D. (2019). Dynamic assessment of base isolation systems for irregular in plan structures: Response spectrum analysis vs nonlinear analysis, *Composite Structures.* **215,** 98-115.

[105] Mazza, F., Vulcano, A. (2012). Effects of near-fault ground motions on the nonlinear dynamic response of base-isolated r.c. framed buildings, *Earthquake Engineering and Structural Dynamics*. **41,** 211-232.

[106] Clemente, P., Bongiovanni, G., Buffarini, G., Saitta, F., Castellano, M. G., Scafati, F. (2019). Effectiveness of HDRB isolation systems under low energy earthquakes, *Soil Dynamics and Earthquake Engineering*. **118,** 207-220.

[107] Rahnavard, R., Thomas, R. J. (2019). Numerical evaluation of steel-rubber isolator with single and multiple rubber cores, *Engineering Structures.* **198,** 109532.

[108] Zuniga-Cuevas, O., Teran-Gilmore, A. (2013). Parametric study on acceleration-based design of low-rise base isolated systems, *Engineering Structures.* **53,** 25–37.

[109] AISC 341-16S. (2016). Seismic Provisions for Structural Steel Buildings, ANSI/AISC, Chicago, IL, American Institute of Steel Construction.

[110] Asgarian B, Sadrinezhad A, Alanjari P. (2010). Seismic performance evaluation of steel moment resisting frames through incremental dynamic analysis, Journal of Constructional Steel Research. **66**, 178–190.

[111] Iranian code of practice for seismic resistant design of buildings. Standard no. 2800. 3rd edition, (2004). Building and Housing Research Center.

[112] AISC (1997). Seismic provisions for structural steel buildings. American Institute of Steel Construction.

[113] FEMA. (2000). Seismic design criteria for new moment-resisting steel frame construction. Federal Emergency Management Agency Report No. 350.

[114] Filiatrault A, Cherry S. (1990). Seismic design spectra for friction-damped structures, Journal of Structural Engineering ASCE. **116(5),** 1334–1355.

[115] Mirtaheri M, Zandi AP, Samadi SS, Samani HR. (2011). Numerical and experimental study of hysteretic behavior of cylindrical friction dampers, Engineering Structures. **33,** 3647–3656.

[116] Lee SH, Park JH, Lee SK, Min KW. (2008). Allocation and slip load of friction dampers for a seismically excited building structure based on storey shear force distribution, Engineering Structures. **30,** 930-940.

[117] Soong TT, Spencer BF Jr. (2002). Supplemental energy dissipation: state-of-the-art and state-of-the practice, Engineering Structures. **24,** 243-259.

[118] Computers and Structures, Inc. (2011). SAP 2000 Advanced 14.0.0. Structural Analysis Program, Berkeley, CA.

[119] Karavasilis, T.L., Bazeos, N., Beskos, D. E. (2006). Maximum displacement profiles for the performance based seismic design of plane steel moment resisting frames, *Engineering Structures.* **28(1),** 9–22.

[120] Park, Y. J., Wen, Y. K., Ang, A.H-S. (1986). Random Vibration of Hysteretic Systems under Bi-Directional Ground Motions, *Earthquake Engineering and Structural Dynamic.* **14,** 543-557.

[121] Ryan, K. L., Chopra, A. K. (2004). Estimating the seismic displacement of friction pendulum isolators based on non-linear response history analysis, *Earthquake Engineering and Structural Dynamics.* **33(3),** 359–373.

[122] Wei, W., Yuan, Y., Igarashi, A., Tan, P., Lemur, H., Zhu, H. (2016). A generalized rate-dependent constitutive law for elastomeric bearings, *Construction and Building Materials.* **106,** 693-699.

[123] Dall'Asta, A., Ragni, L. (2006). Experimental Tests and Analytical Model of High Damping Rubber Dissipating Devices, *Engineering Structures.* **28,** 1874-1884.

[124] Hwang, J. S., Wu, J. D., Pan, T. C., Yang, G. (2002). A Mathematical Hysteretic Model for Elastomeric Isolation Bearings, *Earthquake Engineering and Structural Dynamics.* **31,** 771-789.

[125] Sarno, L. D., Chioccarelli, E., Cosenza, E. (2011). Seismic response analysis of an irregular base isolated building, *Bulletin of Earthquake Engineering.* **9,** 1673-1702.

[126] Nestovito, G., Occhiuzzi, A. (2016). Implementation of smart-passive dampers combined with double concave friction pendulum devices to retrofit an existing highway viaduct exploiting the seismic early warning information, Engineering Structures. **120,** 58-74.

[127] PEER. The Pacific Earthquake Engineering Research Center. User's Manual for the PEER Ground Motion Database Application, University of California, Berkeley, 2011.

[128] Avila, L., Vasconcelos, G., Lourenco, P. B. (2018). Experimental seismic performance assessment of asymmetric masonry buildings. *Engineering Structures,* **155**, 298-314.

[129] SEAOC Seismology Committee (1999). Recommended lateral force requirements and commentary. Structural Engineers Association of California, Sacramento, CA. Uniform Building Code.

[130] Nabid, N., Hajirasouliha, I., Petkovski, M. (2019). Simplified Method for Optimal Design of Friction Damper Slip Loads by Considering Near-Field and Far-Field Ground Motions, *Journal of Earthquake Engineering.* DOI: 10.1080/13632469.2019.1605316.

[131] Wu, Y.M., Samali, B. (2005). Shake table testing of a base isolated model, *Engineering Structures.* **24,** 1203-1215.

APPENDIX

Appendix A: Hysteretic Curves for 3, 6, and 9-Storey Frame with FPB

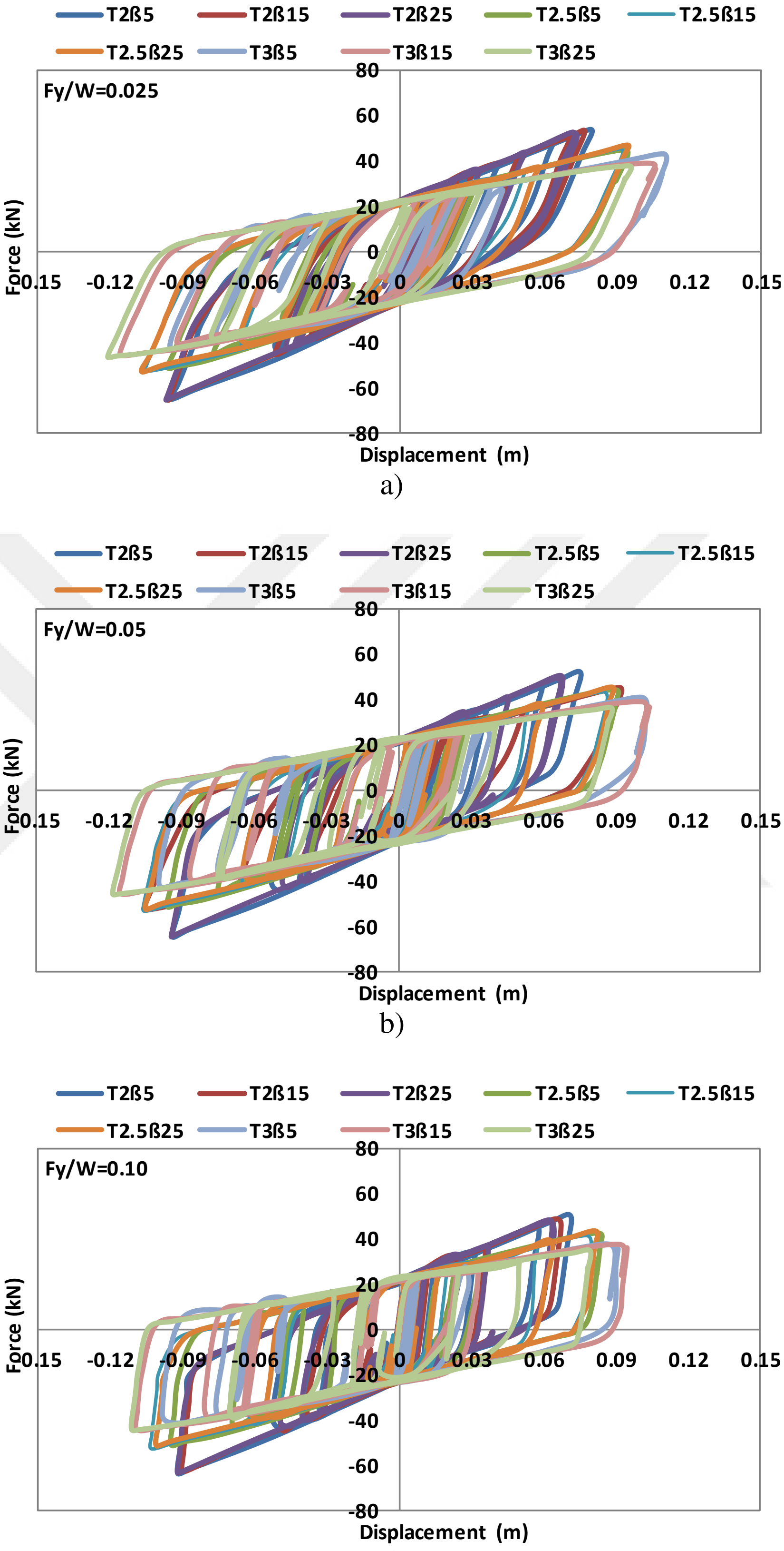

Figure A.1 Bi-linear force-deformation relation of 3-storey frame with FPB under Gazlı earthquake

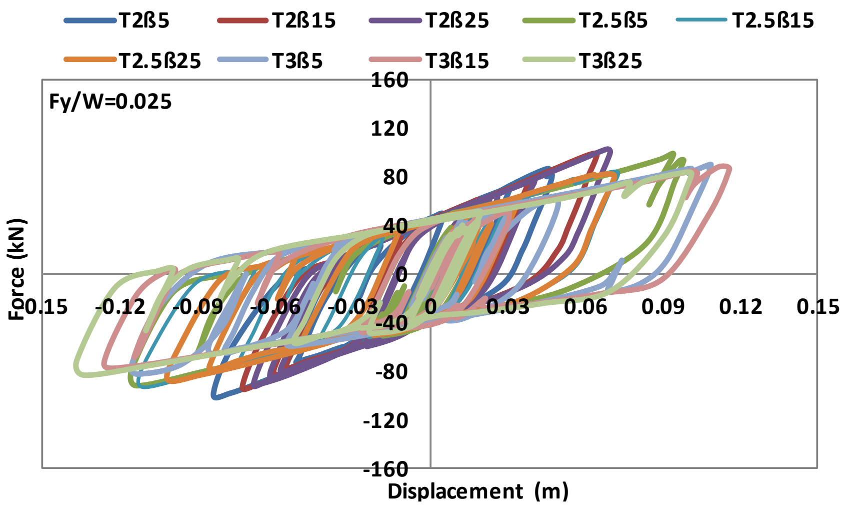

a)

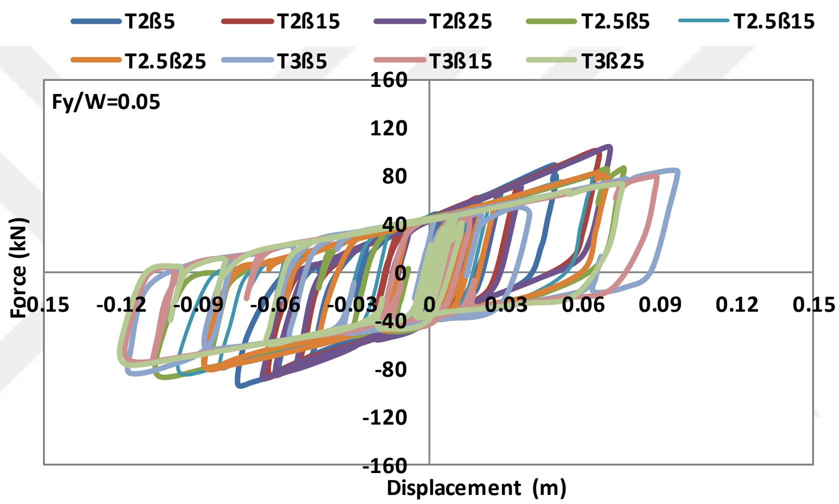

b)

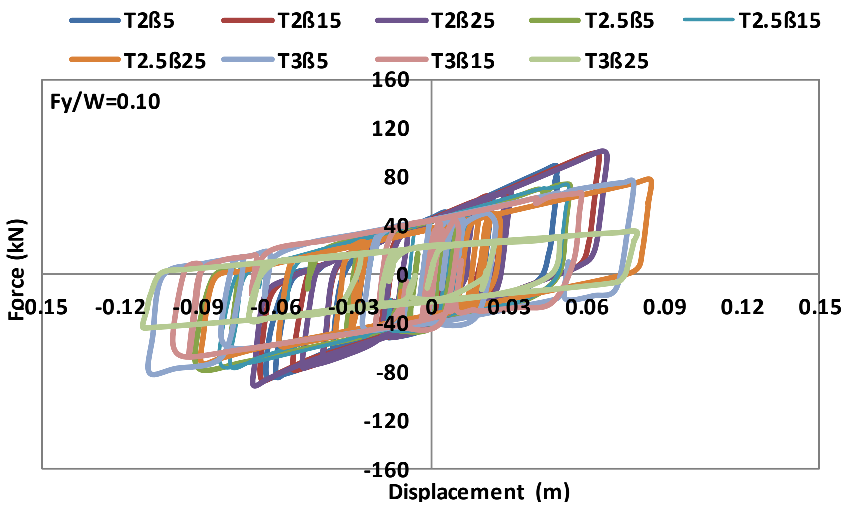

c)

Figure A.2 Bi-linear force-deformation relation of 6-storey frame with FPB under Gazlı earthquake

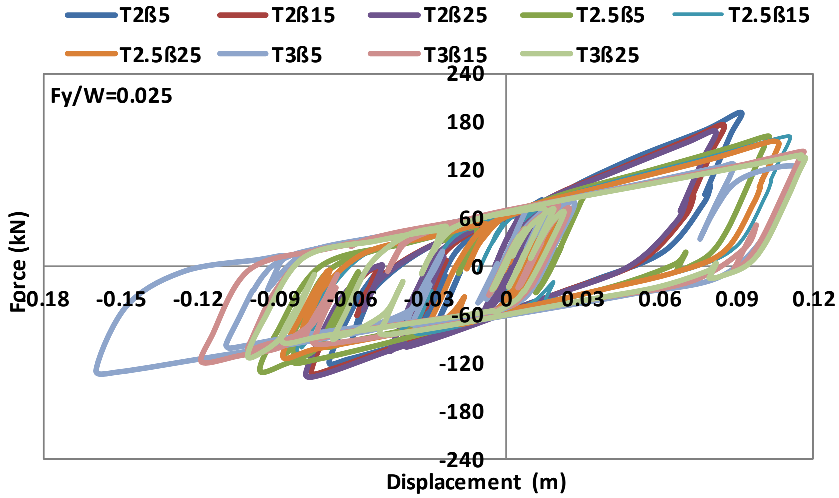

a)

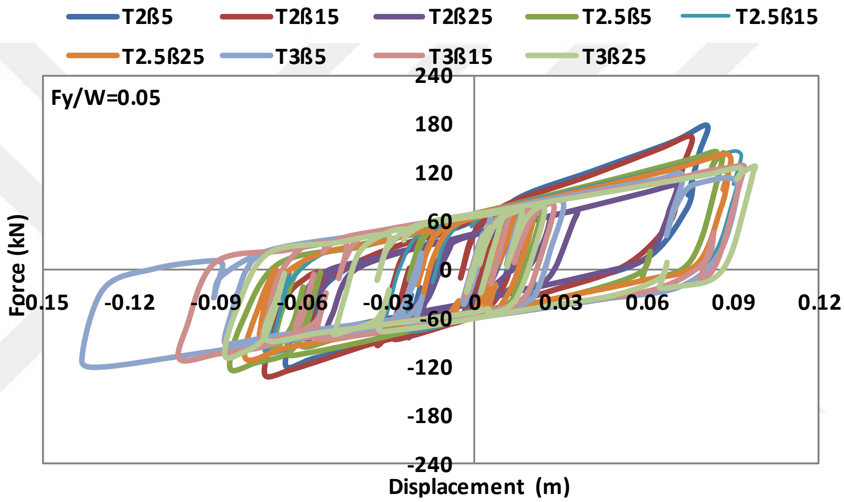

b)

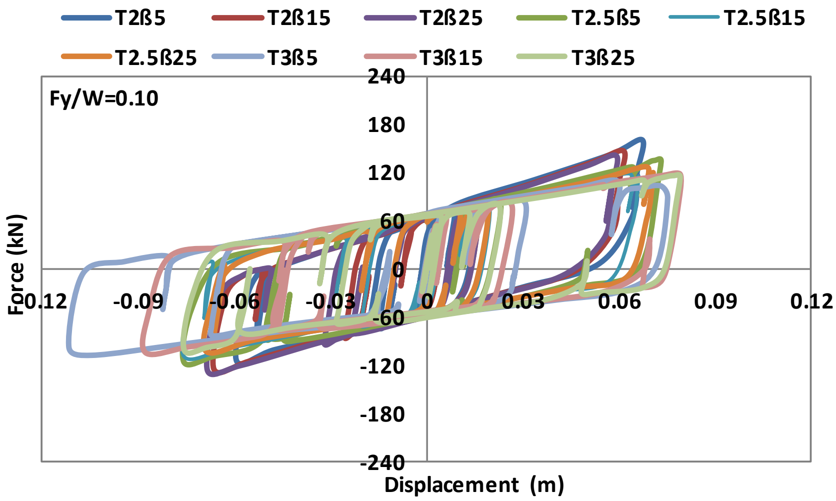

c)

Figure A.3 Bi-linear force-deformation relation of 9-storey frame with FPB under Gazlı earthquake

Appendix B: Hysteretic Curves for 3, 6, and 9-Storey Frame with HDRB

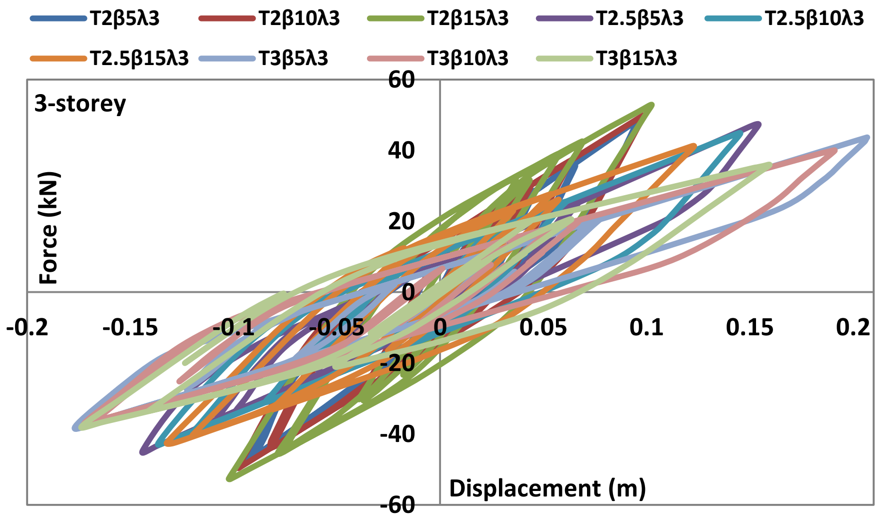

a)

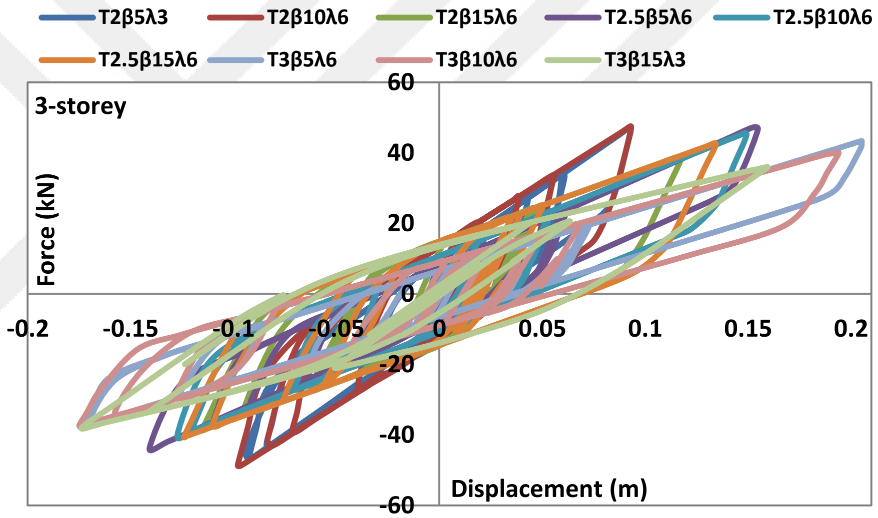

b)

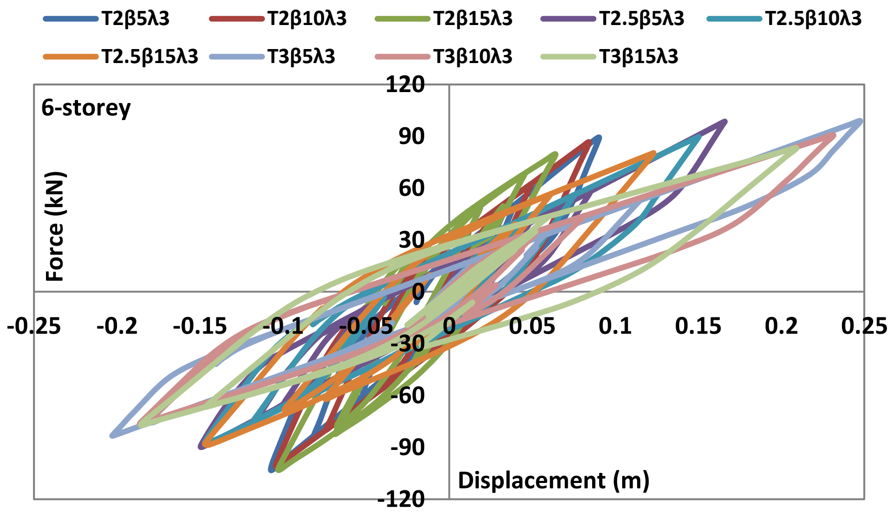

c)

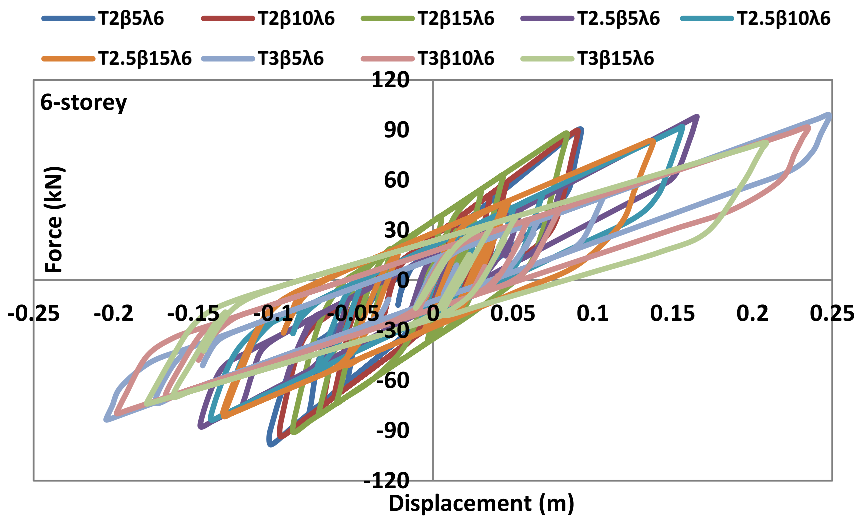

d)

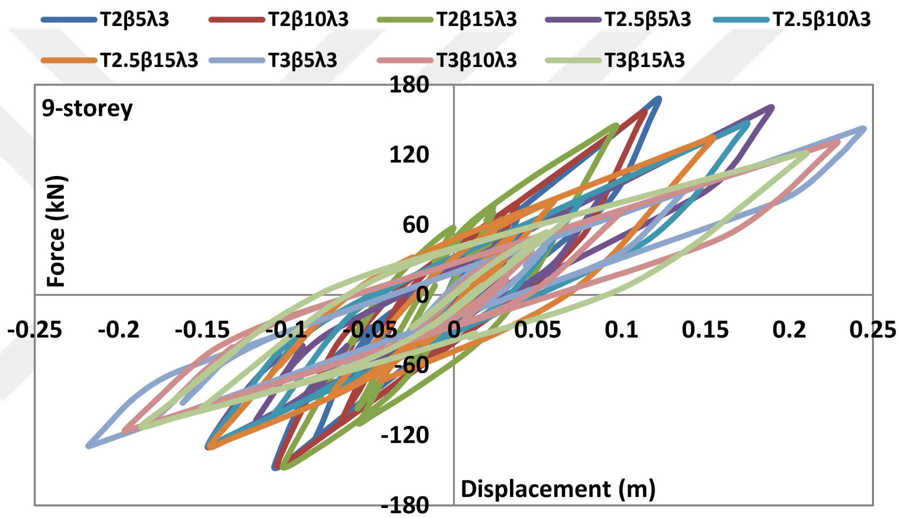

e)

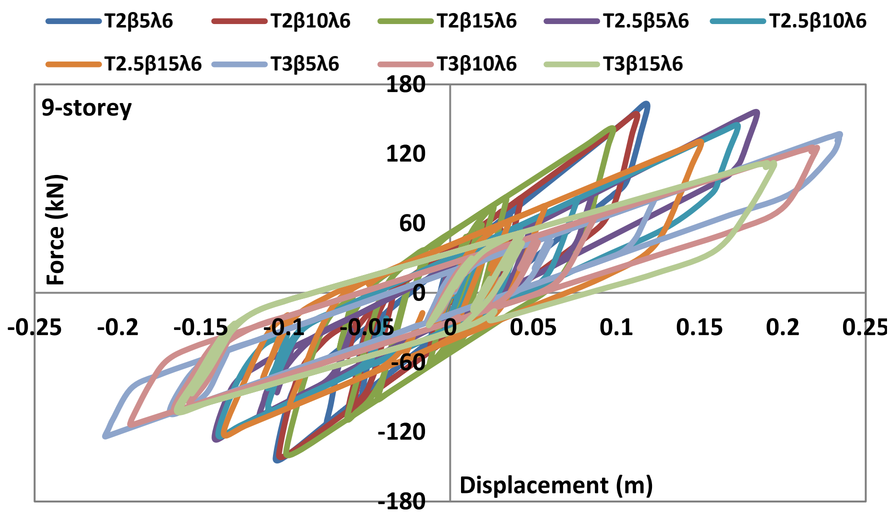

f)

Figure B.1 The force-deformation relation of 3, 6, and 9-storey frame with HDRB under Gazlı earthquake

Appendix C: Hysteretic Curves for 5-Storey Frame with FD, LRB, FPB, HDRB, FD+LRB, FD+FPB, and FD+HDRB

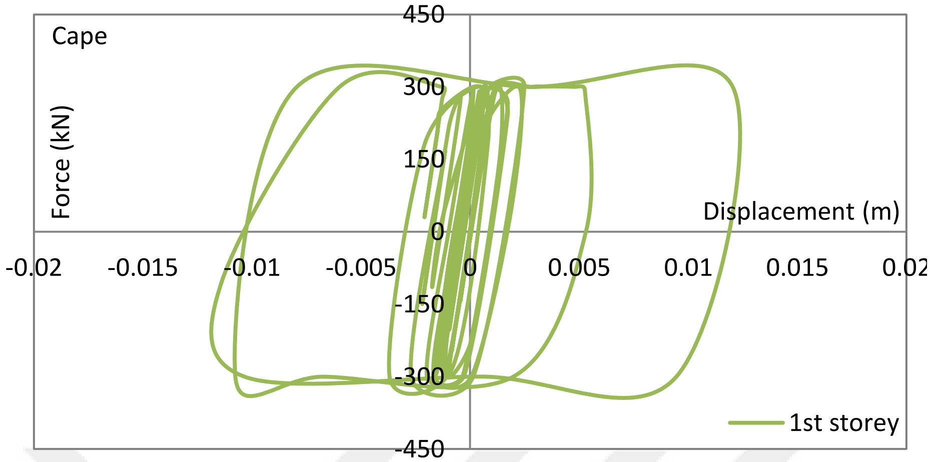

a)

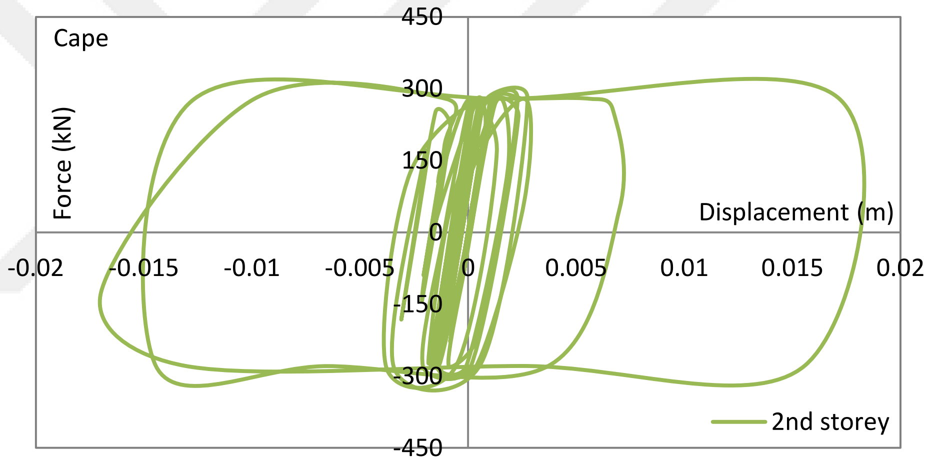

b)

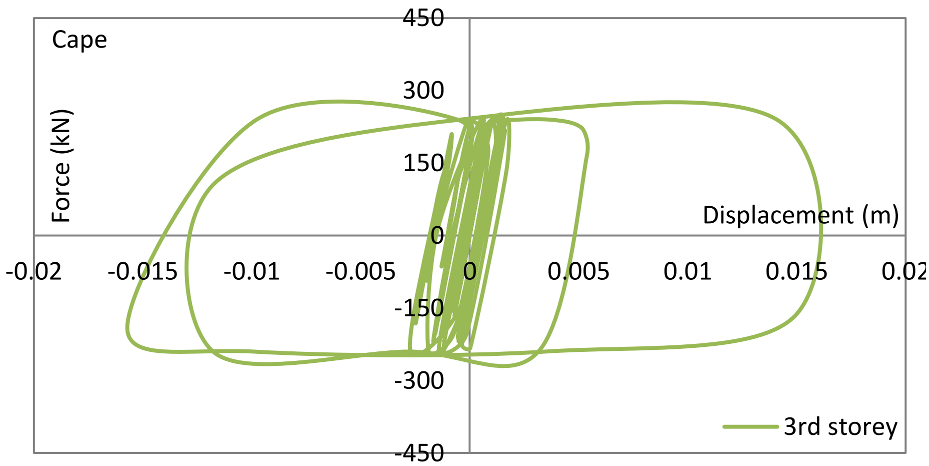

c)

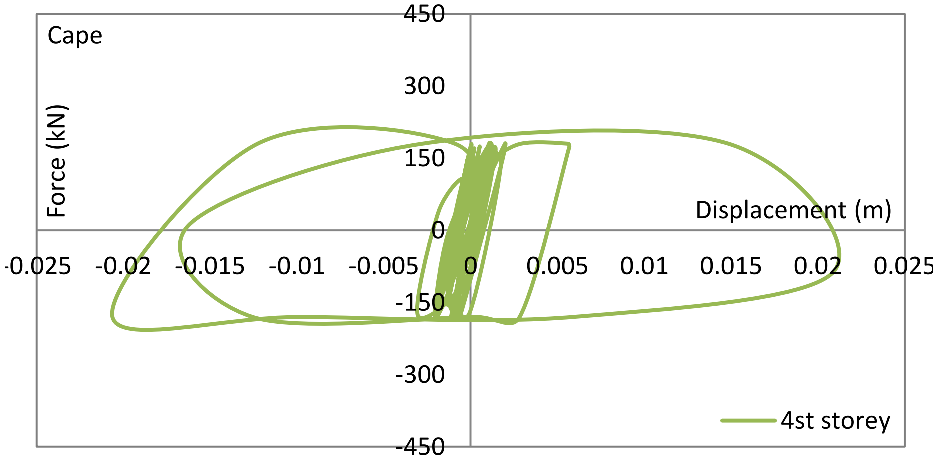

d)

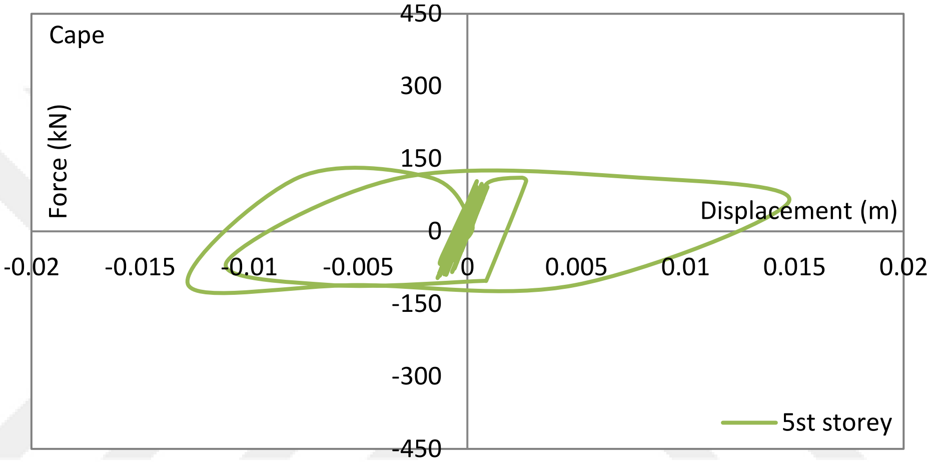

e)

Figure C.1 The force-deformation relation of 5-storey frame with FD under Cape earthquake

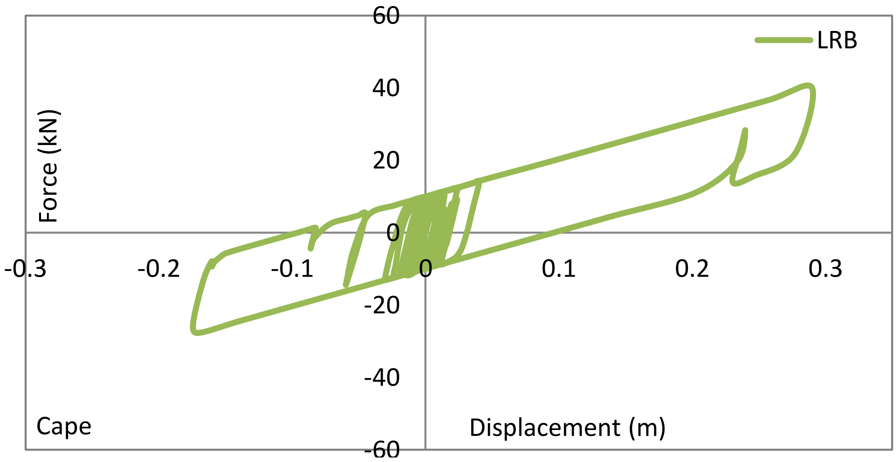

a)

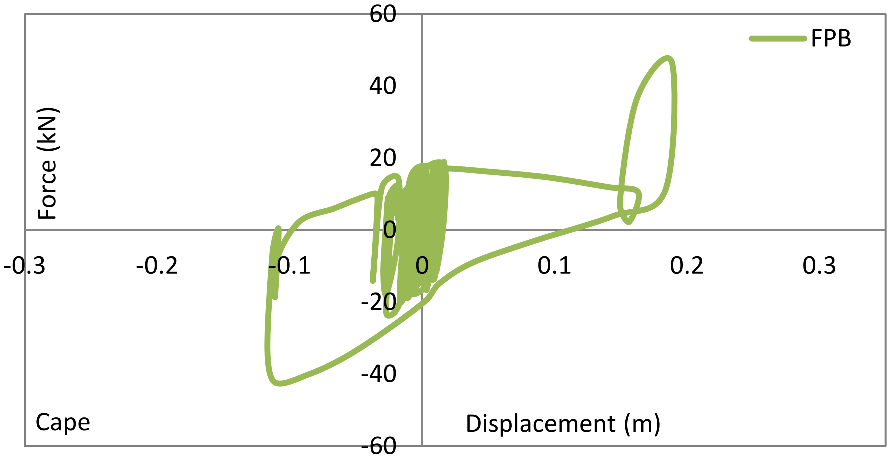
FPB
Force (kN)
Displacement (m)
Cape
60
40
20
0
-20
-40
-60
-0.3
-0.2
-0.1
0
0.1
0.2
0.3

b)

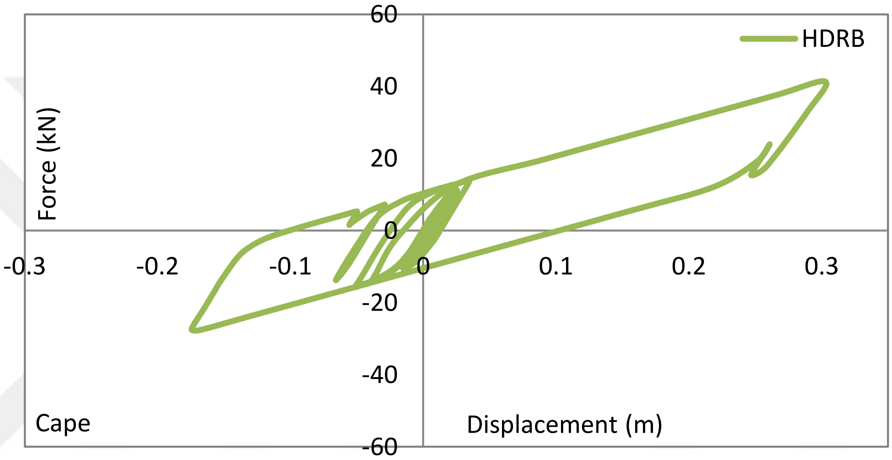
HDRB
Force (kN)
Displacement (m)
Cape
60
40
20
0
-20
-40
-60
-0.3
-0.2
-0.1
0
0.1
0.2
0.3

c)

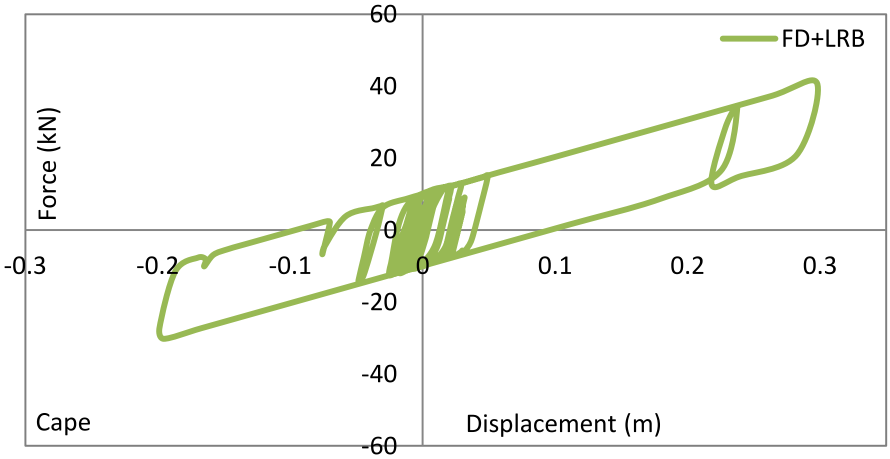
FD+LRB
Force (kN)
Displacement (m)
Cape
60
40
20
0
-20
-40
-60
-0.3
-0.2
-0.1
0
0.1
0.2
0.3

d)

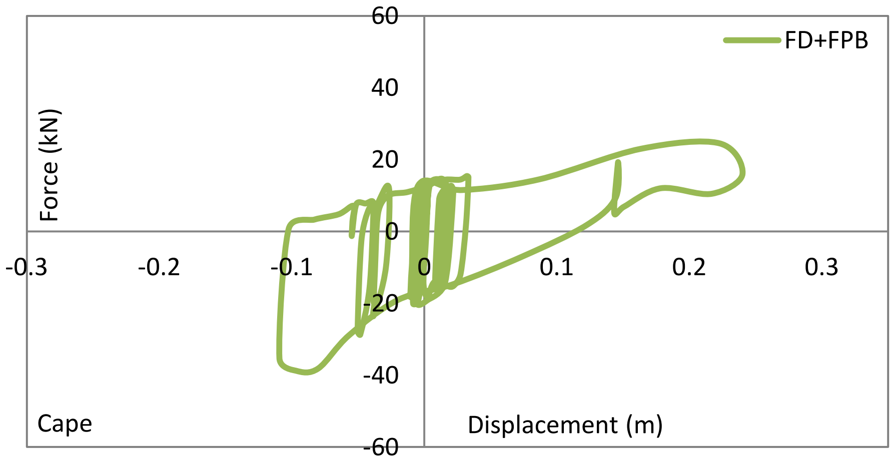

e)

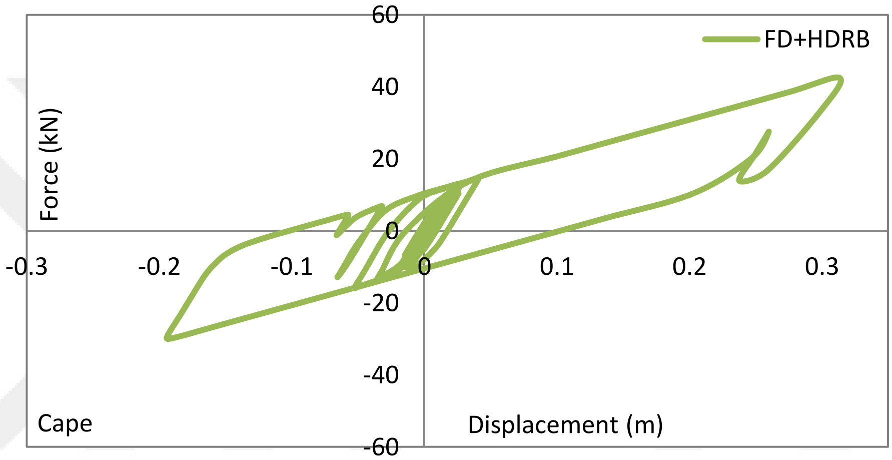

f)

Figure C.2 The force-deformation relation of 5-storey frame with LRB, FPB, HDRB, FD+LRB, FD+FPB, and FD+HDRB under Cape earthquake

PERSONAL INFORMATION

Name and surname	: Ahmet Hilmi DERİNGÖL
Nationality	: T.C.
Birth place and date	: Bünyan/11.12.1986
Marital status	: Married
Phone number	: +90 (532) 795 27 38
Fax	: -
Email	: aderingol@gmail.com

EDUCATION

	Graduate school	Year
M.Sc.	University of Gaziantep	2013
B.Sc.	University of Gaziantep	2010
High school	Sema Yazar Anadolu Lisesi	2004

WORK EXPERIENCE

Years	Place	Enrollment
2011-Present	DHMİ	Chef Engineer
2010-2011	Kilis 7 Aralık University	Research Assistant

PUBLICATIONS

International Journals

a. Deringöl, A.H. and Güneyisi, E.M. (2020). Single and combined use of friction-damped and base-isolated systems in ordinary buildings, *Journal of Constructional Steel Research.* 174, 106308, 1-18.

b. Deringöl, A.H. and Güneyisi, E.M. (2020). Effect of Lead Rubber Bearing on Seismic Response of Regular and Irregular Frames in Elevation, *Pamukkale University Journal of Engineering Sciences.* DOI:10.5505/pajes.2019.49207

c. Deringöl, A.H. and Güneyisi, E.M. (2019). Effect of Friction Pendulum Bearing Properties on Behaviour of Buildings Subjected to Seismic Loads, *Soil Dynamics and Earthquake Engineering*. 125, 105746, 1-20.

d. Deringöl, A.H. (2019). Seismic Performance of Steel Moment Frames with Variable Friction Pendulum Systems under Real Ground Motions, *International Advanced Researches and Engineering Journal*. 2(3), 208-216.

e. Güneyisi, E.M. and Deringöl, A.H. (2018). Seismic Response of Friction Damped and Base-Isolated Frames Considering Serviceability Limit State, *Journal of Constructional Steel Research.* 148, 639-658.

f. Deringöl, A.H. and Bilgin, Huseyin. (2018). Effects of the Isolation Parameters on the Seismic Response of Steel Frames. *Earthquake and Structures*. 15(3), 319-334.

International Conferences

a. Deringöl, A.H. (2017). Seismic Demands of Steel Moment Frames with Lead Rubber Bearings, *International Advanced Researches & Engineering Congress*. 2026-2033, Osmaniye, Turkey.

b. Deringöl, A.H. (2017). Seismic Performance of Steel Moment Frames with Variable Friction Pendulum Systems under Real Ground Motions *International Advanced Researches & Engineering Congress*. 2034-2041, Osmaniye, Turkey.

c. Güneyisi, E.M. and Deringöl, A.H. (2016). Seismic Analysis of Base Isolated Frames with Lead Rubber Bearings, *1st International Conference on Engineering Technology and Applied Sciences.* 623-630, Afyon, Turkey.

d. Deringöl, A.H. and Güneyisi, E.M. (2016). Effect of Friction Damper Placement on the Behaviour of Frame Structures under Seismic Actions, *1st International Conference on Engineering Technology and Applied Sciences.* 940-946, Afyon Kocatepe University, Afyon, Turkey.

e. Deringöl, A.H. and Güneyisi, E.M. (2013). Sürtünme Tipi Enerji Sönümleyicilerin Çelik Yapıların Deprem Davranışına Etkisi, *2. Türkiye Deprem Mühendisliği ve Sismoloji Konferansı,* TDMSK.018. 1-9, Hatay, Turkey.

FOREIGN LANGUAGE: English, German

HOBBIES: Hiking, Travelling, Films, Theatre, Reading, Writing